ASSESSMENT OF SATELLITE DERIVED RAINFALL AND ITS USE IN THE ACRU HYDROLOGICAL MODEL

S SULEMAN

Submitted in fulfillment of the requirements for the degree of MSc. Hydrology

Centre for Water Resources Research
School of Agriculture, Earth and Environmental Sciences
University of KwaZulu-Natal
Pietermaritzburg
December 2017

Supervisor: Ms K.T. Chetty
Co-Supervisor: Mr D.J. Clark

DEDICATED TO:

MY PARENTS, ESSACK AND SUHAIFA SULEMAN AND MY SISTER, TURAIFIA SULEMAN.

ABSTRACT

Many parts of southern Africa are considered water scarce regions. Therefore, sound management and decision making is important to achieve maximum usage with sustainability of the precious resource. Hydrological models are often used to inform management decisions; however model performance is directly linked to the quality of data that is input. Rainfall is a key aspect of hydrological systems. Understanding the spatial and temporal variations of rainfall is of paramount importance to make key management decisions within a management area. Rainfall is traditionally measured through the use of in-situ rain gauge measurements. However, rain gauge measurements poorly represent the spatial variations of rainfall and rain gauge networks are diminishing, especially in southern Africa.

Due to the sparse distribution of rain gauges and the spatial problems associated with rain gauge measurements, the use of satellite derived rainfall is being increasingly advocated. The overall aim of this research study was to investigate the use of satellite derived rainfall into the ACRU hydrological model to simulate streamflow. Key objectives of the study included (i) the validation of satellite derived rainfall with rain gauge measurements, (ii) generation of time series of satellite derived rainfall to drive the ACRU hydrological model, and (iii) validation of simulated streamflow with measured streamflow. The products were evaluated in the upper uMngeni, upper uThukela (summer rainfall) as well as the upper and central Breede catchments (winter rainfall). The satellite rainfall products chosen for investigation in this study included TRMM 3B42, FEWS ARC2, FEWS RFE2, TAMSAT-3 and GPM.

The satellite rainfall products were validated using rain gauges in and around the study sites from 1 January 2010 to 30 April 2017. The rainfall products performed differently at each location with high variation in daily magnitudes of rainfall. Total rainfall volumes over the period of analysis were generally in better agreement with rain gauge volumes with TRMM 3B42 tending to overestimate rainfall volumes whereas the other products underestimated rainfall volumes. The ACRU model was applied using satellite rainfall and rain gauge measurements in the aforementioned study catchments from 1 October 2007 to 30 September 2016. Streamflow results were generally poor and variable amongst products. Daily correlations of streamflow were poor. Total streamflow volumes were in better agreement with total volumes of observed streamflow. TRMM 3B42 and rain gauge driven simulations produced the best results in the summer rainfall region, whereas the FEWS driven simulations produced the best results in the winter rainfall region.

DECLARATION 1 - PLAGIARISM

I, Shuaib Suleman, declare that

(i) The research reported in this dissertation, except where otherwise indicated, is my original work.

(ii) This dissertation has not been submitted for any degree or examination at any other university.

(iii) This dissertation does not contain other persons' data, pictures, graphs or other information, unless specifically acknowledged as being sourced from other persons.

(iv) This dissertation does not contain other persons' writing, unless specifically acknowledged as being sourced from other researchers. Where other written sources have been quoted, then:

(a) their words have been re-written but the general information attributed to them has been referenced;

(b) where their exact words have been used, their writing has been placed inside quotation marks, and referenced.

(vi) This dissertation does not contain text, graphics or tables copied and pasted from the Internet, unless specifically acknowledged, and the source being detailed in the Dissertation and in the References sections.

PREFACE

The work described in this dissertation was carried out in the Centre for Water Resources Research, School of Agriculture, Earth and Environmental Sciences, University of KwaZulu-Natal, Pietermaritzburg under the supervision of Ms K.T. Chetty and Mr D.J. Clark.

The research represents original work by the author and has not otherwise been submitted in any form for any degree or diploma to any tertiary institution. Where use has been made of the work of others it is duly acknowledged in the text

ACKNOWLEDGEMENTS

This Masters Research Project titled "ASSESSMENT OF SATELLITE DERIVED RAINFALL AND ITS USE IN THE ACRU HYDROLOGICAL MODEL" has been funded by the Water Research Commission (WRC) and the National Research Foundation (NRF). I wish to thank the aforementioned institutions for funding this research. I would also like to acknowledge the following people and institutions:

- Ms K.T. Chetty, thank you for all of your support throughout my hydrology career. The years under your guidance has given me a solid foundation for future endeavours.
- Mr D.J. Clark, thank you for the endless support throughout the project. Sharing your technical skills has proven to be invaluable to me and is much appreciated.
- My family, thank you for the constant love, support and motivation.
- My friends, thank you for the support and motivation.
- The Department of Water Affairs and Sanitation of South Africa for providing daily rainfall and streamflow data.
- The South African Weather Service for providing rainfall data.
- Ezemvelo KZN Wildlife for the 2011 Land Cover Dataset.
- The Department of Environmental Affairs for use of the 2013/2014 National Land Cover Dataset.
- NASA/GES DISC for providing TRMM 3B42 and GPM daily rainfall data.
    - Huffman, GJ, Adler, RF, Bolvin, DT, Nelkin, EJ. 2010. The TRMM Multi-satellite Precipitation Analysis (TMPA). Chapter 1 in Satellite Rainfall Applications for Surface Hydrology, Hossain, F and Gebremichael, M, Eds. Springer Verlag, ISBN: 978-90-481-2914-0, 3-22.
    - Huffman, GJ, Bolvin, D, Braithwaite, D, Hsu, K, Joyce, R and Xie, P. 2014. Integrated Multi-satellite Retrievals for GPM (IMERG), version 4.0. NASA's Precipitation Processing Centre, https://gpm1.gesdisc.eosdis.nasa.gov
- The USGS for providing the FEWS daily rainfall.
    - Xie, P and Arkin, PA. 1996. Analyses of global monthly precipitation using gauge observations, satellite estimates, and numerical model predictions. *Journal of Climate*, 9, 840–858.
    - Novella, NS and Thiaw, WM. 2013. African rainfall climatology version 2 for famine early warning systems. *Journal of Applied Meteorology and Climatology*, 52(3): 588-606.

- TAMSAT for providing the TAMSAT version three rainfall data.
    - Tarnavsky, E, Grimes, D, Maidment, R, Black, E, Allan, R, Stringer, M, Chadwick, R and Kayitakire, F. 2014. Extension of the TAMSAT Satellite-based Rainfall Monitoring over Africa and from 1983 to present. *Journal of Applied Meteorology and Climate*, DOI 10.1175/JAMC-D-14-0016.1

TABLE OF CONTENTS

LIST OF TABLES

LIST OF FIGURES

Page

LIST OF ABBREVIATIONS

AMSU	:	Advanced Microwave Sounding Unit
CHIRPS	:	Climate Hazards Group Infrared Precipitation with Station Data
CMAP	:	CPC's Merged Analysis of Precipitation
CMORPH	:	Climate Prediction Centre Morphing Technique
CPC	:	Climate Predication Centre
DEM	:	Digital Elevation Model
DWS	:	Department of Water and Sanitation of South Africa
ET_0	:	Reference Evaporation
EUMETSAT	:	European Organisation for the Exploitation of Meteorological Satellites
FEWSARC	:	Famine Early Warning Systems Network African Rainfall Climatology
FEWSRFE	:	Famine Early Warning Systems Network Rainfall estimator
GOES	:	Geostationary Operational Environmental Satellites
GPM	:	Global Precipitation Mission
NASA	:	National Aeronautics and Space Administration
NOAA	:	National Oceanic and Atmospheric Administration
PERSIANN	:	Precipitation Estimation from Remotely Sensed Information using Artificial Neural Networks
SAHG	:	Satellite Applications and Hydrology Group
SAWS	:	South African Weather Service
TAMSAT	:	Tropical Applications of Meteorology Using Satellite Data and Ground-based Observations
TRMM	:	Tropical Rainfall Measuring Mission
WRC	:	Water Research Commission

1. INTRODUCTION

1.1 Background

Many parts of southern Africa are categorised as water scarce regions and many users share the limited water resource (Lange *et al*., 2007, Jarmain *et al*., 2009). Thus the need for sound water resource management and decision making is important to achieve resource sustainability.

Effective decision making of water resources must be based on factual information and sound knowledge of the dominant hydrological processes that occur in a water management area (Wilk *et al*., 2006; Kongo *et al*., 2010; Xu *et al*., 2014). Understanding and observing these hydrological processes in time and space can only occur through the establishment of monitoring networks (Hughes, 2006; Kongo *et al*., 2010). Subsequently, assessment and sound management of water resources in large catchments of southern Africa prove to be a difficult task due to limited data (Wilk *et al*., 2006). The reality of the situation is that surface rain gauge measurements are sparse, especially in less developed countries and monitoring networks are declining globally (Hughes, 2006). Reliability of data and missing data are areas of concern in monitoring catchment variables (Hughes, 2006). Models may be used to obtain information in areas of insufficient surface monitoring. However, model performance is directly linked to the quality of data that is utilised within them, especially precipitation data which is generally the driver of most hydrological models (Hughes, 2006). Effective and sustainable water resource management requires information and data on the spatial and temporal variations of rainfall within a management area (Wilk *et al*., 2006).

Rainfall is one of the most important climatic variables to consider when analysing the heat, water, momentum and gas exchange budgets (Nysteun *et al*., 1996). However, rainfall is in one of the most difficult to measure (Nysteun *et al*., 1996). Rainfall measurement is made through in-situ surface techniques or through climate model estimates and satellite-based observations. In-situ based measurements using rain gauges are relatively accurate, but can be sparse with limited spatial coverage as they are point measurements (Xu *et al*., 2014; Ciabatta, *et al*., 2015; Amekudzi *et al*., 2016). Remotely sensed observations offer better geographical coverage with large amounts of spatial data that are not accessible through the use of in-situ methods (Jarmain *et al*., 2009; Xu *et al*., 2014; Amekudzi *et al*., 2016). Data is

updated often, freely available and easy to access which has promoted on the use of remote sensing (van Dijk and Renzullo, 2011; Xu *et al*., 2014).

Currently many satellite derived rainfall products are available. Many of the available products obtain inputs from the same sensors, however the algorithms that are used to achieve an estimate through merging, inter-calibrating and interpolating vary greatly among the products (Rauniyar *et al*., 2017). Some of these products include the Tropical Rainfall Measuring Mission (TRMM) series of products, the Famine Early Warning Systems Rainfall Estimator (FEWS-RFE), The CPC's Merged Analysis of Precipitation (CMAP) and The Climate Prediction Centre Morphing Technique (CMORPH), among many others. The increasing availability of remotely sensed products over the past few decades has allowed for the integration of data into models and water budgets where they are most relevant to water resource management (Xu *et al*., 2014).

1.2 Research Problem

Rainfall is measured in many ways namely; in-situ based measurement, climate model estimates and remotely sensed methods. In-situ measurements are generally the most accurate form of measurement, however their spatial distribution is relatively sparse with some areas lacking any form of measurement (Kidd and Levizzani, 2011, Ciabatta *et al*., 2015). In-situ based measurements also measure variables at a very local scale and may not account for the spatial and temporal heterogeneity with regards to rainfall (New *et al*., 2000; Xu *et al*., 2014). In-situ meteorological radar measurements also acquire errors through reflectivity issues (Ciabatta *et al*., 2015). Remotely sensed data provide a useful means of measurement in a world of diminishing rain gauge networks and more specifically in southern Africa, where measurements are relatively poor in terms of accuracy and spatial distribution (Kidd and Levizzani, 2011; Pitman, 2011; Cohen Liechti *et al*., 2012; Xu *et al*., 2014). Satellite observations are not seen as a primary solution to data acquisition and monitoring challenges, but used as a means to obtain measurements where monitoring is absent or inadequate (Jarmain *et al*., 2009; Ciabatta *et al*., 2015).

The availability of satellite data has not been widely utilised within water resource management and there is little evidence of the wide uptake of the information they provide into water resource management (van Dijk and Renzullo, 2011). There are a number of challenges that the field experiences in encouraging the use of satellite derived data in

resource management (Xu *et al*. 2014; Ciabatta *et al*., 2015). Major challenges include technological barriers required to process the satellite data and the lack of knowledge in integrating the satellite data into meaningful applications (van Dijk and Renzullo, 2011; Xu *et al*., 2014; Ciabatta *et al*., 2015).

The increasing availability of satellite observation data and increasing advancements in technology have presented many opportunities for the advancement and inclusion of the data into hydrological models (van Dijk and Renzullo, 2011; Fern'andez-Prieto *et al*., 2012; Xu *et al*., 2014). Models used for a specific application have to be carefully considered in terms of their best fit for the application. According to van Dijk and Renzullo (2011) the success of a model does not only depend on the model itself, but rather the data that is utilised within the model. Ciabatta *et al*. (2015) attribute the scarce use of satellite rainfall data in models to the poor estimation of light rainfall events; insufficient temporal and spatial resolutions and poor data latency for operational purposes. The current nature of hydrological models does not readily accept remotely sensed datasets and are designed to incorporate traditional methods of measurement. Current hydrological model configurations require modification to include satellite derived data or new models need to be developed (Wagener *et al*., 2010; Xu *et al*., 2014). Furthermore, the main focus of utilising satellite derived rainfall within the scientific community is for validation studies to eventually obtain guidelines for the use of specific products in specific regions (Ciabatta *et al*., 2015).

Surface measurements are proving to be insufficient in water resource management, except in developed areas where networks are well established (Xu *et al*., 2014). The global decline in surface monitoring and the sparse nature of networks are hindering sound water resource management due to the lack of information on the processes occurring. Satellite observations are capable of providing extensive data for use in hydrological modelling and ultimately water resource management (Xu *et al.*, 2014). The availability and ease of access to remotely sensed data show promise in a world of diminishing monitoring networks.

1.3 Aims and Objectives

This research study forms part of the WRC K5/2512 project (Clark, 2017a/b) which is a follow on project from the WRC K5/2205 by Clark (2015). Key recommendations of the WRC K5/2205 project were that satellite derived rainfall is to be assessed and utilized in a hydrological model in a summer and winter rainfall region as well as to use the ACRU

hydrological model to simulate streamflows. The recommendations of the K5/2205 project informed the aims and objectives of this research study.

The overall aim of this study was to assess satellite derived rainfall accuracy and the suitability of satellite derived rainfall data to drive the Agricultural Catchments Research Unit Model version 4 (ACRU) (Schulze, 1995; Smithers and Schulze, 2004). The output of the model can be used to enhance decision making within water management. The general aim of this study was to create time series datasets of rainfall estimates at a sub-catchment scale from satellite derived rainfall products and use these datasets as input to the ACRU model to simulate streamflow. The specific objectives of the study were to:

i. To analyse the accuracy and effectiveness of satellite derived rainfall when compared to observed rainfall at monitoring stations.
ii. To validate satellite derived rainfall with in-situ measurement at selected rain gauge stations.
iii. To compare simulated streamflow obtained through driving the ACRU model with satellite derived rainfall and rain gauge measurements with observed streamflow.

1.4 Research Questions

i. How do the in-situ based (rain gauge) rainfall compare to the satellite derived estimates?
ii. How will simulated streamflow generated by the ACRU model driven by satellite derived rainfall and rain gauge measurements compare to observed streamflow?
iii. Does satellite derived rainfall enhance hydrological modelling due to the better spatial and temporal scale that it provides?

1.5 Research Hypothesis

i. H_o: Simulated streamflow obtained from the satellite rainfall products, as a driver to the ACRU model, will compare favourably to the observed streamflow.
ii. H_a: Simulated streamflow obtained from the satellite rainfall products, as a driver to the ACRU model, will not compare favourably to the observed streamflow.

1.6 Organisation of Thesis

The research topic was introduced in Chapter 1. In Chapter 2, rainfall estimation techniques are reviewed as well as literature related to satellite derived rainfall estimation and its use in hydrological modelling. In Chapter 3, the methodology and study sites used in this research study are described. In Chapters 4 and 5, the results of the product validation and the ACRU simulations of streamflow are presented and discussed respectively. In Chapter 6, the conclusions and recommendations are presented. Appendix A describes the statistics used in this study. Appendix B presents the tables of statistics and rainfall time series plots of the validation study. Appendix C presents the time series of streamflow simulations of the ACRU modelling study.

2. LITERATURE REVIEW

Traditionally, rainfall is measured through the use of rain gauges. Alternate techniques of rainfall measurement are made through the use of ground-based radar and satellites. Rain gauge measurements produce accurate results of rainfall at a point scale, but poorly represent rainfall spatially. Sources of errors of rain gauge measurement include wind, adhesion, inclination and splash of rain gauge (Kurtyka, 1953). Rain gauges are sparsely distributed and networks are declining, especially in southern Africa (Pitman, 2011; Hughes, 2006). Ground-based radar provides an intermediate spatial scale of rainfall measurement. However, ground-based radar is limited in detecting weaker rainfall events and topography may cause beam blocking (Wetchayont *et al*., 2013). Satellite derived rainfall measurement has greater spatial scales, however resolutions may be too coarse for meaningful applications (New *et al*., 2000). Table 2.1 summarises the characteristics of rain gauge, ground-based and satellite derived measurement. This Chapter reviews literature focusing on satellite derived rainfall measurement and its use in hydrological modelling.

Table 2.1 Comparison of rain gauge, ground-based radar and satellite derived rainfall measurement (after, New *et al*., 2000; Wetchayont *et al*., 2013).

Rain Gauge Measurement	**Ground-based radar**	**Satellite Derived Measurement**
Poor spatial coverage	Intermediate spatial coverage	Large spatial coverage
Point measurement	Spatial measurement	Spatial measurement
Long records	Short records	Short records
Biases and inhomogeneities	Biases and inhomogenities	Biases, inhomogeneities and discontinuities
Observer errors and logger malfunction	Inter radar calibration errors and beam blocking	Calibration errors and algorithm uncertainty

2.1 Satellite Derived Rainfall Measurement

Rainfall is one of the most influential variables in surface hydrology. Out of all of the hydrological variables, rainfall estimation by satellite, radar or gauge, has been the most extensively studied (Nystuen *et al*., 1996; Lakshmi, 2004). Satellites have near global coverage with regards to remotely sensed rainfall and this is an advantage to areas that lack surface observations (Hu *et al*., 2015). Another advantage is that the availability of satellite products are not limited by administrative factors and they are usually free of charge which

has promoted developments in satellite rainfall estimation (Hu *et al*., 2015). Since rainfall is highly variable in time (less than 30 minutes) and space (1-2 km), accurate representation of rainfall in both time and space are needed for a variety of applications (Lakshmi, 2004). Remotely sensed rainfall estimates offer a solution to the spatial, temporal and in-situ issues that are encountered with in-situ based measurements. Satellite based rainfall estimation offers high spatial resolutions (10-20 km) with revisit times ranging from one to two days (Lakshmi, 2004). Radar rainfall estimates perform better in that it has spatial resolutions of 1-2 km and with temporal resolutions ranging from 15-30 minutes (Lakshmi, 2004). The greater spatial resolutions and finer temporal resolutions of rainfall allow for better monitoring at a management level.

Retrievals of rainfall intensity from low orbiting and geostationary satellites in the past 30 years have been based on passive sensors which utilise the infrared, visible and passive microwave wavelengths (Michaelides *et al*., 2009). The microwave sensors provide estimates over land due to scattering and emission over the sea (Rauniyar *et al*., 2017). Due to the high albedo of clouds, they appear bright in contrast to the earth. Thus, rainfall can be estimated in the visible range because deep clouds appear brighter and thick clouds are associated with rainfall (Kidd and Levizzani, 2011). The visible range also allows for investigating of cloud top texture which can also provide useful information about rainfall. Kidd and Levizzani (2011) report that the relationship between rainfall and cloud brightness is relatively poor and imagery presented in the visible range need to be used in conjunction with other observational methods, such as the use of rain gauge for calibration. Infrared observations can be more useful as it can be operated during the night, unlike the visible range which is limited to operating during the day. The infrared spectrum is used to measure cloud top temperatures and the measurements share an indirect relationship to rainfall rates (Rauniyar *et al*., 2017). Tall, large clouds are associated with heavy rainfall and a simple rainfall estimation can be derived from cloud top temperatures, even though the relationship between rainfall and cloud top temperatures is indirect (Kidd and Levizzani, 2011). The passive microwave range utilises the fact that the earth naturally emits microwaves. Microwave frequencies are responsive to internal cloud processes and rainfall is the main source of attenuation within this range (Michaelides *et al*., 2009). Two processes allow for the observation of rainfall in the microwave region and these are that rain drops cause an increase in microwave radiation and precipitating ice particles cause scattering which decrease the microwave radiation (Michaelides *et al*., 2009; Kidd and Levizzani, 2011). Low frequency

channels are used to observe rainfall due to the low and constant background radiometric signal over water (Kidd and Levizzani, 2011). Active microwave remote sensing based retrievals are probably the most direct approach of rainfall measurement by satellite. Microwaves penetrate into the cloud and therefore interact with the hydrometeors which causes backscatter which is proportional to the number of hydrometeors, thus often providing more accurate results in terms of rainfall intensity (New *et al*., 2000; Kidd and Levizzani, 2011).

Passive microwave data are collected by Low Earth Orbiting (LEO) satellites. However, there exists a large global spatial gap in that the data collected only covers 80% of the earth's surface (Huffman *et al*., 2010; Rauniyar *et al*., 2017). Infrared data are collected by a constellation of Geosynchronous Earth Orbit (GEO) satellites. They possess high spatial and temporal resolutions. However, the estimates are less reliable for cold cirrus clouds, non-precipitating clouds and low warm clouds (Ebert *et al.*, 2007). Rauniyar *et al*. (2017) report that studies show that infrared estimates are poor at fine spatial and temporal scales. To overcome these limitations and to maximise the benefits many satellite rainfall products have blended microwave estimates with infrared estimates (Rauniyar *et al*., 2017). Many techniques also include gauge or modelled data into the estimation process to achieve enhanced global coverage as well as finer spatial and temporal resolutions (Rauniyar *et al*., 2017).

2.2 Satellite Derived Rainfall Products

The launch of the first operational radar, the Tropical Rainfall Measuring Mission (TRMM) in 1997, has laid the ground work down for on-board satellite measurement of rainfall (Michaelides *et al*., 2009). Since then many satellite derived rainfall products have been developed. Many product algorithms make use of multi-sensors to achieve a rainfall estimate. Commonly used satellite rainfall products include CMORPH, TAMSAT, TRMM, FEWS (ARC2, RFE2), PERSIANN and CHIRPS. The most common and popular products are reviewed below.

2.2.1 Famine Early Warning Systems Rainfall Estimator (FEWS RFE 2.0)

The Climate Prediction Centre (CPC), part of the National Oceanic and Atmospheric Administration (NOAA), developed the Rainfall Estimator (RFE) product in 1995 (Herman *et al*. 1997). This was developed to meet the need for higher spatial resolution daily rainfall

estimates to support the United States Agency for International Development (USAID) and Famine Early Warning Systems Network (FEWS-NET) (Novella and Thiaw, 2013). Novella and Thiaw (2013) report that the product is unique in that it has a high spatial resolution of 0.1˚ (10 km x 10 km), and its ability to combine satellite and gauge data to produce daily rainfall estimations at a near real-time basis over Africa. In 2001, the CPC implemented the second generation of the RFE which includes an advanced RFE algorithm. Love *et al*. (2004) reports that the advanced algorithm enhanced computational efficiency, estimation accuracy and reduced the bias errors. The RFE 2.0 obtains inputs from four different sources, of which three are satellite-based sources (Love *et al*., 2004). These are from the daily rain gauge data of the Global Telecommunications System (GTS); the Geostationary Operational Environmental Satellite (GOES) precipitation index (GPI) which is calculated from infrared cloud-top temperatures from EUMETSAT; rainfall estimates based on the Advanced Microwave Sounding Unit (AMSU-B), which replaced the older AMSU-A; and estimates based on the Special Sensor Microwave Imager (SSM/I) (Novella and Thiaw, 2013).

The SSM/I algorithm uses an 85 GHz channel to detect radiation by precipitation sized particles within the layer of cloud (Ferraro *et al*., 1996). Over the land surface the algorithm uses scattering techniques and over the ocean low frequency emission techniques are used provided that insignificant scattering exists (Xie, 2001). The SSM/I measures brightness temperature which is caused by the presence of liquid precipitation (Xie, 2001). AMSU-B rainfall rate data is retrieved in a similar process as the SSM/I (Xie, 2001). Half hourly rainfall amounts from GOES Precipitation Index (GPI) are derived from EUMETSAT's Meteosat's infrared cloud top temperatures (Xie, 2001). A total daily rainfall estimate obtained from the GPI is input in the RFE 2.0 algorithm (Xie, 2001). The final step includes GTS data to obtain a final daily RFE 2.0 rainfall estimate (Xie, 2001). NOAA CPC report that up to 1000 stations are available for use in Africa, however due to poor gauge data and maintenance less than 500 are actually used daily. Satellite measurements that are bias-corrected are used to determine the extent and spatial distribution of a rainfall event and the magnitude of rainfall is determined by rain gauge measurements (Novella and Thiaw, 2013). The data is merged due to sources containing random errors, bias and not being spatially adequate. Information regarding the FEWS RFE 2 product is presented in Table 2.2.

Table 2.2 Information regarding the FEWS RFE 2.0 product.

Attribute	Information
Temporal Resolution	Daily
Spatial Resolution	5˚, 2.5˚, 1˚, 0.5˚, 0.25˚, 0.1˚
File formats	Geotiff, shapefile, binary
Source	NOAA National Weather Service Climate Prediction Centre (FEWS-Net) http://www.cpc.ncep.noaa.gov/fews/fewsdata/africa/rfe2
Availability	January 2001- present

2.2.2 Famine Early Warning Systems African Rainfall Climatology (FEWS ARC 2.0)

The African Rainfall Climatology (ARC, version 2) is a daily product for monitoring rainfall over Africa (Novella and Thiaw, 2013). The original version of ARC (ARC 1) is based on the same algorithm used in the FEWS RFE 2 product, however the algorithm excludes inputs from the microwave range which may affect the estimation accuracy (Novella and Thiaw, 2013). The main purpose of the FEWS ARC 1.0 was to develop a consistent and continuous rainfall dataset. The strength of FEWS ARC 2.0 are to provide daily images of rainfall anomalies over different time scales in order to identify and understand trends in rainfall anomalies at a near real-time scale (Novella and Thiaw, 2013). The FEWS RFE 2 product obtains inputs from geostationary infrared data and 24 hour rainfall accumulations obtained from the Global Telecommunication System (GTS) rain gauge data over Africa (Novella and Thiaw, 2013). There are two key differences between FEWS RFE 2.0 and ARC 2.0. Firstly, ARC 2.0 incorporates only a subset of the inputs incorporated in RFE 2.0 (Novella and Thiaw, 2013). Geostationary infrared data are used to obtain GPI estimates and gauge data are used as inputs (Novella and Thiaw, 2013). Secondly, to obtain the GPI only three hourly infrared cloud-top temperatures are used as opposed to half hourly being utilised in the RFE 2.0 (Novella and Thiaw, 2013). Infrared data and longer historical rain gauge data were used in developing the ARC 2 algorithm to produce a more consistent and stable dataset as well as to remove a bias introduced in processing that affected the ARC 1 product (Novella and Thiaw, 2013). Novella and Thiaw (2013) report that ARC 2 offers many advantages when compared to other products with long term rainfall datasets. It provides long term high resolution historical datasets at a daily real-time scale; the product operates at a high spatial resolution of 0.1˚; and the products dataset consistency can be attributed to the use of a single algorithm with two consistent inputs, being calibrated infrared imagery and fixed gauge rainfall which minimizes the bias that would be caused by using different gauges (Novella

and Thiaw, 2013). The same merging algorithm used in the FEWS RFE 2.0 is used in the FEWS ARC 2.0. Due to the consistent inputs, long dataset, and high resolution, ARC 2 is useful to monitor and understand climate change and climate variability at a local scale (Novella and Thiaw, 2013). Information for the FEWS ARC 2.0 product is presented in Table 2.3.

Table 2.3 Information regarding the FEWS ARC 2.0 product.

Attribute	**Information**
Temporal Resolution	Daily
Spatial Resolution	0.1˚x0.1˚
File formats	Geotiff, shapefile, binary
Source	NOAA National Weather Service Climate Prediction Centre (FEWS-Net) http://www.cpc.ncep.noaa.gov/fews/fewsdata/africa/arc2
Availability	January 1983- present

2.2.3 Tropical Rainfall Measuring Mission 3B42 (TRMM 3B42)

The Tropical Rainfall Measuring Mission is a shared mission of the National Aeronautics and Space Agency of the USA (NASA) and the National Space Development Agency (NASDA) of Japan (Kummerow *et al*., 1998). The purpose of the mission was to measure characteristics of tropical rainfall and the associated latent heating (Kumerrow *et al*. 1998; Prakash and Gairola, 2014). Launched in 1997, the TRMM mission laid the foundation for the use of radar in rainfall monitoring and has been available since 1998 proving useful in applications in hydrometeorology as well as climatology (Michaelides *et al*., 2009; Prakash and Gairola, 2014). The detailed specifications of TRMM are described by Kumerrow *et al*. (1998).

The TRMM 3B42 product utilises various satellite systems and gauge data to produce estimates at a spatial resolution of 0.25˚ and at a temporal scale of 3 hours of which the daily product is derived from (Dinku *et al*., 2007; Prakash and Gairola, 2014). The rainfall instruments on-board the TRMM satellite comprise of the Visible and Infrared Radiometer System (VIRS), precipitation radar (PR) and the TRMM Microwave Imager (TMI) (Kumerow *et al*., 1998) The TMI is based on the SSM/I and is a nine channel passive microwave radiometer; The PR provides 3-D rainfall structure, obtains quantities measurements over the earth and improves TRMM retrieval accuracy; the VIRS is a five-channel imaging spectroradiometer and operates from 0.6 μm to 1.2 μm (Kumerrow *et al*., 1998). There are four algorithms associated with TRMM rainfall measurement (Kummerow

et al., 1998). The full algorithm descriptions can be found at NASA's Precipitation Processing System website. The four algorithms are briefly described below:

i. Radar Algorithms

TRMM uses a single frequency radar which operates at the Ku-Band which is sensitive to moderate rainfall rates. The TRMM radar is able to obtain rain drop particle size distribution where either the number of drops within specified ranges or the median drop size is measured.

ii. Radiometer Algorithms

TRMM uses nine passive frequencies. The frequencies range from 10 GHz to 183 GHz. Low frequencies respond to liquid rain drops in the cloud and the high frequencies respond to snow in the cloud. In areas of clean air, brightness temperatures are linked to surface emission, where-as light rainfall events may contaminate surface emission. Bayesian Datasets are used to reduce assumptions from passive measurements. Models and calculations of brightness temperatures are used to generate multi-frequency brightness temperatures that are linked to precipitation profiles.

iii. Combined Radar and Radiometer Algorithms

Information on the micro and macro-physical characteristics of precipitating clouds are obtained by the combination which is used to reduce uncertainty within radiometer and radar retrieval algorithms. The combination of these retrievals produce particle size distribution, brightness temperatures and a hydrometeor profile. The attenuation obtained by the radar measurements are constrained by the radiometer signal.

iv. Multi-Satellite Algorithms

Multi-satellite algorithms include rainfall measurements from the international constellation of satellites to obtain a high resolution product. Microwave and radiometer/radar measurements are generally of high quality whereas measurements by thermal infrared as of lower quality, but are make more frequent measurements (temporal) due to their low orbit. The combined radar and radiometer algorithm is chosen as a standard, thereafter the other rainfall datasets are calibrated to that standard where

high quality data is primarily used. Monthly gauged data is used to remove bias that may occur in the satellite data.

Daily estimates are produced by computing an average of the three hour estimates throughout the day (Prakash and Gairola, 2014). The products are available at a post-real time and a near-real time basis. Information for the TRMM 3B42 daily product is presented in Table 2.4.

Table 2.4 Information regarding the daily TRMM 3B42 product.

Attribute	**Information**
Temporal Resolution	Daily
Spatial Resolution	0.25˚x0.25˚
File formats	NetCDF, HDF, Binary
Source	http://mirador.gsfc.nasa.gov/
Availability	January 1998- present

2.2.4 Global Precipitation Mission (GPM)

Following the discontinuation of TRMM in 2015, the Global Precipitation Mission (GPM) was launched in February 2014 by NASA and JAXA. The GPM is a constellation based mission which provides a new scope of snow and rainfall measurement to better understand the Earth's precipitating cycles (Hou *et al.,* 2014). GPM provides near real-time data with a higher accuracy than TRMM and a temporal resolution of three hours (Hou *et al*., 2014). TRMM validation activities and algorithms focuses more on medium to heavy rainfall events over tropical oceans whereas, GPM observes light rainfall events as well as cold season snow fall (Hou *et al.*, 2014). GPM obtains retrievals from microwave radiometers in conjunction with brightness temperatures and a common hydrometeor database which incorporates radar measurements (Hou *et al.,* 2014). GPM has a much larger global coverage compared to TRMM which allows for enhanced measurement over land, different climate regimes and over the high and middle latitudes (Hou *et al*., 2014). Information for the GPM rainfall product is presented in Table 2.5.

Table 2.5 Information regarding the GPM product.

Attribute	**Information**
Temporal Resolution	Three hour, daily
Spatial Resolution	0.1˚x0.1˚
File formats	NetCDF4, HDF5
Source	https://gpm1.gesdisc.eosdis.nasa.gov/data
Availability	March 2014- present

The algorithm basis is similar to that of TRMM. However, there a few key differences. In the radar algorithm, GPM operates with two frequencies, the Ku-Band and the Ka-Band (Hou *et al*., 2014). The Ka-Band is more sensitive to falling snow and lighter rainfall events, therefore drop size as well as drop distribution can be obtained (Hou *et al*., 2014). The radiometer algorithm operates through thirteen passive frequencies as opposed to nine in TRMM (Hou *et al*., 2014).

2.2.5 CPC's Merged Analysis of Precipitation (CMAP)

The CPC's Merged Analysis of Precipitation is a product that produces images of 2.5˚ spatial resolution and consists of monthly and pentad aggregations (temporal scale) (Dinku *et al*., 2007). The algorithm used is based on a merging technique, described by Xie and Arkin (1996). The merging technique utilises inputs from precipitation indices derived from infrared estimates from the Geostationary Operational Environmental Satellite (GOES), passive microwave retrievals and gauge data (Dinku *et al*., 2007). Dinku *et al*. (2007) report that estimates produced using two steps. The first step is the merging of infrared data and passive microwave data in a maximum likelihood approach and then bias is removed with the use of surface gauge data through a blending technique. The merged products are then produced by determining the structure of rainfall which formulates the Poisson equation. Datasets for the pentad and monthly products are available from 1979. Information for the CMAP product is presented in Table 2.6.

Table 2.6 Information regarding the CMAP product.

Attribute	**Information**
Temporal resolution	Monthly aggregations, Pentad
Spatial resolution	2.5˚x 2.5˚
File format	NetCDF
Source	http://www.esrl.noaa.gov/psd/
Availability	1979- present

2.2.6 The Climate Prediction Centre Morphing Technique (CMORPH)

The Climate Prediction Centre Morphing Technique (CMORPH) is a relatively new product that merges different passive microwave data with infrared data (Dinku *et al*., 2007). The product incorporates estimates from AMSU-B, AMSR-E, TMI (from the TRMM satellite) and the SSM/I (Joyce *et al*., 2004). The CMORPH technique is not a rainfall estimation algorithm, but a means by which different rainfall algorithms can be combined (Joyce *et al*.,

2004). The technique uses rainfall estimates from passive microwave data and then propagates the features in space with the use of motion vectors which are derived from 30 minute infrared data obtained from geostationary satellites (Joyce *et al*., 2004). The product determines feature motions from infrared data which determines the displacement vector used for "morphing" the time intervals between microwave observations (Joyce *et al*., 2004; Dinku *et al*., 2007). Dinku *et al*. (2007) reports that that the product combines the accuracy of passive microwave retrievals with the high temporal resolution of the infrared data. Thus, the product is classified as passive-microwave with the indirect use of infrared data, where infrared data are used when microwave data are not available (Dinku *et al*., 2007, Joyce *et al*., 2004). The product is flexible in that it can incorporate many different rainfall algorithms to obtain a rainfall estimate (Joyce *et al*., 2004). The product is available from 2002 at a high spatial and temporal resolution of 8 km and 30 minutes respectively. The product offers bias corrected data as well as "raw" uncorrected data (Joyce *et al*., 2004). Information for the CMORPH product is presented in Table 2.7.

Table 2.7 Information regarding the CMORPH product.

Attribute	**Information**
Temporal Resolution	30 min, 3 hourly, Daily
Spatial Resolution	0.25˚x0.25˚, 0.08˚ x 0.08˚
File formats	Binary
Source	http://ftp.cpc.ncep.noaa.gov/gov/precip/CMORPH_V1.0/RAW/0.25deg-DLY_00Z
Availability	December 2002-December 2015

2.2.7 Precipitation Estimation from Remotely Sensed Information using Artificial Neural Networks (PERSIANN)

The Precipitation Estimation from Remotely Sensed Information using Artificial Neural Networks (PERSIANN) for the estimation of rainfall is consistently enhanced by the University of Arizona. The artificial neural algorithm uses longwave infrared imagery to obtain cloud texture to produce rainfall rates (Sorooshian *et al*., 2000). Low orbiting passive microwave estimates provide model parameters which are constantly updated (Hsu and Sorooshian, 2009). The fundamental algorithm that drives the product is flexible in that it allows for incorporation of various forms of data as they become available (Sorooshian *et al*., 2000). The algorithm has been constantly developing since 2000 which has been producing near real-time estimates which have been utilised in global rainfall research (Hsu and Sorooshian, 2009). Information for the PERSIANN product is presented in Table 2.8.

Table 2.8 Information regarding the PERSIANN product.

Attribute	Information
Temporal Resolution	1 hour, 3 hour, 6 hour, daily, monthly, yearly
Spatial Resolution	0.25˚x0.25˚
File formats	Binary
Source	http://chrs.web.uci.edu/persiann/data.html
Availability	March 2000-present

2.2.8 Tropical Applications of Meteorology Using Satellite Data and Ground-Based Observations (TAMSAT)

The TAMSAT technique obtains a rainfall estimate by combining geostationary Meteosat data with gauge data through a calibration process focused on drought monitoring (Tarnavsky *et al*., 2014; Maidment *et al*., 2017). Up till 2009, TAMSAT only operated in the north and south-eastern areas of Africa (Tarnavsky *et al*., 2014). In that time, only rainy seasons were considered, May-October for the Northern Hemisphere and November-April for the Southern Hemisphere and rain gauged input data used in the calibration varied based on quality and availability of the measurement on the day (Tarnavsky *et al*., 2014). The current product utilises specific rain gauge measurements within the calibration (Tarnavsky *et al*., 2014). The rainfall algorithm is based on Meteosat TIR imagery obtained every 15 minutes, from July 2006 to present, and every 30 minutes prior (Maidment *et al*., 2017). The algorithm uses cold cloud duration (CCD) to obtain rainfall estimates (Maidment *et al*., 2017). The product has been updated to include the whole of Africa, including Madagascar, and the time period of available observations extends from January 1983 to present (Maidment *et al*., 2017; Tarnavsky *et al*., 2014). In January 2017, the TAMSAT Group released version 3 (TAMSAT-3) which is operating alongside version 2 (TAMSAT-2) due to current users still using TAMSAT-2 (Maidment *et al*., 2017). TAMSAT operates at a 0.0375˚ x 0.0375˚ spatial resolution and at pentad, decadal and daily temporal resolutions. Some of the limitations of TAMSAT include the product's inability to detect rain producing clouds where warm rain mechanisms are dominant (eg. mountainous regions and coastal areas) (Maidment *et al*., 2017). The TAMSAT-2 version, and prior versions, focused on frequent, low rainfall amounts to better monitor droughts which often produces a dry bias (underestimation), especially when the data is disaggregated to a daily resolution (Maidment *et al*., 2017). Information for the TAMSAT-3 product is presented in Table 2.9.

Table 2.9 Information regarding the TAMSAT-3 product.

Attribute	Information
Temporal Resolution	Daily, Dekadal, monthly, pentad, seasonal
Spatial Resolution	0.0375˚x0.0375˚
File formats	NetCDF3
Source	https://www.tamsat.org.uk/data/rfe
Availability	1983-present

2.3 Remotely Sensed Rainfall in Hydrological Modelling

Over the last decade there have been significant efforts to integrate satellite derived data into modelling (Xu *et al*., 2014). Some of the parameters included in models are rainfall, soil moisture, total evaporation and leaf area indices (Xu *et al,* 2014). The value satellite derived estimates can provide include parameter estimation and data assimilation for use as input in hydrological models (Xu *et al*., 2014).

Vergara *et al*. (2014) report that there is significant uncertainty from sampling errors with products of low temporal and spatial resolutions and that even though the uncertainties may be quantified, the data may not be viable for use in certain hydrological modelling applications due to their coarse resolutions. The uncertainties involved in the processes of satellite derived estimation and the lack of knowledge of incorporating the satellite derived rainfall into hydrological models has led to a reluctant use of the data. Most studies highlight the effect of catchment size and product resolution on the error of rainfall propagation in hydrological model simulations (Seyyedi *et al*., 2014). Most of these studies have concluded that downscaling of rainfall products may significantly enhance runoff simulations.

The importance of high resolution data has promoted the development of many rainfall disaggregation or downscaling techniques. Immerzeel *et al*. (2009) downscaled the TRMM3B43 product using an exponential relationship between the product and the Normalized Difference Vegetation Index (NDVI) from 25 km to 1 km. Jia *et al*. (2011) downscaled TRMM 3B43 from 25 km to 1 km based on a statistical scheme on the relationship of terrain elevation, NDVI and rainfall. Haas and Born (2011) have developed a two-step approach to downscale satellite data with ground-based data over Morocco's heterogeneous terrain. Most downscaled approaches for reanalysis datasets have focused on obtaining consistent statistics between the runoff produced and the downscaled datasets (Seyyedi *et al*., 2014). Most studies within the remotely sensed rainfall field focus on

validation of the products or quantifying errors within the data. Relatively few studies in southern Africa have been conducted where models were driven by satellite derived rainfall.

2.4 Case Studies

Several studies have investigated satellite derived rainfall and its incorporation in a wide variety of applications (i.e. drought monitoring, forecasting and hydrological modelling). Many studies evaluated product accuracy using individual gauge measurements (e.g. Hirpa *et al*., 2010; Bumke *et al*., 2016; Alijanian *et al*., 2017). Some evaluated products using gauge-adjusted radar (e.g. Islam *et al*., 2012). Many studies evaluated products in terms of hydrological modelling where streamflows simulated are compared to observed flows (e.g. Collischonn *et al*., 2008; Falck *et al*., 2015). However, only a few are briefly described below.

Thorne *et al*. (2001) compared the two algorithms of TAMSAT (northern and southern) and estimates from the CPC against rain gauge measurement over southern Africa. The study validated the products against data from 800 gauges in southern Africa using a kriging approach. It was found that the TAMSAT products estimated rainfall better over the plateau region where rain gauge measurement was poor and only the Cold Cloud Duration (CCD) was used. The CPC estimates performed better over mountainous regions. The CPC estimates performance was found to be satisfactory. The study found that product estimations were generally of better accuracy where rain gauges were present and used in the calibration.

Grimes and Diop (2003) investigated the feasibility of driving a simple rainfall-runoff with daily satellite derived rainfall obtained from Meteosat infrared data. The study also included numerical weather prediction (NWP) analysis models to investigate if the rainfall estimates could be enhanced. The study took place in Mali, West Africa, specifically in the Bakoye catchment, and focused on the wet seasonal months for three years. The validation study showed that the NWP enhanced rainfall estimates. The study found that when the NWP models were used, river flows were enhanced when compared to observed measurements. However, in the absence rain gauge estimates for calibration of the rainfall data, the performance of the model was reduced, where the NWP model performed better than the uncorrected satellite derived rainfall data.

Dinku *et al*. (2007) validated 10 different rainfall products over complex topography in East Africa (Ethiopia) against a station network. The study site ranged from sea level to an

elevation of 4620 m. The ten products included Global Precipitation Climatology Project (GPCP-MS, GPCP-SG), CMAP, TRMM 3B43, TRMM 3B42, NOAA-CPC African rainfall estimation algorithm, GPCP one-degree-daily (1DD), CMORPH and TAMSAT. The study found that CMAP, TRMM 3B42, TRMM 3B43, CMORPH and TAMSAT performed reasonably well.

Hughes (2006) investigated the potential of using satellite derived rainfall through validation against gauge data. The study used PERSIANN and the GCPC 1DD dataset over the Kafue River, Zambia; Okavango River Basin, Botswana, Namibia and Angola; Thukela River Basin, South Africa; and the Kat River Basin, South Africa. The study found that short satellite derived rainfall records are a hindrance to modelling. It was found that the satellite data also ignore the influences of topography on precipitation. The type of model being used to incorporate satellite rainfall is important. Model uncertainty and data quality are considerable in these studies. Satellite data should be further processed (e.g. bias corrected) to obtain better results.

Collischonn *et al*. (2008) incorporated TRMM 3B42 rainfall estimates into a large-scale hydrological model. The study was conducted in the Tapajo´s river basin, located in the Amazon River Basin. Three hourly TRMM 3B42 data was aggregated to obtain a daily dataset and was validated against gauges. It was found that the satellite derived data performed reasonably well when compared to gauge data mimicking the rainfall regime of the area reasonably well. It was found that the data differed at a point scale when compared to gauge data, but data were similar when compared at an area scale. Hydrographs generated by the model with TRMM 3B42 as a driver are comparable with the results of the model driven by gauge data.

Sawunyama and Hughes (2008) used the Climate Prediction Center African daily precipitation climatology (CPCAPC) product to drive the Pitman model in selected quaternary catchments in South Africa. A non-linear technique to correct the satellite rainfall was applied using historical gauge data. The correction showed to improve simulations compared to the use of raw data. The study highlights that there are still spatial and temporal problems associated with transferring information from different scales. However, the authors report that there is potential for satellite derived rainfall use in models in the future.

Clark (2015) validated and drove the ACRU hydrological model with CMORPH, FEWS RFE 2, FEWSARC 2 and TRMM 3B42 in the uMngeni and Sabie-Sand catchments located in South Africa. Satellite rainfall products performed differently in different locations. The products proved favourable with rain gauge measurements in the uMngeni catchment and less favourably in the Sabie-Sand catchment. The coarse resolution and bias in the satellite derived rainfall estimates proved a problem in accurately estimating rainfall when compared to the rain gauge measurements. Streamflow results were variable among locations and no clear trends were apparent among product driven simulations. Model input uncertainty was also found to affect the accuracy of results.

Alazzy *et al*. (2017) evaluated the PERSIANN-CDR, CMORPH (corrected), TRMM 3B42RT and TRMM 3B42 rainfall products and incorporated the products into the HEC-HMS model. The study took place in the Ganzi River Basin, Tibetan Plateau. Results showed that CMORPH and TRMM 3B42 performed better than the other products at a seasonal and annual scale. Results showed that TRMM 3B42 and CMORPH underestimated rainfall of medium and high intensities, while PERSIANN and TRMM 3B42RT overestimated at these intensities. Simulation results showed that the TRMM 3B42 performed significantly better than the other products and performed better than the model driven by gauge estimates. The study concludes that TRMM 3B42 is a viable source of data for the Tibetan Plateau area.

Rauniyar *et al*. (2017) investigated the seasonal and regional rainfall rate retrieval uncertainties using nine satellite rainfall products. These products included TRMM 3B42RT, TRMM 3B42V7, CMORPH (raw data), CMORPH (corrected), GSMaP-MVK, GSMaP-Gauge, PERSIANN, PERSIANN-CDR and CHIRPS. The products were evaluated at sub-daily, daily, monthly, seasonally and intra-seasonally. The study was conducted in a maritime climate over Sarawak, Malaysia. It was found that there were considerable differences between products and no product outperformed the others across all temporal resolutions.

Najmaddin *et al*. (2017) evaluated the TRMM TMPA 3B42 and TRMM 3B42RT in the Lesser Zab, northeast Iraq and incorporated the rainfall estimates into the Leicester Model for Semi-Arid Regions (LEMSAR). The data was bias-corrected using rain gauge data. Validation of the satellite data showed a slight underestimation, even though bias corrected. Model simulations of streamflow showed that the corrected TRMM 3B42RT data and was

poor using uncorrected data. The study concluded that corrected TRMM data is a viable data source for rainfall-runoff modelling and results are enhanced when data is corrected.

Beck *et al*. (2017) evaluated 23 satellite derived rainfall products at a global scale using gauge data and hydrological modelling. Thirteen non-gauge corrected satellite rainfall products were evaluated using 76 086 globally located gauge measurements. Ten gauge corrected satellite rainfall products were evaluated using the conceptual HBV model (Bergström, 1992; Seibert and Vis, 2012) with obtaining streamflow records of 9053 catchments that are < 50000 km^2. Non-gauge corrected products included CHIRP version 2, CMORPH, ERA-Interim, GSMaP version 5/6, GridSat, JRA-55, MSWEP-ng version 1.2, MSWEP-ng version 2, NCEP-CFSR, PERSIANN, PERSIANN-CCS, SM2RAIN-ASCAT and TRMM TMPA 3B42RT. Gauge corrected products included CHIRPS version 2, CMORPH-CRT, CPC-Unifed, GPCP-1DD version 1.2, MSWEP version 1.2, MSWEP version 2.0, PERSIANN-CDR, V1R1, PGF, TMPA 3B42 V7 and WFDEI-CRU. The study found considerable differences between the spatio-temporal accuracy of the products. The study found that the MSWEP-ng version 1.2 and version 2 generally performed the best when compared to gauge measurements. The study found that products that directly incorporated gauge measurements generally performed better, i.e CPC Unified and MSWEP V1.2 and V2.0. However, the study found that the gauge-corrected products may not achieve accurate results in ungauged catchments.

2.5 Summary of Key Findings

There are many satellite derived products that are available for use with their own defining spatial and temporal resolutions. Even though products may share sensor information, the algorithms used to achieve rainfall estimates, vary significantly. From the literature, it is shown that satellite derived products perform uniquely in different locations on earth, thus product selection for the specific application is important. Many studies focus on the validation of satellite derived rainfall estimates against gauge measurements to quantify uncertainties associated with satellite derived rainfall measurement. The majority of rainfall product validation does not occur within Africa and specifically southern Africa. Validations of satellite derived estimates using hydrological models show promise, however, the most appropriate model for the application is an important decision. Meaning, model uncertainty may introduce further uncertainty in output results. Model uncertainty is generally a difficult task to quantify, where uncertainty of model inputs need to be reduced in-order to obtain

representative results of the satellite derived rainfall performance. Only a minority of literature focuses on the use of satellite derived rainfall incorporation into hydrological models in Africa, and more specifically, South Africa. Furthermore, the use of satellite derived rainfall estimates in the ACRU hydrological model has not been extensively studied and the only incorporation of satellite derived rainfall into the ACRU hydrological model is presented by Clark (2015).

* * * * * * * *

The satellite derived products chosen to be utilised in this study were based on free of charge, daily temporal resolution, fine spatial resolution, latest product versions available, coverage over South Africa and the latency of data release to the public. The products chosen to be assessed include TRMM 3B42 V7, GPM (IMERGV4), FEWS RFE2, FEWS ARC2 and TAMSATV3. The FEWS and TAMSAT products were chosen as they provide specific coverage over Africa at fine spatial resolutions. The TRMM 3B42 product being one of the most commonly used satellite derived products is compared to its successor GPM as well as the FEWS and TAMSAT products.

This research study forms part of the WRC K5/2512 project (Clark, 2017a/b) which is a follow on from the WRC K5/2205 project (Clark, 2015). The ACRU model is chosen to simulate streamflow based on the recommendation of the WRC K5/2205 project (Clark, 2015) where the ACRU model was successfully driven by satellite derived rainfall. The term driven is referred to using rainfall as input to drive the model to simulate streamflow. The ACRU hydrological model is suggested as it is a daily time step, physical-conceptual model that is sensitive to land use (Warburton *et al*., 2010).

The literature review and the recommendations of the WRC K5/2205 project (Clark, 2015) informed the methodology of this research study.

3. METHODOLOGY

The Water Research Commission (WRC) project K5/2205 (Clark, 2015) was undertaken from 2013 to 2015. The WRC K5/2512 project, of which this research is a part of, is a follow on from the WRC K5/2205 project. Some of the WRC K5/2205 project specific objectives included a review of methodologies and data sources for quantifying water use; to integrate the different data sources into a single framework or water account; to apply the water account to assess sectoral water use in study areas of South Africa; and to quantify errors and uncertainties associated with poor or missing data. Some of the key decisions made in the WRC K5/2205 project were that the ACRU model should be used and that the use of remotely sensed data as inputs to the model should be investigated; and to concentrate efforts on variables that are likely to be sensitive, one of which being rainfall. The WRC K5/2205 project recommended the investigation of remotely sensed rainfall at a scale relevant to modelling and to use the ACRU hydrological model to simulate streamflow. Another recommendation was to investigate and apply satellite derived rainfall in a winter rainfall region, as the study areas of the WRC K5/2205 project were only situated in summer rainfall regions.

The methodology applied in this study was designed to answer the research questions posed in Chapter 1, which were:

i. How do the in-situ based (rain gauge) rainfall compare to the satellite derived estimates?
ii. How will simulated streamflow generated by the ACRU model driven by satellite derived rainfall and rain gauge measurements compare to observed streamflow?
iii. Does satellite derived rainfall enhance hydrological modelling due to the better spatial and temporal scale that it provides?

3.1 Study Sites

Three study sites were selected for this study. The upper uMngeni and upper uThukela catchments are located in a summer rainfall region and the upper and central Breede catchment is located in a winter rainfall region. Figure 3.1 displays the locations of the study sites in South Africa, with specific details of the catchments presented in the sections below.

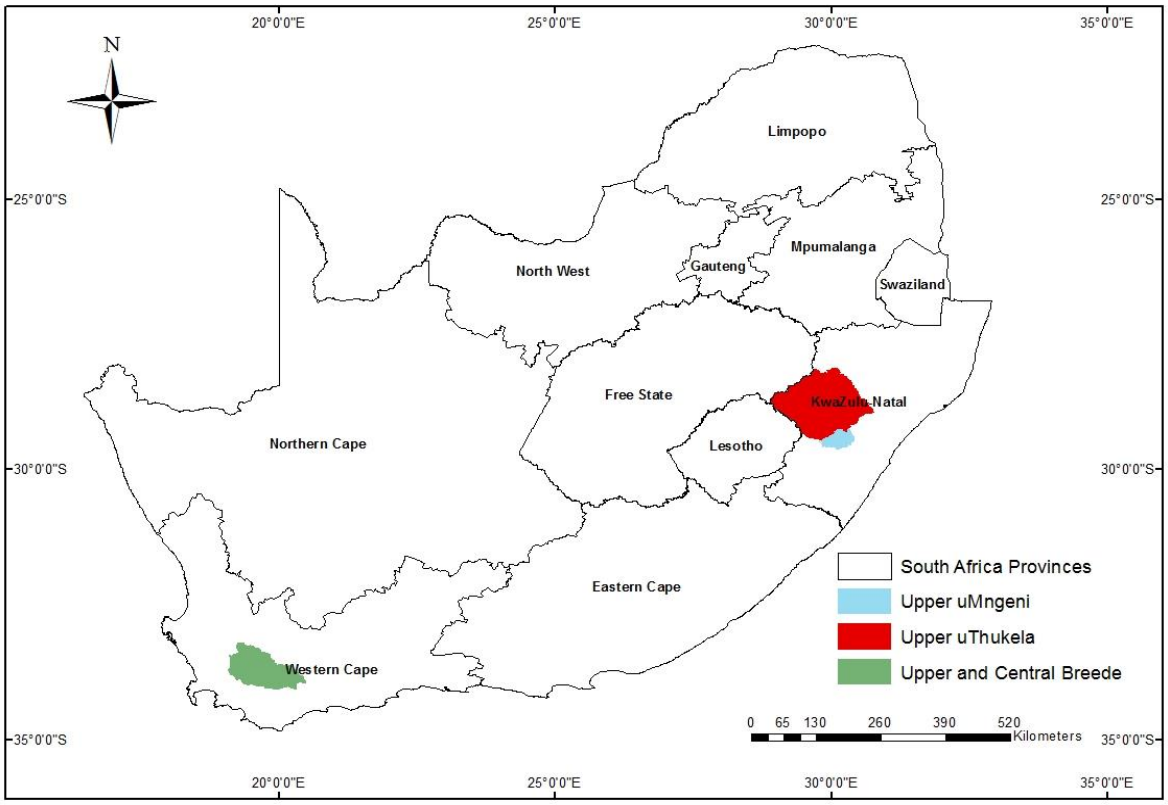

Figure 3.1 Location of study sites in South Africa

3.2 Upper uMngeni Catchment

The uMngeni catchment situated in KwaZulu-Natal, South Africa experiences a sub-humid climate and spans over an area of 4455 km^2 (Warburton *et al*., 2010; Warburton *et al*., 2011; Warburton *et al*., 2012). Dominant land uses in the catchment consist of urbanised areas, commercial sugarcane and commercial forestry (Warburton *et al*., 2012). Rural areas consist of commercial and subsistence agriculture, extensive irrigated agriculture, sugarcane and commercial forestry (DWAF, 2004) (Figure 3.5). The altitude (Figure 3.3) ranges from 1913 m in the western parts of the catchment to sea level at the catchment outlet located at the Indian Ocean (Warburton *et al*., 2010). The mean annual precipitation (Figure 3.4) varies from 700 mm per annum in the middle reaches to 1550 mm per annum in the west reaches of

the catchment (Warburton *et al*., 2010). Mean annual temperatures range from 20 ˚C at the ocean to 12 ˚C in the escarpment areas and the catchment experiences a range of 1567 mm to 1737 mm of mean annual potential evaporation (Warburton *et al*., 2010). Four large dams are located in the uMngeni catchment regulating the Mgeni River, namely, Midmar Dam, Albert Falls Dam, Nagle Dam and Inanda Dam with approximately 300 small farm dams (Warburton *et al*., 2010; Warburton *et al*., 2012). Transfers occur from the Mooi River in the uThukela catchment.

In this study, the sub-Quaternary catchment boundaries used by Warburton (2011) and Umgeni Water (the bulk water supplier of the uMngeni catchment) were used. The uMngeni catchment consists of the U20 Tertiary Catchment. For this study only the upper uMngeni sub-Quaternary catchments are used. The uMngeni catchment and sub-catchment delineation are presented in Figure 3.2.

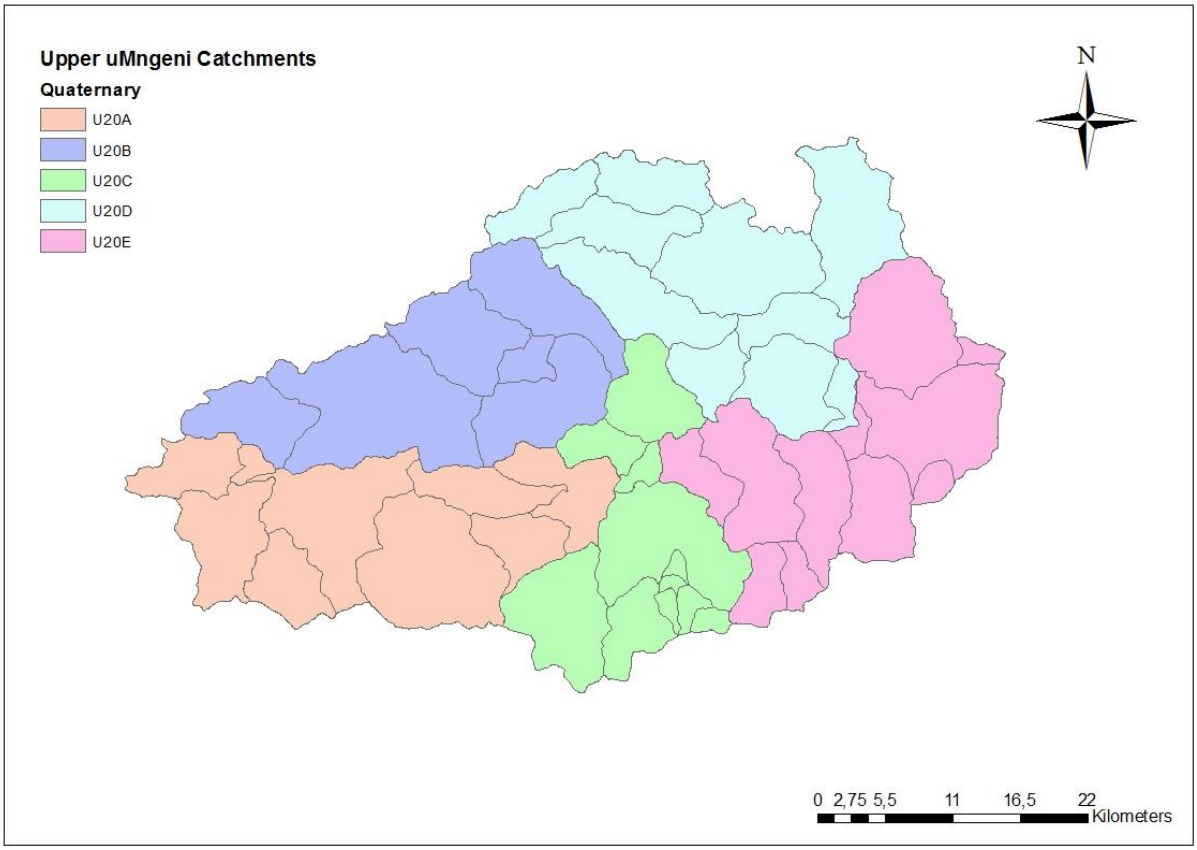

Figure 3.2 Quaternary and sub-quaternary catchments in the upper uMngeni Catchment

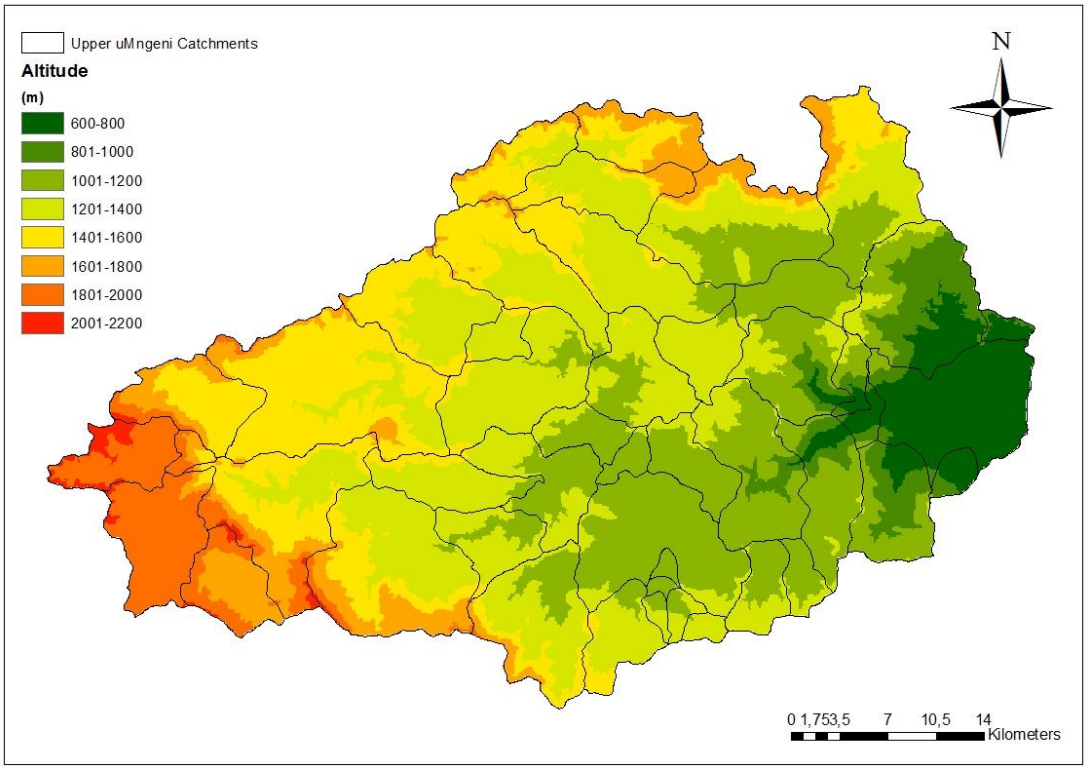

Figure 3.3 Altitude of the upper uMngeni (Weepener *et al*., 2011b)

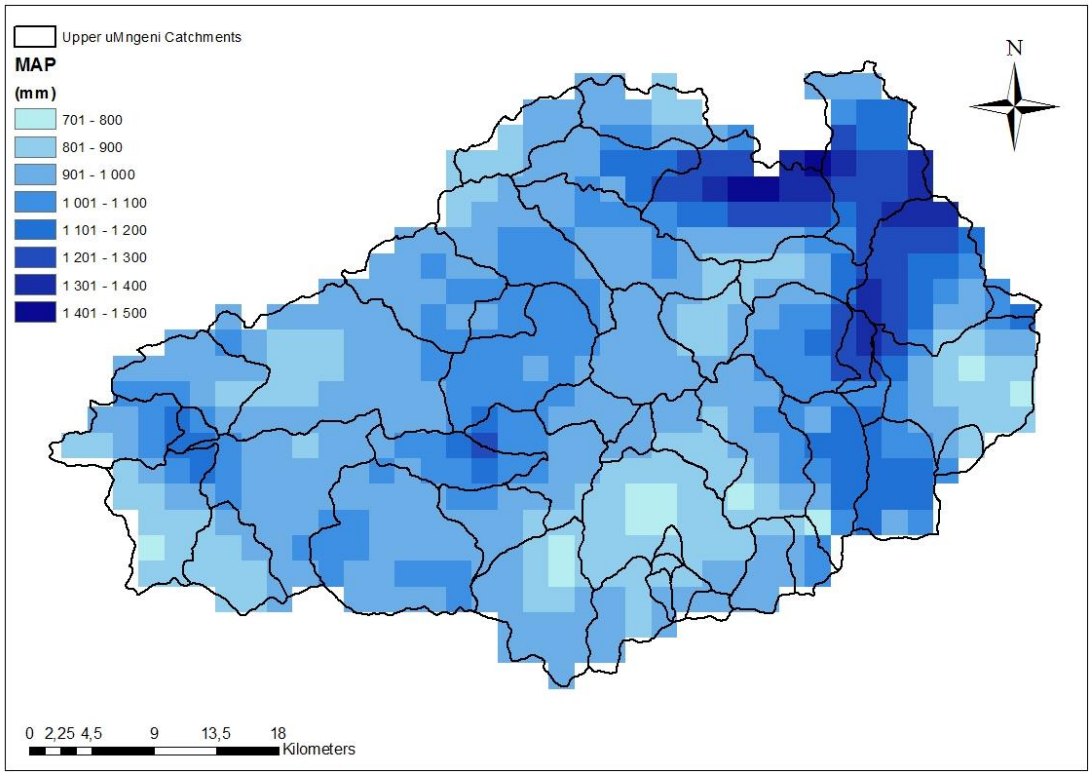

Figure 3.4 Mean Annual Precipitation of the upper uMngeni (Lynch, 2004)

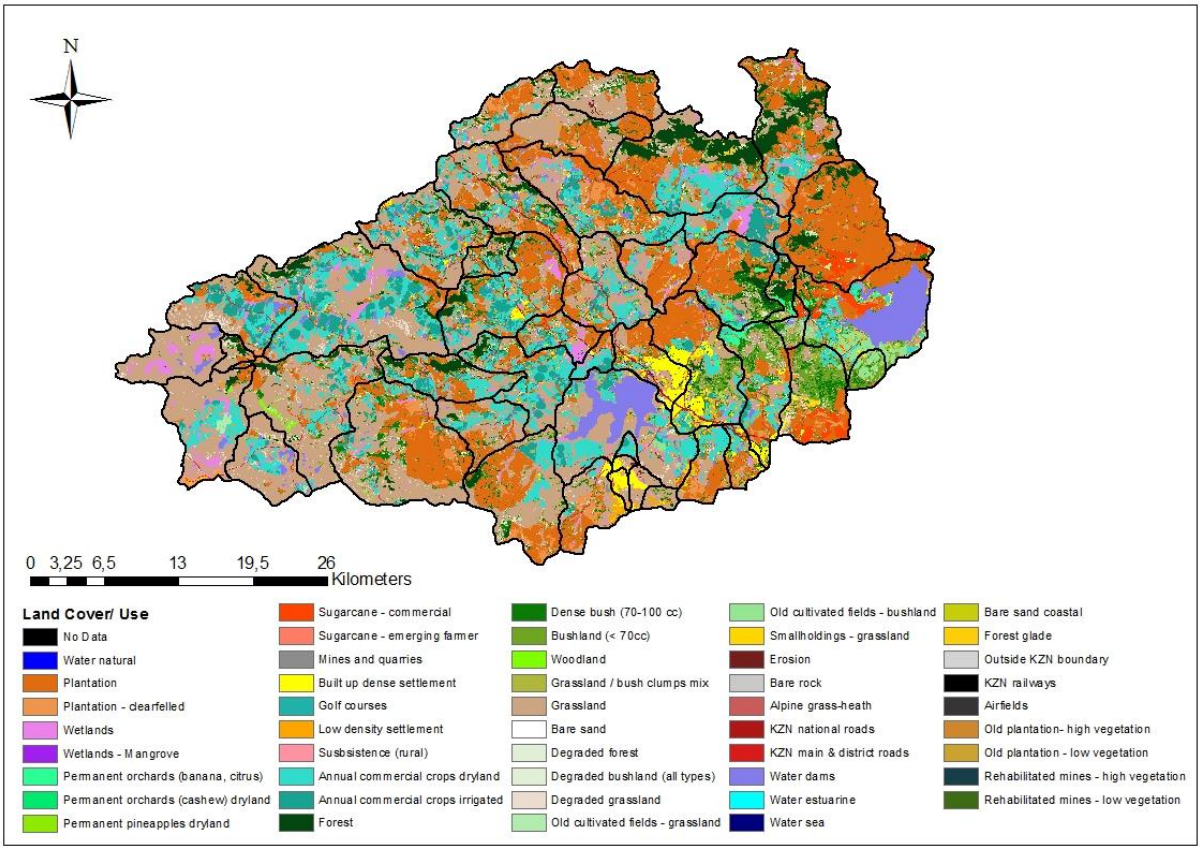

Figure 3.5 Land use/cover for the upper uMngeni (Ezemvelo KZN Wildlife and GeoTerraImage, 2013)

3.3 Upper uThukela Catchment

The uThukela catchment spans over 16129 km^2, with its source of water in the Drakensberg which drains into the Indian Ocean. Altitude in the catchment (Figure 3.7) range from 3451 m in the west to 474 m in the east. The catchment experiences warm summers with high rainfall and cool dry winters (Andersson *et al*., 2011; Clark, 2017a). The mean annual precipitation (Figure 3.8) ranges from 2000 mm in the west to 500 mm in the central parts of the catchment (Andersson *et al*., 2011). The catchment experiences between 1600 mm to 2000 mm of mean potential evapotranspiration (Andersson *et al*., 2011). The main land uses (Figure 3.9) in the catchment consist of unimproved grassland, forest plantations, agriculture and grazing pastures (DWAF, 2004; Andersson *et al*., 2011). Extensive irrigated agriculture occurs in the western and southern parts of the catchment (Clark, 2017a).

For the purposes of this study secondary catchments V1, 2, 6 and 7 will be investigated. The National Freshwater Ecosystem Priority Areas (NFEPA) Catchments (Nel *et al.*, 2011a) were adjusted to delineate the boundaries of the upper uThukela catchment and sub-catchment in

the K5/2512 project. The sub-catchment delineation from the WRC project K5/2512 by Clark (2017b) will be used in this study (Figure 3.6).

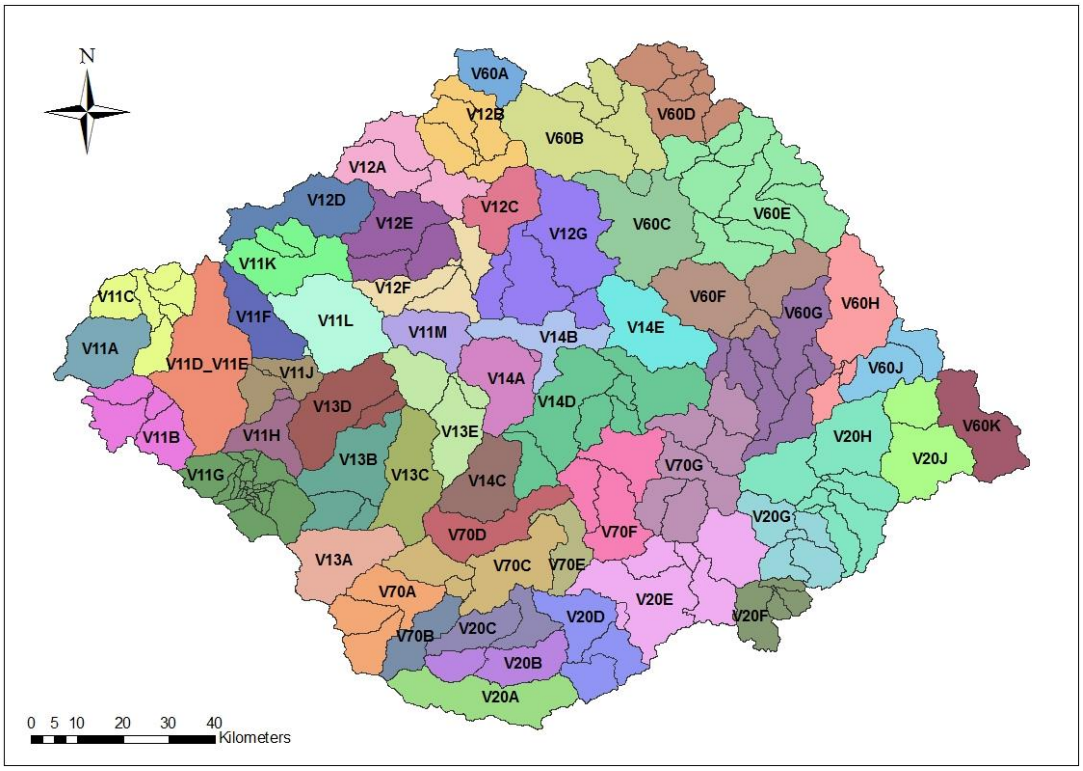

Figure 3.6 Quaternary and sub-quaternary catchments of the upper uThukela

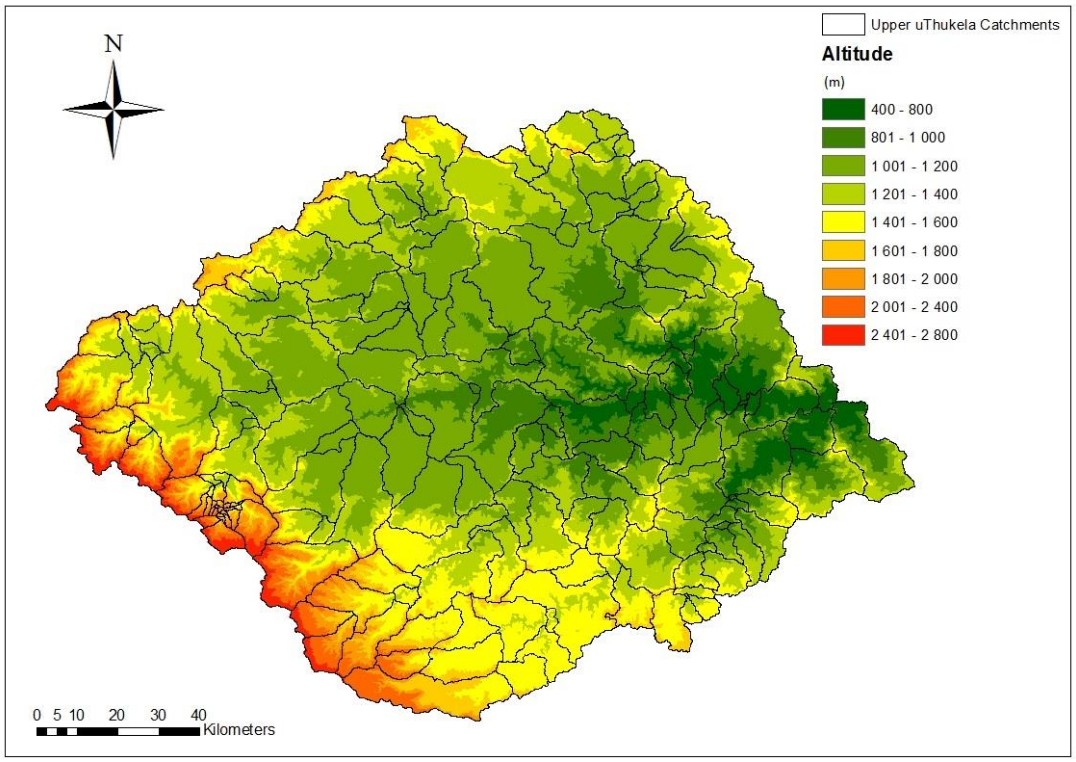

Figure 3.7 Altitude of the upper uThukela (Weepener *et al*., 2011b)

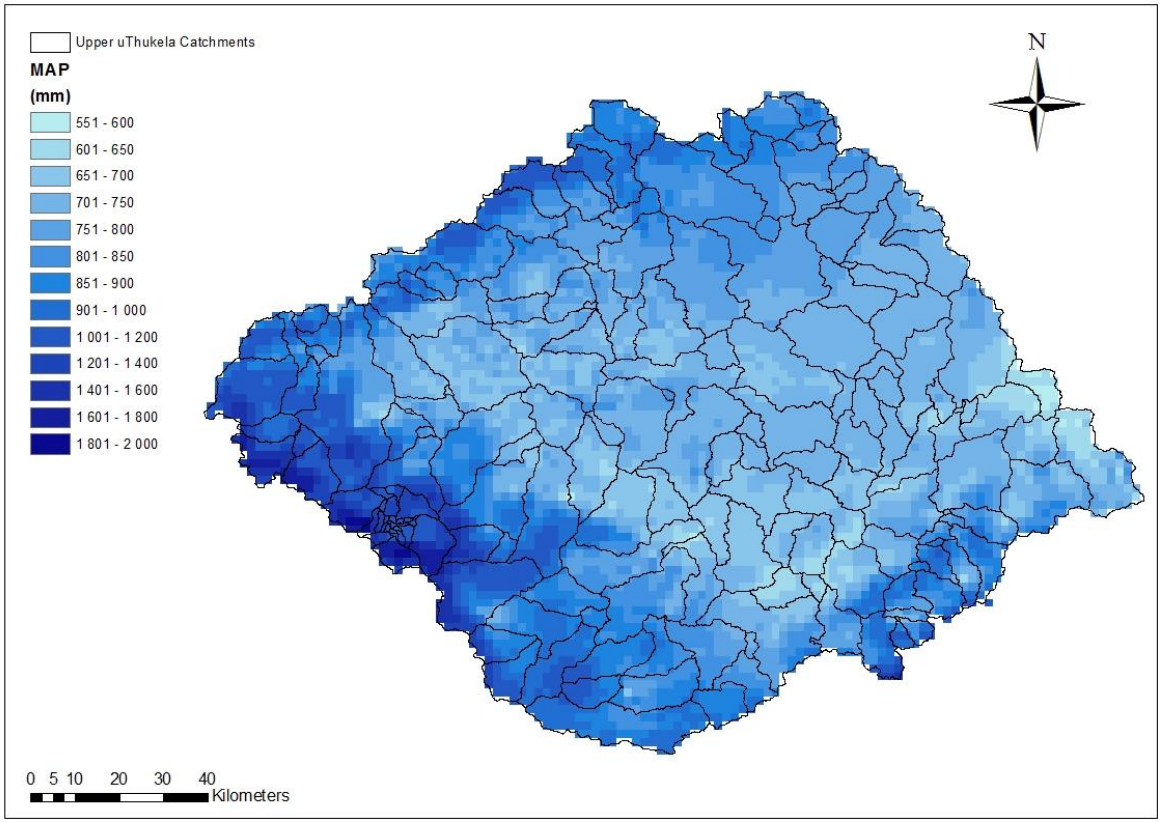

Figure 3.8 Mean Annual Precipitation of the upper uThukela catchment (Lynch, 2004)

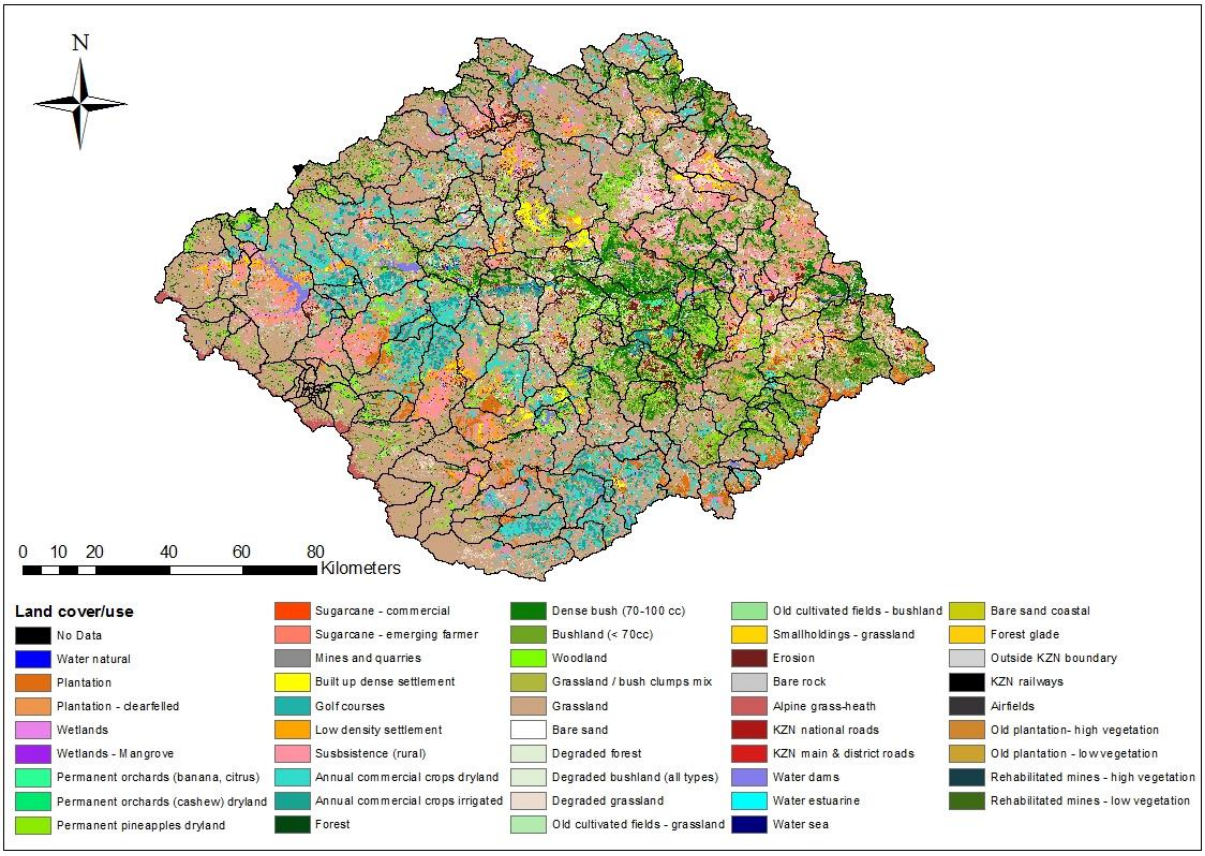

Figure 3.9 Land cover/use of the upper uThukela catchment (Ezemvelo KZN Wildlife and GeoTerraImage, 2013)

3.4 Upper and Central Breede Catchment

The upper and central Breede catchment is located in the Western Cape, South Africa and has an area of 7405 km^2. The catchment falls within the Breede-Gouritz Water Management Area, which is in a winter rainfall region. The Breede catchment is divided into five hydrological sub-areas. These sub-areas are the Upper Breede, Overberg East, Lower Breede Overberg West and Riviersonderend. The main river in the catchment is the Bree River which is sourced in the north-west of the catchment and flows into the Indian Ocean (Clark, 2017b). The upper and central Breede catchment topography varies from east to west (Figure 3.11). Altitude ranges from 2232 m in the northern parts to 79 m in the south-eastern parts of the catchment (Clark, 2017b) (Figure 3.11). The mountainous regions located in the south-west of the catchment experience an MAP of 2000 mm (Figure 3.12). The central and north-eastern areas experience an MAP of 250 mm (Figure 3.12). Agriculture is the dominant land use in the catchment (Figure 3.13). Agriculture in the catchment includes fruit orchards, irrigated vineyards, dryland grain crops and livestock (Clark, 2017b). Groundwater is used for agriculture in many parts of the catchment (Clark, 2017b).

In this study the H1, H2, H3, H4 and H5 Secondary catchments are investigated. The National Freshwater Ecosystem Priority Areas (NFEPA) Catchments (Nel *et al.*, 2011a) were modified to delineate the boundaries of the upper and central Breede catchment and sub-Quaternaries in the K5/2512 project. The delineation from the WRC project K5/2512 by Clark (2017b) will be used in this study (Figure 3.10).

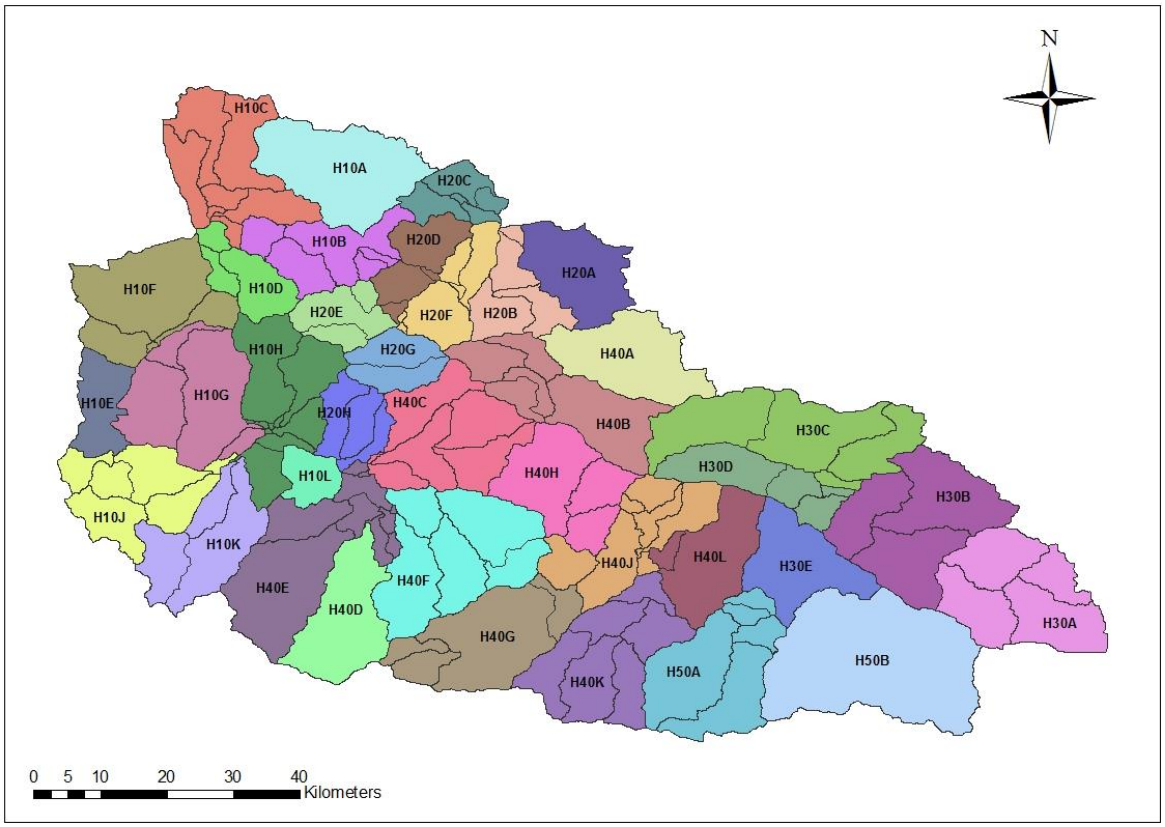

Figure 3.10 Quaternary and sub-quaternary catchments of the upper and central Breede catchment.

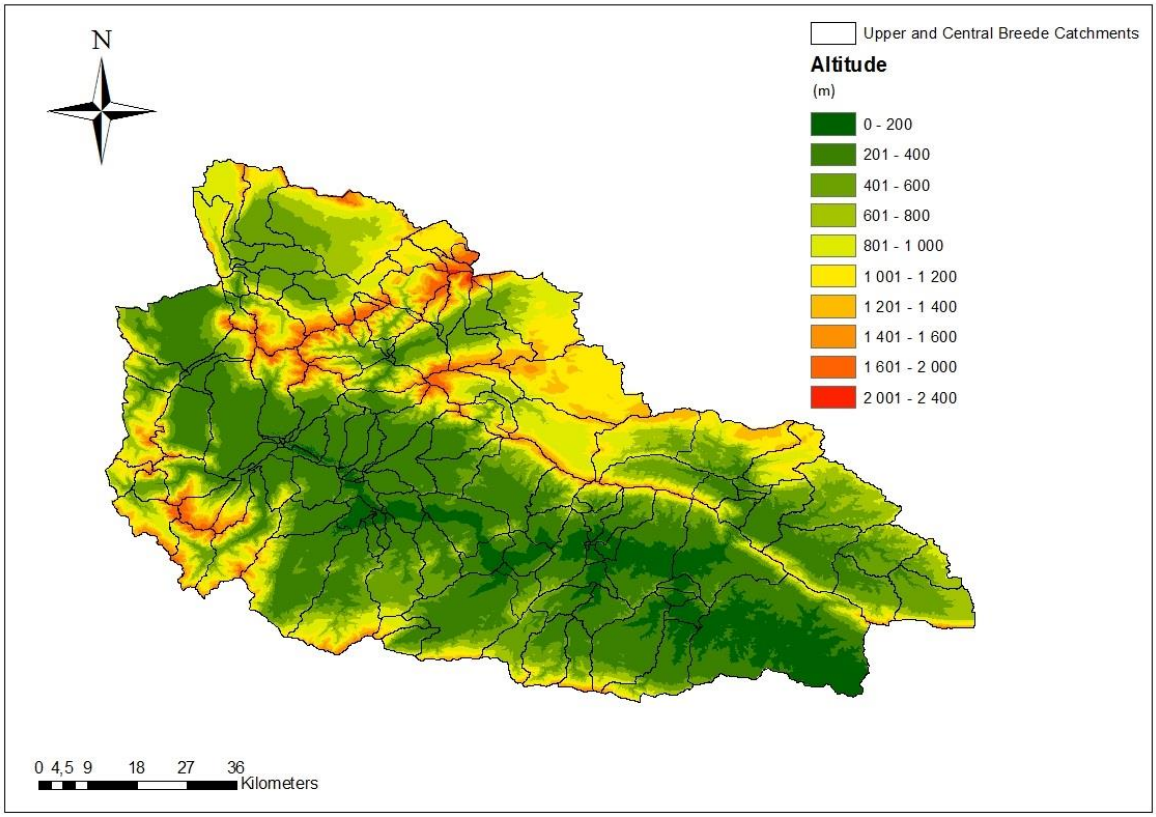

Figure 3.11 Altitude of the upper and central Breede (Weepener *et al*., 2011b)

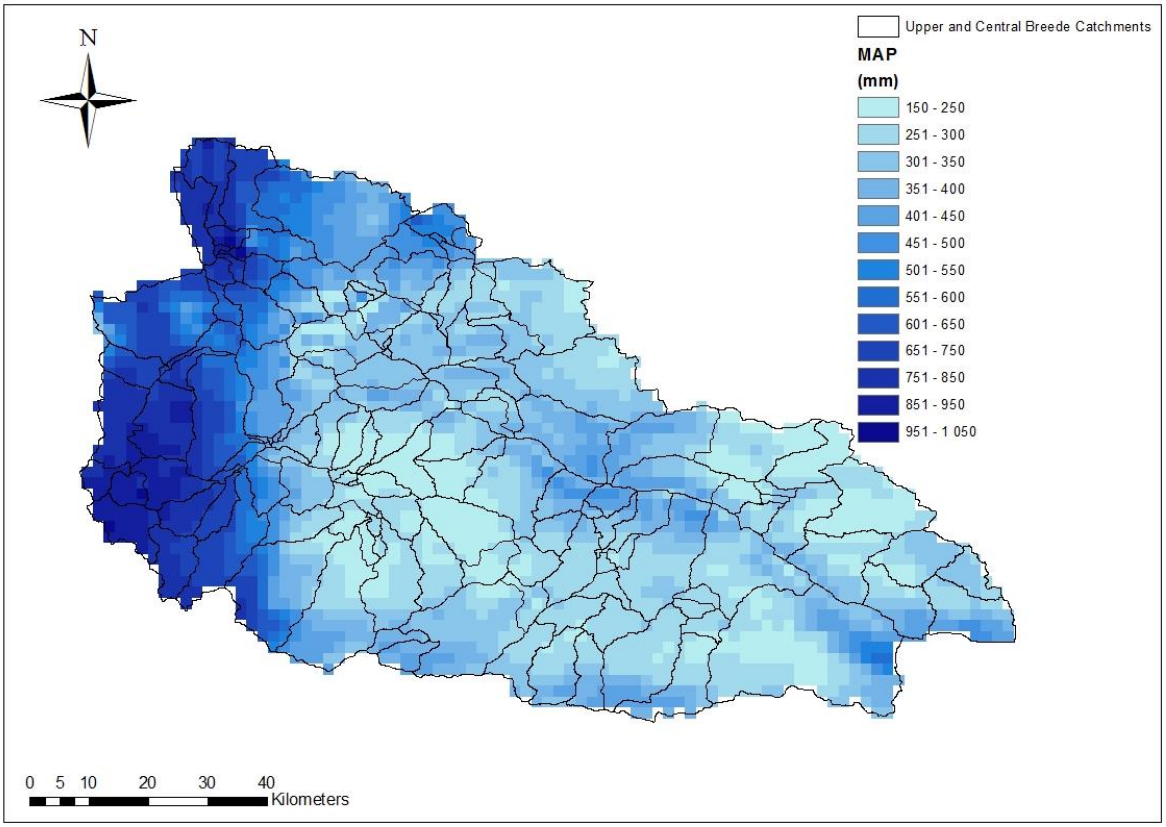

Figure 3.12 Mean Annual Precipitation of the upper and central Breede (Lynch, 2004)

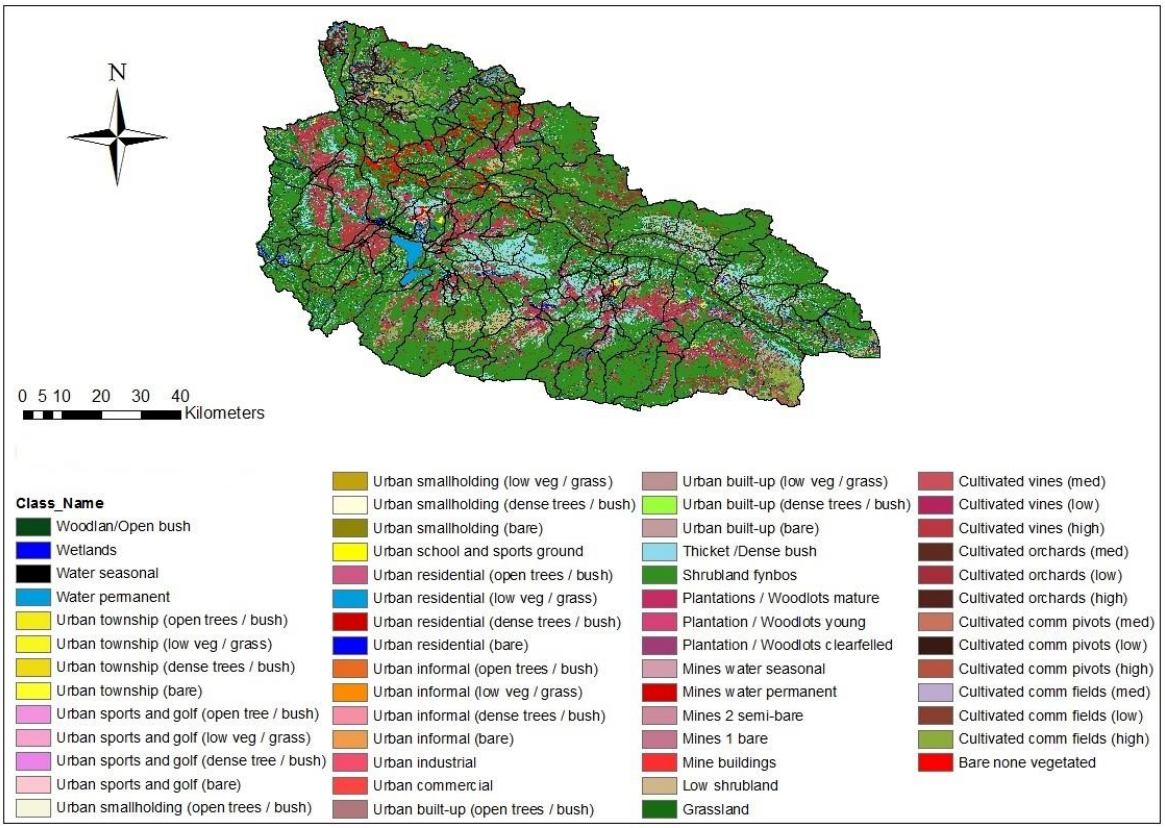

Figure 3.13 Land cover/use for the upper and central Breede Catchment (DEA and GTI, 2015)

3.5 Satellite Derived Rainfall Data Acquisition

Satellite rainfall products were chosen based on daily temporal resolution, fine spatial resolution, product latency and coverage of study areas. FEWS and TAMSAT produce specific coverage over Africa, whereas TRMM 3B42 and GPM produce global coverage. TAMSAT V3 estimates are produced at the finest scale when compared to the other products. In-order to obtain the satellite rainfall product rainfall estimates, online registration with the products were necessary. Thereafter, rainfall product data was made available. Data was downloaded for the period 1 October 2007 to 30 April 2017. The validation study required data for the period 1 January 2010 to 30 April 2017 (due to rain gauge data quality). The modelling study required data for the period 1 October 2007 to 30 September 2016 (limited by ET_0 data, described in Chapter 3.8). Data for the GPM product was downloaded from 12 March 2014 to 30 April 2017, due to data availability. Table 3.1 summarises the product characteristics which were used in this research study.

Table 3.1 Summary of product details utilised in this research.

	TRMM3B42 V7	**FEWSARC2**	**FEWSRFE2**	**TAMSAT V3**	**GPM (IMERGV4)**
Spatial (km)	25 x 25	10 x 10	10 x 10	3.75 x 3.75	10 x 10
Temporal	Daily	Daily	Daily	Daily	Daily
Format	NetCDF 4	Geotiff	Geotiff	NetCDF 3	NetCDF 4

3.6 Rain Gauge Data Acquisition

Daily rain gauge measurements were essential for use in the verification study as well as to drive the ACRU model. Daily rainfall measurements obtained from rain gauges were supplied from the Department of Water and Sanitation of South Africa (DWS) and the South African Weather Service (SAWS). Poor rain gauge coverage and poor quality of rainfall data were inherent in all of the study areas.

Daily rainfall measurements were downloaded from 1 January 2010 to 30 April 2017 for use in the validation study. The dates selected for the validation study were based on a common period with the best quality of data across all rain gauges. The gauges selected were based on data quality and gauges operating throughout the study period, i.e. gauges with the least amount of missing data and patched data. The selected rain gauges are presented in Chapter 4.

Daily rainfall used in the modelling study was provided through the DWS and SAWS from 1 October 2007 to 30 September 2016. The chosen rain gauges to drive the ACRU model are presented in Chapter 5.

3.7 Python Scripts

In-order to process the satellite rainfall estimates into time series of a common format, computer scripts were essential.

The validation of satellite derived rainfall estimates required point estimates of rainfall to be extracted from the datasets. The scripts were designed to access and read the data in the different formats that they were supplied. The scripts extract the rainfall estimate produced in the pixel where the rain gauge is situated. A time series of product rainfall estimates were output in Comma Separated Value (CSV) format from the various rain gauge locations. The satellite product estimates were then compared with rain gauge measurements where performance statistics were used to achieve an understanding of the satellite rainfall product performance in the study areas. Missing data was not included in the analysis.

The modelling study required daily time series of satellite rainfall product estimates to be produced at a sub-catchment scale. The functions of the scripts were designed to produce an area-weighted rainfall estimate over a sub-catchment scale. This is because sub-catchments are covered by portions of pixels (Figure 3.14). Therefore, the influence of a pixel estimate to the final estimate produced is directly linked to the amount of area the pixel occupies in the sub-catchment. The script then averages the area-weighted rainfall pixels occupied within the sub-catchment to produce a daily rainfall estimate for the sub-catchment. A time series of area-weighted daily rainfall is output in CSV format for each sub-catchment in the study sites for use in the ACRU model.

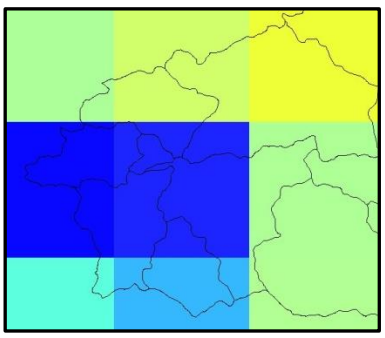

Figure 3.14 Example of how sub-catchments are covered by portions of pixels.

3.8 ACRU Model Configurations

The ACRU hydrological model version 4 (Schulze, 1995; Schulze and Smithers, 2004) was used to model the study sites. The ACRU model is a daily time step, multilevel, physical-conceptual and multi-purpose model that was developed by the School of Bioresources Engineering and Environmental Hydrology at the University of KwaZulu-Natal, South Africa (Warburton *et al*., 2010). A list of studies where the ACRU model was extensively utilised is provided by Warburton *et al*. (2010). The conceptualisations of the processes are presented in Figure 3.15.

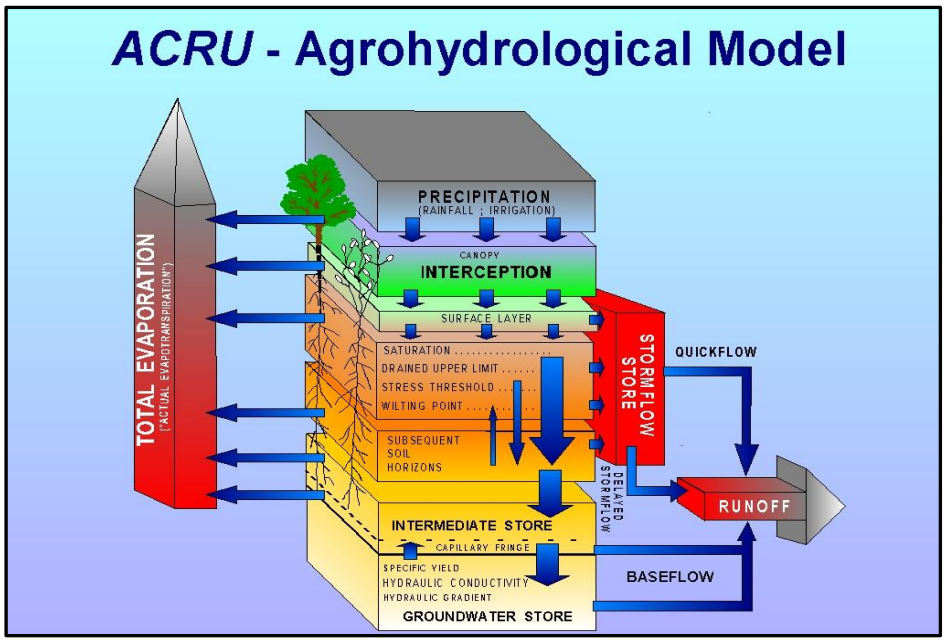

Figure 3.15 The conceptualisations of the process within the ACRU model (Schulze, 1995; Schulze and Smithers, 2004).

3.8.1 Datasets/information used in the model configurations

Mean altitude for each sub-catchment was obtained through the use of the 90 m resolution flow path improved DEM produced by Weepener *et al*. (2011a). Flow paths of the rivers in the upper uMngeni were provided through a shapefile by Weepener *et al*. (2011b); and the upper uThukela and upper and central Breede by Nel *et al.* (2011b). River nodes are located at river confluences as well as where rivers intersected sub-catchment boundaries. The dams input into the model were obtained through the use of DWS registered dams database (DSO, 2014) as well as with the use of Google Earth for confirmation. Smaller unregistered farm dams were lumped as they do affect runoff, but were not considered for irrigation purposes. Natural land cover was obtained through the use of the Acocks (1988) dataset, for which

hydrological properties were obtained from Schulze (2004) for each Acocks Veld Type. Land cover/use was obtained through the use of the 2011 Ezemvelo KZN Wildlife dataset and GeoTerraImage (2013) for the upper uMngeni and upper uThukela. Land cover/use for the upper and central Breede sub-catchments were obtained through the use of the 2013/2014 national land cover/use raster dataset for South Africa (DEA and GTI, 2015). Soils data was obtained through the use of the dataset by Schulze and Horan (2008). Dominant soil types for each land cover/use within each sub-catchment were then used to determine the soil hydrological properties for input into the model. The MAP configured into the model was obtained through the use of the dataset by Lynch (2004). The rainfall seasonality dataset provided by Schulze and Maharaj (2008a) was used to configure the model. The Satellite Applications Hydrology Group (SAHG) reference evaporation, ET_0, dataset (http://sahg.ukzn.ac.za/soil_moisture/et) was used to obtain a time series of ET_0 of each sub-catchment. The ET_0 data was adjusted by a factor of 1.2 to obtain A-Pan estimates for input into the ACRU model. ET_0 data is limited from 2007 to present, which influenced the modelling period. Maximum and minimum air temperatures were obtained through the use of datasets by Schulze and Maharaj (2008b) and Schulze and Maharaj (2008c). Areal mean values were computed for each sub-catchment where monthly values of daily maximum and minimum temperatures were input into the ACRU model. Frost occurrences in the sub-catchments were obtained through use of the dataset by Schulze and Maharaj (2008d).

The ACRU model configuration for the upper uMngeni was obtained from the WRC project K5/2205 (Clark, 2015). One inter-catchment transfer is present in the catchment, being a transfer from the Mooi River into the Mpofana River which flows into the Lions River. The flow data was obtained at Gauge V2H015 provided by the DWS which was used in conjunction with data obtained from Umgeni Water to determine daily transfers. A detailed description of the model configuration for the upper uMngeni catchment is presented in the WRC K5/2205 project (Clark, 2015).

The ACRU model configuration for the upper uThukela catchment was obtained from the WRC project K5/2512 (Clark, 2017a). Three inter-catchment transfers occur in the upper uThukela catchment. These are the Drakensberg Pump Storage Scheme, Ingula Pump Storage Scheme and Mooi-uMngeni Transfer Scheme. A detailed description of the model configuration for the upper uThukela catchment is presented in the WRC K5/2512 project (Clark, 2017a).

The ACRU model configuration for the upper and central Breede was obtained from the WRC project K5/2512 (Clark, 2017b). Due to a low MAP and intensive agriculture, there exists extensive water infrastructure in the catchment (Clark, 2017b). These are in the form of dams, canals, river diversions and pipelines. The transfers included consist of water transferred from the Smalblaar River into the Holsloot River; the Holsloot River diversion into Brandvlei Dam; water from the Bree River into Brandvlei Dam during winter; the Spek River into the Valsgat River; and The Valsgat River diversion into the neighbouring Berg-Olifant Water Management Area. Many other transfers have not yet been included due to lack of information. Irrigation and urban water use is assumed to be extracted from the registered dams. A detailed description of the model configuration for the upper and central Breede catchment is presented in the WRC K5/2512 project (Clark, 2017b).

3.9 ACRU Modelling

The ACRU model was driven by the satellite derived rainfall product estimates as well as by rain gauge measurements, as it is traditionally done, for comparison with the satellite driven results. The model output a time series of simulated streamflow in m^3/day, which was converted to m^3/second to compare against weir gauge flow data supplied in m^3/second. The model was run from 1 October 2007 to 30 September 2016. However, the first hydrological year was omitted from the analysis as it was used as a "warm up" where the hydrological processes are initialised within the model. Simulated streamflows were compared to daily weir gauge flow data obtained from DWS[1]. Performance statistics were calculated to obtain an understanding of the modelled streamflows based on the different rainfall products and rain gauges. The locations of the weirs where modelled streamflows are compared to observed flows are presented in Chapter 5. The weirs were selected based on limiting the impact of dam and water transfer influence on observed and simulated streamflow as the streamflow is highly controlled. Discrepancies in dam release and water transfer data will incorrectly reflect the performance of the modelled streamflow produced by the satellite products and rain gauges.

A poor network of operational rain gauges exists within the study sites. For the rain gauge driven simulations, rain gauge measurements had to be adjusted to represent rainfall in sub-catchments that were not gauged. The ungauged sub-catchments assigned to a driver rain

[1] From: http://www.dwa.gov.za/Hydrology/Verified/hymain.aspx

gauge were based on similar altitude, MAP and distance from the rain gauge. The adjustment factors for each ungauged sub-catchment were calculated through the use of precipitation correction (PPTCORR) factors for each month. The monthly median values of each sub-catchment were calculated from a median rainfall raster dataset by Lynch (2004). The monthly median values of the driver rain gauge were also calculated. The PPTCORR for each month was applied to the driver rain gauge measurements to obtain rainfall records to drive ungauged sub-catchments.

$$PPTCORR = \frac{Subcatchment\ Median}{Rain\ Gauge\ Median}$$

4. RESULTS AND DISCUSSION: PRODUCT VALIDATION

This Chapter addresses the validation of the satellite derived rainfall product estimates with in-situ rain gauge measurements.

It is important to quantify satellite derived rainfall product estimates through the use of defined metrics in-order to assess uncertainties. The metrics provide a means of measuring the performance of products with those of ground-based gauges. The validation focuses on spatial and temporal patterns as well as consistency among the product estimates (when compared to rain gauge measurements). The analyses included in the validation study are:

i. Time series analysis

ii. Bias, where a value of 1 relates to no bias in the dataset when compared to gauge measurements

iii. Mean Absolute error (MAE), which indicates the average magnitude of errors between datasets, regardless of whether the error is positive or negative.

iv. Root Mean Square Error (RMSE), which indicates the average magnitude of errors between gauge measurements and product estimates.

v. Relative Volume Error (RVE), which is the percentage difference in total volume between gauge measurements and product estimates.

vi. Coefficient of determination (R^2), which indicates the linear relationship between gauge measurements and product estimates. Values range from 0 to 1, where a value of 1 indicates a perfect linear relationship.

vii. Probability of Detection (POD), which indicates the fraction of gauge measurements that are correctly estimated by the product (Amekudzi *et al*., 2016). Values range from 0 to 1, where 0 indicates no skill and 1 indicates perfect skill. POD is sensitive to missed events only (Amekudzi *et al*., 2016).

viii. False Alarm Ratio (FAR), which indicates the fraction of product estimates that are not confirmed by gauge measurements (Amekudzi *et al*., 2016). The values range

from 0 to 1, where 0 indicates perfect skill and 1 indicates no skill. FAR is sensitive to false estimates only (Amekudzi *et al.*, 2016).

ix. Critical Success Index (CSI), which is also a measure of accuracy between datasets. Vales range from 0 to 1, where 0 indicates no skill and 1 indicates perfect skill. CSI is sensitive to missed events and false alarms (Amekudzi *et al.*, 2016).

The analyses used to validate the satellite derived rainfall were based on current assessment methodologies. The selected analyses are considered appropriate to be used in the validation of satellite derived rainfall products against rain gauge measurements, whereby reliable conclusions can be drawn. The statistical equations used are included in Appendix A.

The products (grid point) are compared to various rain gauges (point rain gauges) situated within and around the study sites. TRMM3B42, FEWSARC2, FEWSRFE2 and TAMSATV3 are compared over the period of 1 January 2010 to 30 April 2017. GPM was analysed over the period of 12 March 2014 to 30 April 2017 due to GPM data availability. In-order to validate the product estimates, daily rain gauge data was obtained from the Department of Water and Sanitation (DWS) as well as the South African Weather Service (SAWS). Stations chosen were limited to the quality of the rainfall record during the validation period (i.e. to limit missing days and poor record values). The upper uMngeni and upper uThukela are discussed together based on their locations within a summer rainfall region.

4.1 Upper uMngeni and Upper uThukela

Various rain gauges were used in the validation process within and around the study catchments. Rain gauge details are provided in Table 4.1 and Figure 4.1. Appendix B presents the daily time series of all products against rain gauge measurements, average monthly total rainfall plots and the complete tables of statistics at the rain gauge sites.

Table 4.1 Rain gauges used in the uMngeni and uThukela Catchments.

Station	Station Name	Latitude	Longitude
V3E002	Chelmsford @ Chelmsford Dam	29,94974	-27,95460
U3E004	Cotton Lands @ Hazelmere Dam	31,04144	-29,61701
U2E002	Driefontein @ Cedara	30,28308	-29,53368
V1E008	Eendracht @ Driel Barrage	29,28722	-28,76705
U2E010	Inanda Dam	30,87227	-29,72506
V2E002	Rietvlei @ Craigie Burn Dam	30,28308	-29,16703
0268883 6	Mooi River (SAWS)	30,00200	-29,21800
0239698 5	Pietermaritzburg (SAWS)	30,40200	-29,62700

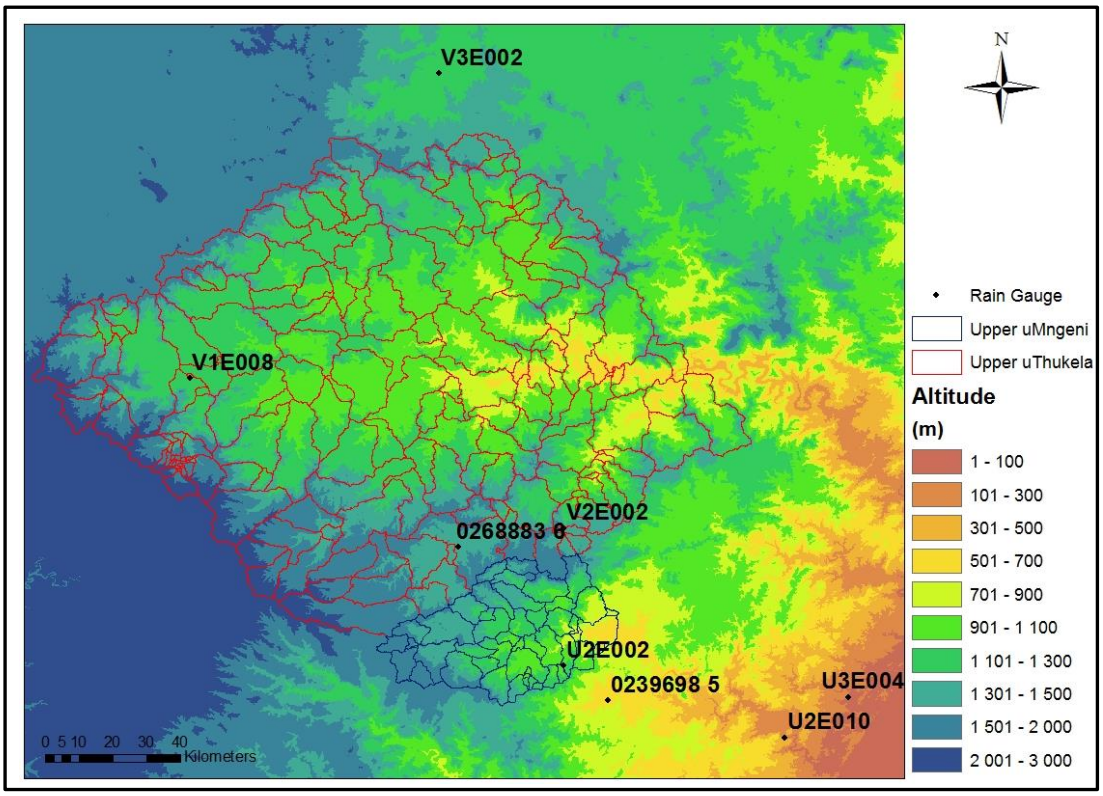

Figure 4.1 Location of rain gauges in uMngeni and uThukela with altitude (Weepener *et al.*, 2011b).

Satellite rainfall product estimation of rainfall were variable at each location. No definite trends exist among the products when compared to rain gauge measurements on a daily temporal scale where products either consistently overestimated or underestimated rainfall (Time series presented in Appendix B). Cumulative (Figure 4.2a-h) and average monthly rainfall total plots (Appendix B) show that the products are in closer agreement with rain gauge measurements at a monthly, seasonal and yearly scale. The products often inaccurately estimated the daily magnitudes of rainfall when compared to rain gauge measurements (Time

series presented in Appendix B). Apart from the FEWS products at gauge 0239698 5 (Pietermaritzburg), R^2 values achieved were low indicating that the satellite rainfall products correlated poorly to rain gauge measurements at a daily temporal scale (Table 4.2). TAMSAT-3 produced the poorest correlation when compared to rain gauge measurements at a daily scale, whereas both FEWS products generally had the best daily correlation to rain gauge measurements of all products.

Total volumes of the satellite products of analysis were in closer agreement with total volumes measured by the rain gauges over the whole period of analysis (Table 4.2, Figure 4.2a-h). TRMM 3B42 often overestimated total rainfall volumes, where bias values where above 1 (Table 4.2). Apart from rain gauge U2E010, GPM underestimated total rainfall volumes, where bias values were below 1 (Figure 4.2a-h). TAMSAT-3 performed variably in terms of estimating total rainfall volumes over the whole period of analysis, where 50 % of the cases overestimated total volumes of rainfall. Both FEWS products often produced the closest agreement to rain gauge total volumes when compared to the other products.

POD, FAR and CSI metrics were calculated at 0 mm and 5 mm thresholds (Appendix B). POD values for the FEWS products were generally closer to 1 across all gauging sites at the 0 mm threshold. FAR and CSI values were found to be generally poor for all products at 0 mm, with FAR being high and CSI being low. Meaning that the satellite products estimated rainfall more frequently when the rain gauge recorded 0 mm of rainfall. This could be because the products may be estimating rainfall from cold non-precipitating clouds. The algorithms make use of cloud top temperatures and cloud brightness which may indicate rainfall, where-as no rainfall occurs at the ground level. Both FEWS products generally produce better POD, FAR and CSI values when compared to the other products across all gauge sites. GPM generally produced lower POD, higher FAR and lower CSI when compared to TRMM3B42 at the 0 mm threshold. At the 5 mm threshold all products performed well achieving values close to 1 (POD and CSI) and 0 (FAR). This shows the limitations experienced by the products in detecting light rainfall events.

Table 4.2 Summary of statistics comparing satellite product estimates to rain gauge measurements.

		V3E002	U3E004	U2E002	V1E008	U2E010	V2E002	0268883	02396985
TRMM 3B42	**Bias**	0.90	1.02	0.84	0.97	1.15	1.18	1.25	1.16
	RVE %	-9.66	1.74	-16.49	-3.22	14.79	18.08	25.23	16.09
	R^2	0.40	0.25	0.26	0.35	0.22	0.30	0.18	0.31
FEWS ARC2	**Bias**	0.82	1.06	0.79	0.96	1.14	1.03	1.05	0.95
	RVE %	-18.33	5.73	-21.49	-3.53	14.17	3.18	4.63	-5.07
	R^2	0.43	0.43	0.59	0.42	0.37	0.32	0.26	0.86
FEWS RFE2	**Bias**	0.98	0.83	0.80	1.00	0.92	1.03	1.10	0.98
	RVE %	-1.52	-16.89	-20.27	0.25	-8.31	2.54	9.54	-1.67
	R^2	0.50	0.40	0.57	0.43	0.41	0.48	0.33	0.87
TAMS AT-3	**Bias**	0.88	0.97	0.84	0.91	1.23	1.13	1.17	1.13
	RVE %	-12.18	-3.10	-15.52	-9.25	23.12	12.67	16.54	13.12
	R^2	0.21	0.07	0.11	0.15	0.07	0.16	0.14	0.12
GPM	**Bias**	0.87	0.90	0.56	0.73	1.13	0.90	0.87	0.81
	RVE %	-12.55	-9.84	-43.77	-9.25	13.12	-10.46	-13.20	-18.98
	R^2	0.30	0.17	0.27	0.19	0.29	0.22	0.43	0.33

(a) V3E002 (Chelmsford at Chelmsford Dam)

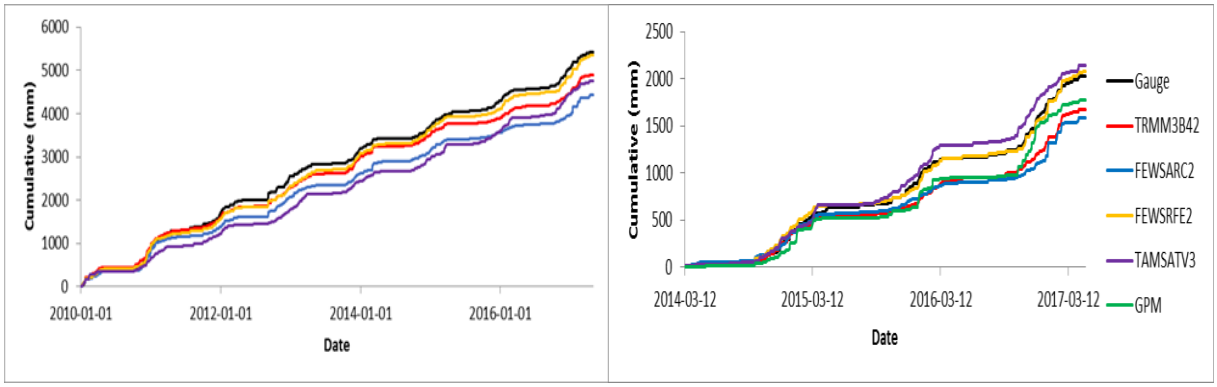

(b) U3E004 (Cotton Lands at Hazelmere Dam)

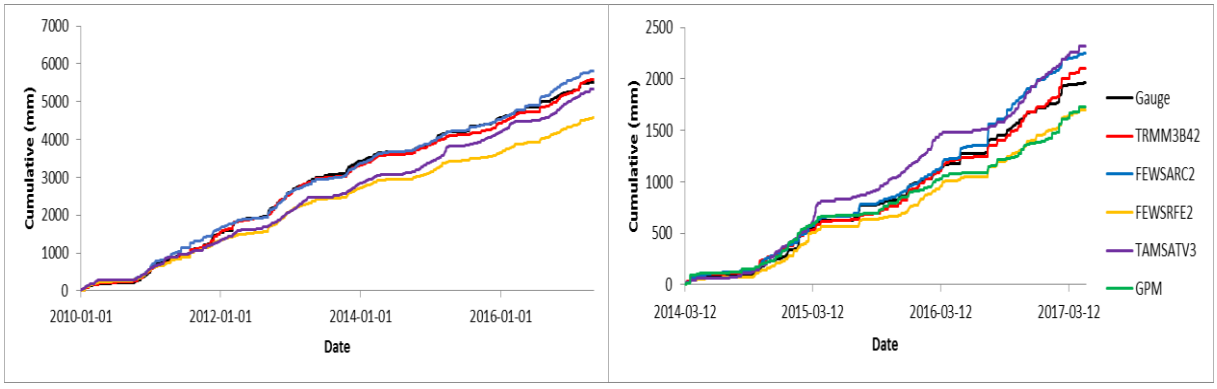

(c) U2E002 (Driefontein at Cedara)

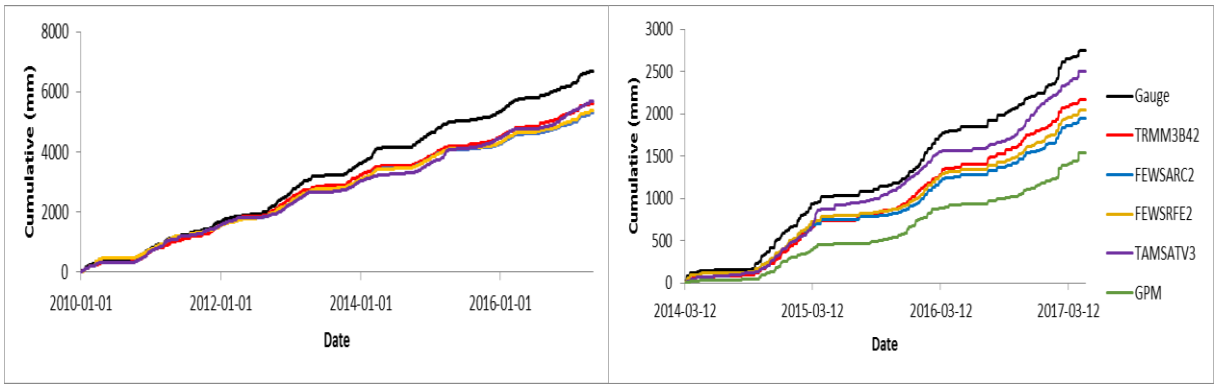

(d) V1E008 (Eendracht at Driel Barrage)

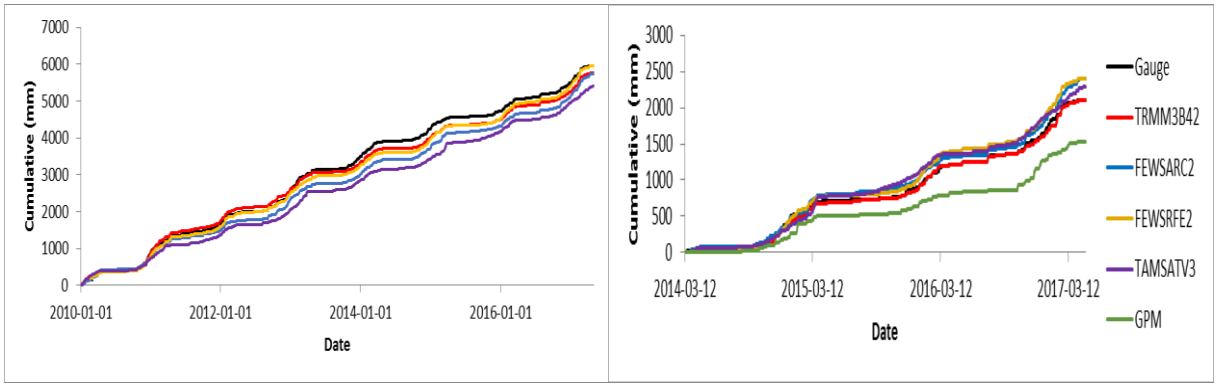

(e) U2E010 (Inanda Dam)

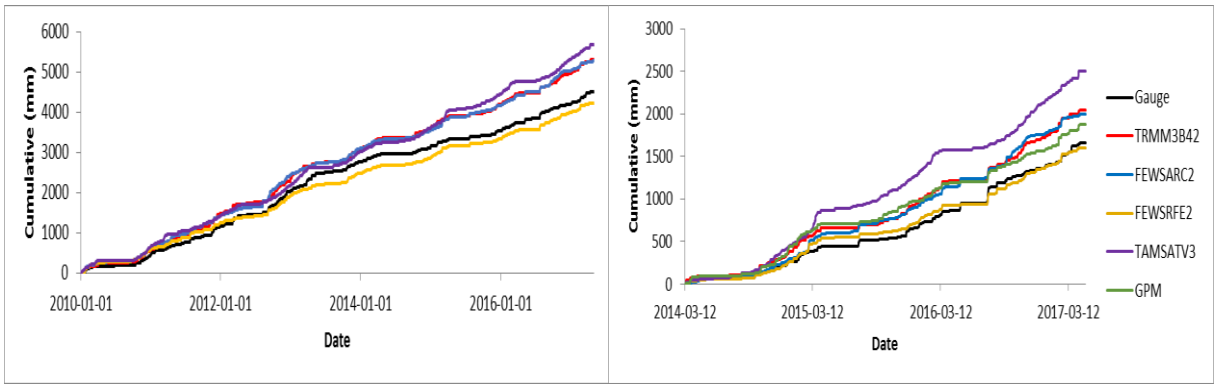

(f) (Rietvlei at Craigie Burn dam)

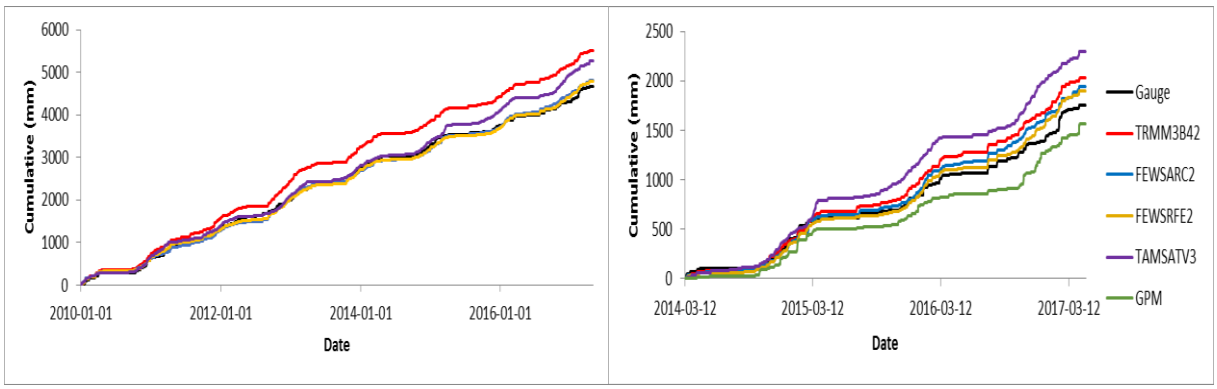

(g) 0268883 6 (Mooi River SAWS)

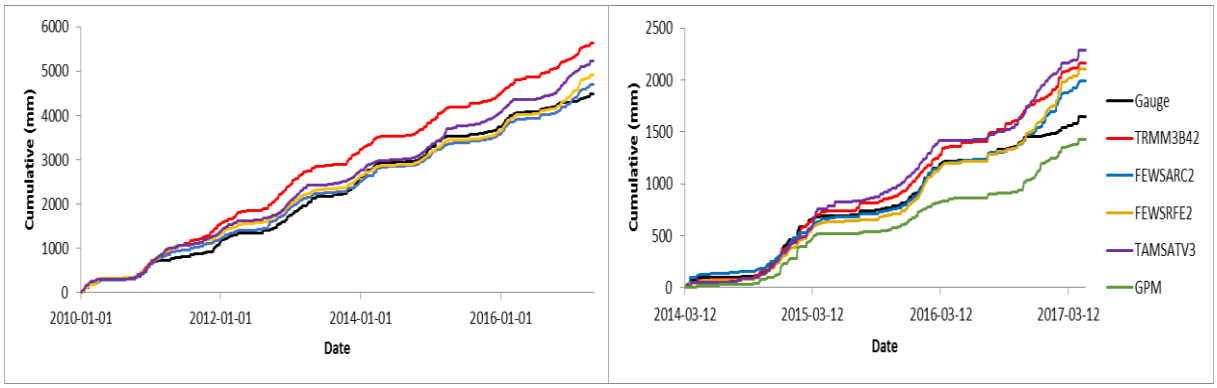

(h) 0239698 5 (Pietermaritzburg SAWS)

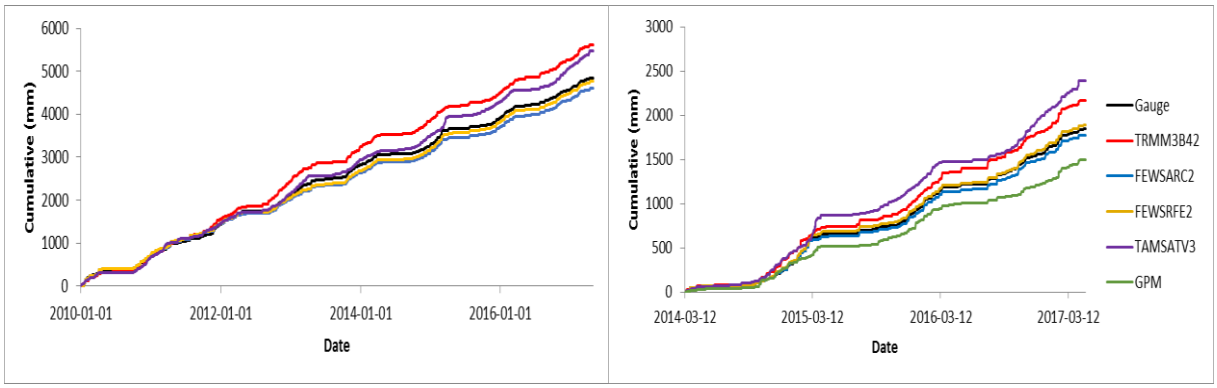

Figure 4.2a-h Graphs of accumulated rainfall of the product estimates and rain gauge measurements. The graphs on the left depict whole period of analysis and the graphs on the right depict the GPM period of analysis.

4.2 Upper and Central Breede

Various rain gauges were used in the validation process within and around the study catchments. Rain gauge details are provided in Table 4.3 and Figure 4.3. Appendix B presents the daily time series of all products against rain gauge measurements, average monthly total rainfall plots and the complete tables of statistics at the rain gauge sites.

Table 4.3 Rain gauges used in the Breede catchment.

Station	Station Name	Latitude	Longitude
0022729 X	Worcester (SAWS)	19,41800	-33,66300
H1E007	Doorn @ Kwaggaskloof Dam	19,25083	-33,83472
H9E002	Krantzkloof @ Korinte-Vet Dam	21,16250	-34,00638
H6E001	The Waters Kloof @ Theewaterskloof Dam	19,29189	-34,07591
H4E007	Haweqwas Stateforest @ Stettynskloof Dam	19,47412	-33,76092
H3E002	Montagu	20,12747	-33,79537
H2E003	Lakenvlei @ lakenvallei Dam	19,58274	-33,36261

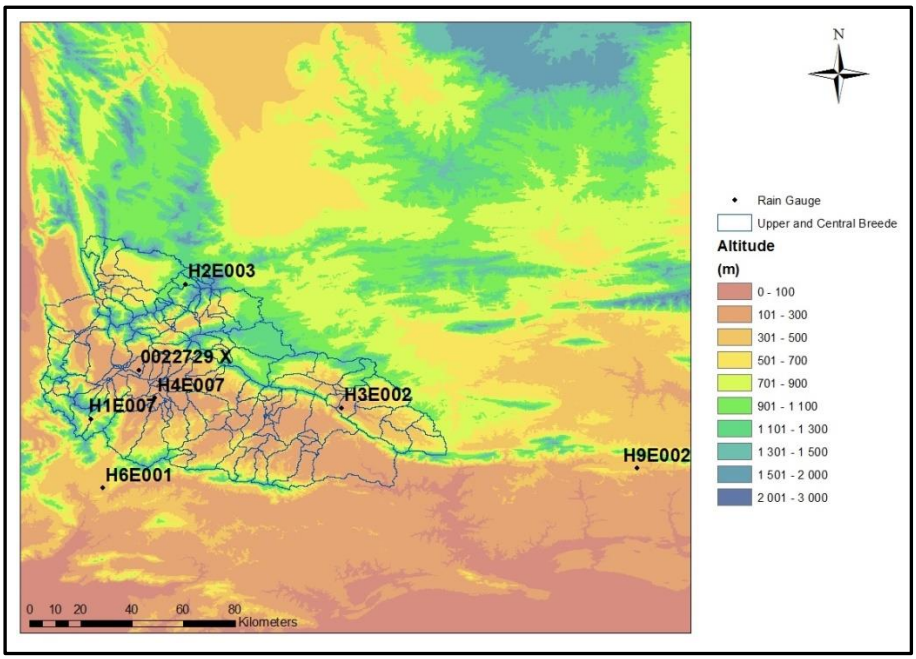

Figure 4.3 Location of rain gauges in Breede catchment with altitude (Weepener *et al*., 2011b).

Satellite rainfall products estimation of rainfall were inconsistent and generally poor across all locations. Daily rainfall estimates were generally underestimated when compared to the rain gauge measurements (Time series presented in Appendix B). R^2 values achieved were low indicating that the satellite rainfall products correlated poorly to rain gauge measurements at a daily temporal scale (Table 4.4). It is noted that the TAMSAT-3 product consistently produced the lowest R^2 values (Table 4.4), indicating the poorest correlation to daily rain gauge measurements. Both FEWS products achieved higher R^2 values than the other products when compared to daily rain gauge measurements (Table 4.4). Cumulative (Figure 4.4a-g) and average monthly rainfall total plots (Appendix B) show that the products are in closer agreement with rain gauge measurements at a monthly, seasonal and yearly scale, noting that the majority of rainfall occurs in winter in this region.

Satellite products generally poorly estimated total rainfall volumes when compared to rain gauge total volumes over the whole period of analysis. Apart from a few cases, the products generally underestimated total rainfall volumes (Table 4.4). It is observed that TAMSAT-3 produced the closest agreement to rain gauge total volumes, even though daily correlations of rainfall were the poorest when compared to rain gauge measurements. GPM generally produced the highest percentage of underestimation at each rain gauge location when compared to the other products.

POD, FAR and CSI metrics were calculated at 0 mm and 5 mm thresholds (Appendix B). POD for the FEWS products were generally higher across all gauging sites at the 0 mm threshold when compared to the other products which were considerably lower. FAR and CSI values were found to be generally poor for all products at 0 mm, with FAR being high and CSI being low. This means that the products estimated rainfall much more frequently than confirmed by gauge measurements at a 0 mm threshold. GPM generally produced higher FAR and CSI when compared to TRMM3B42 at the 0 mm threshold. TAMSAT had the worst POD, FAR and CSI, further exposing the products poor performance of detecting rainfall at a daily scale in the region. At the 5 mm threshold all products performed well achieving values close to 1 (POD and CSI) and 0 (FAR). This shows the limitations satellite derived rainfall experience in detecting light rainfall events as well as the effect of cold non-precipitating clouds on inaccurate estimation. The Breede region experiences a Mediterranean climate with mid-latitude weather systems, predominantly frontal rainfall (Thorne *et al*., 2001). The satellite products perform poorly in detecting daily rainfall in this region which may be due to their inability to accurately estimate rainfall generated from this weather system experienced in the Breede region.

Table 4.4 Summary of statistics comparing satellite product estimates to rain gauge measurements.

		0022729 X	H1E007	H9E002	H6E001	H4E007	H3E002	H2E003
TRMM3B42	**Bias**	1.69	1.39	0.45	0.72	0.45	0.80	0.66
	RVE %	69.28	38.79	-54.77	-27.86	-55.42	-19.82	-33.85
	R^2	0.39	0.42	0.20	0.34	0.23	0.24	0.17
FEWSARC2	**Bias**	1.53	1.42	0.50	1.05	0.48	0.79	0.47
	RVE %	53.06	42.45	-49.80	4.72	-51.85	-20.91	-53.12
	R^2	0.70	0.34	0.54	0.53	0.51	0.24	0.25
FEWSRFE2	**Bias**	1.30	1.10	0.41	0.76	0.37	0.65	0.45
	RVE %	30.46	10.19	-59.48	-23.78	-62.71	-34.54	-55.49
	R^2	0.69	0.44	0.52	0.45	0.33	0.31	0.28
TAMSAT	**Bias**	1.05	0.98	0.69	0.88	0.42	0.65	0.57
	RVE %	4.52	-1.80	-31.23	-11.66	-57.66	-35.18	-43.18
	R^2	0.02	0.02	0.02	0.03	0.01	0.03	0.01
GPM	**Bias**	0.88	0.69	0.21	0.46	0.24	0.38	0.37
	RVE %	-12.43	-31.22	-78.95	-54.14	-75.70	-61.76	-62.56
	R^2	0.32	0.21	0.19	0.20	0.18	0.15	0.07

(a) 0022729 X (Worcester)

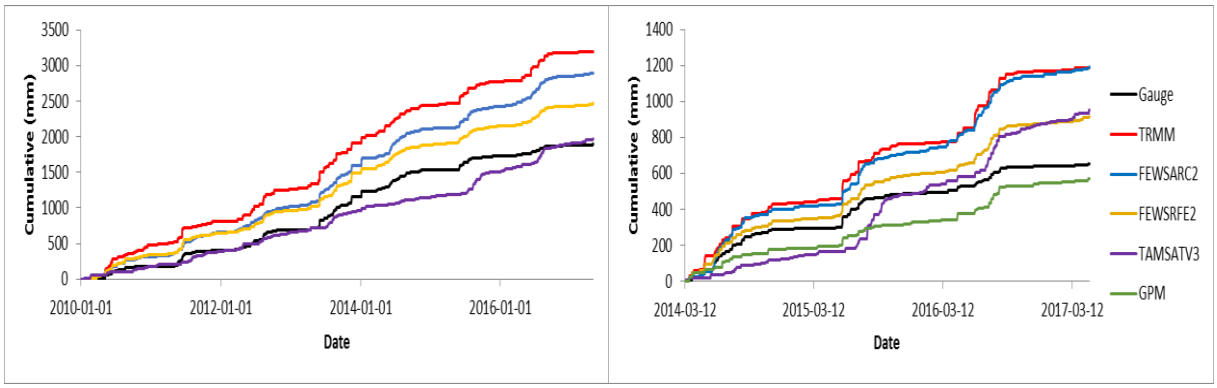

(b) H1E007 (Doorn at Kwaggaskloof Dam)

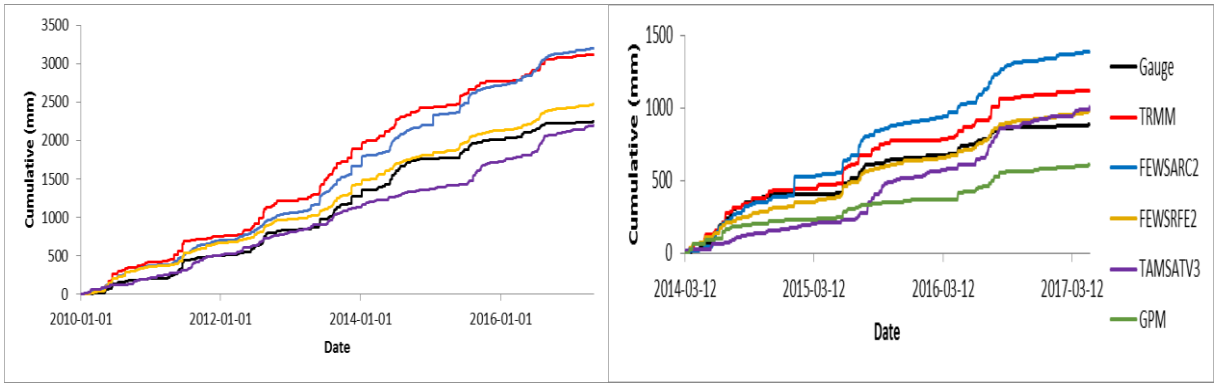

(c) H9E002 (Krantzkloof at Korinte-Vet Dam)

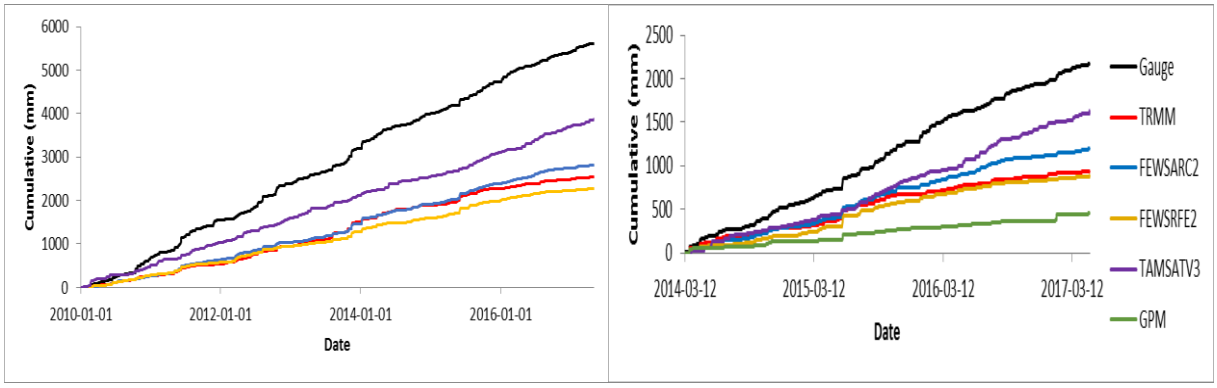

(d) H6E001 (Thee Waters Kloof at Theewaterskloof Dam)

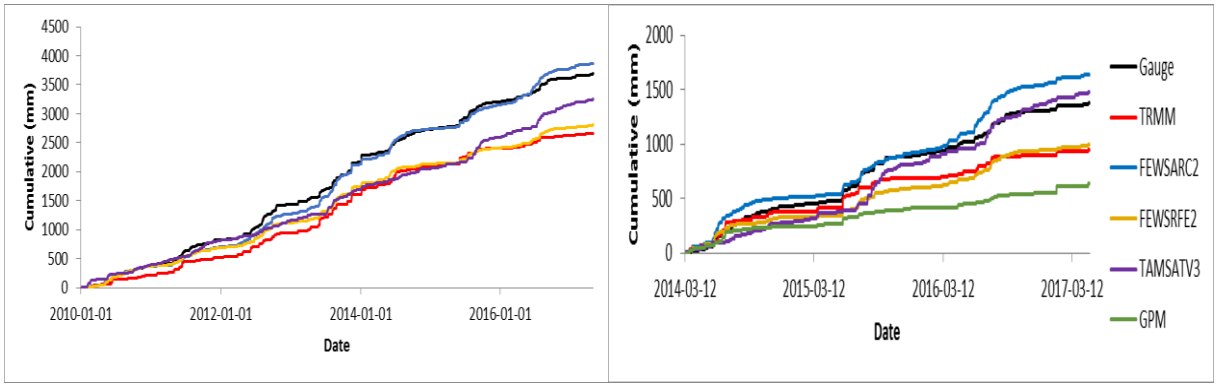

(e) H4E007 (Haweqwas Stateforest at Stettynskloof Dam)

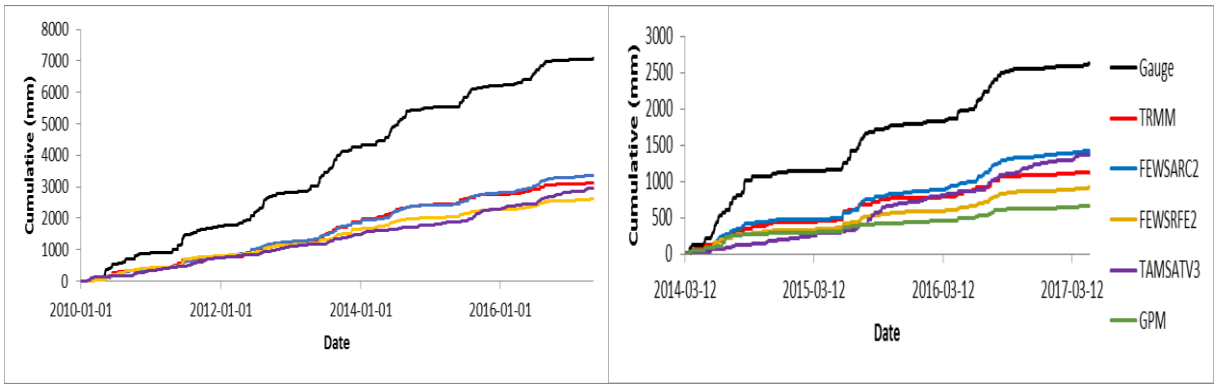

(f) H3E002 (Montagu)

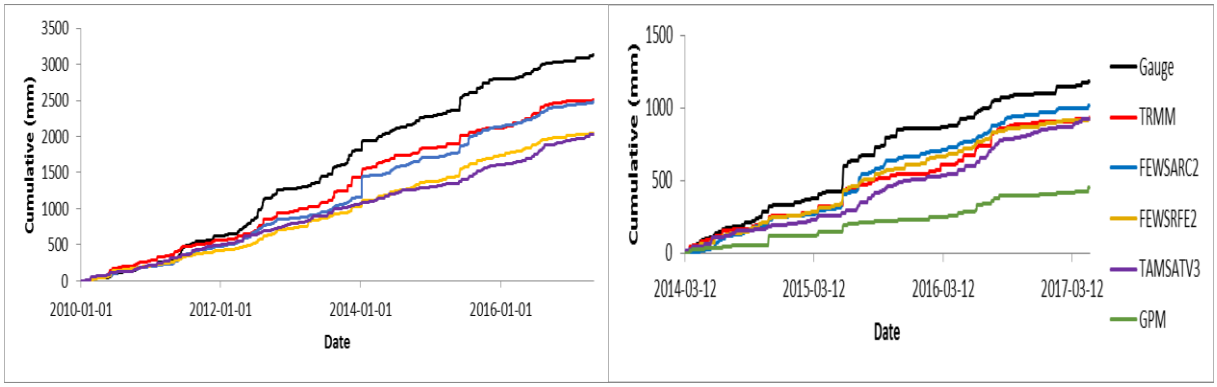

(g) H2E003 (Lakenvlei at Lakenvallei Dam)

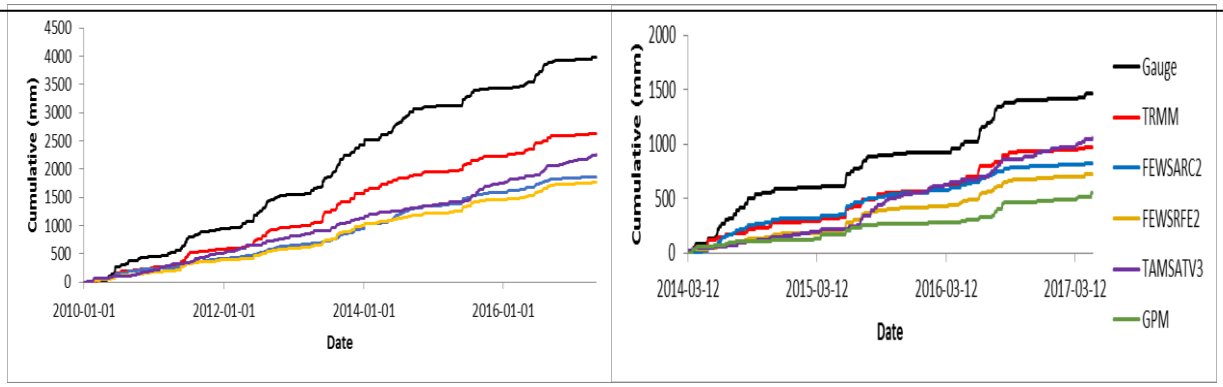

Figure 4.4a-g Graphs of accumulated rainfall of the product estimates and rain gauge measurements. The graphs on the left depict the whole period of analysis and the graphs on the right depict the GPM period of analysis.

4.3 Summary of Findings of the Validation Study

The satellite rainfall products produced inconsistent results when compared to rain gauges across all three study sites. The satellite rainfall products where in better agreement to rain gauge measurements in the upper uMngeni and upper uThukela than in the Breede region. This could be attributed to the products ability to estimate rainfall from convective rainfall

mechanisms which is the dominant mechanism of the upper uMngeni and upper uThukela region (Thorne *et al*., 2001).

Total, monthly and seasonal rainfall volume estimations were found to be in better agreement with rain gauge volume totals than the correlations at the daily scale, more so in the uMngeni and uThukela than in the Breede region. Satellite measurements make use of cloud top temperatures and brightness temperatures to obtain rainfall measurements. Measurements obtained from cold cirrus clouds, non-precipitating clouds and low warm clouds provide less reliable rainfall results (Ebert *et al*., 2007). Meaning that satellite rainfall products may recognise rainfall events from these types of clouds, when no rainfall actually occurred at the ground level or the products provide an inaccurate measurement of rainfall. The upper Breede catchment rainfall is highly influenced by the warm Indian Ocean and cold Atlantic Ocean (Bangira *et al*,. 2015). Both oceans meet along the Western Cape coast where convergence and frontal rainfall occurs. Satellite product rainfall estimation ability may be affected by the rainfall mechanisms that occur in the region which results in inaccurate rainfall estimates (Thorne *et al*., 2001; Maidment *et al*., 2017). The FEWS and TAMSAT-3 products utilise rain gauge inputs to calibrate the satellite derived data. Absence of rain gauges in the area may have affected the accuracy of rainfall estimates produced.

Rain gauge measurements neglect the spatial variations of topography, where-as satellite derived rainfall neglect the estimation errors caused by different orographic rainfall regimes (Hughes, 2006, Kimani *et al*., 2017). The satellite derived products could replicate seasonal, monthly and yearly rainfall patterns, however the magnitudes of daily rainfall differ when compared to rain gauge measurements which may be due to the different orographic rainfall types caused by complex topography in some cases. In evaluating satellite products using rain gauge measurements, it is important to note the spatial heterogeneity that exists when comparing a point value obtained from a rain gauge with a pixel estimate from a satellite product. Products produce a spatially averaged estimate of rainfall within the pixel area, where-as rain gauges record rainfall of a specific point location. Product limitations that affect estimates include sampling frequency; type of orbit, especially those of polar orbiting retrievals; the rainfall diurnal cycle as well as the uncertainties associated with product algorithms (Amekudzi *et al*., 2016).

5. RESULTS AND DISCUSSION: ACRU MODELLING

This Chapter presents and discusses the results of the ACRU modelling. The Chapter addresses the comparison of simulated streamflow generated by the ACRU model to observed streamflow. The statistical analyses used in this chapter include time series analysis, total streamflow, mean, maximum, bias, mean absolute error (MAE), root mean square error (RMSE), relative volume error (RVE%), coefficient of correlation (R^2) and standard deviation (STD Dev). The statistical equations are presented in Appendix A. The time series of all streamflow simulations are presented in Appendix C.

5.1 Upper uMngeni Catchment

The uMngeni catchment streamflow modelling was analysed at three streamflow gauges at weirs in the catchment (Table 5.1). Figure 5.1 shows the location of rain gauges used to drive the sub-catchments as well as the location of the streamflow gauges in the catchment. The rain gauge U2E006 was used as the driver rain gauge for the catchments shaded in light pink and rain gauge U2E003 was used as the driver rain gauge for the catchments shaded in light green (Figure 5.1).

Table 5.1 Weir details used in the uMngeni modelling.

Weir Gauge	**Name**	**Latitude**	**Longitude**
U2H006	Karkloof @ Shafton	-29.38175	30.27775
U2H007	Lions River (Mpofana River @ Weltervreden	-29.44258	30.14852
U2H013	Mgeni River @ Petrus Stroom	-29.51261	30.09441

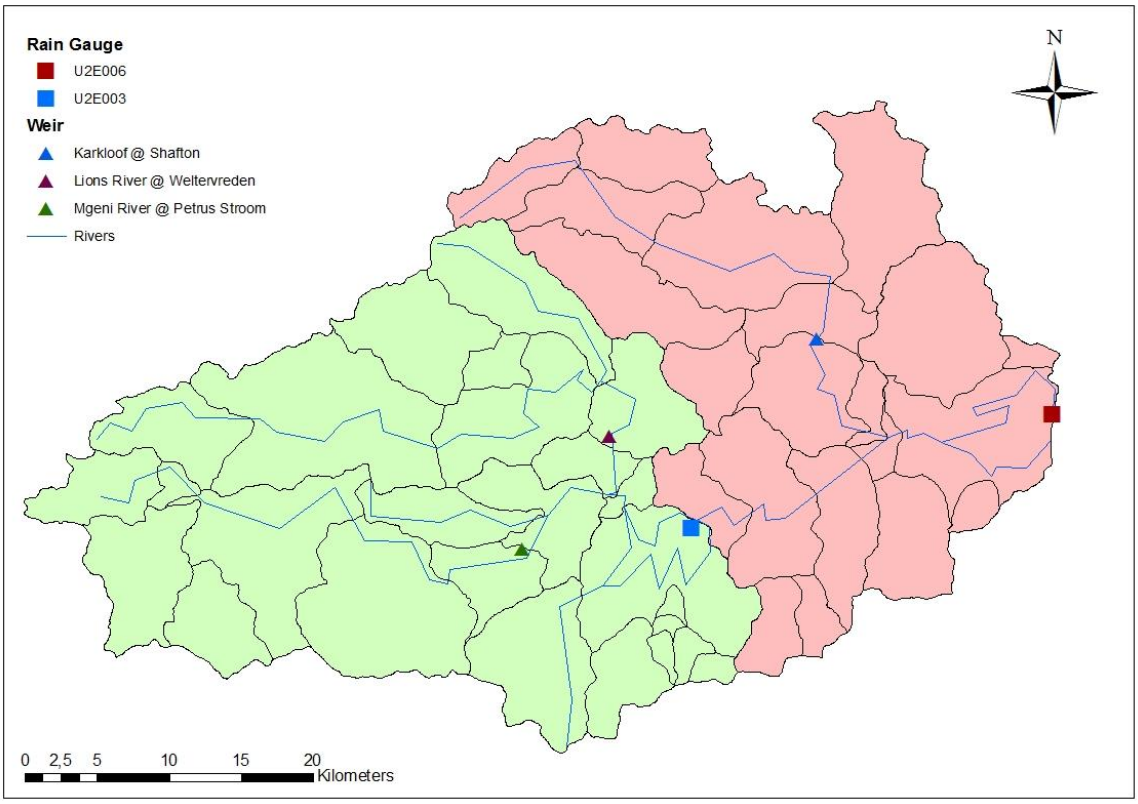

Figure 5.1 Weir and Rain Gauge locations with respect to catchment boundaries.

5.1.1 U2H006 (Karkloof @ Shafton)

The streamflow of all simulations were poorly represented at a daily scale. The simulations did not accurately represent the variations of daily streamflow magnitudes when compared to observed streamflow. R^2 values were low (Table 5.2) which indicated the poor correlation of simulated streamflow to observed streamflow at a daily scale. FEWS RFE2, TAMSAT-3 and GPM produced the lowest values of R^2 when compared to the other simulations, as the daily variation in streamflow was poorly represented (Time series presented in Appendix C). The rain gauge driven simulation produced the closest statistical agreement to observed streamflow through-out the whole period of analysis when compared to other simulations. All simulations of streamflow produced an underestimation of streamflow volumes (Bias, RVE%), with the rain gauge driven simulation underestimating streamflow the least (Figure 5.2 and 5.3). The FEWS RFE2 driven simulation produced the highest degree of underestimation of streamflow over the whole period of analysis. FEWS RFE2 raw satellite data are corrected by rain gauge measurements in terms of magnitude (Novella and Thiaw, 2013). There may be an absence of rain gauges used in the algorithm in this region which may attribute to the poor spatial rainfall estimates which in-turn produced poor streamflow

results. Of the satellite product driven simulations, TRMM 3B42 produced the closest agreement to observed streamflow at this weir with the highest correlation to daily streamflow and the closest agreement to total streamflow volume than the other products.

Table 5.2 Statistics comparing observed streamflow and simulated streamflows at Gauge U2H006 (Karkloof @ Shafton).

	Weir Gauge	**Rain Gauge**	**TRMM3B42**	**FEWSARC2**	**FEWSRFE2**	**TAMSATv3**	
Total (m^3)	5.10×10^8	4.04×10^8	2.35×10^8	9.15×10^7	4.49×10^7	1.19×10^8	
Max (m^3/s)	57,97	46,61	38,65	35,57	18,11	19,26	
Mean (m^3/s)	2,09	1,60	0,93	0,36	0,18	0,47	
BIAS		0,79	0,46	0,18	0,09	0,23	
MAE (m^3/s)		0,42	1,09	1,66	1,84	1,55	
RMSE (m^3/s)		3,58	3,16	3,78	3,57	3,47	
RVE (%)		-20,85	-53,98	-82,07	-91,21	-76,59	
RSQ		0,25	0,22	0,03	0,07	0,05	
STD Dev (m^3/s)		3,51	2,85	2,71	2,49	2,48	
	Weir Gauge	**Rain Gauge**	**TRMM3B42**	**FEWSARC2**	**FEWSRFE2**	**TAMSATv3**	**GPM**
Total (m^3)	5.50×10^7	8.56×10^7	2.09×10^7	1.67×10^7	4.83×10^6	2.32×10^7	1.71×10^7
Max (m^3/s)	10,46	33,40	15,64	33,46	1,79	19,26	43,38
Mean (m^3/s)	0,87	1,36	0,33	0,27	0,08	0,37	0,27
BIAS		1,56	0,38	0,30	0,09	0,42	0,31
MAE (m^3/s)		0,48	0,54	0,60	0,79	0,50	0,60
RMSE (m^3/s)		1,75	1,48	1,52	1,31	1,58	2,35
RVE (%)		55,75	-62,01	-69,55	-91,22	-57,87	-68,82
RSQ		0,04	0,07	0,29	0,24	0,01	0,02
STD Dev (m^3/s)		2,62	1,18	1,43	0,89	1,14	1,73

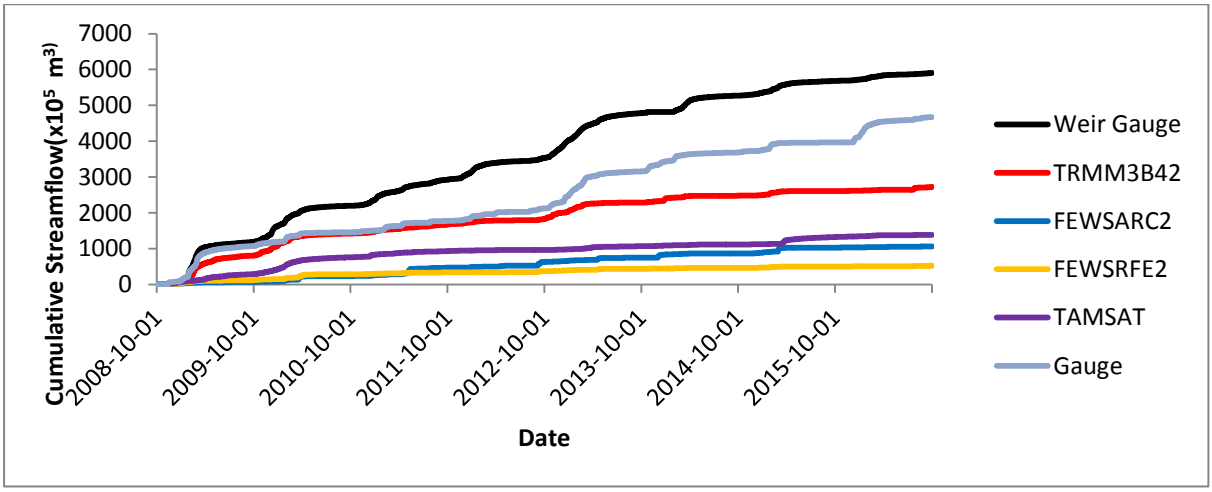

Figure 5.2 Accumulated streamflow for the period 1/10/2008-30/09/2016.

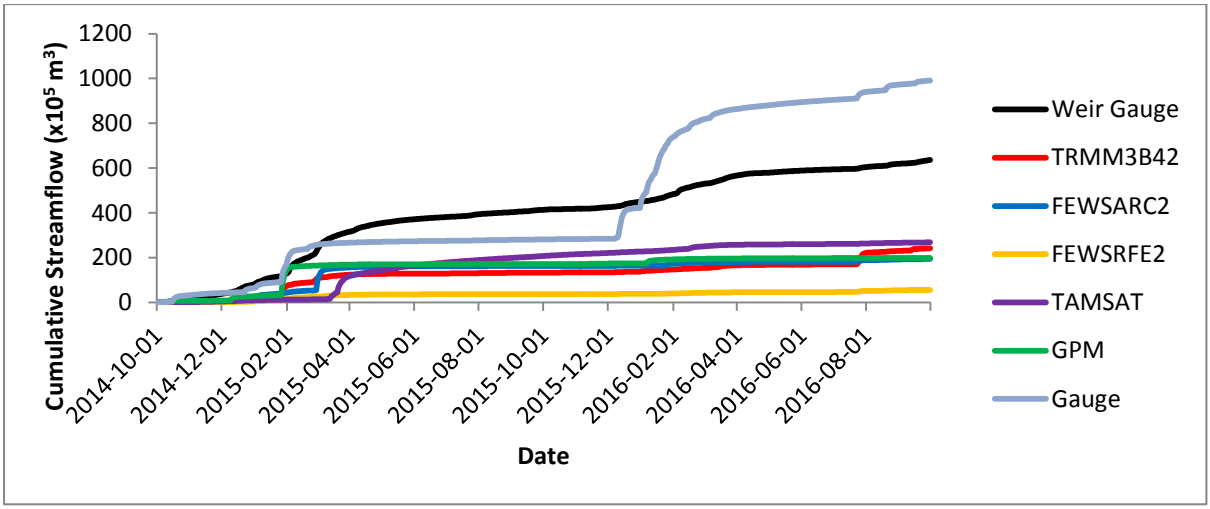

Figure 5.3 Accumulated streamflow for period 1/10/2014-30/19/2016.

5.1.2 U2H007 (Lions River @ Weltervreden)

The streamflows were well represented temporally across all simulations (Appendix C). However, the daily magnitudes of streamflow varied across all simulations (Appendix C). Over the whole period of analysis, both FEWS products and TAMSAT-3 produced an underestimation of total streamflow volumes (RVE %-Table 5.3, Figure 5.4). The TAMSAT-3 driven simulation produced the closest agreement to total observed streamflow volume (RVE %) over the whole period of analysis, even though daily correlations were poor. The rain gauge and TRMM 3B42 driven simulations produced an overestimation of streamflow over the whole period of analysis, with TRMM 3B42 producing a slightly lower percentage of overestimation when compared to the rain gauge driven simulation (Bias, RVE %- Table 5.3, Figure 5.4). It was observed that during the GPM period of analysis, all products

produced an overestimation of streamflow with GPM providing the closest statistical results (Table 5.3, Figure 5.5). The TRMM 3B42 driven simulation produced the closest statistical agreement with observed streamflow over the whole period with the highest correlation (R^2) to daily observed streamflow (Table 5.3). This was due to a closer correlation with high and low flows.

Table 5.3 Statistics comparing observed streamflow and simulated streamflows at Gauge U2H007 (Lions River @ Weltervreden).

	Weir Gauge	**Rain Gauge**	**TRMM3 B42**	**FEWSAR C2**	**FEWSRFE2**	**TAMSATv3**	
Total (m^3)	5.54 x 10^8	7,40 x 10^8	7,06 x 10^8	4,41 x 10^8	3,97 x 10^8	4,83 x 10^8	
Max (m^3/s)	26,61	31,98	56,72	50,45	19,22	17,46	
Mean (m^3/s)	2,19	2,93	2,80	1,75	1,57	1,91	
BIAS		1.34	1,27	0,80	0,72	0,87	
MAE (m^3/s)		0,74	0,60	0,44	0,62	0,28	
RMSE (m^3/s)		3,05	2,94	2,24	2,17	2,17	
RVE (%)		33,60	27,50	-20,28	-28,28	-12,75	
RSQ		0,31	0,45	0,26	0,21	0,21	
STD Dev (m^3/s)		2,97	3,13	2,23	2,00	2,07	
	Weir Gauge	**Rain Gauge**	**TRMM3 B42**	**FEWSAR C2**	**FEWSRFE2**	**TAMSATv3**	**GPM**
Total (m^3)	1,28 x 10^8	2,36 x 10^8	1,83 x 10^8	1,71 x 10^8	1,63 x 10^8	1,81 x 10^8	1,62 x 10^8
Max (m^3/s)	8,10	26,94	19,84	22,65	7,08	17,44	10,82
Mean (m^3/s)	2,03	3,74	2,91	2,71	2,59	2,86	2,57
BIAS		1,84	1,44	1,34	1,28	1,41	1,27
MAE (m^3/s)		1,71	0,88	0,68	0,56	0,84	0,54
RMSE (m^3/s)		1,72	1,87	1,58	1,26	1,57	1,32
RVE (%)		84,46	43,63	33,82	27,69	41,27	26,68
RSQ		0,31	0,50	0,56	0,62	0,56	0,59
STD Dev (m^3/s)		2,79	1,94	1,80	1,63	1,75	1,65

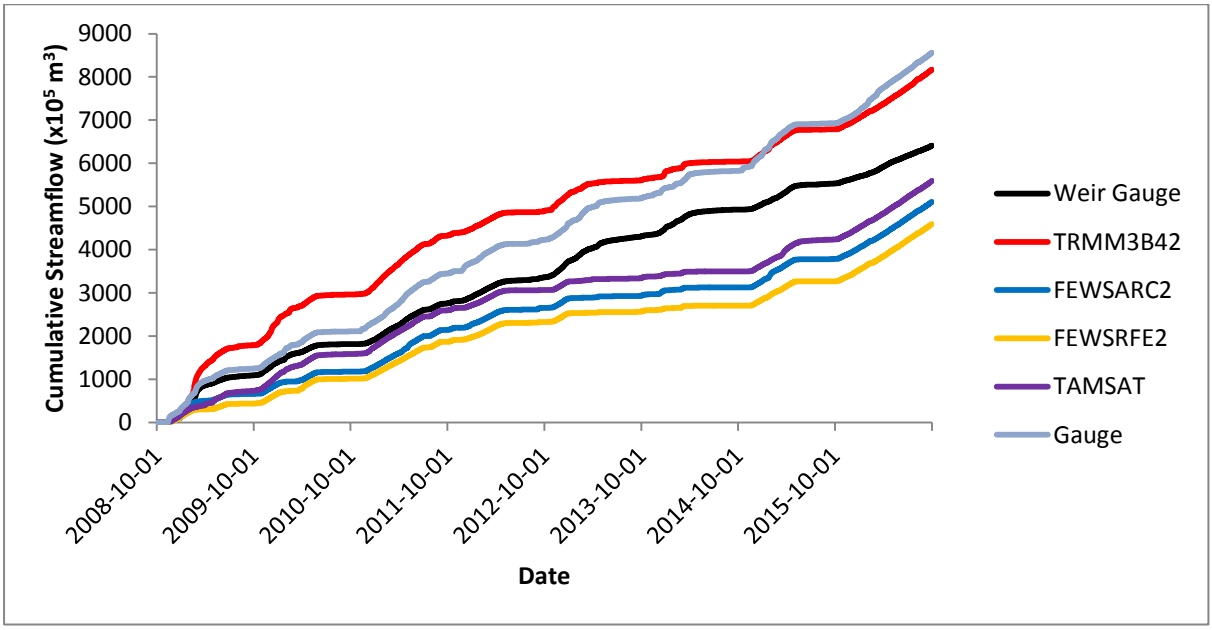

Figure 5.4 Accumulated streamflow for the period 1/10/2008-30/09/2016.

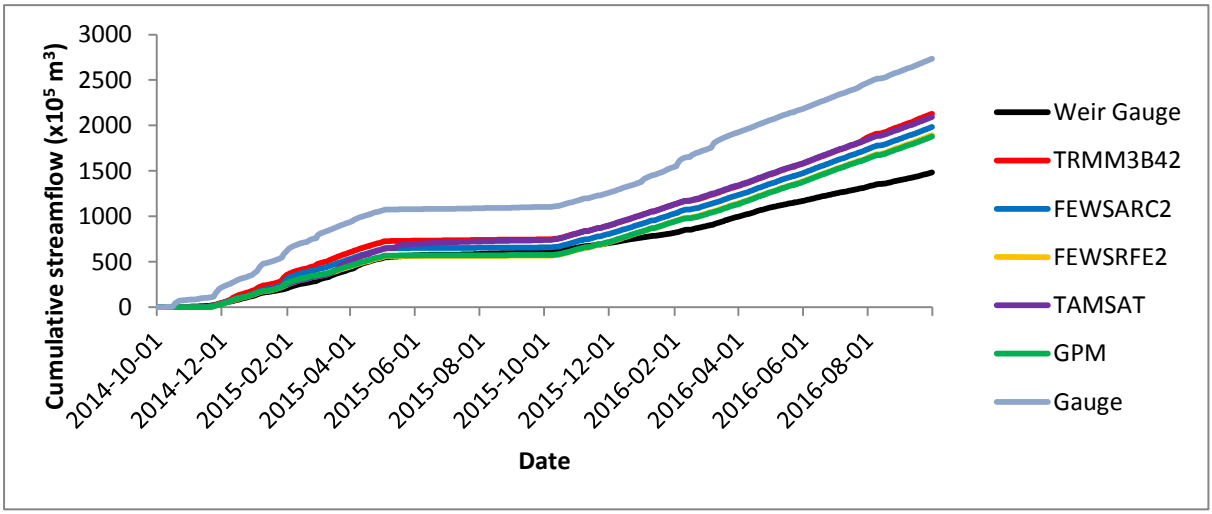

Figure 5.5 Accumulated streamflow for the period 1/10/2014- 30/09/2016.

5.1.3 U2H013 (Mgeni River @ Petrus Stroom)

The streamflow of all simulations were poorly represented at a daily scale (Appendix C). The simulations did not accurately represent the variations of high and low flows when compared to observed streamflow (Appendix C). All simulations underestimated streamflow which was indicated by the low values of bias and RVE % (Table 5.4, Figures 5.6 and 5.7). The TRMM 3B42 driven simulation produced the closest agreement to observed streamflow with the highest correlation (R^2) of daily streamflow with observed streamflow. The TAMSAT-3 driven simulation produced the poorest statistical agreement when compared to observed streamflow. TAMSAT-3 produced the lowest R^2 (Table 5.4) indicating the poorest daily

correlation with observed streamflow. The TAMSAT-3 driven simulation produced the highest percentage of underestimation (RVE %) of streamflow when compared to the other simulations of streamflow. It is observed that the catchments represented by this streamflow gauge involve complex topography. The satellite derived products may inaccurately estimate rainfall generated by the complex topography which may have been amplified through the modelling process that used averaged area-weighted rainfall estimates. This may be the cause of underestimation of streamflow across all satellite rainfall products.

Table 5.4 Statistics comparing observed streamflow and simulated streamflows at Gauge U2H013 (Mgeni River @ Petrus Stroom).

	Weir Gauge	**Rain Gauge**	**TRMM3 B42**	**FEWSARC 2**	**FEWSRFE2**	**TAMSATv3**	
Total (m^3)	1,71 x 10^9	6,48 x 10^8	6,41 x 10^8	4,50 x 10^8	3,98 x 10^8	3,73 x 10^8	
Max (m^3/s)	91,64	61,68	50,74	91,21	47,01	28,10	
Mean (m^3/s)	6,77	2,57	2,54	1,78	1,58	1,48	
BIAS		0,38	0,3	0,26	0,23	0,22	
MAE (m^3/s)		4,21	4,18	4,99	5,20	5,30	
RMSE (m^3/s)		8,53	8,21	9,50	9,59	10,26	
RVE (%)		-62,09	-60,50	-73,71	-76,75	-78,21	
RSQ		0,39	0,45	0,26	0,34	0,15	
STD Dev (m^3/s)		7,59	7,55	7,53	7,34	7,21	
	Weir Gauge	**Rain Gauge**	**TRMM3 B42**	**FEWSARC 2**	**FEWSRFE2**	**TAMSATv3**	**GPM**
Total (m^3)	2,43 x 10^8	7,88 x 10^7	6,93 x 10^7	8,91 x 10^7	6,24 x 10^7	8,44 x 10^7	2,04 x 10^7
Max (m3/s)	44,84	17,65	20,30	65,65	10,69	28,10	3,63
Mean (m3/s)	3,85	1,25	1,10	1,41	0,99	1,34	0,32
BIAS		0,32	0,28	0,37	0,26	0,35	0,08
MAE (m3/s)		2,60	2,75	2,44	2,86	2,51	3,52
RMSE (m3/s)		2,63	5,44	5,66	5,59	5,95	6,19
RVE (%)		-67,63	-71,53	-63,38	-74,37	-65,30	-91,60
RSQ		0,29	0,25	0,13	0,27	0,02	0,21
STD Dev		4,11	4,10	4,59	4,04	4,21	4,12

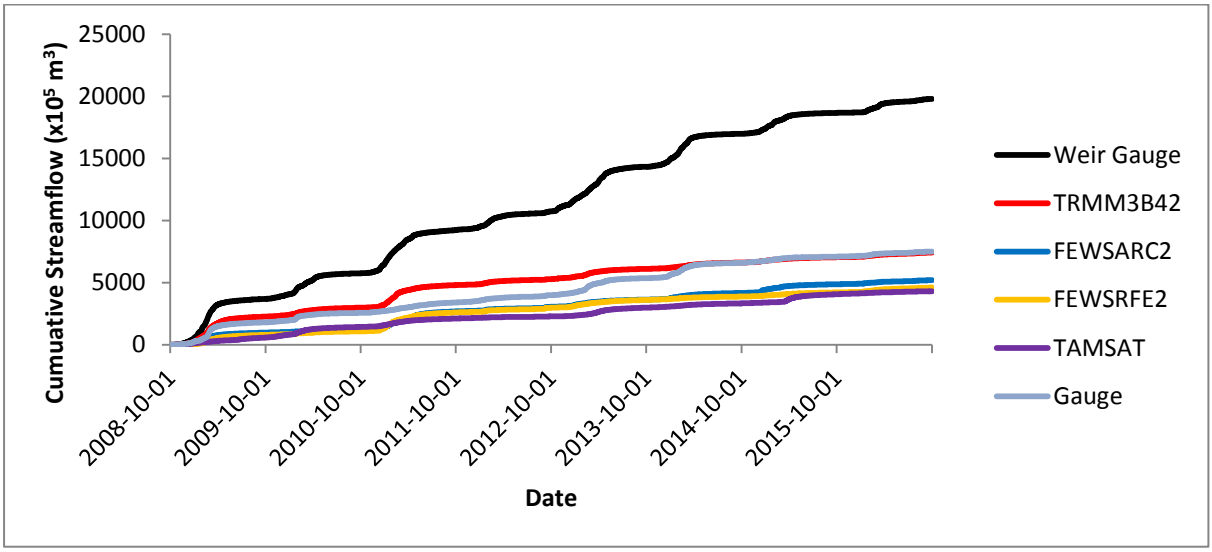

Figure 5.6 Accumulated streamflow for the period 1/10/2008-30/09/2016.

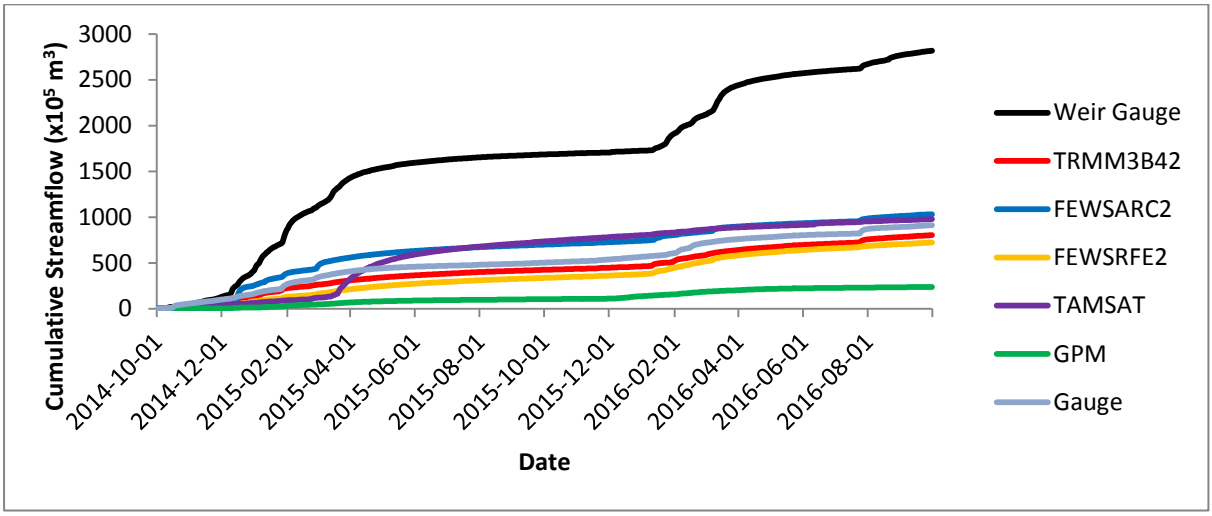

Figure 5.7 Accumulated streamflow for the period 1/10/2014-30/09/2016.

5.2 Upper uThukela Catchment

The upper uThukela catchment streamflow modelling was analysed at three streamflow gauges in the catchment (Table 5.5). Figure 5.8 shows the locations of rain gauges used to drive the sub-catchments as well as the location of the streamflow gauges in the catchment. The rain gauge 0268883 6 was used as the driver rain gauge for the catchments shaded in pink and rain gauge V3E002 was used as the driver rain gauge for the catchments shaded in light green (Figure 5.8).

Table 5.5 Weir details used in the uThukela modelling.

Weir Gauge	Name	Latitude	Longitude
V6H004	Sondags River @ Kleinfontein	-28.40458	30.01280
V7H017	Boesmans River @ Drakensberg Loc 1	-29.18516	29.63708
V2H006	Little Mooi River @ Dartington	-29.26619	29.86800

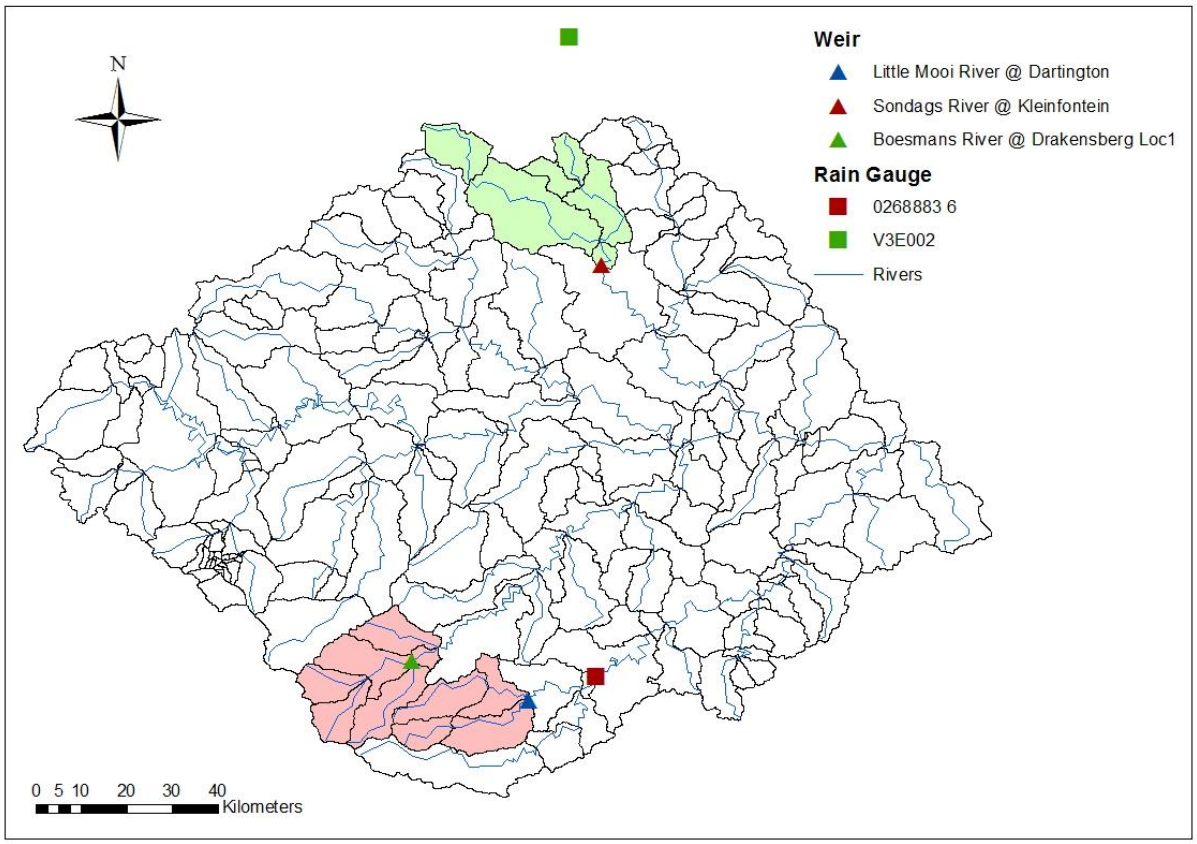

Figure 5.8 Weir and rain gauge locations with respect to catchment boundaries.

5.2.1 V6H004 (Sondags River @ Kleinfontein)

The streamflow of all simulations were poorly represented at a daily scale (Appendix C). The simulations did not accurately represent the variations of high and low flows when compared to observed streamflow (Appendix C). R^2 values of all simulations were low which indicated a poor correlation of streamflow between simulations and observed streamflow at a daily scale (Table 5.6). The TAMSAT-3 driven simulation produced the lowest R^2 value (Table 5.6) indicating the poorest daily correlation with observed streamflow. Over the whole period of analysis, total streamflow volumes were underestimated (RVE %), with the TAMSAT-3

driven simulation underestimating streamflow volume the greatest and the rain gauge driven simulation underestimating streamflow volume the least (Table 5.3). The rain gauge and TRMM 3B42 driven simulations produced the closest statistical agreement with observed streamflow over the period of analysis with TAMSAT-3 producing the worst (Table 5.3, Figure 5.9). The GPM driven simulation produced the highest percentage of underestimation during the period of analysis (RVE %-Table 5.6, Figure 5.10).

Table 5.6 Statistics comparing observed streamflow and simulated streamflows at Gauge V6H004 (Sondags River @ Kleinfontein).

	Weir Gauge	**Rain Gauge**	**TRMM3 B42**	**FEWSAR C2**	**FEWSRFE2**	**TAMSATv3**	
Total (m^3)	$6{,}14 \times 10^8$	$6{,}09 \times 10^8$	$5{,}61 \times 10^8$	$3{,}77 \times 10^8$	$3{,}59 \times 10^8$	$1{,}89 \times 10^8$	
Max (m^3/s)	75,90	87,59	92,05	109,74	118,65	47,35	
Mean (m^3/s)	2,43	2,41	2,22	1,49	1,42	0,75	
BIAS		0,99	0,91	0,61	0,58	0,31	
MAE (m^3/s)		0,02	0,21	0,94	1,01	1,68	
RMSE (m^3/s)		6,08	5,93	6,76	6,06	6,37	
RVE (%)		-0,96	-8,77	-38,64	-41,51	-69,19	
RSQ		0,29	0,25	0,18	0,20	0,04	
STD Dev (m^3/s)		6,30	5,89	6,23	5,66	4,73	
	Weir Gauge	**Rain Gauge**	**TRMM3 B42**	**FEWSAR C2**	**FEWSRFE2**	**TAMSATv3**	**GPM**
Total (m^3)	$3{,}39 \times 10^7$	$4{,}17 \times 10^7$	$2{,}73 \times 10^7$	$7{,}02 \times 10^7$	$4{,}99 \times 10^7$	$6{,}44 \times 10^7$	$1{,}84 \times 10^7$
Max (m^3/s)	16,53	30,16	12,65	96,88	34,24	34,65	12,09
Mean (m^3/s)	0,54	0,66	0,43	1,11	0,79	1,02	0,29
BIAS		1,23	0,80	2,07	1,47	1,90	0,54
MAE (m^3/s)		0,12	0,10	0,57	0,25	0,48	0,24
RMSE (m^3/s)		1,27	1,61	5,68	2,42	2,87	1,52
RVE (%)		23,04	-19,54	107,31	47,24	90,15	-45,72
RSQ		0,06	0,15	0,15	0,20	0,18	0,18
STD Dev (m^3/s)		2,05	1,44	4,47	2,20	2,50	1,35

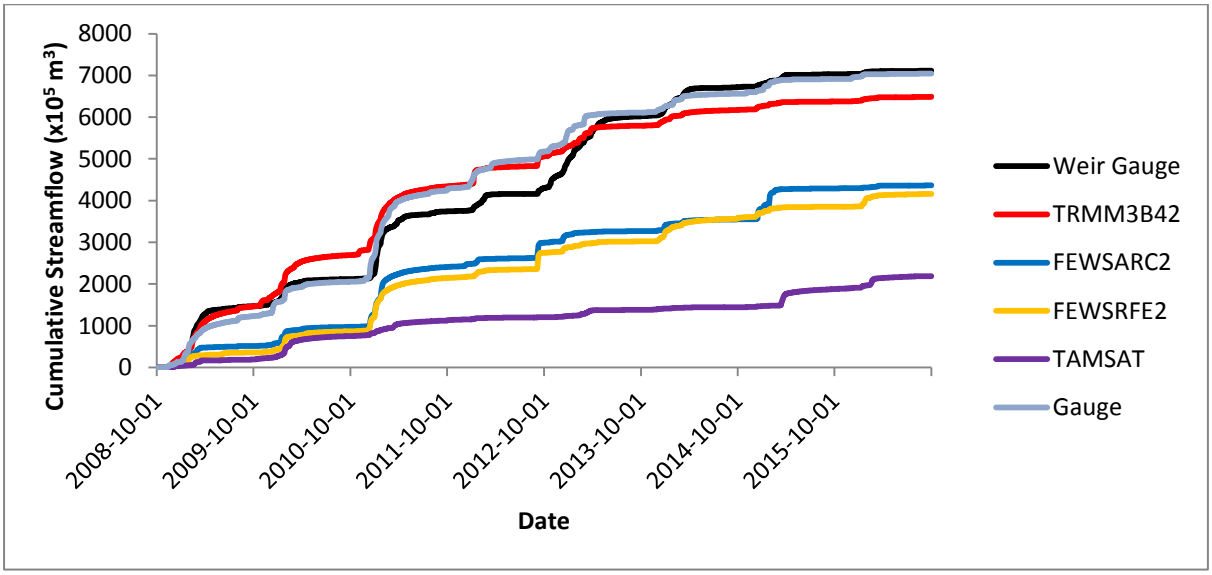

Figure 5.9 Accumulated streamflow for the period 1/10/2008-30/09/2016.

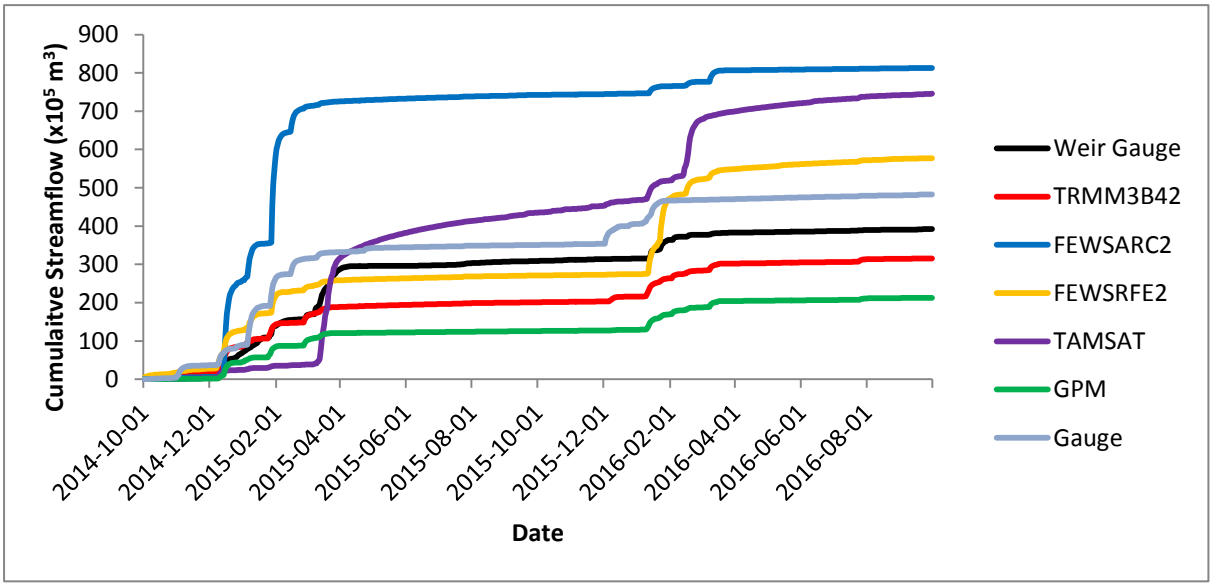

Figure 5.10 Accumulated streamflow for the period 1/10/2014-30/09/2016.

5.2.2 V7H017 (Boesmans River @ Drakensberg Loc 1)

The streamflow of all simulations were poorly represented at a daily scale (Appendix C). The simulations did not accurately represent the variations of high and low flows when compared to observed streamflow (Appendix C). R^2 values of all simulations were low which indicated a poor correlation of streamflow between simulations and observed streamflow at a daily scale (Table 5.7). The poorest daily correlation (R^2) over the whole period of analysis was produced by the FEWS ARC2 product. The TRMM 3B42 driven simulation produced the highest R^2 value when compared to the other simulations of streamflow. All simulations of streamflow underestimated the total volume of streamflow when compared to the total

volume of observed streamflow over the period of analysis (Bias, RVE %-Table 5.7, Figures 5.11 and 5.12). The FEWS RFE2 driven simulation produced the highest percentage of underestimation where-as the TRMM 3B42 driven simulation produced the lowest percentage of underestimation (Table 5.7). The GPM driven simulation produced the highest percentage of underestimation when compared to the other satellite product driven simulations over the period of analysis (Bias, RVE %-Table 5.7). The TRMM 3B42 driven simulation produced the closest statistical agreement with observed streamflow, whereas FEWS ARC2 produced the worst.

It is observed that the catchments represented by this streamflow gauge involve complex topography. The satellite derived products may inaccurately estimate rainfall generated by the complex topography which may have been amplified through the modelling process that used averaged area-weighted rainfall estimates. This may be the cause of underestimation of streamflow across all satellite rainfall products.

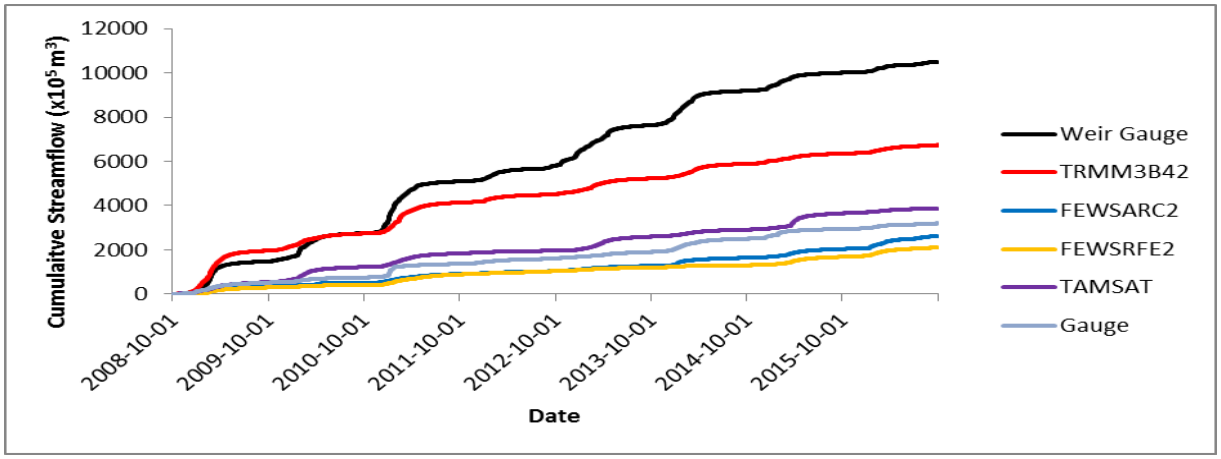

Figure 5.11 Accumulated streamflow for the period 1/10/2008-30/09/2016.

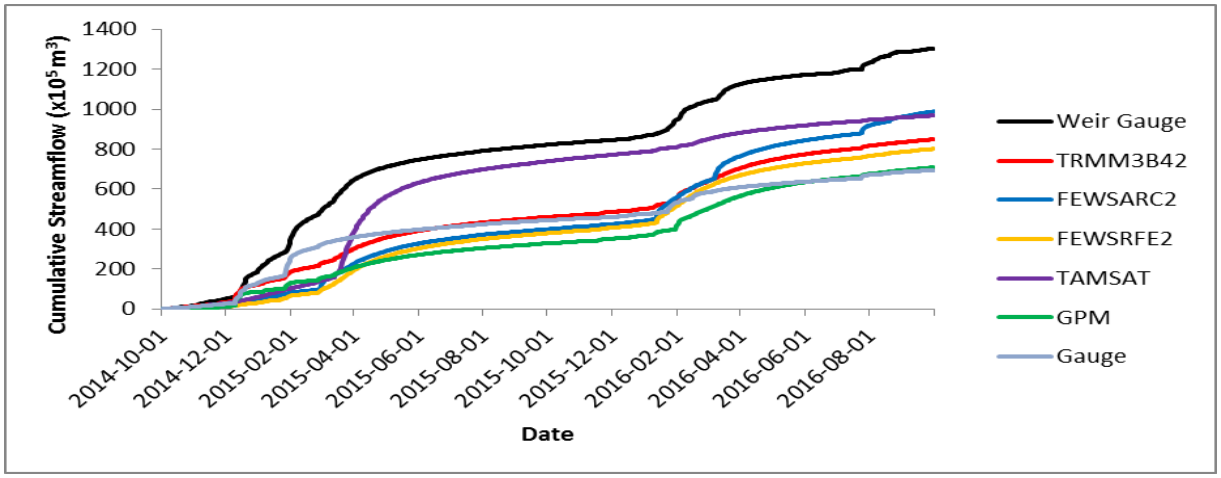

Figure 5.12 Accumulated streamflow for the period 1/10/2014-30/09/2016.

Table 5.7 Statistics comparing observed streamflow and simulated streamflows at Gauge V7H017 (Boesmans River @ Drakenberg Loc 1).

	Weir Gauge	**Rain Gauge**	**TRMM3 B42**	**FEWSARC 2**	**FEWSRFE2**	**TAMSATv3**	
Total (m^3)	$9{,}06 \times 10^8$	$2{,}76 \times 10^8$	$5{,}82 \times 10^8$	$2{,}26 \times 10^8$	$1{,}81 \times 10^8$	$3{,}35 \times 10^8$	
Max (m^3/s)	60,62	35,32	42,49	28,34	14,20	24,99	
Mean (m^3/s)	3,59	1,09	2,31	0,90	0,72	1,33	
BIAS		0,30	0,64	0,25	0,20	0,37	
MAE (m^3/s)		2,50	1,28	2,69	2,87	2,26	
RMSE (m^3/s)		5,22	4,55	5,89	5,95	5,48	
RVE (%)		-69,56	-35,76	-75,00	-79,97	-63,04	
RSQ		0,34	0,37	0,09	0,14	0,19	
STD Dev (m^3/s)		4,37	4,67	4,26	4,21	4,22	
	Weir Gauge	**Rain Gauge**	**TRMM3 B42**	**FEWSARC 2**	**FEWSRFE2**	**TAMSATv3**	**GPM**
Total (m^3)	$1{,}12 \times 10^8$	$6{,}00 \times 10^7$	$7{,}33 \times 10^7$	$8{,}53 \times 10^7$	$6{,}92 \times 10^7$	$8{,}36 \times 10^7$	$6{,}12 \times 10^7$
Max (m^3/s)	18,41	32,92	20,82	23,23	13,32	24,99	20,53
Mean (m^3/s)	1,78	0,95	1,16	1,35	1,10	1,32	0,97
BIAS		0,53	0,65	0,76	0,62	0,74	0,54
MAE (m^3/s)		0,83	0,62	0,43	0,68	0,45	0,81
RMSE (m3/s)		1,16	2,30	2,55	2,28	2,82	2,46
RVE (%)		-46,56	-34,70	-24,03	-38,41	-25,56	-45,52
RSQ		0,27	0,16	0,10	0,15	0,07	0,11
STD Dev (m^3/s)		2,23	1,99	2,14	1,89	2,31	1,99

5.2.3 V2H006 (Little Mooi River @ Dartington)

The streamflow of all simulations were poorly represented at a daily scale (Appendix C). The simulations did not accurately represent the variations of high and low flows when compared to observed streamflow (Appendix C). R^2 values of all simulations were low which indicated a poor correlation of streamflow between simulations and observed streamflow at a daily scale (Table 5.8). The TAMSAT-3 driven simulations of streamflow produced the lowest R^2 when compared to the other simulations indicating the poorest correlation with daily observed streamflow. The rain gauge driven simulation produced the highest R^2 when compared to the other simulations indicating the best daily correlation with observed streamflow from all simulations. All simulations underestimated total streamflow volumes when compared to the total streamflow volume of the observed streamflow (Bias, RVE %-Table 5.8). Both FEWS product driven simulations underestimated streamflow by the highest percentage when compared to the other simulations (Table 5.8, Figure 5.13 and 5.14). The TRMM 3B42 driven simulation showed the closest agreement to total streamflow volume when compared to total observed streamflow volume. The TRMM 3B42 driven simulation produced the closest statistical agreement with observed streamflow.

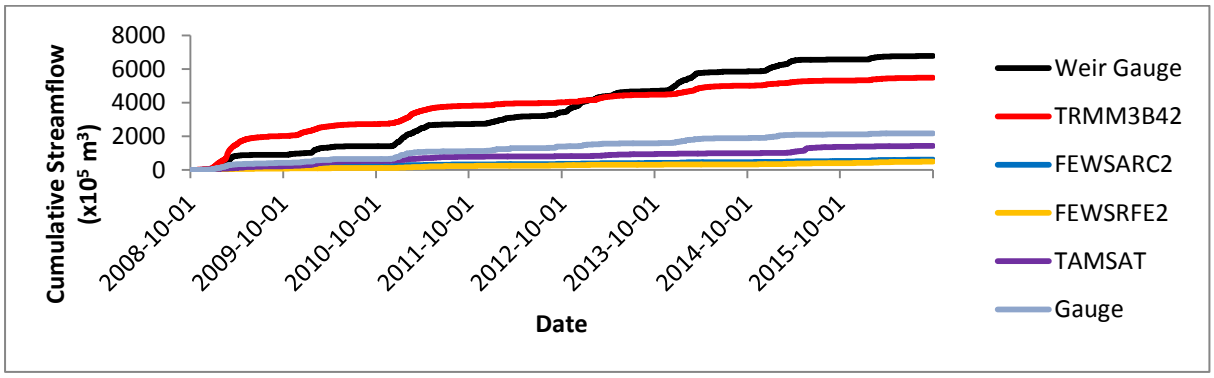

Figure 5.13 Accumulated streamflow for the period 1/10/2008-30/09/2016.

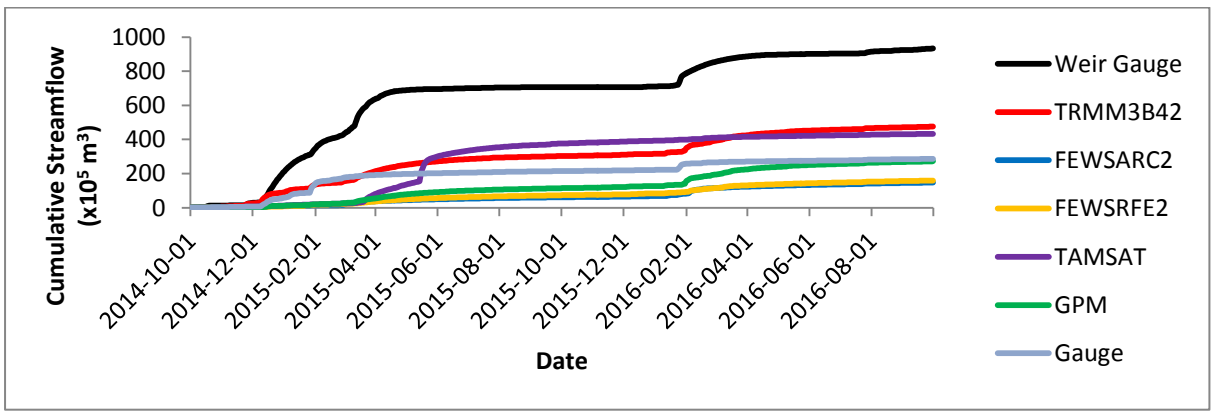

Figure 5.14 Accumulated streamflow for the period 1/10/2014-30/09/2016.

Table 5.8 Statistics comparing observed streamflow and simulated streamflow at V2H006 (Little Mooi River @ Dartington)

	Weir Gauge	**Rain Gauge**	**TRMM3 B42**	**FEWSAR C2**	**FEWSRF E2**	**TAMSATv 3**	
Total (m^3)	$5{,}86 \times 10^8$	$1{,}88 \times 10^8$	$4{,}74 \times 10^8$	$5{,}28 \times 10^7$	$4{,}23 \times 10^7$	$1{,}23 \times 10^8$	
Max (m^3/s)	18,12	24,78	59,35	9,19	5,88	32,91	
Mean (m^3/s)	2,32	0,75	1,88	0,21	0,17	0,49	
BIAS		0,32	0,81	0,09	0,07	0,21	
MAE (m^3/s)		1,58	0,44	2,11	2,15	1,83	
RMSE (m^3/s)		3,86	4,10	4,44	4,51	4,49	
RVE (%)		-67,89	-19,17	-90,99	-92,77	-78,99	
RSQ		0,24	0,22	0,13	0,11	0,01	
STD Dev (m^3/s)		3,27	3,95	3,07	3,07	3,13	
	Weir Gauge	**Rain Gauge**	**TRMM3 B42**	**FEWSAR C2**	**FEWSRF E2**	**TAMSATv 3**	**GPM**
Total (m^3)	$8{,}06 \times 10^7$	$2{,}47 \times 10^7$	$4{,}11 \times 10^7$	$1{,}27 \times 10^7$	$1{,}37 \times 10^7$	$3{,}74 \times 10^7$	$2{,}35 \times 10^7$
Max (m^3/s)	17,24	16,38	17,31	8,25	3,12	32,91	11,86
Mean (m^3/s)	1,28	0,39	0,65	0,20	0,22	0,59	0,37
BIAS		0,31	0,51	0,16	0,17	0,46	0,29
MAE (m^3/s)		0,88	0,63	1,07	1,06	0,68	0,90
RMSE (m^3/s)		1,15	2,33	2,64	2,64	3,22	2,56
RVE (%)		-69,37	-49,05	-84,25	-82,98	-53,58	-70,83
RSQ		0,26	0,18	0,05	0,06	0,00	0,06
STD Dev (m^3/s)		2,00	1,96	1,85	1,83	2,27	1,87

5.3 Upper and Central Breede Catchment

The upper and central Breede catchment streamflow modelling was analysed at three streamflow gauges at weirs in the catchment (Table 5.9). Figure 5.15 shows the location of the rain gauges used to drive the sub-catchments as well as the location of the streamflow gauges in the catchment. The rain gauge 0022729 X was used as the driver rain gauge for the catchments shaded in pink and H1E003 was used as the driver rain gauge for the catchments shaded in light green (Figure 5.15).

Table 5.9 Weir details used in the upper and central Breede catchment modelling.

Weir Gauge	**Name**	**Latitude**	**Longitude**
H1H013	Koekedou River @ Ceres	-33.35972	19.29833
H4H016	Keisers @ Mc Gregor Toeken Geb	-33.93944	19.84055
H4H018	Poesjenels @ Le Chasseur	-33.86777	19.71611

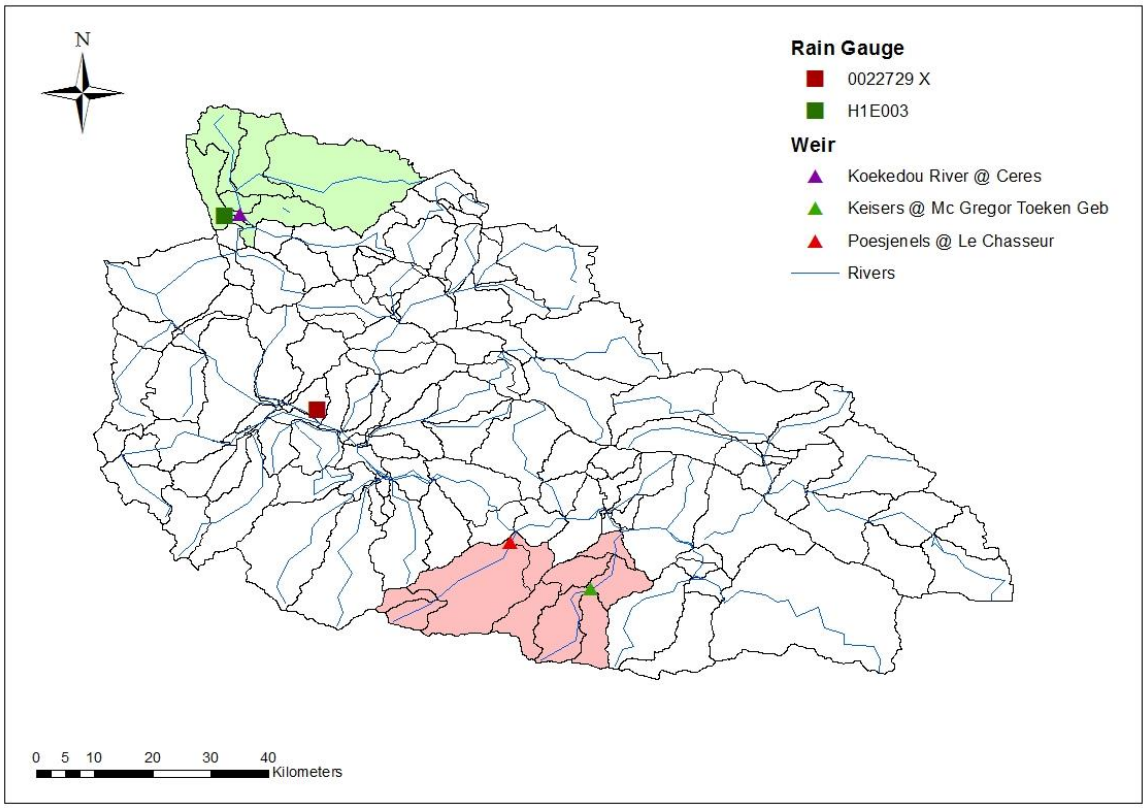

Figure 5.15 Weir and driver rain gauge locations with respect to sub-catchment boundaries.

5.3.1 H1H013 (Koekedou River @ Ceres)

The streamflow of all simulations were remarkably poorly simulated (Appendix C). The simulations did not represent the variations of high and low flows when compared to observed streamflow (Appendix C). The satellite rainfall product driven simulations produced poor daily correlations as well as produced high percentages of underestimation of total streamflow volumes when compared to the observed streamflow (Figures 5.16 and 5.17, Bias, RVE %-Table 5.10). RMSE's were low due to the simulated streamflow data not representing fluctuations of streamflow, this is shown by the low mean and maximum values achieved when compared to observed streamflow mean values (Table 5.10). The rain gauge driven simulation produced the closest daily correlation (R^2) and overestimated total streamflow volume when compared to observed streamflow (Table 5.10, Figures 5.16 and 5.17).

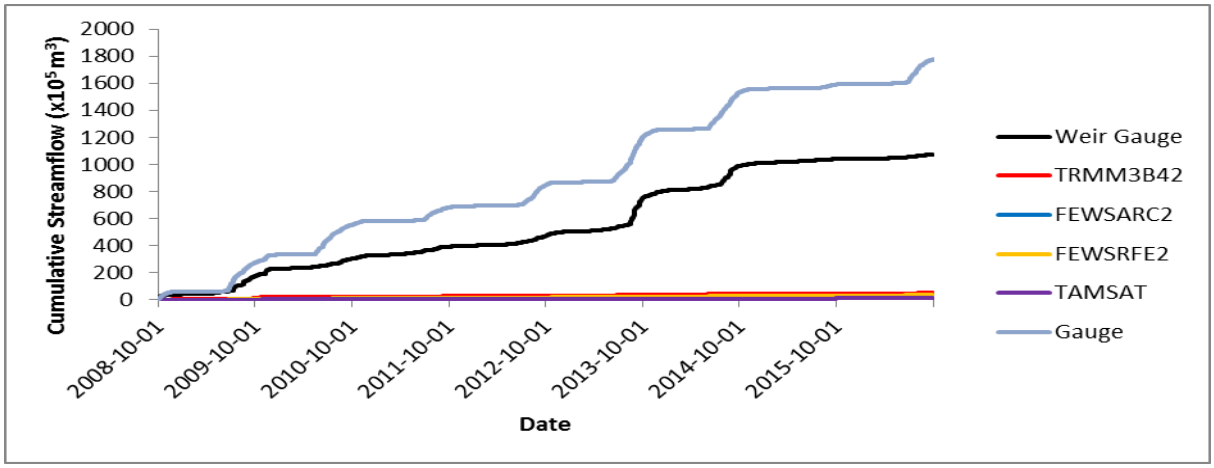

Figure 5.16 Accumulated streamflow for the period 1/10/2008-30/09/2016.

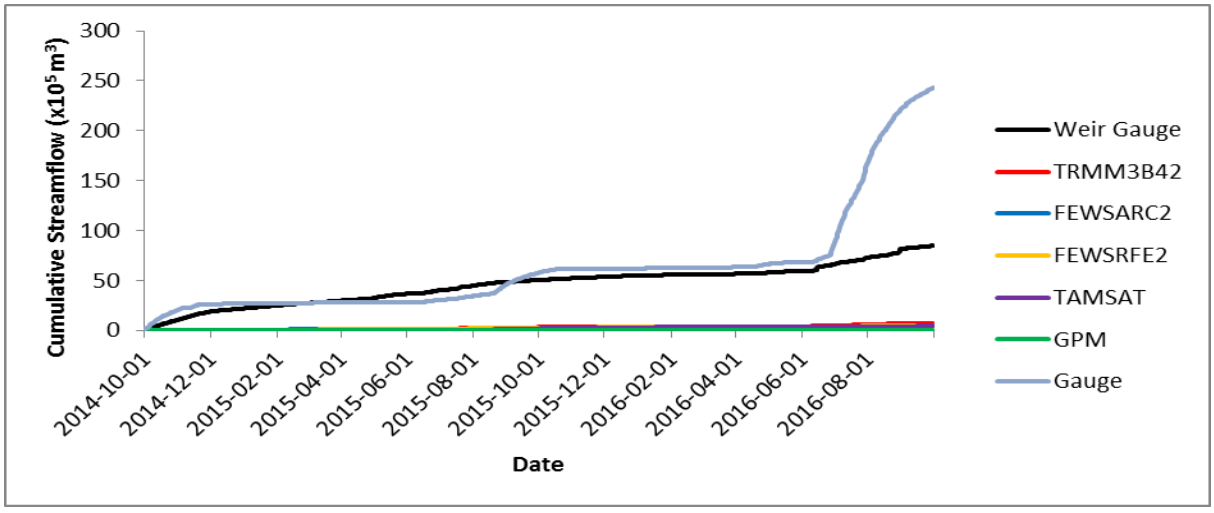

Figure 5.17 Accumulated streamflow for the period 1/10/2014-30/09/2016.

Table 5.10 Statistics comparing observed streamflow and simulated streamflow at H1H013 (Koekedou River @ Ceres).

	Weir Gauge	**Rain Gauge**	**TRMM3 B42**	**FEWSAR C2**	**FEWSRF E2**	**TAMSA Tv3**	
Total (m^3)	$9{,}28 \times 10^7$	$1{,}53 \times 10^8$	$4{,}30 \times 10^6$	$1{,}70 \times 10^6$	$2{,}93 \times 10^6$	$1{,}06 \times 10^6$	
Max (m^3/s)	13,83	11,34	1,16	0,41	0,44	0,10	
Mean (m^3/s)	0,37	0,61	0,02	0,01	0,01	0,00	
BIAS		1,65	0,05	0,02	0,03	0,01	
MAE (m^3/s)		0,24	0,35	0,36	0,36	0,36	
RMSE (m^3/s)		0,88	0,95	0,96	0,96	0,96	
RVE (%)		65,40	-95,36	-98,16	-96,84	-98,86	
RSQ		0,38	0,05	0,03	0,04	0,02	
STD Dev (m^3/s)		0,96	0,66	0,66	0,66	0,66	
	Weir Gauge	**Rain Gauge**	**TRMM3 B42**	**FEWSAR C2**	**FEWSRF E2**	**TAMSA Tv3**	**GPM**
Total (m^3)	$7{,}33 \times 10^6$	$2{,}10 \times 10^7$	$6{,}51 \times 10^5$	$4{,}22 \times 10^5$	$4{,}23 \times 10^5$	$3{,}81 \times 10^5$	$7{,}00 \times 10^4$
Max (m^3/s)	2,56	4,96	0,22	0,41	0,15	0,10	0,02
Mean (m^3/s)	0,12	0,33	0,01	0,01	0,01	0,01	0,00
BIAS		2,87	0,09	0,06	0,06	0,05	0,01
MAE (m^3/s)		0,22	0,11	0,11	0,11	0,11	0,11
RMSE (m^3/s)		0,34	0,19	0,19	0,19	0,20	0,20
RVE (%)		186,58	-91,11	-94,24	-94,23	-94,80	-99,04
RSQ		0,11	0,03	0,00	0,08	0,00	0,02
STD Dev (m^3/s)		0,51	0,13	0,13	0,13	0,13	0,13

The extremely poor performance of the products at this location warranted an extra validation study to further understand the performance. The products were validated at rain gauge H1E008 (Ceres Dam). Performance of the products produced poor results with a considerable underestimation of rainfall at the point scale (Table 5.11). It is noted that the area of interest involves complex topography which may be the cause of the products inability to estimate rainfall in this region, which is further exploited when used to drive the model which

produced poor streamflow results. The products may be unable to estimate rainfall produced due to the aforementioned mid-latitude weather systems as well as topographical influences (Thorne *et al*., 2001).

Table 5.11 Validation of products at H1E003.

	Rain Gauge	**TRMM 3B42**	**FEWSA RC2**	**FEWS RFE2**	**TAMSAT v3**	**Rain Gauge (GPM analysis)**	**GPM**
Total (mm)	10553,50	2951,10	2364,11	2784,80	2752,90	2023,20	569,90
Max (mm)	100,00	108,00	102,63	87,50	54,10	28,30	32,70
Mean (mm)	3,94	1,10	0,88	1,04	1,03	0,69	0,50
BIAS		0,28	0,22	0,26	0,26		0,72
MAE (mm)		2,84	3,06	2,90	2,91		0,20
RMSE (mm)		11,38	9,74	10,54	12,87		2,88
RVE (%)		-72,04	-77,60	-73,61	-73,91		-28,17
RSQ		0,18	0,26	0,33	0,00		0,22

5.3.2 H4H016 (Keisers @ Mc Gregor Toeken Geb)

The streamflow of all simulations were poorly represented at a daily scale (Appendix C). The simulations did not represent the variations of high and low flows when compared to observed streamflow (Appendix C). The daily correlations (R^2) of all simulations were low indicating a poor relationship with daily observed streamflow (Table 5.13). The TAMSAT-3 driven simulation produced the lowest R^2 value indicating the poorest correlation to daily observed streamflow. Both FEWS driven simulations produced the highest values of R^2 when compared to the other simulations. Apart from TAMSAT-3 and GPM, all simulations overestimated streamflow volumes (RVE%-Table 5.13, Figure 5.18 and 5.19). The rain gauge driven simulation produced the highest percentage (RVE %) of overestimation when compared to the other simulations. Both FEWS driven simulations produced the closest agreement with total streamflow volumes. The GPM driven simulation produced the poorest statistical agreement with observed streamflow. GPM performed poorly in estimating rainfall in this region.

The southern border involves complex topography in the catchments represented by this streamflow gauge. The satellite derived products may inaccurately estimate rainfall generated by the complex topography which may have been amplified through the modelling process that used averaged area-weighted rainfall estimates. This may be the cause of inaccuracy of streamflow across all satellite rainfall products.

Table 5.12 Statistics comparing observed streamflow and simulated streamflow at H4H016 (Keisers @ Mc Gregor Toeken Geb).

	Weir Gauge	**Rain Gauge**	**TRMM3 B42**	**FEWSA RC2**	**FEWSRF E2**	**TAMSATv 3**	
Total (m^3/s)	$4{,}50 \times 10^7$	$1{,}05 \times 10^8$	$8{,}52 \times 10^7$	$4{,}63 \times 10^7$	$4{,}90 \times 10^7$	$1{,}93 \times 10^7$	
Max (m^3/s)	37,98	26,01	19,83	15,22	10,70	2,48	
Mean (m^3/s)	0,18	0,42	0,34	0,18	0,19	0,08	
BIAS		2,34	1,89	1,03	1,09	0,43	
MAE (m^3/s)		0,24	0,16	0,01	0,02	0,10	
RMSE (m^3/s)		1,26	1,21	1,13	1,15	1,23	
RVE (%)		133,83	89,43	2,89	8,99	-57,04	
RSQ		0,12	0,20	0,25	0,18	0,01	
STD Dev		1,07	1,11	0,94	0,91	0,88	
	Weir Gauge	**Rain Gauge**	**TRMM3 B42**	**FEWSA RC2**	**FEWSRF E2**	**TAMSATv 3**	**GPM**
Total (m^3)	$9{,}12 \times 10^6$	$1{,}31 \times 10^7$	$1{,}26 \times 10^7$	$1{,}16 \times 10^7$	$5{,}37 \times 10^6$	$3{,}74 \times 10^6$	$6{,}22 \times 10^4$
Max (m^3/s)	11,35	1,14	14,79	2,33	0,86	0,45	0,01
Mean (m^3/s)	0,14	0,21	0,20	0,18	0,09	0,06	0,01
BIAS		1,43	1,38	1,27	0,59	0,41	0,01
MAE (m^3/s)		0,06	0,06	0,04	0,06	0,09	0,14
RMSE (m^3/s)		0,32	0,73	0,59	0,61	0,63	0,64
RVE (%)		43,50	38,20	27,21	-41,09	-58,98	-99,32
RSQ		0,04	0,24	0,13	0,09	0,00	0,04
STD Dev (m^3/s)		0,48	0,72	0,48	0,45	0,45	0,45

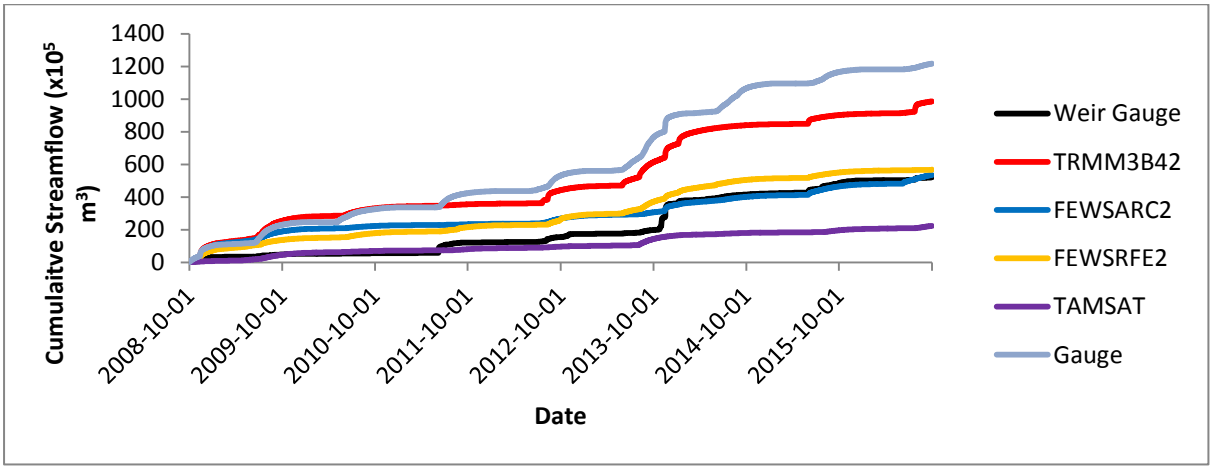

Figure 5.18 Accumulated streamflow for the period 1/10/2008-30/09/2016.

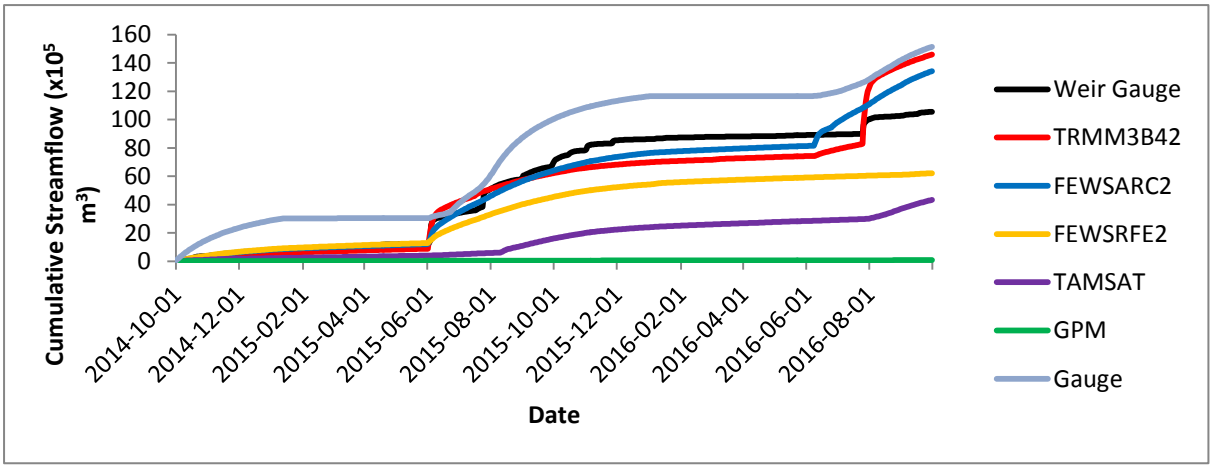

Figure 5.19 Accumulated streamflow for the period 1/10/2014-30/09/2016.

5.3.3 H4H018 (Poesjenels @ Le Chasseur)

The streamflow of all simulations were poorly represented at a daily scale (Appendix C). The simulations did not represent the variations of high and low flows when compared to observed streamflow (Appendix C). The daily correlations (R^2) of all simulations were low indicating a poor relationship with daily observed streamflow (Table 5.13). The TRMM 3B42 driven simulation produced the highest R^2 indicating the closest correlation to daily observed streamflow. Apart from TAMSAT-3 and GPM, all simulations overestimated streamflow volumes (RVE %- Table 5.13, Figure 5.20 and 5.21). The TRMM 3B42 simulation produced the highest total volume of streamflow when compared to the other simulations. The GPM driven simulation produced the highest percentage of underestimation compared to the other simulations (Figure 5.21). The FEWS RFE2 driven simulation produced the closest agreement to total streamflow volume when compared to observed streamflow. Even though the TAMSAT-3 driven simulation produced the poorest daily correlation to observed

streamflow, the total volume of simulated streamflow was in closer agreement with observed streamflow than the rain gauge, TRMM 3B42, FEWS ARC2 and GPM driven simulations of streamflow.

The southern border involves complex topography in the catchments represented by this streamflow gauge. The satellite derived products may inaccurately estimate rainfall generated by the complex topography which may have been amplified through the modelling process that used averaged area-weighted rainfall estimates. This may be the cause of inaccuracy of streamflow across all satellite rainfall products.

Table 5.13 Statistics comparing observed streamflow and simulated streamflow at H4H018 (Poesjenels @ Le Chasseur).

	Weir Gauge	**Rain Gauge**	**TRMM3 B42**	**FEWSAR C2**	**FEWSRF E2**	**TAMSATv 3**	
Total (m^3)	$6,09 \times 10^7$	$1,89 \times 10^8$	$2,34 \times 10^8$	$1,59 \times 10^8$	$8,72 \times 10^7$	$4,79 \times 10^7$	
Max (m^3/s)	5,21	8,34	46,69	18,33	34,97	3,96	
Mean (m^3/s)	0,28	0,75	0,93	0,63	0,35	0,19	
BIAS		2,74	3,39	2,30	1,26	0,69	
MAE (m^3/s)		0,48	0,65	0,36	0,07	0,08	
RMSE (m^3/s)		1,15	2,37	1,18	1,11	0,75	
RVE (%)		174,39	239,09	130,16	26,39	-30,59	
RSQ		0,15	0,18	0,09	0,09	0,03	
STD Dev (m^3/s)		0,95	1,87	0,95	0,93	0,58	
	Weir Gauge	**Rain Gauge**	**TRMM3 B42**	**FEWSAR C2**	**FEWSRF E2**	**TAMSATv 3**	**GPM**
Total (m^3)	$1,55 \times 10^7$	$2,89 \times 10^7$	$3,29 \times 10^7$	$2,59 \times 10^7$	$4,29 \times 10^6$	$1,09 \times 10^7$	$6,35 \times 10^5$
Max (m^3/s)	5,21	3,46	38,53	6,44	0,48	1,98	0,40
Mean (m^3/s)	0,25	0,46	0,52	0,41	0,08	0,17	0,01
BIAS		1,87	2,12	1,67	0,32	0,70	0,04
MAE (m^3/s)		0,21	0,27	0,16	0,17	0,07	0,24
RMSE (m^3/s)		0,39	1,93	0,78	0,67	0,72	0,73
RVE (%)		86,67	111,98	66,79	-68,28	-29,89	-95,90
RSQ		0,10	0,02	0,04	0,20	0,02	0,07
STD Dev (m^3/s)		0,65	1,42	0,61	0,50	0,53	0,50

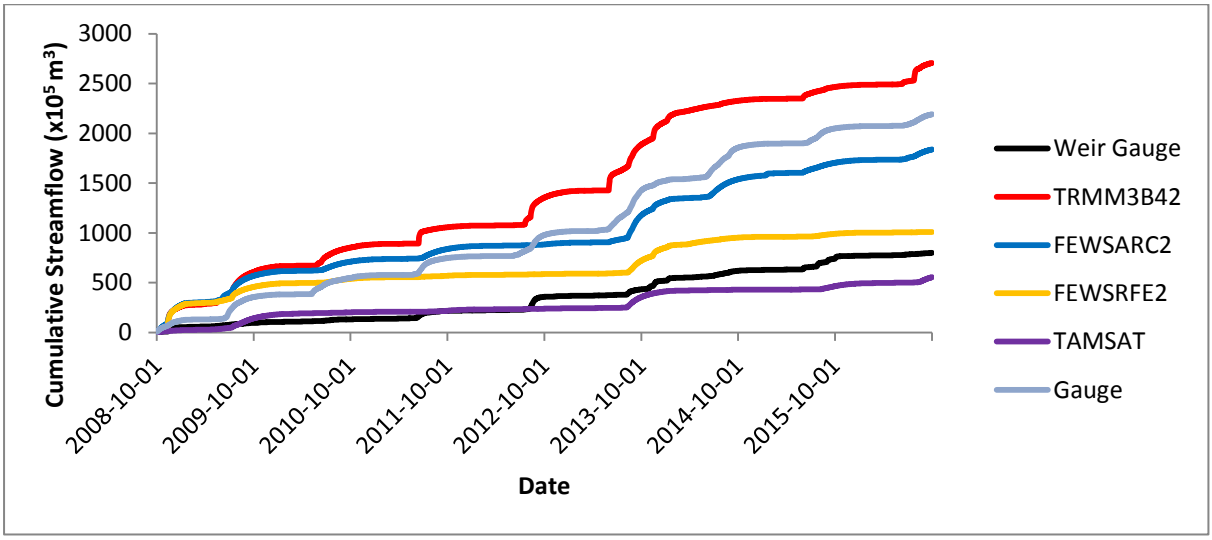

Figure 5.20 Accumulated streamflow for the period 1/10/2008-30/09/2016

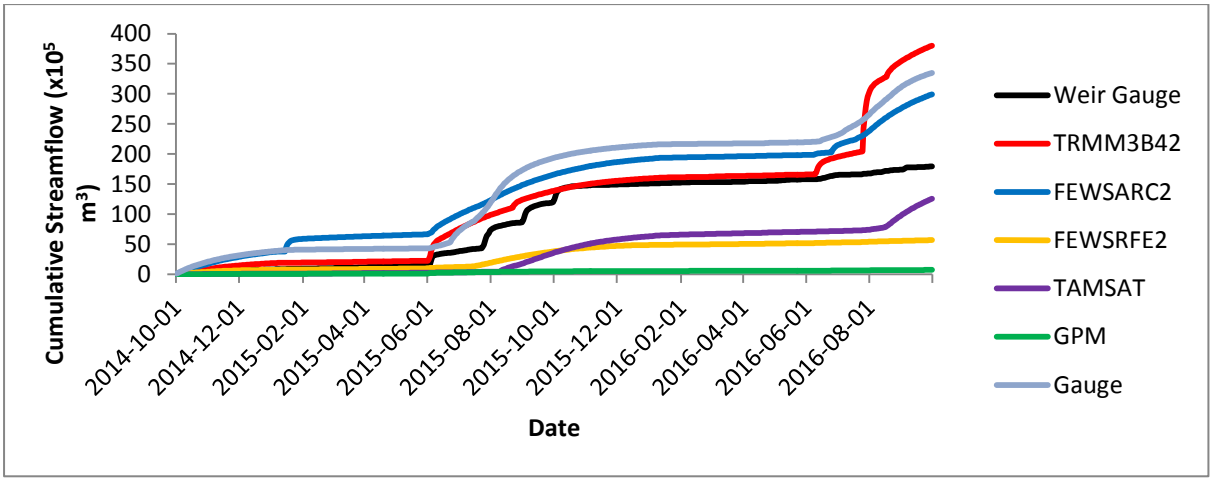

Figure 5.21 Accumulated streamflow for the period 1/10/2014-30/09/2016.

5.4 Summary of Findings of the ACRU Streamflow Modelling

The satellite derived rainfall products were used an input to the ACRU model to simulate streamflow in the upper uMngeni, upper uThukela and upper and central Breede catchments. Even though the products may have performed poorly at a point spatial scale, it was important to evaluate the products at the larger spatial scale that they offer. Rain gauge measurements were also used as input to the model to provide a reference for the evaluation of satellite derived products as the use of rain gauge data is the traditional approach to streamflow modelling. The simulated streamflow produced by the products and rain gauge data were compared to daily flow data obtained at various weir gauging locations across the study catchments. Keeping in mind that the study sites are functioning catchments where-by transfers, irrigation and water use by various sectors occur at a daily scale, weir gauges

chosen for the analysis were chosen based on reducing the anthropogenic influences on streamflow, such as dams and water transfers which regulate streamflow.

In the upper uMngeni catchment products produced relatively poor streamflow results across all three weir gauge sites. The products produced a considerable underestimation of streamflow, except at gauge U2H007 where TRMM 3B42 produced an overestimation of streamflow over the whole period when compared to observed streamflow. It is noted at this gauge all products overestimated streamflow during the GPM period of analysis. Apart from the U2H007 case, GPM produced a considerable underestimation of streamflow. TAMSAT-3 produced a poor daily correlation with observed streamflow, however total estimated streamflow volumes were in closer agreement with total rain gauge volumes when compared to the FEWS products. Both FEWS products performed poorly with high levels of underestimation. Rain gauge driven simulations produced results with closer daily correlation and total streamflow volumes with observed streamflow when compared to the satellite rainfall product driven simulations. However, due to TRMM 3B42's tendency to overestimate rainfall, the simulations of streamflow produced the best daily correlation and volume of streamflow when compared to the other satellite product driven simulations.

In the upper uThukela catchment, simulations of streamflow were better temporally represented when compared to the streamflow modelling in the other study sites. However, the magnitudes of streamflow were poorly correlated with observed streamflow at a daily scale. Satellite product driven simulations generally underestimated streamflow with both FEWS products underestimating streamflow the most. The TRMM 3B42 and rain gauge driven simulations produced the best statistical results when compared to the other streamflow simulations. Rain gauge driven simulations often produced a better correlation at a daily scale, however total streamflow volumes were generally poorly represented. The TRMM 3B42 product produced the best estimation of total streamflow volumes when compared to the other simulations.

In the upper and central Breede, product performances were variable across all weir gauging sites. The case presented at H1H013 (Koekedou River @ Ceres) showed all products to perform outstandingly poorly, and the rain gauge driven simulation produced the best streamflow results when compared to observed streamflow. Apart from H1H013, TRMM 3B42 driven simulations produced an overestimation of streamflow, especially at gauge H4H018 (Poesjenels @ Le Chasseur). The GPM product performed poorly in this region

producing the poorest streamflow results in terms of magnitude and temporally representing observed streamflow. TAMSAT-3 driven simulations produced streamflow that was poorly correlated with daily observed streamflow, however total streamflow volumes were in better agreement than the TRMM 3B42 and rain gauge driven simulations, as seen at weir H4H016 and H4H018. Both FEWS driven simulations performed better at weir gauges H4H016 and H4H018 when compared to the other simulations. Rain gauge driven simulated streamflow results were poor and did not necessarily outperform the TRMM 3B42 and FEWS streamflow results, however the streamflow produced had a better daily correlation with observed streamflow at a daily scale.

The sparse nature of rain gauges in the catchments meant that rain gauges that were used to drive the sub-catchments were not necessarily in or close to the sub-catchments. Therefore a precipitation correction factor had to be calculated and applied to the rain gauge data to represent the rainfall in those sub-catchments with similar altitude and MAP. Uncertainty arises as sub-catchments are driven with rain gauge measurements that are not entirely representative of the area, however that is the reality in regions of diminishing rain gauge networks. Results show that rain gauge driven simulations are relatively poor and do not necessarily outperform TRMM 3B42 in the summer rainfall region and FEWS in the winter rainfall region in terms of streamflow volumes, even though rain gauge driven simulations produce a better daily correlation with observed streamflow. Rain gauges neglect the spatial variations of rainfall in terms of topography (Hughes, 2006), which may also explain the poor rain gauge driven streamflow results, especially in the Breede region which involves complex topography. The satellite products may be unable to accurately estimate rainfall produced by the mid-latitude weather systems that occur in the Breede region, which may explain the poor satellite product streamflow results. The satellite derived products could replicate seasonal rainfall patterns, however the magnitudes of rainfall may differ when compared to rain gauge measurements due to the different orographic rainfall types caused by complex topography which negatively impacts the accuracy of simulated streamflow produced.

Observed data quality is always of question. To reduce uncertainty, where observed streamflow data was missing, the simulated streamflow produced was excluded in the statistical analysis. However, missing rain gauge data within a record was patched with rainfall data of a rain gauge that was situated closest to the rain gauge. This had to be done as ACRU is a daily time step model. Streamflow gauge data also contains inaccuracies, especially in operational catchments where the catchments are far from “natural” with many

processes taking place daily which may not be documented accurately, as found in Sawunyama and Hughes (2008). The inaccuracies in streamflow data increases the uncertainty involved in the simulated streamflow results. Overtopping of the weir is also not measured in some cases, which may have affected results.

Satellite rainfall algorithms spatially average rainfall over a pixel area. The scripts used produce an averaged area-weighted estimate of rainfall in the respective sub-catchment. An average of the whole sub-catchment rainfall may not necessarily represent the rainfall events that may occur, as a high magnitude rainfall event may be averaged by a low magnitude event that covers a larger area of the sub-catchment. This may have impacted the high flows produced in the simulations and may be a cause of underestimation of simulated streamflows.

Model uncertainty is a considerable factor in streamflow modelling. Model performance is directly linked to the quality of information and data used to configure the model. The information and data that is required as input to model may not always be straight forward to obtain or accurate. One such example, is that irrigation requirements were input in the model, however accurately identifying irrigated areas are limited due to insufficient data which affects the volumes of streamflows simulated. The configurations of the models that were used were initial configurations. A number of water transfers were not represented in the upper uThukela and upper and central Breede configuration (See Clark, 2017a/b), however the final configurations will include all water transfers. However, the streamflow gauges selected in this study were not affected by water transfers. The model configurations remained constant during all of the simulations.

6. CONCLUSIONS AND RECOMMENDATIONS

This Chapter presents the conclusions of this research study. The Chapter also presents the recommendations for future studies, derived from this research study.

6.1 Conclusion

Many parts of southern Africa are considered water scarce regions whereby many users share the limited resource (Lange *et al*., 2007, Jarmain *et al*., 2009). Therefore, sound management and decision making is important to achieve sustainability of the resource. Hydrological models are often used in water resource management to support decision making. The successes of models however, are dependent on the quality and availability of data that are used within the model. Rainfall is an important hydrological variable to consider in water resource management. Understanding the spatial and temporal variations of rainfall is important to achieve effective water resource management. Rainfall is traditionally measured through the use of in-situ rain gauge measurements. However, rain gauge measurements poorly represent the spatial variations of rainfall and rain gauge networks are diminishing especially in southern Africa.

Satellite derived rainfall provide a useful means of measurement, especially in regions of poor monitoring. The ease of access, availability, cost effectiveness and larger geographical coverage has made satellite derived rainfall a viable option for use in water resource management. However, there has been a reluctant uptake of the use of satellite derived rainfall. This can be attributed to the lack of technological power to process the data, uncertainty involved with satellite derived estimation, lack of knowledge to integrate the data into meaningful applications, reluctance to use methods other than the traditional measurement as well as the insufficient spatial and temporal resolutions needed for operational purposes (Xu *et al*., 2014, Ciabatta *et al*., 2015). The current nature of many hydrological models also do not accommodate for the incorporation of satellite derived rainfall (Xu *et al*., 2014). Model configurations are fixed into incorporating tradition methods of parameter measurement and model reconfiguration will be needed to incorporate satellite derived rainfall.

This research study forms part of the WRC K5/2512 project (Clark, 2017) which is a follow on of the WRC K5/2205 project (Clark, 2015). The overall aims of this research study was to

compare satellite derived rainfall product estimates with in-situ rain gauge measurements as well as to use the satellite derived rainfall to drive the ACRU hydrological model. In-order to meet these objectives various specific objectives were outlined. The satellite derived rainfall products that were used in this study include TRMM 3B42, FEWS ARC2, FEWS RFE2, TAMSATV3 and GPM (IMERGV4). The products were evaluated in the upper uMngeni, upper uThukela and upper and central Breede catchments. This was to test the methodology in both summer and winter rainfall regions.

The products were analysed at various rain gauge sites in and around the study catchments. The time period of analysis was from 1 January 2010 to 30 April 2017. GPM was analysed from 12 March 2014 to 30 April 2017 due to data availability. Product performances were highly variable across all rain gauge sites. Products generally portrayed the temporal patterns of rainfall seasonally, monthly and yearly, however the satellite products produced a poor daily correlation with rainfall magnitudes when compared to rain gauge measurements. No product clearly outperformed the other. GPM, TRMM's successor, did not necessarily outperform TRMM 3B42. TRMM 3B42 generally produced an overestimation of rainfall, whereas GPM generally produced an underestimation of rainfall across all three study areas. Both FEWS products performed poorly in the upper uMngeni and upper uThukela, whereas they performed better than the other products in the upper Breede with a general underestimation throughout. TAMSAT-3 notably performed the poorest with considerably poor correlations with rain gauge measurements at a daily scale. Total rainfall volumes of the products were in better agreement with total rainfall volumes of the rain gauges. TAMSAT-3 provided agreement with total rainfall volumes of the rain gauge in the Breede, where most products performed poorly, even though daily correlations were generally worse than the other products. Satellite products may be unable to accurately estimate rainfall generated in complex topographical areas, as seen in the Breede region. It is acknowledged that uncertainty exists in comparing a point value with a spatial estimate as well as uncertainty exists within the product algorithms. Overall, the products performed better in the upper uMngeni and upper uThukela than the upper and central Breede. The satellite products may inaccurately estimate rainfall due to the mid-latitude weather systems, frontal and orographic rainfall regimes of the Breede region (Thorne *et al*., 2001).

Even though the products may have performed poorly at a point scale, it was important to evaluate the products at the larger spatial scale. The satellite rainfall products were used to drive the ACRU hydrological model configured for all three study catchments. The model

was also driven with rain gauge measurements to obtain a reference whereby simulated streamflow driven with satellite derived rainfall could be compared with the traditional method of hydrological modelling using rain gauge measurements.

In the upper uMngeni, the satellite products performed poorly with a general underestimation throughout and a poor daily temporal representation of streamflow. Simulated streamflow results were generally poorly correlated with observed streamflow. Total volume of streamflow over the whole period was generally poor when compared to streamflow gauge totals. Rain gauge driven simulations had better daily correlation with observed streamflow than the product driven simulations and generally produced better results than the products in some cases, however TRMM 3B42 results were generally of similar quality to that of the rain gauge driven simulations.

In the upper uThukela catchment, satellite products produced better temporal representations of streamflow than the uMngeni, however the daily magnitudes were poorly represented. FEWS and GPM driven simulations produced a consistent underestimation of streamflow. Rain gauge and TRMM 3B42 driven simulations produced the best results, with the rain gauge driven simulations providing better correlation at a daily scale with observed streamflow. TRMM 3B42 driven simulations generally had better agreement with total streamflow volumes when compared to total observed streamflow volumes.

In the upper and central Breede, TRMM 3B42 and FEWS satellite product driven simulations generally overestimated streamflow, with TRMM 3B42 causing a considerable overestimation of streamflow. TAMSAT-3 and GPM driven simulations consistently underestimated streamflow over the whole period. FEWS and TASMAT-3 generally provided the best results in terms of total streamflow volumes over the whole period when compared to the other simulations. The satellite products may be unable to accurately estimate rainfall due to the mid-latitude weather systems, frontal and orographic rainfall regimes of the Breede region (Thorne *et al*., 2001) which negatively impacted streamflows.

The rain gauge and TRMM 3B42 driven simulations provided the closest agreement to observed streamflow in the summer rainfall region, where-as the FEWS driven simulations provided the closest agreement to streamflow in the winter rainfall region. TRMM 3B42 tended to overestimate rainfall in general which produced an overestimation of streamflow and generally improved simulations in the summer rainfall region. GPM and TAMSAT-3

tended to underestimate rainfall which caused an underestimation of streamflow in general. Both FEWS satellite products performed inconsistently in the validation study, however produced closer agreement to streamflow in the winter rainfall region. Where rainfall is underestimated/overestimated by the satellite products, the streamflow will consequently be underestimated/overestimated by the ACRU model as the model is highly dependant on rainfall. Total streamflow volumes were well simulated at a monthly, seasonal and yearly scale, but poorly simulated at a daily scale. Simulated streamflow generated by the ACRU model is highly dependent on the rainfall input.

The sparse nature of rain gauges in the study catchments poorly represents rainfall over the whole catchment, whereas product performance was variable at each location. Algorithm and model uncertainty have considerable roles to play in utilising satellite derived rainfall for management and decision making. The satellite products are not suitable for use directly into hydrological models without bias correction, and several studies have demonstrated that daily data has larger variations compared to monthly data, hence if used in hydrological models the results will differ greatly. The type of application in which the satellite derived rainfall is used is important. Satellite derived rainfall show potential for use in applications where total volumes are of interest, such as water budgets. Satellite derived rainfall may hinder applications that require finer spatial scales and accurate daily rainfall magnitude estimation. However, with increasing technological capacity, satellite derived rainfall show promise in supplying rainfall measurements in a world of diminishing rain gauge networks.

6.2 Recommendations

The recommendations presented below address the limitations experienced in this research study as well as to assist future studies.

i. Ideally to address the limitation of comparing a point value to a spatial estimate, a dense rain gauge network is needed. However, the reality is that dense networks do not exist, especially in developing countries. Satellite rainfall products should then be compared to a spatial representation of rainfall constructed through the use of rain gauge measurements. Rain gauge kriging is a method used to overcome the spatial limitations of rain gauge measurements, as used in Thorne *et al*. (2001). Kriging is a method used for obtaining optimal areal estimates from a point estimate (Journel and Huijbrets, 1978; Thorne *et al*., 2001).

ii. Product resolution is too coarse for fine scale modelling. Downscaling the satellite derived rainfall products may increase model performance at fine scales which may improve results at the larger scale. Downscaled estimates may also improve the correlation when compared to rain gauge measurements.

iii. The products display bias, such as TRMM 3B42 with a general overestimation, and FEWS, GPM and TAMSAT with a general underestimation. A bias correction applied to the datasets may enhance satellite derived results which may be more representative to the rainfall of a specific area.

iv. Satellite derived data is not seen as a primary replacement of ground-based measurements. The products were shown to operate variably in different locations. Satellite rainfall data should be used in conjunction with ground-based data, whereby satellite data may be used to create measurements that are more spatially representative with the local accuracy of the rain gauge.

v. In complex topographical areas, rain gauge and radar networks should be prioritised.

vi. Satellite derived rainfall is spatially distributed within the pixel area. This may neglect peak events which may be averaged out and further exacerbated by the area- weighted averaging over the catchments. The ACRU hydrological model needs to be modified to operate at a gridded scale and accommodate gridded input datasets. This would allow the model to accept a variety of raster datasets and this would allow the model to better spatially represent processes, especially that of rainfall. This may increase the accuracy of streamflow simulations when compared to observed streamflow as the gridded data would be more spatially representative of the hydrological processes that occur over a whole catchment.

vii. Modelling uncertainty needs to be reduced. The models were not further verified during this research study. Insufficient data has a significant role to play in the assumptions built into the model, as seen with water transfers for example. More detailed data is required in certain cases to improve model performance in-order to reduce model uncertainty. Parameters such as soil depths and runoff responses input into the model may need to be adjusted to more accurately represent the streamflow generating processes that occur in the catchments.

viii. Product algorithms are constantly being updated. TRMM 3B42 version seven, FEWS versions two, GPM version four, TAMSAT version three were used in this study as these were current during the time period of this study. It is important for

future studies to use the most updated version of the products as algorithm updates may reduce bias and may provide more accurate results.

ix. Product performance is highly variable amongst locations. Even though products may produce global or continental coverage, it is important to understand the rainfall generating mechanisms of the region at a localised level when choosing products. One such example is that of TAMSAT. TAMSAT is limited in detection of warm rain producing mechanisms such as in coastal or mountainous areas (Maidment *et al*., 2017). Product limitations should be considered to increase the accuracy of the satellite derived estimates depending on the location and the respective rainfall mechanisms. Rainfall time series may also be generated using a variety of products over different locations of sub-catchments instead of one product, which may enhance catchment modelling.

7. REFERENCES

Acocks, J. 1988. Veld Types of South Africa. Memoirs of the Botanical Survey of South Africa No.57. 3rd Edition. Botanical Research Institute, Pretoria, South Africa.

Alazzy, AA, Lü, H, Chen, R, Ali, AB, Zhu, Y and Su, J. 2017. Evaluation of Satellite Precipitation Products and Their Potential Influence on Hydrological Modeling over the Ganzi River Basin of the Tibetan Plateau. *Advances in meteorology*, 1-23.

Alijanian, M, Rakhshandehroo1, GR, Mishra, AK and Dehghani, M. 2017. Evaluation of satellite rainfall climatology using CMORPH, PERSIANN-CDR, PERSIANN, TRMM, MSWEP over Iran, *International Journal of Climatology*, in press.

Amekudzi, LK, Osei, MA, Atiah, WA, Aryee, JNA, Ahiataku, MA, Quansah, E, Preko, K, Danuor, SK and Fink, AH. 2016. Validation of TRMM and FEWS Satellite Rainfall Estimates with Rain Gauge Measurement over Ashanti Region, Ghana. *Atmospheric and Climate Sciences*, 6, 500-518.

Andersson, JC, Zehnder, AJ, Rockström, J and Yang, H. 2011. Potential impacts of water harvesting and ecological sanitation on crop yield, evaporation and river flow regimes in the Thukela River basin, South Africa. *Agricultural Water Management*, 98(7): 1113-1124.

Bangira, T, Maathuis, BHP, Dube, T and Gara, TW. 2015 Investigating flash floods potential areas using ASCAT and TRMM satellites in the Western Cape Province, South Africa, *Geocartography International*, 30(7), 737-754.

Beck, HE, Vergopolan, N, Pan1, M, Levizzani, V, van Dijk, AIJM, Weedon, G, Brocca, L, Pappenberger, F, Huffman7, GJ and Wood, EF. 2017. Global-scale evaluation of 23 precipitation datasets using gauge observations and hydrological modelling. *Hydrology Earth Systems Science Discusions*. 1-23.

Bergström, S. 1992. The HBV model—its structure and applications, SMHI Reports RH 4, Swedish Meteorological and Hydrological Institute (SMHI), Norrköping, Sweden.

Bumke, K, König-Langlo, G, Kinzel, J and Schröder, M. 2016. HOAPS and ERA-Interim precipitation over the sea: validation against shipboard in-situ measurements, *Atmospheric Measurement Techniques*, (9), 2409–2423, 2016.

Ciabatta, L, Brocca, L, Massari, C, Moramarco, T, Gabellani, S, Puca, S and Wagner, W. 2015. Rainfall-runoff modelling by using SM2RAIN-derived and state-of-the-art satellite rainfall products over Italy. *International Journal of Applied Earth Observsation Geoinf*ormation, (48), 163-173.

Clark, DJ. 2015. Development of a methodology for water use quantification and accounting. In ed: Clark, DJ. 2015. Development and assessment of an integrated water resources accounting methodology for South Africa. Water Research Commission, Pretoria, South Africa, Report K5/2205.

Clark, DJ. 2017a. Further Development and Assessment of an Integrated Water Resources Accounting Methodology for South Africa. Water Research Commission, Pretoria, South Africa, Report K5/2512, Deliverable 4.

Clark, DJ. 2017b. Further Development and Assessment of an Integrated Water Resources Accounting Methodology for South Africa. Water Research Commission, Pretoria, South Africa, Report K5/2512, Deliverable 5.

Cohen Liechti, T, Matos, JP, Boillat, JL, and Schleiss, AJ. 2012. Comparison and evaluation of satellite derived precipitation products for hydrological modelling of the Zambezi River Basin. *Hydrology and Earth System Sciences*, 16(2): 489-500.

Collischonn, B, Collischonn, W and Tucci, CEM. 2008. Daily hydrological modelling in the Amazon basin using TRMM rainfall estimates. *Journal of Hydrology*, 360(1): 207-216.

DEA and GTI. 2015. 72 Class GTI South African National Land Cover Dataset (2013/2014). Produced by GeoTerraImage Pty Ltd (GTI) for the Department of Environmental Affairs (DEA), Pretoria, South Africa.

Dinku, T, Ceccato, P, Grover-Kopec, E, Lemma, M, Connor, SJ and Ropelewski, CF. 2007. Validation of satellite rainfall products over East Africa's complex topography. *International Journal of Remote Sensing*, 28 (7): 1503-1526.

DSO. 2014. List of Registered Dams in South Africa, 2014. List of Registered Dams Oct 2014.xls available from https://www.dwa.gov.za/DSO/Publications.aspx. Dam Safety Office (DSO), Departnment of Water Affairs, Pretoria, South Africa.

DWAF. 2004. National Water Resource Strategy. Department of Water Affairs and Forestry, Pretoria, RSA.

Ebert, EE, Janowiak, JE and Kidd, C. 2007. Comparison of near-real-time precipitation estimates from satellite observations and numerical models, *Bulletin American Meteorological Society*, (88), 47–64.

Ezemvelo KZN Wildlife and GeoTerraImage. 2013. KwaZulu-Natal Land Cover 2011 V1. Unpublished GIS Coverage [Clp_KZN_2011_V1_grid_w31.zip]. P. O. Box 13053, Cascades, Pietermaritzburg, 3202, South Africa.

Falck, AS, Maggioni, V, Tomasella, J, Vila, DA and Diniz, FLR. 2015. Propagation of satellite precipitation uncertainties through a distributed hydrologic model: A case study in the Tocantins-Araguaia basin in Brazil, *Journal of Hydrology*, (527), 943–957.

Fern'andez-Prieto, D, van Oevelen, P, Su, Z and Wagner, W. 2012. Advances in Earth observation for water cycle science. *Hydrology Earth System Science,* 16, 543-549.

Grimes, D and Diop, M. 2003. Satellite-based rainfall estimation for river flow forecasting in Africa. I: Rainfall estimates and hydrological forecasts. *Hydrological Sciences Journal*, 48(4), 567-584.

Haas, R and Born, K. 2011. Probabilistic downscaling of precipitation data in a subtropical mountain area: a two-step approach. *Nonlinear Processes Geophysics*, 18, 223–234.

Herman, A, Kumar, V, Arkin, PA and Kousky, JV .1997. Objectively determined 10-day African rainfall estimates created for famine early warning. *Inernational Journal of Remote Sensing*. 18, 2147–2159.

Hirpa, FA, Gebremichael, M, and Hopson, T. 2010. Evaluation of high-resolution satellite precipitation products over very complex terrain in Ethiopia, *Journal of Applied Meteorology and Climatology*, (49), 1044–1051.

Hou, AY, Kakar, RK, Neeck, S, Azarbarzin, AA, Kummerow, CD, Kojima, M, Oki, R, Nakamura, K and Iguchi, T. 2014. The Global Precipitation Measurement Mission. *American Meteorological Society*, 95 (5): 701–722.

Hsu, KL and Sorooshian, S. 2009. Satellite-based precipitation measurement using PERSIANN system. *Hydrological Modelling and the Water Cycle*, 27-48.

Hu, Q, Yang, H, Meng, X, Wang, Y and Deng, P. 2015. Satellite and gauge rainfall merging using geographical weighted regression. Remote Sensing and GIS for Hydrology and Water Resources (IAHS Publ. 368, 2015) (Proceedings RSHS14 and ICGRHWE14, Guangzhou, China, August 2014)

Huffman, GJ, Adler, RF, Bolvin, DT and Nelkin, EJ. 2010. The TRMM Multi-satellite Precipitation Analysis (TMPA), in Satellite Rainfall Applications for Surface Hydrology, 3–22, Springer, New York.

Hughes, DA. 2006. Comparison of satellite rainfall data with observations from gauging station networks. *Journal of Hydrology*, 327(3): 399-410.

Immerzeel, WW, Rutten, MM and Droogers, P. 2009. Spatial downscaling of TRMM precipitation using vegetative response on the Iberian Peninsula. *Remote Sensing Environment*, 113, 362–370

Islam, T, Rico-Ramirez, MA, Han, D, Srivastava, PK, and Ishak, AM. 2012. Performance evaluation of the TRMM precipitation estimation using ground-based radars from the GPM validation network, *Journal of Atmospheric and Solar-Terrestrial Physics*, 77, 194–208

Jarmain, C, Bastiaansen, W, Mengistu, MG, and Kongo, V. 2009. A Methodology for Near-Real Time Spatial Estimation for Evaporation, WRC Report No. 1751/1/09, ISBN 978-1-77005-725-8.

Jia, S, Zhu, W, L″u, A and Yan, T. 2011. A statistical spatial downscaling algorithm of TRMM precipitation based on NDVI and DEM in the Qaidam Basin of China, *Remote Sensing Environment*, 115, 3069–3079

Journel, AG and Huijbrets, CJ. 1978. Mining Geostatistics. (New York: Academic).

Joyce, RJ, Janowiak, JE, Arkin, PA and Xie, P. 2004. CMORPH: A method that produces global precipitation estimates from passive microwave and infrared data at high spatial and temporal resolution. *Journal of Hydrometeorology* 5(3): 487-503.

Kidd, C, and Levizzani, V. 2011. Status of satellite precipitation retrievals. *Hydrology and Earth System Sciences*, 15(4): 1109-1116.

Kimani, MW, Hoedjes, JCB and Su, Z. 2017. An Assessment of Satellite-Derived Rainfall Products Relative to Ground Observations over East Africa. *Remote Sensing*, 9(5), 430.

Kongo, VM, Kosgei, JR, Jewitt, GPW and Lorentz, SA. 2010. Establishment of a catchment monitoring network through a participatory approach in a rural community in South Africa. *Hydrology and Earth System Sciences*, 14(12): 2507-2525.

Kummerow, C, Barnes, W, Kozu, T, Shiue, J and Simpson, J. 1998. The Tropical Rainfall Measuring Mission (TRMM) sensor package. *Atmospheric and Ocean Technology* 15, 809–817.

Kurtyka, JC. 1953: Precipitation measurements study. Investigation Rep. 20, Department of Registration and Education and the State Water Survey Division, Urbana, Illinois.

Lakshimi, V. 2004. Use of satellite remote sensing in hydrological predictions in ungauged basins. In XX Congresso da ISPRS (12-23).

Lange, GM, Mungatana, E, and Hassan, R. 2007. Water accounting for the Orange River Basin: An economic perspective on managing a transboundary resource. *Ecological economics*, 61(4): 660-670.

Love, TB, Kumar, V, Xie, P and Thiaw, W. 2004: A 20-year daily Africa precipitation climatology using satellite and gauge data. Preprints, 14th Conf. on Applied Meteorology, Seattle, WA, *American Meteorological Society*, 5(4).

Lynch, S. 2004. Development of a Raster Database of Annual, Monthly and Daily Rainfall for Southern Africa. WRC Report 1156/1/04. Water Research Commission, Pretoria, South Africa.

Maidment, RI, Grimes, D, Black, E, Tarnavsky, E, Young, M, Greatrex, H, Allan, RP, Stein, T, Nkonde, E, Senkunda, S and Alcantara, EMU. 2017.A new, long-term daily satellite-based rainfall dataset for operational monitoring in Africa. *Nature Scientific Data*, 4: 170063 DOI:10.1038/sdata.2017.63.

Michaelides, S, Levizzani, V, Anagnostou, E, Bauer, P, Kasparis, T and Lane, JE. 2009. Precipitation: Measurement, remote sensing, climatology and modelling. *Atmospheric Research*, 94(4), 512-533.

Najmaddin, PM, Whelan, MJ and Balzter, H. 2017. Application of Satellite-Based Precipitation Estimates to Rainfall-Runoff Modelling in a Data-Scarce SemiArid Catchment. *Climate*, 5, 32.

Nel, JL, Driver, A, Strydom, WF, Maherry, AM, Petersen, C, Hill, L, Roux, DJ, Nienaber, S, van Deventer, H, Swartz, E and Smith-Adao, LB. 2011a. FEPA Rivers Based on DWS 1:500,000 River Layer. NFEPA_Rivers.shp. WRC Report No. TT 500/11, Water Research Commission, Pretoria, South Africa.

Nel, JL, Driver, A, Strydom, WF, Maherry, AM, Petersen, C, Hill, L, Roux, DJ, Nienaber, S, van Deventer, H, Swartz, E and Smith-Adao, LB. 2011b. River FEPA Sub-Quaternary Catchments. River_FEPAs.shp. WRC Report No. TT 500/11, Water Research Commission, Pretoria, South Africa.

New, M, Todd, M, Hulme, M and Jones, P. 2000. Precipitation measurements and trends in the twentieth century. *International Journal of Climatology*, 21(15), 1889-1922.

Novella, NS and Thiaw, WM. 2013. African rainfall climatology version 2 for famine early warning systems. *Journal of applied meteorology and climatology*, 52(3), 588-606.

Nystuen, JA, Proni, JR, Black, PG and Wilkerson, JC. 1996. A comparison of automatic rain gauges. *Journal of Atmospheric and Oceanic Technology*, 13(1), 62-73.

Pitman, WV. 2011. Overview of water resource assessment in South Africa: Current state and future challenges. *Water SA*, 37(5): 659-664.

Prakash, S, and Gairola, RM. 2014. Validation of TRMM-3B42 precipitation product over the tropical Indian Ocean using rain gauge data from the RAMA buoy array. *Theoretical and applied climatology*, 115(3-4), 451-460.

Rauniyar, SP, Protat, A and Kanamori, H. 2017. Uncertainties in TRMM-Era multisatellie-based tropical rainfall estimates over the Maritime Continent. *Earth and Space Science*, 4, 275-302, doi: 10.1002/2017EA000279.

Sawunyama, T and Hughes, DA. 2008. Application of satellite-derived rainfall estimates to extend water resource simulation modelling in South Africa. *Water SA*, 34(1),1-9.

Schulze, RE. 1995. Hydrology and Agrohydrology: A Text to Accompany the *ACRU* 3.00 Agrohydrological Modelling System. Water Research Commission, Pretoria South Africa.

Smithers, JC. and Schulze, RE. 2004. *ACRU* Agrohydrological Modelling System: User Manual Version 4.00, School of Bioresources Engineering and Environmental Hydrology, University of KwaZulu-Natal, South Africa.

Schulze, RE and Horan, MJC. 2008. Section 4.2: Soils Hydrological Attributes. In: ed. Schulze, RE, South African Atlas of Climatology and Agrohydrology. WRC Report 1489/1/06. Water Research Commission, Pretoria, South Africa.

Schulze, RE and Maharaj, M. 2008a. Section 6.5: Rainfall Seasonality. In: ed. Schulze, RE, South African Atlas of Climatology and Agrohydrology. WRC Report 1489/1/06. Water Research Commission, Pretoria, South Africa.

Schulze, RE and Maharaj, M. 2008b. Section 7.3: Daily Maximum Temperatures. In: ed. Schulze, RE, South African Atlas of Climatology and Agrohydrology. WRC Report 1489/1/06. Water Research Commission, Pretoria, South Africa.

Schulze, RE and Maharaj, M. 2008c. Section 7.5: Daily Minimum Temperatures. In: ed. Schulze, RE, South African Atlas of Climatology and Agrohydrology. WRC Report 1489/1/06. Water Research Commission, Pretoria, South Africa.

Schulze, RE and Maharaj, M. 2008d. Section 9.3: Frequency of Frost Occurrences. In: ed. Schulze, RE, South African Atlas of Climatology and Agrohydrology. WRC Report 1489/1/06. Water Research Commission, Pretoria, South Africa.

Seibert, J and Vis, MVP. 2012. Teaching hydrological modelling with a user-friendly catchment-runoff-model software package, *Hydrology and Earth System Sciences*, 16, 3315–3325.

Seyyedi, H, Anagnostou, EN, Beighley, E and McCollum, J. 2014. Satellite-driven downscaling of global reanalysis precipitation products for hydrological applications. *Hydrology and Earth System Sciences*, 18(12), 5077-5091.

Sorooshian, S, Hsu, KL, Gao, X, Gupta, HV, Imam, B and Braithwaite, D. 2000. Evaluation of PERSIANN system satellite-based estimates of tropical rainfall. *American Meteorological Society*, 81(9): 2035-2046.

Sawunyama, T, Hughes, DA. 2008. Application of satellite-derived rainfall estimates to extend water resource simulation modelling in South Africa. *Water SA*, 48, 1816-7950

Tarnavsky, E, Grimes, D, Maidment, RI, Stringer, M, Chadwick, R, Allan, RP, Black, E and Kayitakire. 2014. Extension of the TAMSAT Satellite-based Rainfall Monitoring over Africa and from 1983 to present. *Journal of Applied Meteorology and Climatology*, 53(12), 2805: 2822.

Thorne, V, Coakeley, P, Grimes, D and Dugdale, G .2001. Comparison of TAMSAT and CPC rainfall estimates with rain gauges, for southern Africa, *International Journal of Remote Sensing*, 22:10.

van Dijk, AI and Renzullo, LJ. 2011. Water resource monitoring systems and the role of satellite observations. *Hydrology and Earth System Sciences* 13(7), 1337-1347.

Vardon, M, Lenzen, M, Peevor, S, and Creaser, M. 2007. Water accounting in Australia. *Ecological Economics*, 61(4), 650-659.

Vergara, H, Hong, Y, Gourley, JJ, Anagnostou, EN, Maggioni, V, Stampoulis, D and Kirstetter, PE. 2014. Effects of resolution of satellite-based rainfall estimates on hydrologic modelling skill at different scales. *Journal of Hydrometeorology*, 15(2), 593-613.

Warburton, ML, Schulze, RE and Jewitt, GPW. 2010. Confirmation of ACRU model results for applications in land use and climate change studies. *Hydrology and Earth System Sciences*, 14(12), 2399-2414.

Warburton, ML, Schulze, RE and Jewitt, GPW. 2012. Hydrological impacts of land use change in three diverse South African catchments. *Journal of Hydrology*, 414,118-135.

Warburton, ML. 2011. Challenges in modelling hydrological responses to impacts and interactions of land use and climate change. Unpublished Doctor of Philosophy in Hydrology thesis, School of Bioresources Engineering and Environmental Hydrology, University of KwaZulu-Natal, Pietermaritzburg

Weepener, HL, van den Berg, HM, Metz, M and Hamandawana, H. 2011a. The development of a hydrologically improved Digital Elevation Model and derived products for South Africa based on the SRTM DEM. WRC Report 1908/1/11. Water Research Commission, Pretoria, South Africa.

Weepener, HL, van den Berg, HM, Metz, M and Hamandawana, H. 2011b. Gap-filled DEM based on SRTM 90m DEM. SRTM90m_Gapfilled.tif. WRC Report 1908/1/11, Water Research Commission, Pretoria, South Africa.

Wetchayont, P, Hayasaka, T. Satomura, T, Katagiri, S, and Baimoung, S. 2013. Retrieval of Rainfall by Combining Rain Gauge, Ground-Based Radar and Satellite Measurements over Phimai, Thailand. SOLA, 9(0), 166-169.

Wilk, J, Kniveton, D, Andersson, L, Layberry, R, Todd, MC, Hughes, D, Ringrose, S and Vanderpost, C. 2006. Estimating rainfall and water balance over the Okavango River Basin for hydrological applications. *Journal of Hydrology*, 331(1), 18-29.

Xie, P and Arkin, PA. 1996. Global precipitation: A 17-year monthly analysis based on gauge observations, satellite estimates, and numerical model outputs. *Bulletin of the American Meteorological Society*, 78(11), 2539-2558.

Xie, P. 2001. CPC RFE version 2.0. NOAA CPC Training Guide, *Presented at the Drought Monitoring Centre*, Nairobi, Kenya.

Xu, X, Li, J, and Tolson, BA. 2014. Progress in integrating remote sensing data and hydrologic modelling. *Progress in Physical Geography*, 38(4), 464-498.

8. APPENDICES

This chapter presents the Appendices of this research study.

8.1 Appendix A

This section provides the statistical approaches used in this study.

$$Bias = \frac{\int_{i=1}^{n}(Ti)}{\int_{i=1}^{n}(Gi)}$$

$$MAE = \frac{1}{n}\sum_{i=1}^{n}|(\mathrm{Ti} - \mathrm{Gi})|$$

$$RMSE = \sqrt{\frac{1}{n}\sum_{i=1}^{n}(Ti - Gi)^2}$$

$$RVE = \frac{Ti - Gi}{Gi}\ X\ 100$$

$$POD = \frac{H}{H + M}$$

$$FAR = \frac{F}{H + F}$$

$$CSI = \frac{H}{H + F + M}$$

Where, Ti = Satellite estimates

Gi = Observed gauge measurements

H= Hits (Events observed by both satellite and gauge)

M = Misses (Events observed by the gauge only)

F= False alarms (Events observed by the satellite and not the gauge)

Further details are reviewed in Amekudzi *et al*. (2016).

8.2 Appendix B

This section provides the time series graphs and statistical tables produced in Chapter 4, which is the product validation against rain gauge data.

8.2.1 Summer rainfall region

- V3E002 (Chelmsford at Chelmsford Dam)

Time series of the products against gauge measurements are presented below.

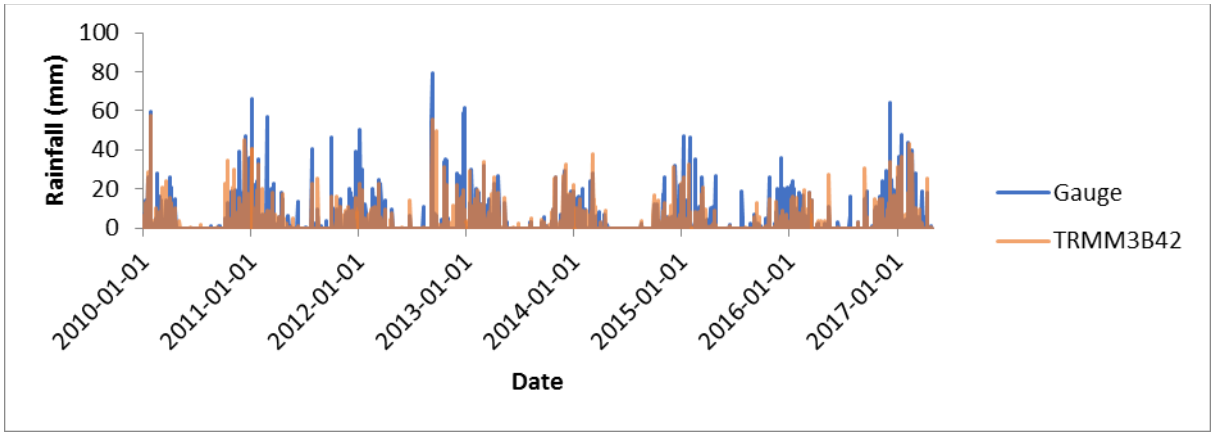

Figure 8.1 Time series of TRMM 3B42 against V3E002 measurements.

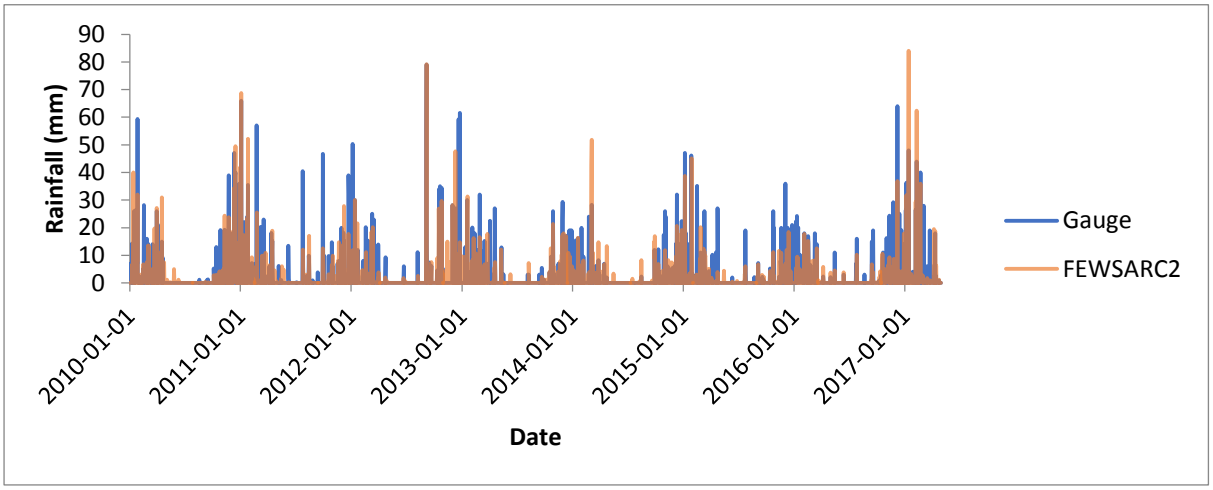

Figure 8.2 Time series of FEWS ARC2 against V3E002 measurements.

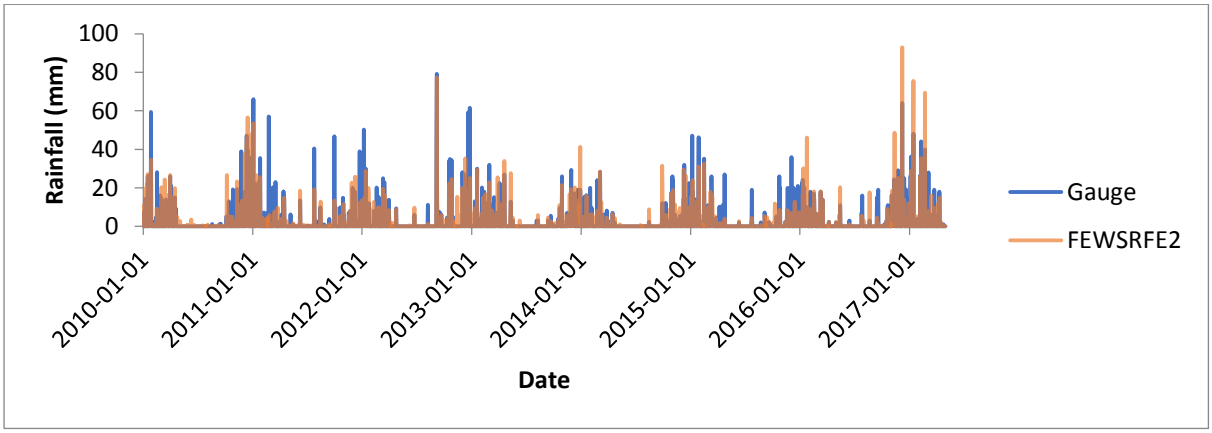

Figure 8.3 Time series of FEWS RFE2 against V3E002 measurements.

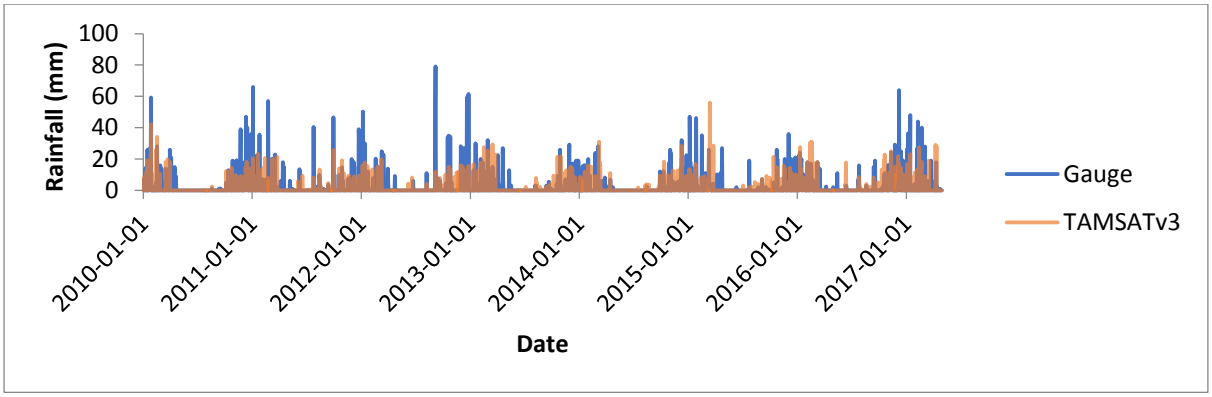

Figure 8.4 Time series of TAMSAT-3 against V3E002 measurements.

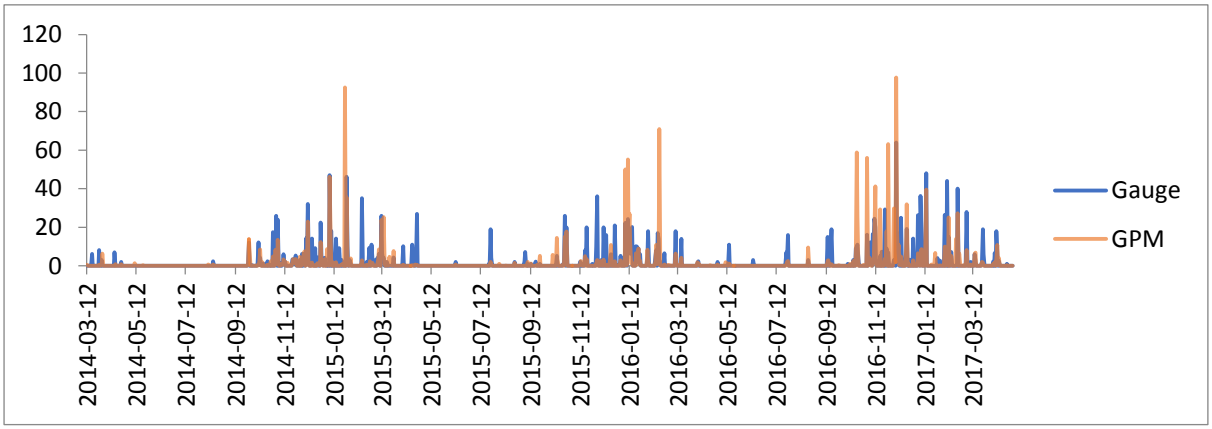

Figure 8.5 Time series of GPM against V3E002 measurements.

Average monthly rainfall totals are presented below.

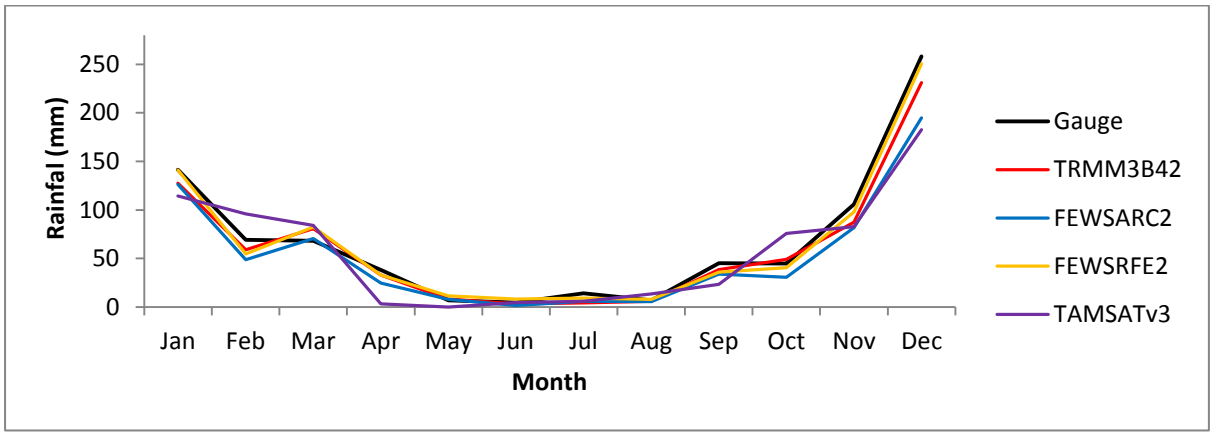

Figure 8.6 Average monthly rainfall totals at V3E002.

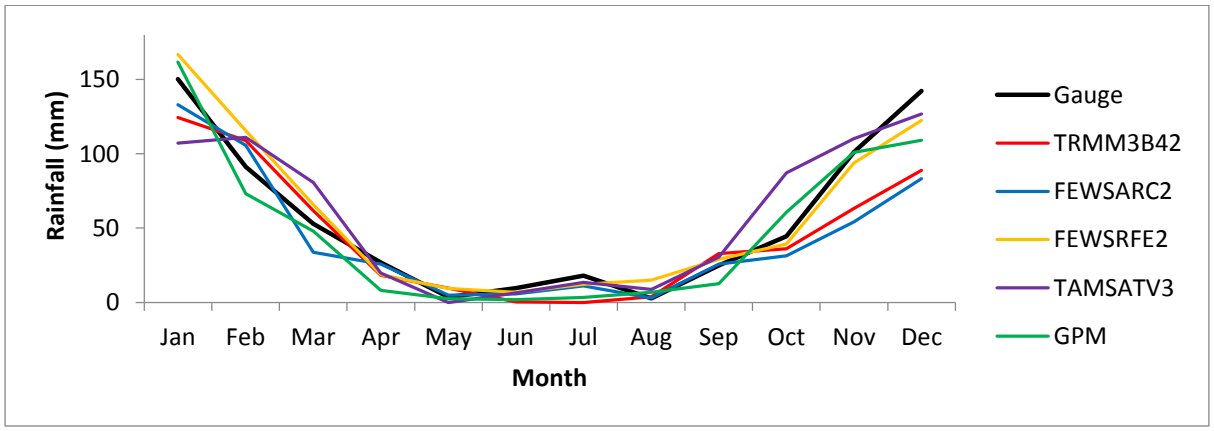

Figure 8.7 Average monthly rainfall totals at V3E002 during the GPM period of analysis.

Accumulated rainfall is presented below.

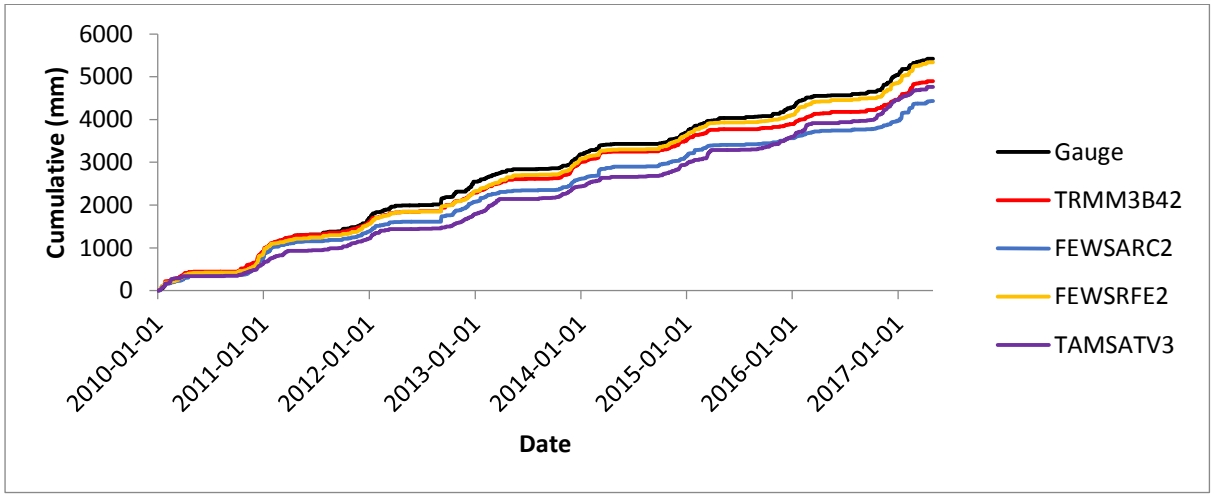

Figure 8.8 Accumulated rainfall at V3E002.

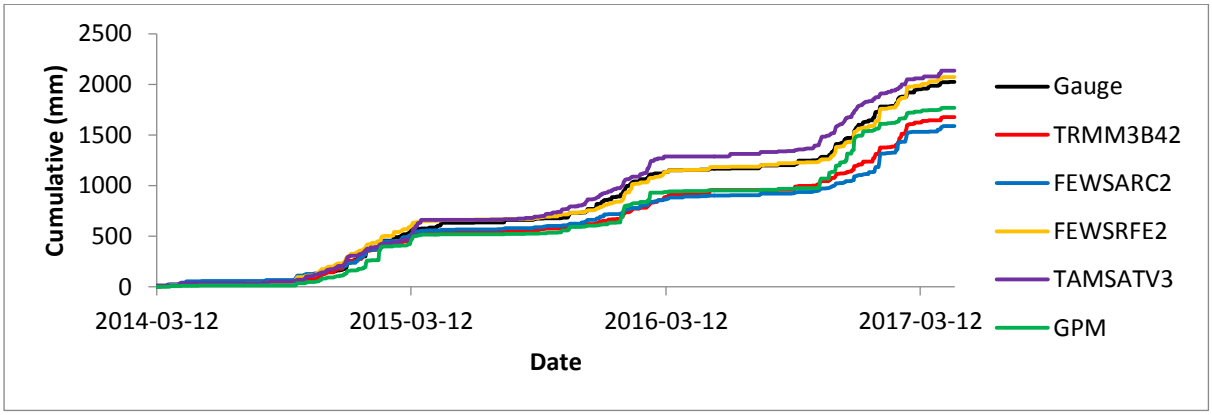

Figure 8.9 Accumulated rainfall at V3E002 during the GPM period of analysis.

Tables of statistics are presented below.

Table 8.1 Statistics produced at V3E002.

	Gauge	TRMM3B42	FEWSARC2	FEWSRFE2	TAMSATv3
Total (mm)	5422,70	4899,10	4428,80	5340,50	4762,30
Max (mm)	79,10	57,50	84,00	93,00	55,90
Mean (mm)	2,03	1,83	1,65	1,99	1,78
BIAS		0,90	0,82	0,98	0,88
MAE (mm)		0,20	0,37	0,03	0,25
RMSE (mm)		5,28	4,50	4,87	6,16
RVE (%)		-9,66	-18,33	-1,52	-12,18
RSQ		0,40	0,43	0,50	0,21
0 mm					
POD		0,80	0,69	0,87	0,60
FAR		0,40	0,42	0,46	0,44
CSI		0,52	0,46	0,50	0,41
5 mm					
POD		0,98	0,98	0,99	1,00
FAR		0,02	0,03	0,02	0,04
CSI		0,96	0,96	0,97	0,96

Table 8.2 Statistics produced at V3E002 during the GPM period of analysis.

	Gauge	TRMM3B42	FEWSARC2	FEWSRFE2	TAMSATv3	GPM
Total (mm)	2023,20	1675,80	1588,10	2071,90	2135,90	1769,30
Max (mm)	64,00	42,90	84,00	93,00	55,90	97,70
Mean (mm)	1,77	1,46	1,39	1,81	1,86	1,54
BIAS		0,83	0,78	1,02	1,06	0,87
MAE (mm)		0,30	0,38	0,04	0,10	0,22
RMSE (mm)		4,79	2,80	4,58	5,62	6,22
RVE (%)		-17,17	-21,51	2,41	5,57	-12,55
RSQ		0,37	0,40	0,51	0,22	0,30
0 mm						
POD		0,80	0,73	0,91	0,68	0,89
FAR		0,38	0,42	0,43	0,43	0,36
CSI		0,54	0,48	0,53	0,45	0,59
5 mm						
POD		0,98	0,96	1,00	1,00	0,96
FAR		0,00	0,00	0,00	0,03	0,00
CSI		0,98	0,96	1,00	0,97	0,96

- U3E004 (Cotton Lands at Hazelmere Dam)

The time series of all products are presented below.

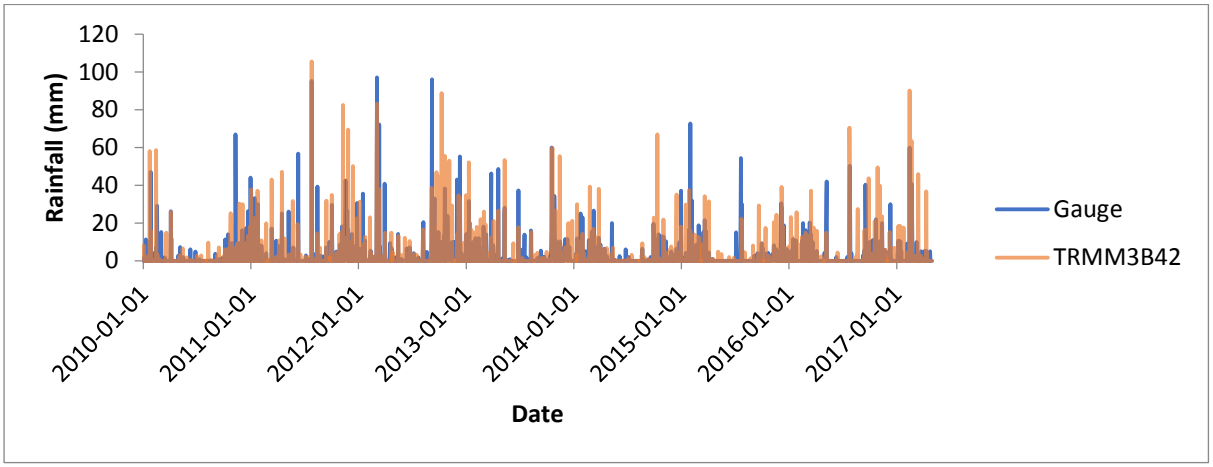

Figure 8.10 Time series of TRMM 3B42 against U3E004 measurements.

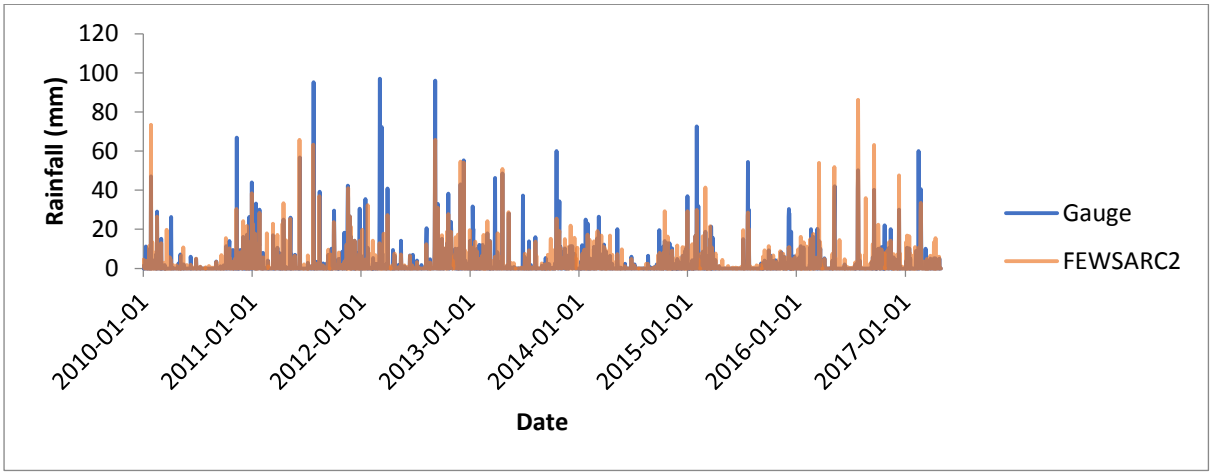

Figure 8.11 Time series of FEWS ARC2 against U3E004 measurements.

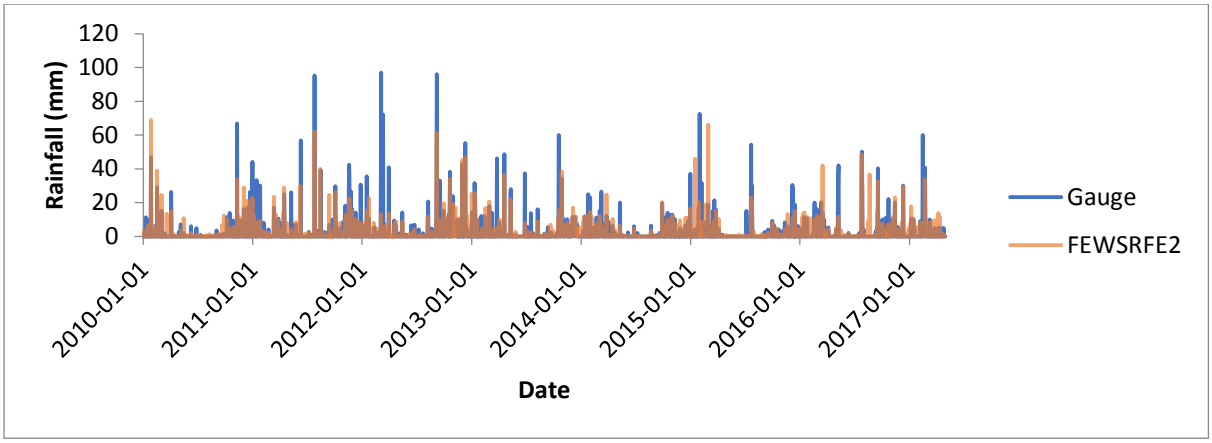

Figure 8.12 Time series of FEWS RFE2 against U3E004 measurements.

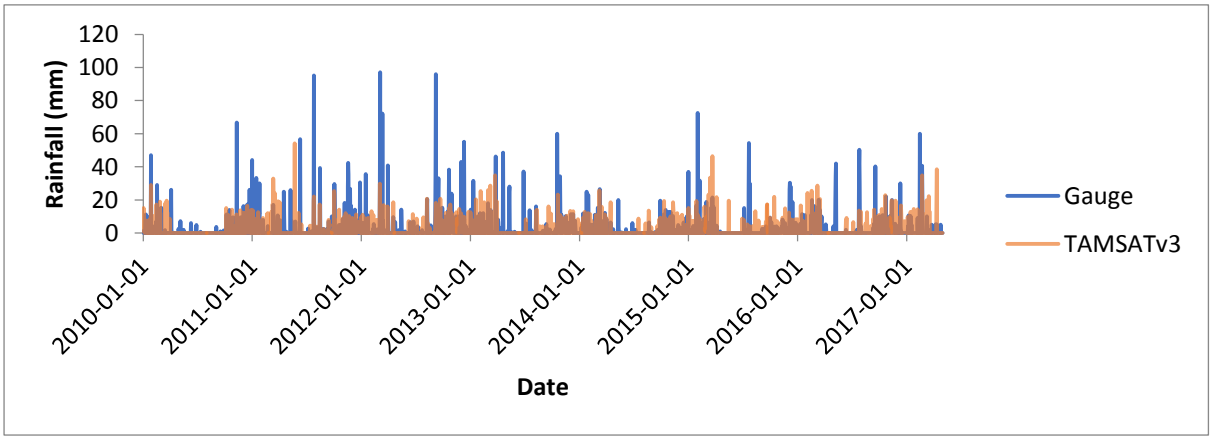

Figure 8.13 Time series of TAMSAT-3 against U3E004 measurements.

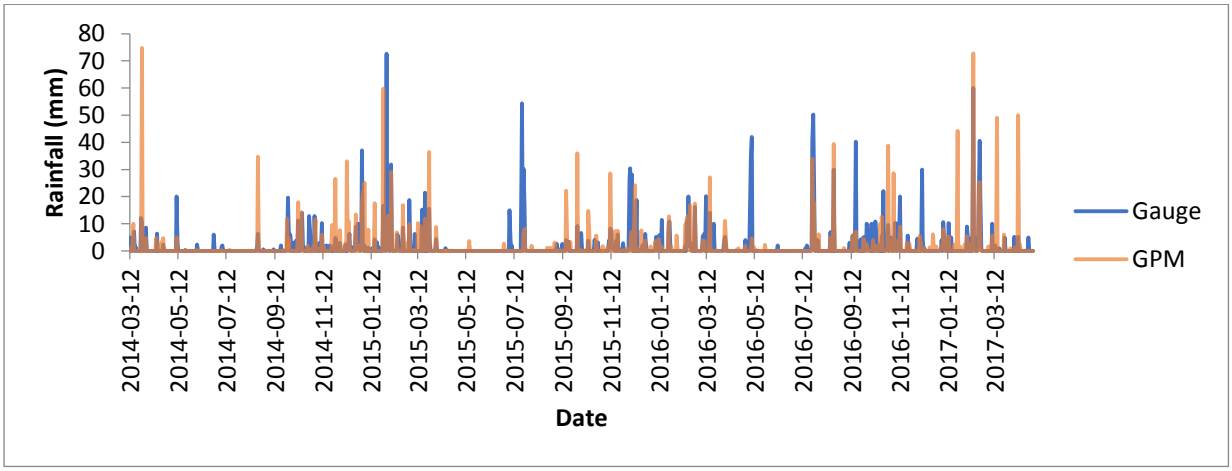

Figure 8.14 Time series of GPM against U3E004 measurements.

Average monthly totals are presented below.

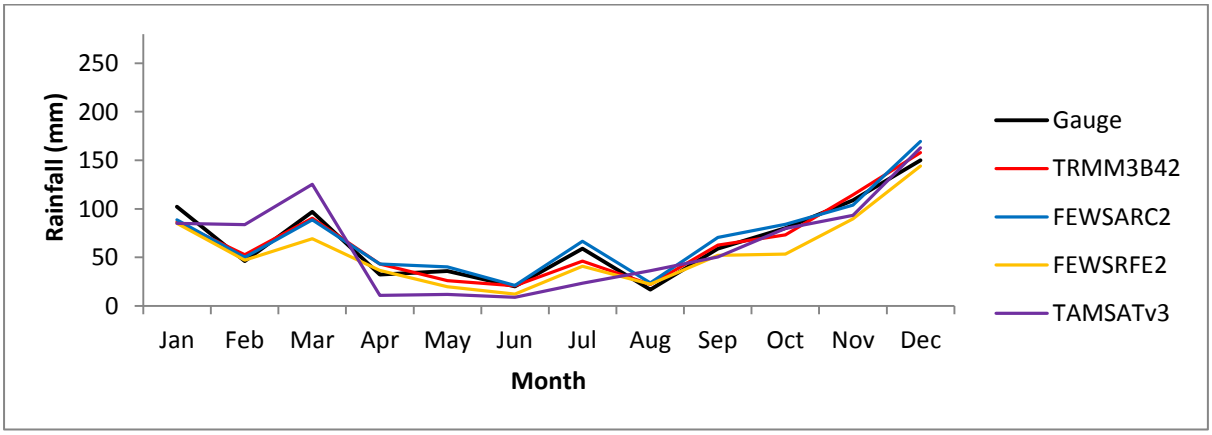

Figure 8.15 Average monthly rainfall totals at U3E004.

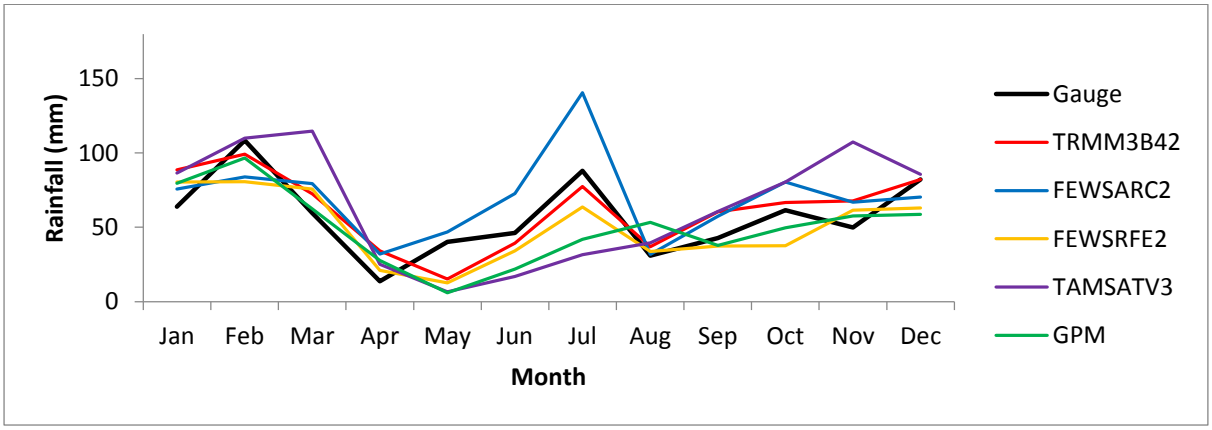

Figure 8.16 Average monthly rainfall totals at U3E004 during the GPM period of analysis.

Accumulated rainfall is presented below.

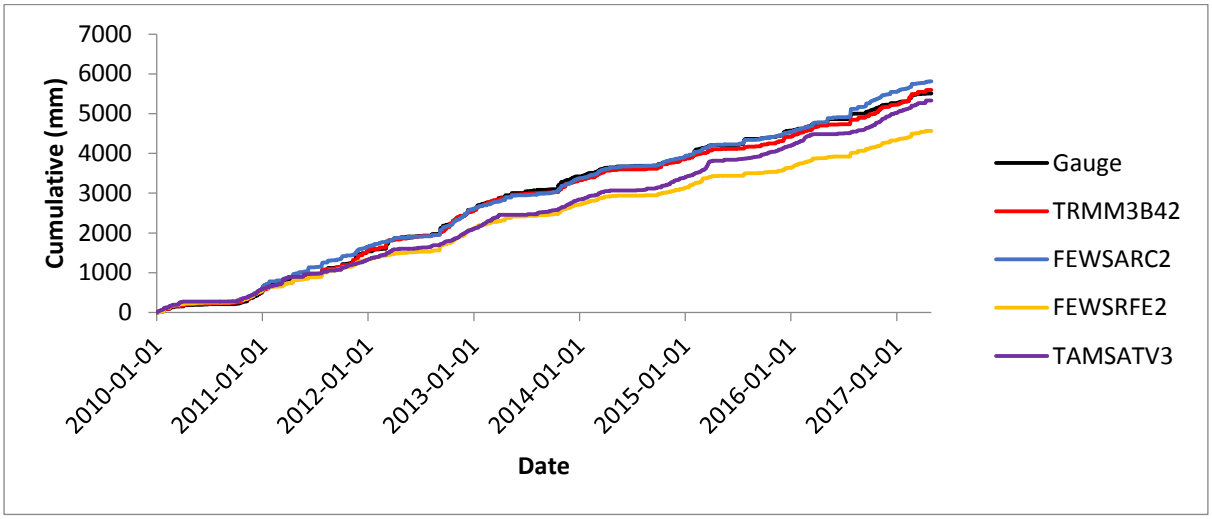

Figure 8.17 Accumulated rainfall at U3E004.

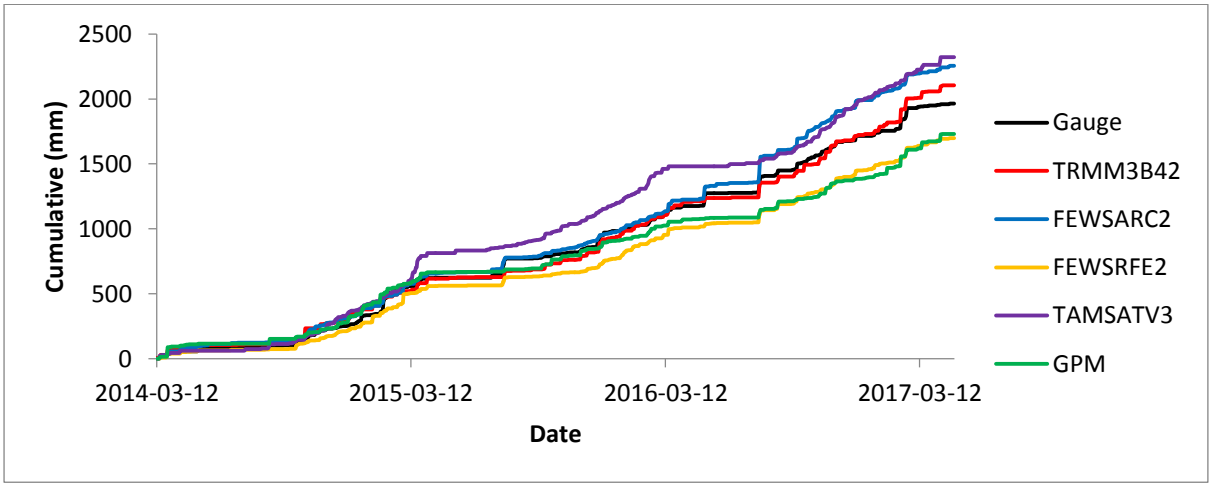

Figure 8.18 Accumulated rainfall at U3E004 during the GPM period of analysis.

Table 8.3 Statistics produced at U3E004.

	Gauge	TRMM3B42	FEWSARC2	FEWSRFE2	TAMSATv3
Total (mm)	5498,00	5593,80	5812,80	4569,20	5327,30
Max (mm)	97,00	105,50	86,20	68,90	54,20
Mean (mm)	2,05	2,09	2,17	1,71	1,99
BIAS		1,02	1,06	0,83	0,97
MAE (mm)		0,04	0,12	0,35	0,06
RMSE (mm)		7,59	5,05	5,59	7,45
RVE (%)		1,74	5,73	-16,89	-3,10
RSQ		0,25	0,43	0,40	0,07
0 mm					
POD		0,50	0,83	0,84	0,50
FAR		0,44	0,44	0,44	0,57
CSI		0,36	0,50	0,51	0,30
5 mm					
POD		0,99	0,98	0,99	0,99
FAR		0,01	0,04	0,02	0,02
CSI		0,98	0,95	0,97	0,97

Table 8.4 Statistics produced at U3E004 during the GPM period of analysis.

	Gauge	TRMM3B42	FEWSARC2	FEWSRFE2	TAMSATv3	GPM
Total (mm)	1920,10	2103,60	2254,60	1697,10	2321,90	1731,10
Max (mm)	72,60	90,10	86,20	66,00	46,50	74,70
Mean (mm)	1,68	1,84	1,97	1,48	2,03	1,51
BIAS		1,10	1,17	0,88	1,21	0,90
MAE (mm)		0,16	0,29	0,19	0,35	0,16
RMSE (mm)		6,53	2,05	4,86	6,52	6,51
RVE (%)		9,56	17,42	-11,61	20,93	-9,84
RSQ		0,25	0,55	0,36	0,07	0,17
0 mm						
POD		0,47	0,83	0,80	0,53	0,57
FAR		0,44	0,45	0,45	0,59	0,50
CSI		0,34	0,49	0,48	0,30	0,36
5 mm						
POD		1,00	0,97	1,00	0,98	0,98
FAR		0,02	0,06	0,03	0,02	0,00
CSI		0,98	0,92	0,97	0,96	0,98

- U2E002 (Driefontein at Cedara)

The time series of the products are presented below.

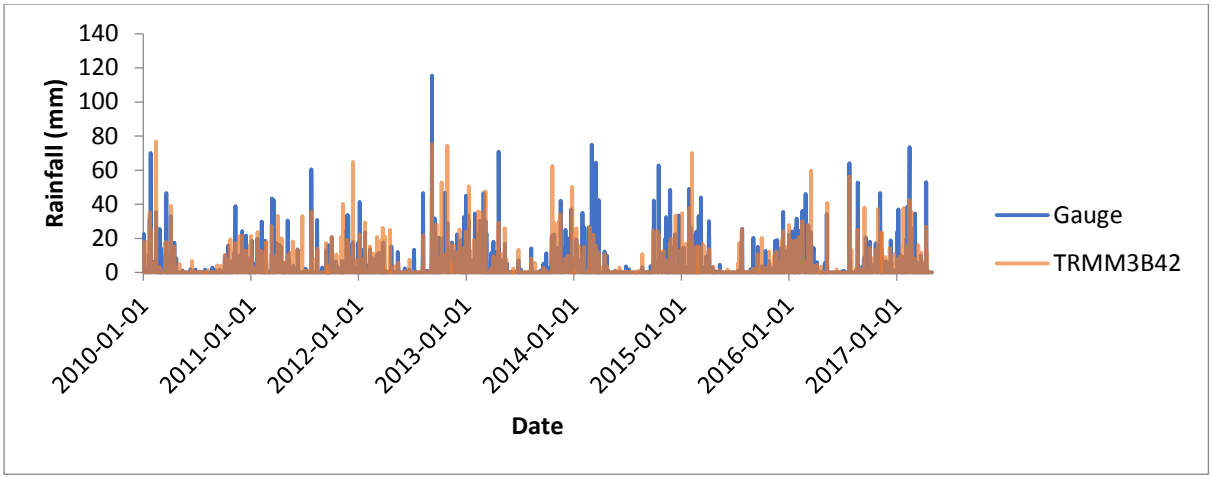

Figure 8.19 Time series of TRMM 3B42 against U2E002 measurements.

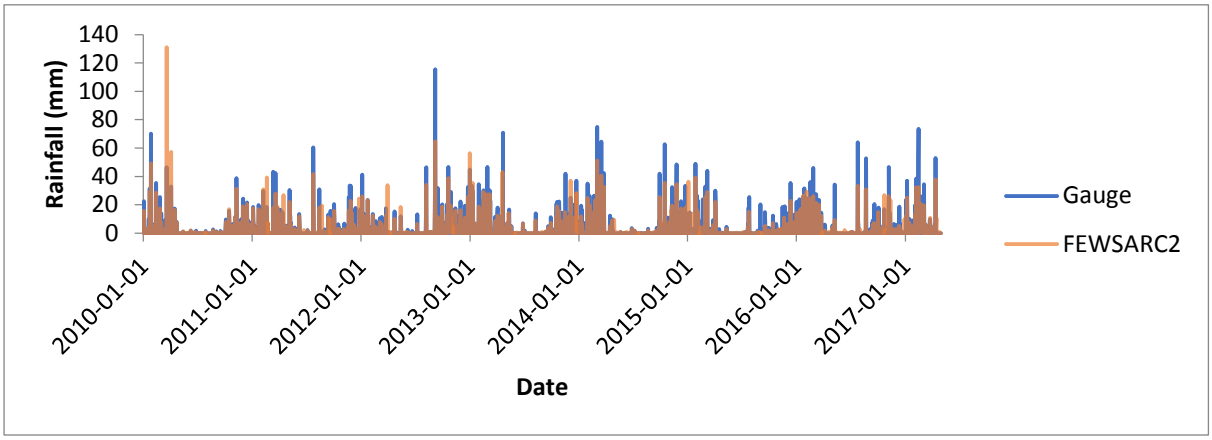

Figure 8.20 Time series of FEWS ARC2 against U2E002 measurements.

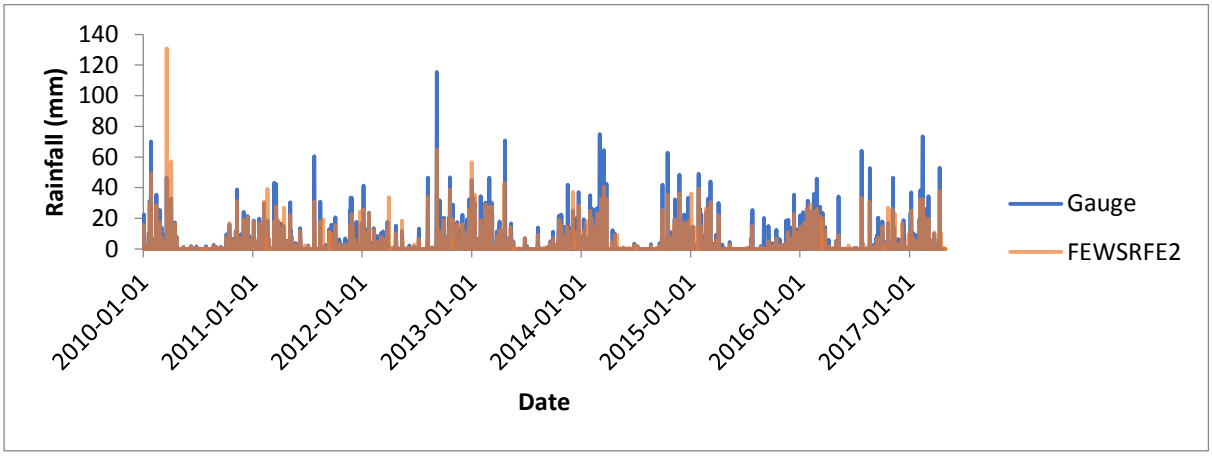

Figure 8.21 Time series of FEWS RFE2 against U2E002 measurements.

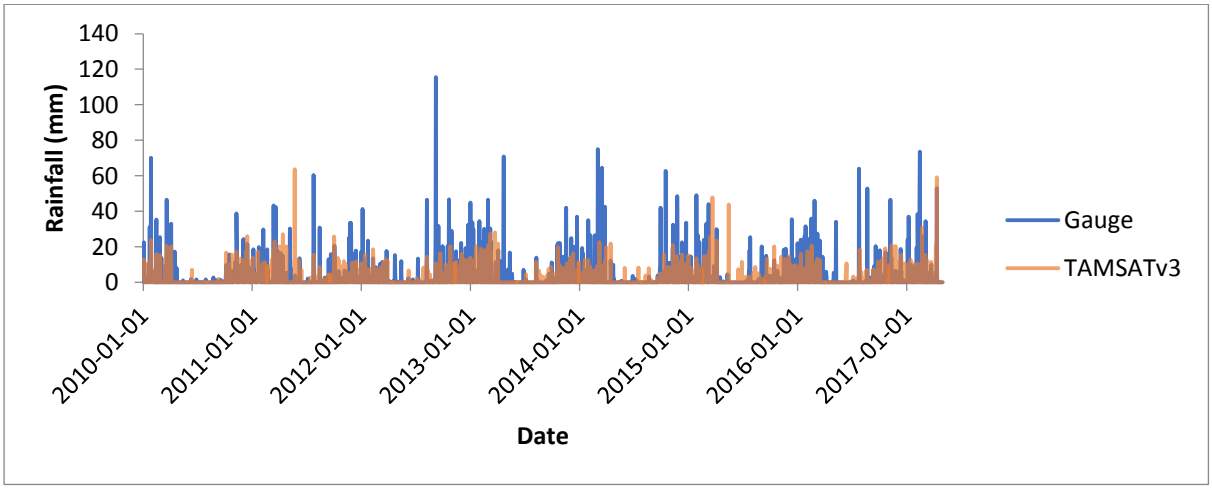

Figure 8.22 Time series of TAMSAT-3 against U2E002 measurements.

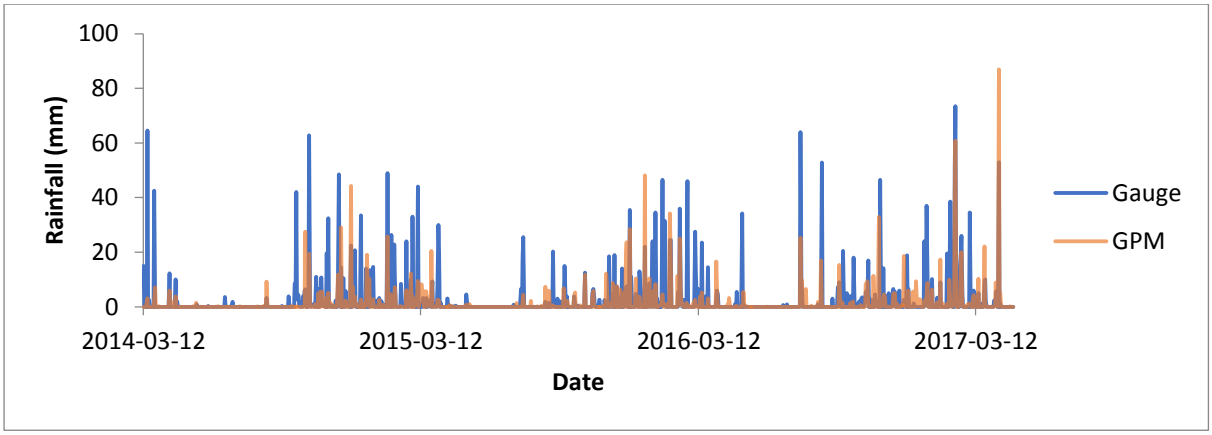

Figure 8.23 Time series of GPM against U2E002 measurements.

Average monthly rainfall totals are presented below.

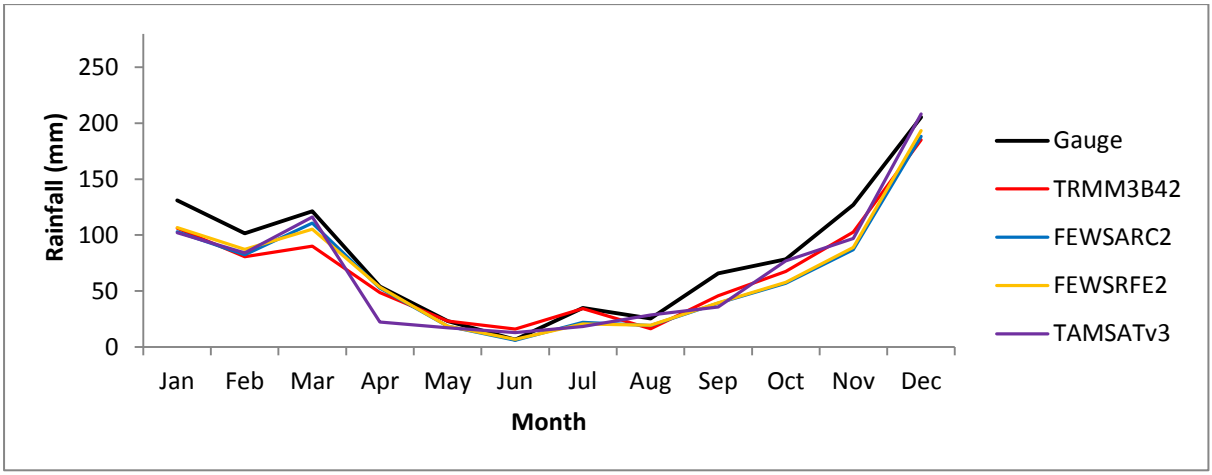

Figure 8.24 Average monthly rainfall totals at U2E002.

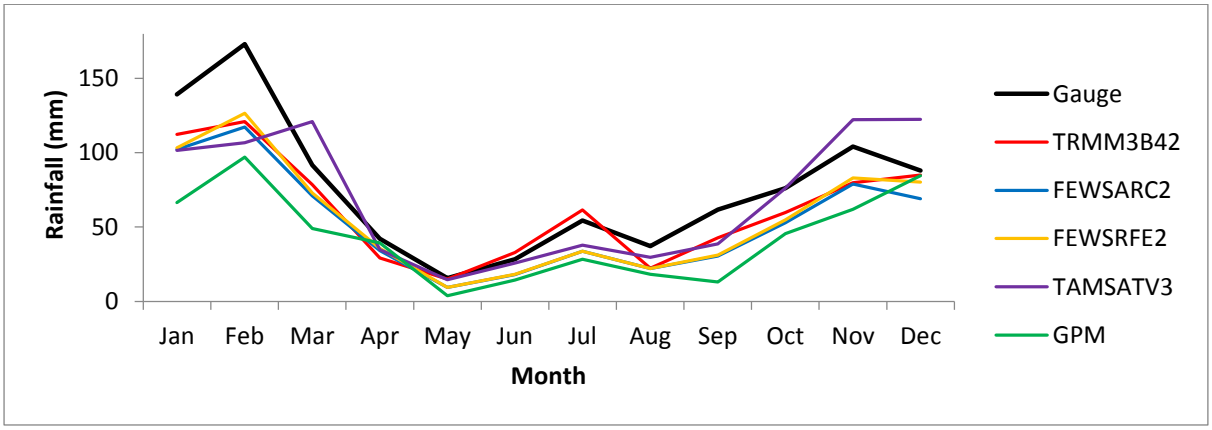

Figure 8.25 Average monthly rainfall totals at U2E002 during the GPM period of analysis.

Accumulated rainfall is presented below.

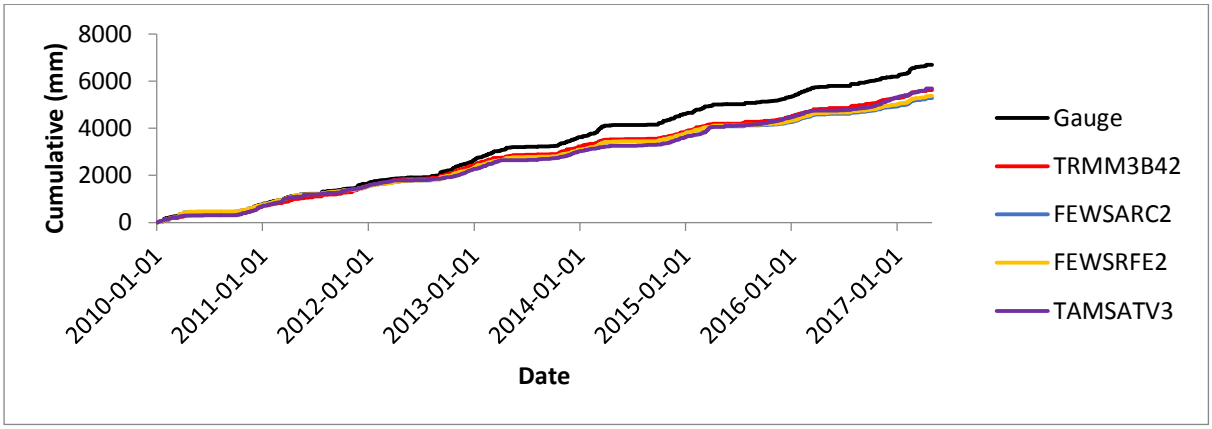

Figure 8.26 Accumulated rainfall atU2E002.

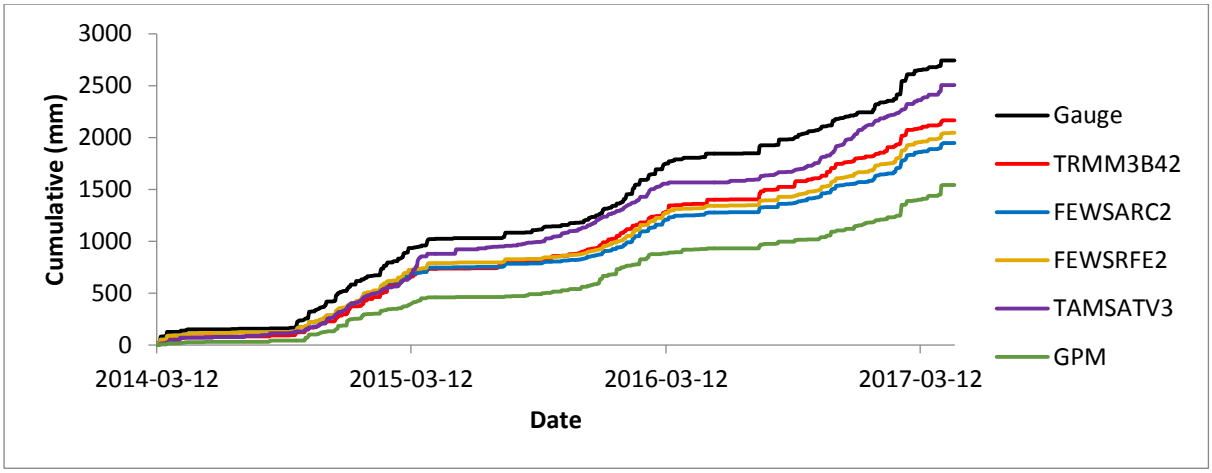

Figure 8.27 Accumulated rainfall at U2E002 during the GPM period of analysis.

Table 8.5 Statistics produced atU2E002.

	Gauge	TRMM3B42	FEWSARC2	FEWSRFE2	TAMSATv3
Total (mm)	6731,20	5621,20	5284,60	5366,90	5686,70
Max (mm)	115,50	76,90	131,00	131,00	63,70
Mean (mm)	2,51	2,10	1,97	2,00	2,12
BIAS		0,84	0,79	0,80	0,84
MAE (mm)		0,41	0,54	0,51	0,39
RMSE (mm)		7,31	4,22	5,20	7,70
RVE (%)		-16,49	-21,49	-20,27	-15,52
RSQ		0,26	0,59	0,57	0,11
0 mm					
POD		0,55	0,87	0,88	0,56
FAR		0,41	0,35	0,35	0,49
CSI		0,40	0,59	0,60	0,36
5 mm					
POD		1,00	0,97	0,97	1,00
FAR		0,01	0,00	0,00	0,03
CSI		0,99	0,97	0,97	0,97

Table 8.6 Statistics produced at U2E002 during the GPM period of analysis.

	Gauge	TRMM3B42	FEWSARC2	FEWSRFE2	TAMSATv3	GPM
Total (mm)	2743,30	2164,90	1946,80	2043,50	2504,90	1542,50
Max (mm)	73,50	70,10	40,60	40,60	59,10	86,90
Mean (mm)	2,39	1,89	1,70	1,78	2,19	1,35
BIAS		0,79	0,71	0,74	0,91	0,56
MAE (mm)		0,50	0,70	0,61	0,21	1,05
RMSE (mm)		7,04	2,30	4,82	7,75	6,85
RVE (%)		-21,08	-29,03	-25,51	-8,69	-43,77
RSQ		0,27	0,64	0,64	0,11	0,27
0 mm						
POD		0,53	0,85	0,87	0,59	0,61
FAR		0,40	0,39	0,40	0,52	0,46
CSI		0,39	0,55	0,55	0,36	0,40
5 mm						
POD		1,00	0,95	0,95	1,00	0,95
FAR		0,01	0,00	0,00	0,03	0,02
CSI		0,99	0,95	0,95	0,97	0,93

- V1E008 (Eendracht at Driel Barrage)

The time series of the products are presented below.

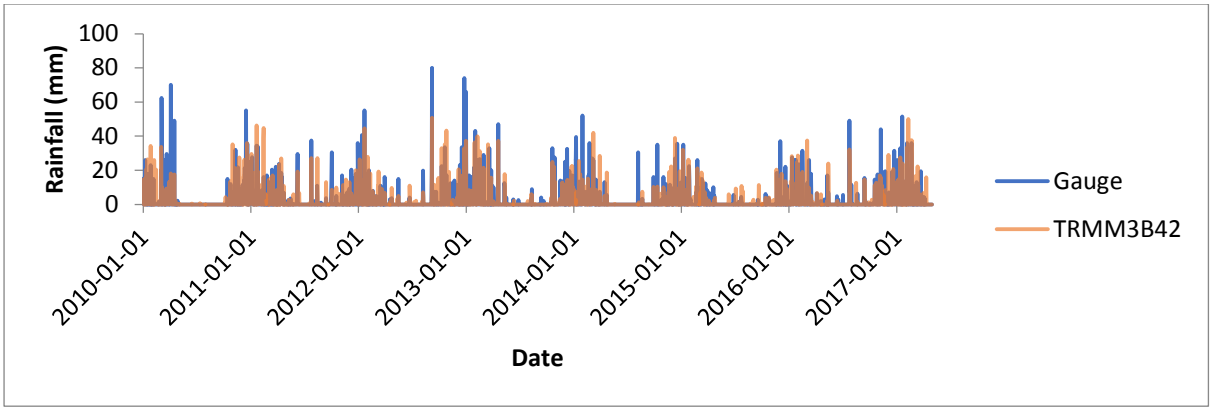

Figure 8.28 Time series of TRMM 3B42 against V1E008 measurements.

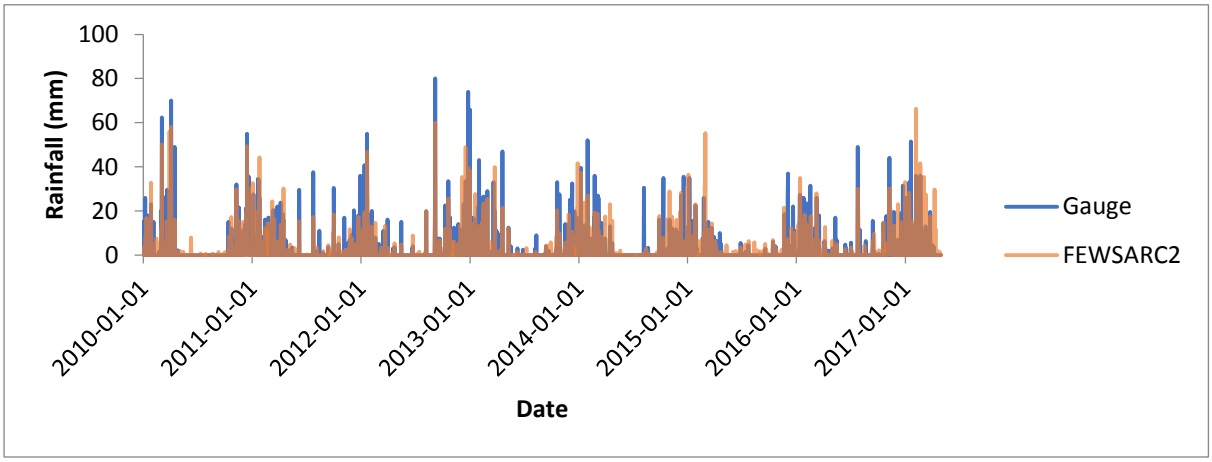

Figure 8.29 Time series of FEWS ACR2 against V1E008 measurements.

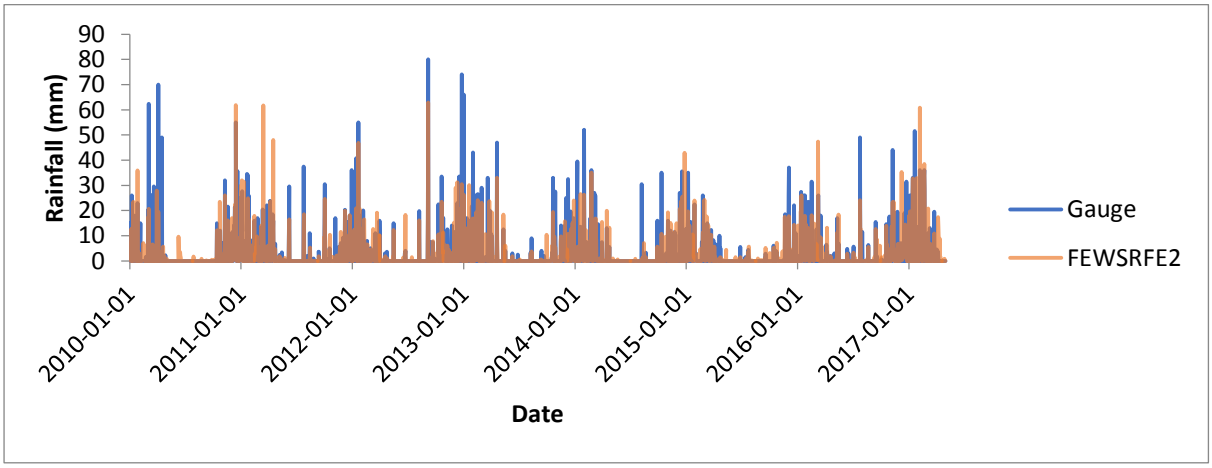

Figure 8.30 Time series of FEWS RFE2 against V1E008 measurements.

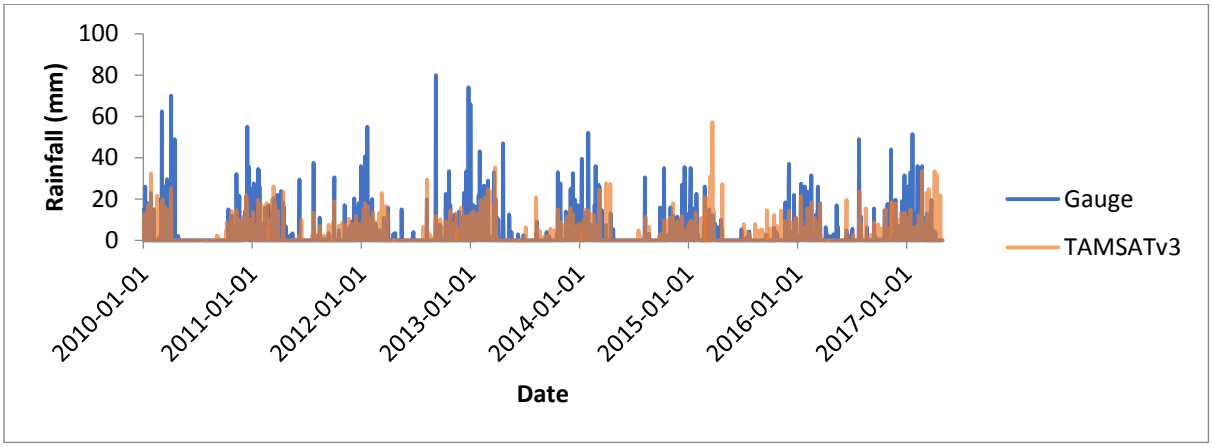

Figure 8.31 Time series of TAMSAT-3 against V1E008 measurements.

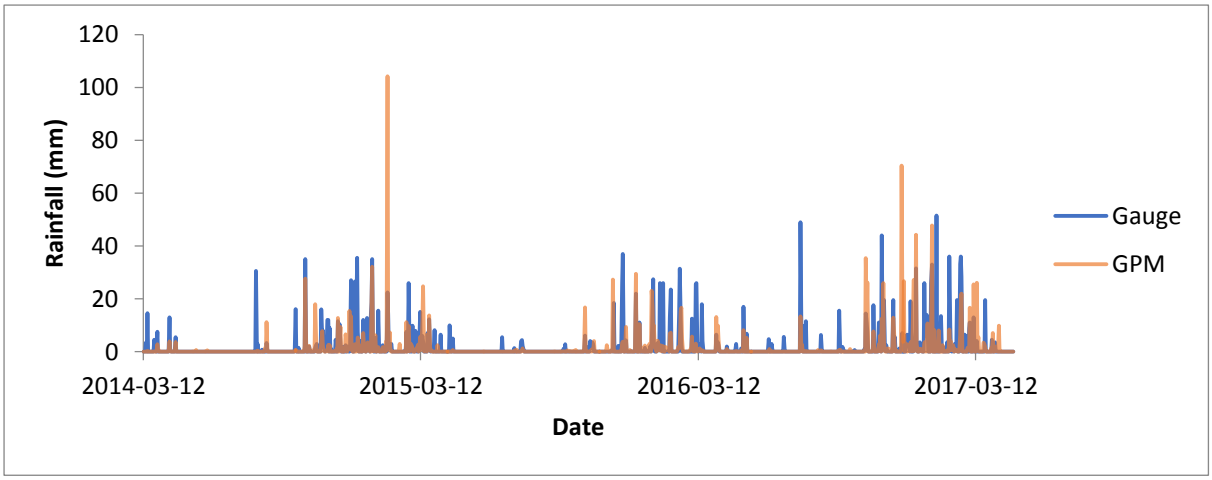

Figure 8.32 Time series of GPM against V1E008 measurements.

Average monthly totals are presented below.

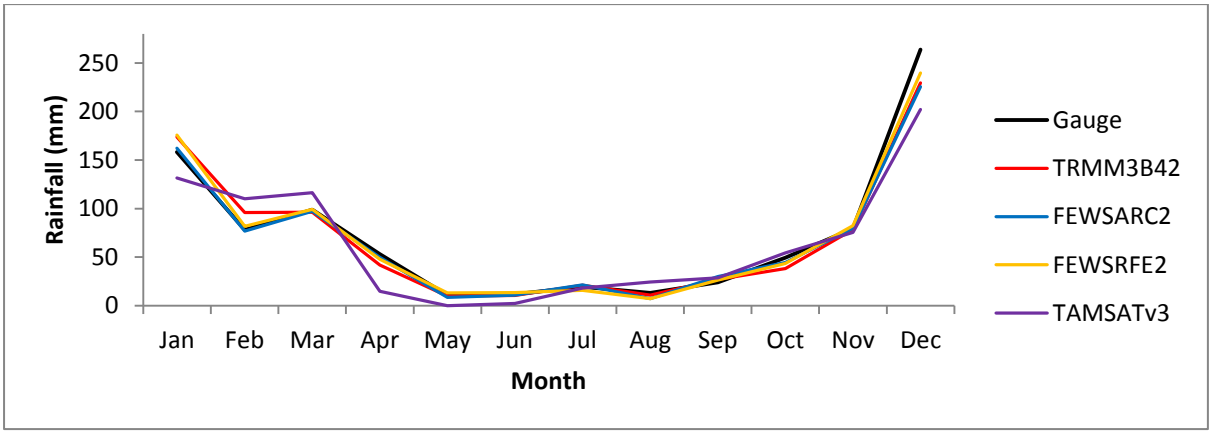

Figure 8.33 Average monthly rainfall totals at V1E008.

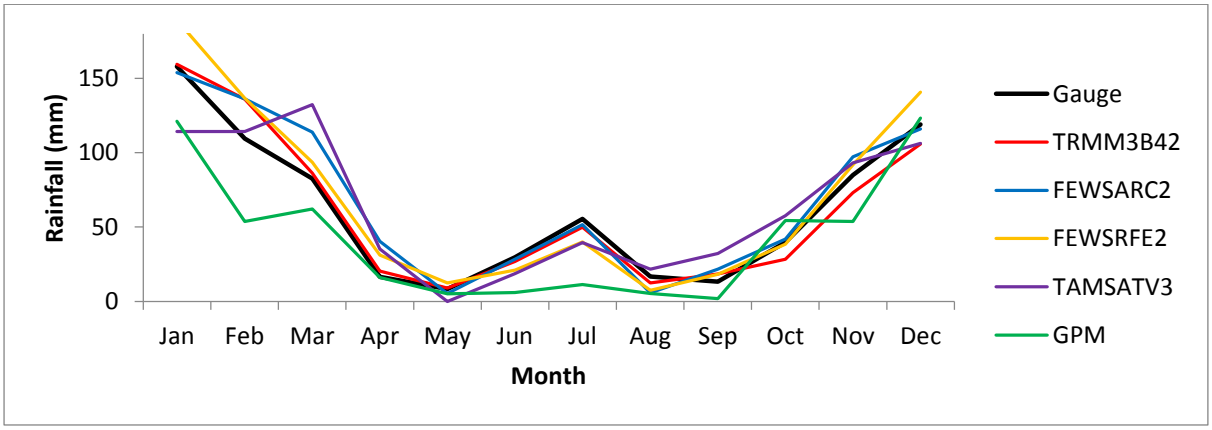

Figure 8.34 Average monthly rainfall totals at V1E008 during the GPM period of analysis.

Accumulated rainfall is presented below.

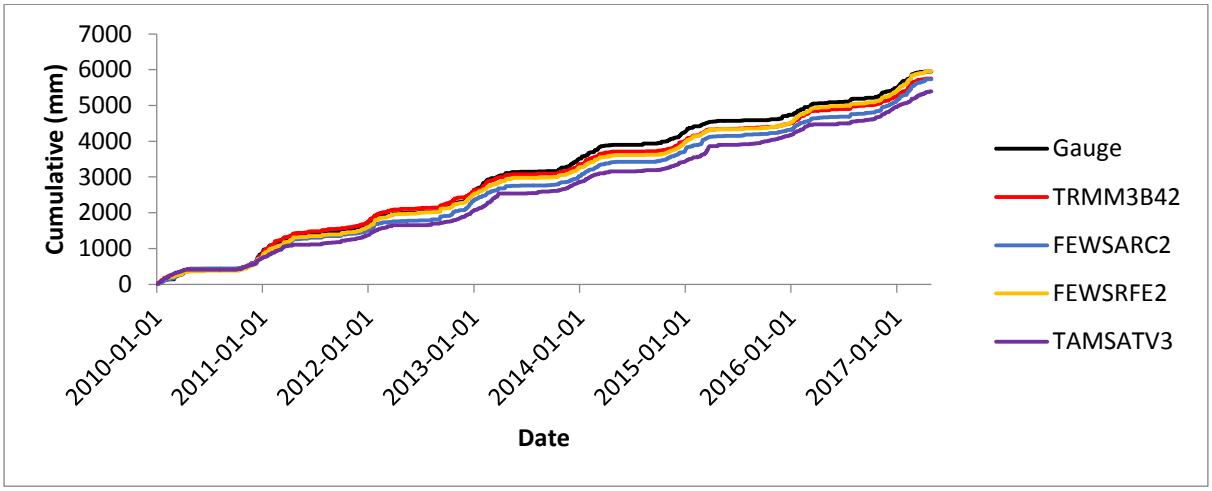

Figure 8.35 Accumulated rainfall atV1E008.

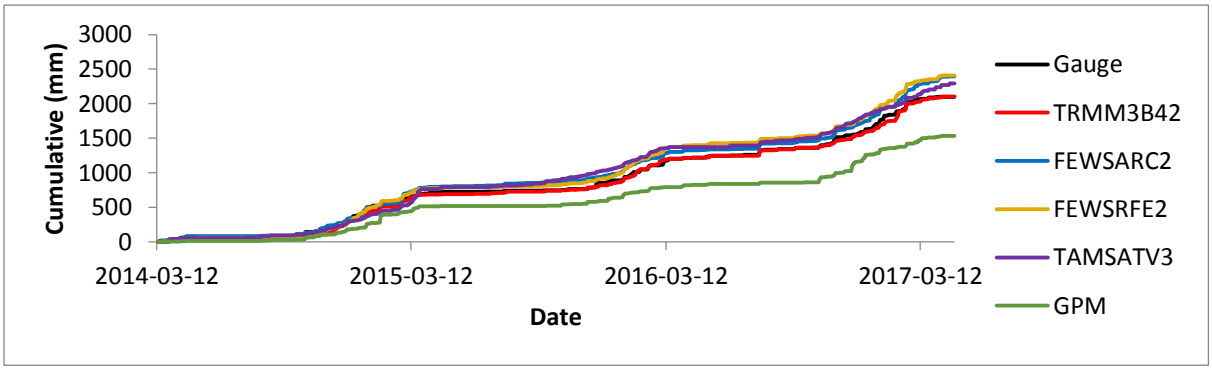

Figure 8.36 Accumulated rainfall at V1E008 during the GPM period of analysis.

Table 8.7 Statistics produced at V1E008.

	Gauge	TRMM3B42	FEWSARC2	FEWSRFE2	TAMSATv3
Total (mm)	5946,00	5754,40	5736,40	5960,90	5396,20
Max (mm)	80,00	50,70	66,20	62,90	57,10
Mean (mm)	2,22	2,15	2,14	2,23	2,02
BIAS		0,97	0,96	1,00	0,91
MAE (mm)		0,07	0,08	0,01	0,21
RMSE (mm)		5,82	4,45	5,32	6,62
RVE (%)		-3,22	-3,53	0,25	-9,25
RSQ		0,35	0,42	0,43	0,15
0 mm					
POD		0,78	0,74	0,86	0,65
FAR		0,40	0,48	0,47	0,49
CSI		0,52	0,44	0,49	0,40
5 mm					
POD		0,98	1,00	0,98	0,99
FAR		0,02	0,03	0,03	0,03
CSI		0,96	0,97	0,95	0,96

Table 8.8 Statistics produced at V1E008 during the GPM period of analysis.

	Gauge	TRMM3B42	FEWSARC2	FEWSRFE2	TAMSATv3	GPM
Total (mm)	2096,70	2103,70	2395,30	2408,10	2291,50	1532,30
Max (mm)	51,50	50,00	66,20	60,80	57,10	104,20
Mean (mm)	1,83	1,84	2,09	2,10	2,00	1,34
BIAS		1,00	1,14	1,15	1,09	0,73
MAE (mm)		0,01	0,26	0,27	0,17	0,49
RMSE (mm)		5,24	2,65	4,63	5,94	6,05
RVE (%)		0,33	14,24	14,85	9,29	-26,92
RSQ		0,31	0,29	0,44	0,15	0,19
0 mm						
POD		0,73	0,77	0,85	0,67	0,79
FAR		0,42	0,50	0,49	0,51	0,40
CSI		0,48	0,44	0,47	0,40	0,51
5 mm						
POD		0,99	1,00	0,98	0,98	1,00
FAR		0,00	0,00	0,00	0,00	0,00
CSI		0,99	1,00	0,98	0,98	1,00

- U2E010 (Inanda Dam)

The time series of the products are presented below.

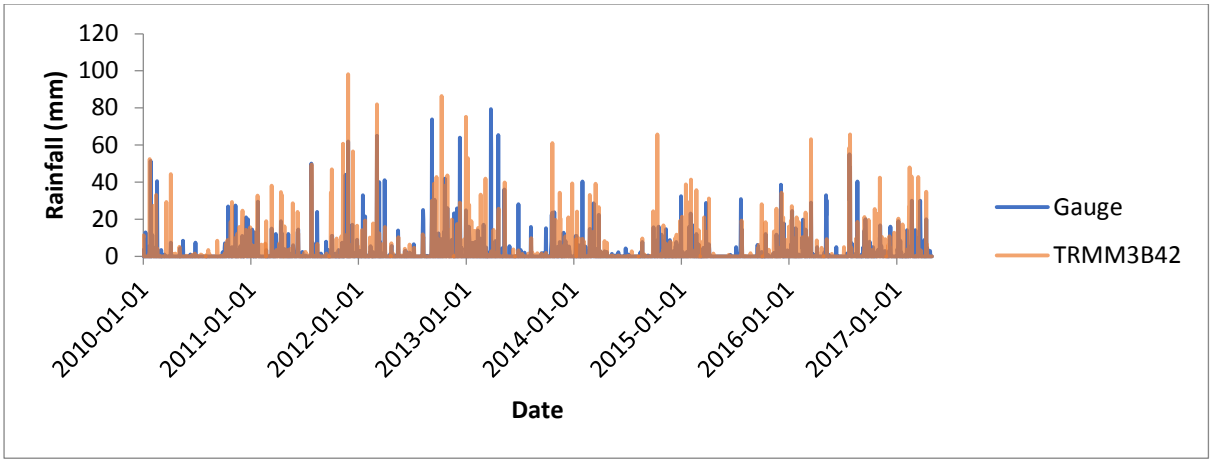

Figure 8.37 Time series of TRMM 3B42 against U2E010 measurements.

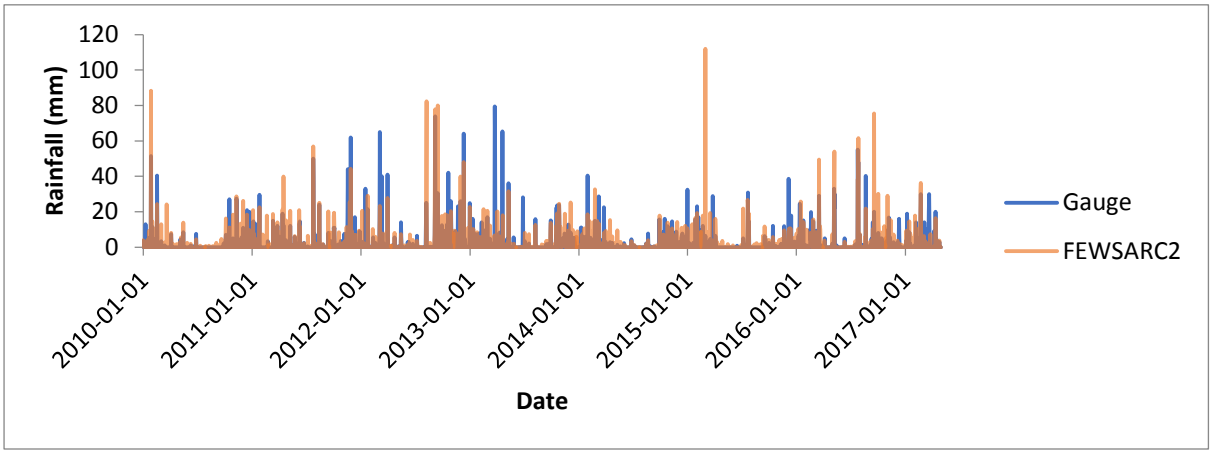

Figure 8.38 Time series of FEWS ARC2 against U2E010 measurements.

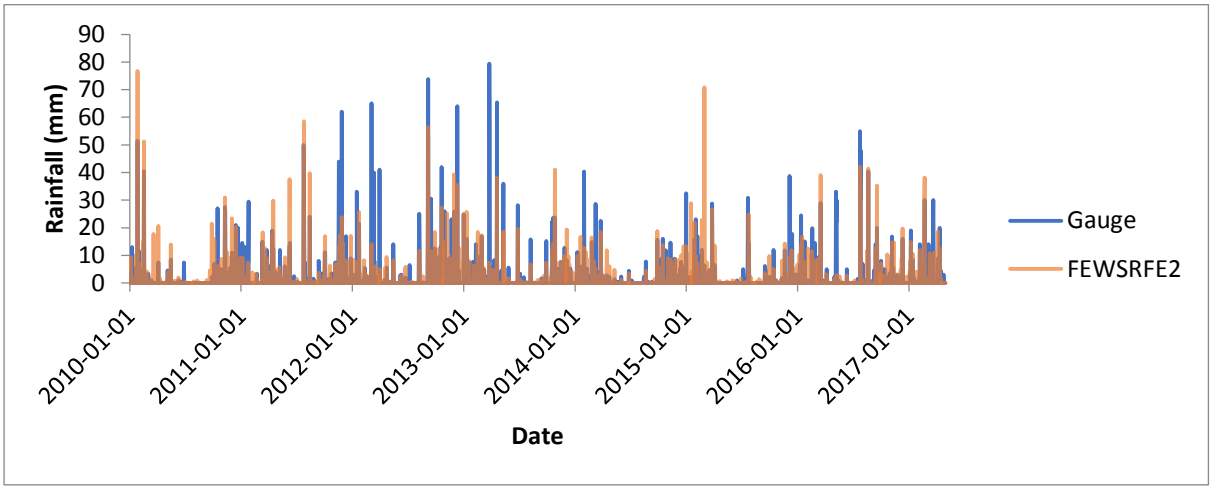

Figure 8.39 Time series of FEWS RFE2 against U2E010 measurements.

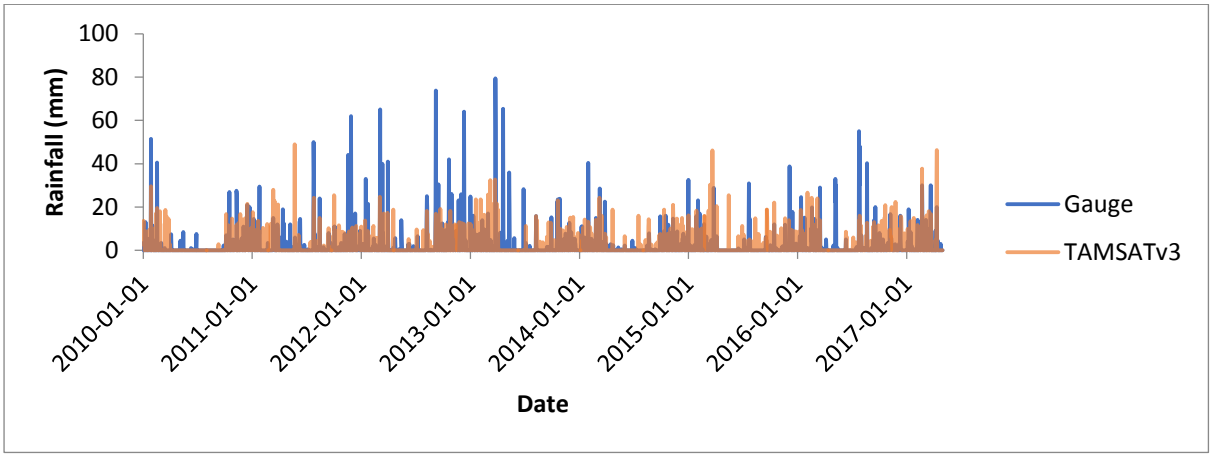

Figure 8.40 Time series of TAMSAT-3 against U2E010 measurements.

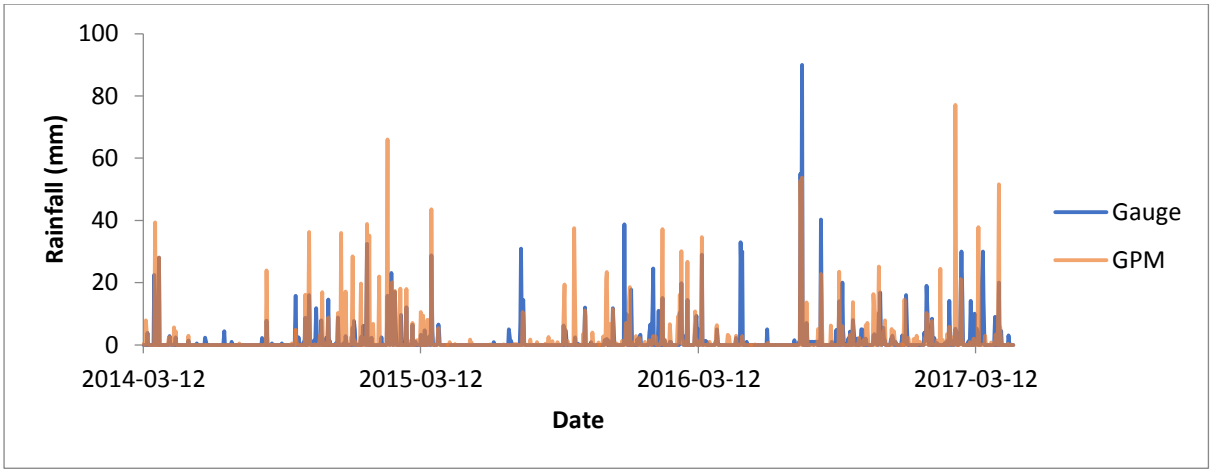

Figure 8.41 Time series of GPM against U2E010 measurements.

Average monthly rainfall totals are presented below.

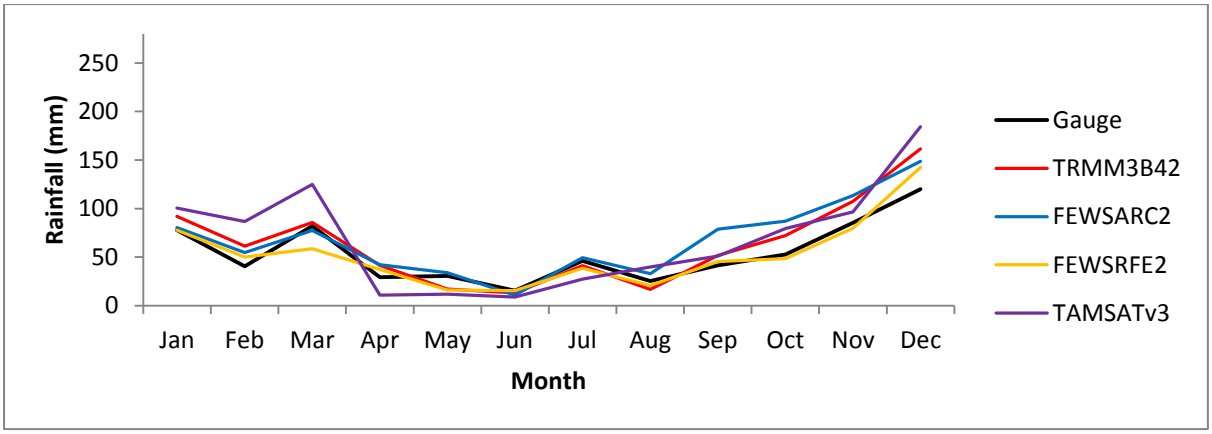

Figure 8.42 Average monthly rainfall totals at U2E010.

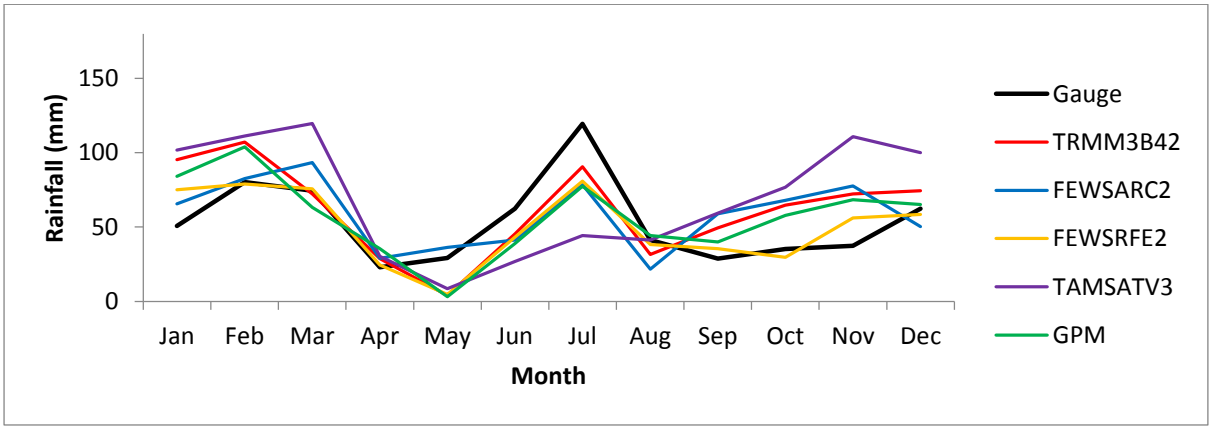

Figure 8.43 Average monthly rainfall totals at U2E010 during the GPM period of analysis.

Accumulated rainfall is presented below.

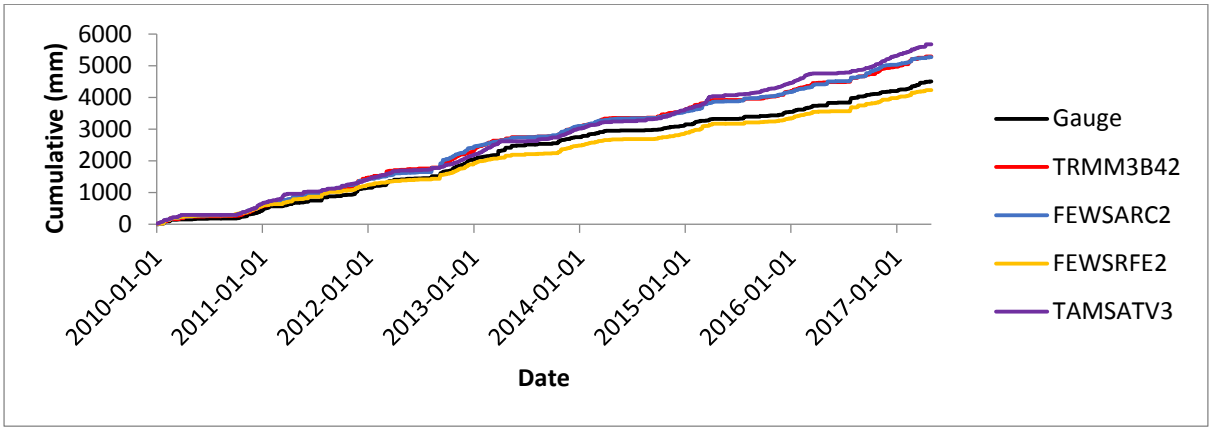

Figure 8.44 Accumulated rainfall at U2E010.

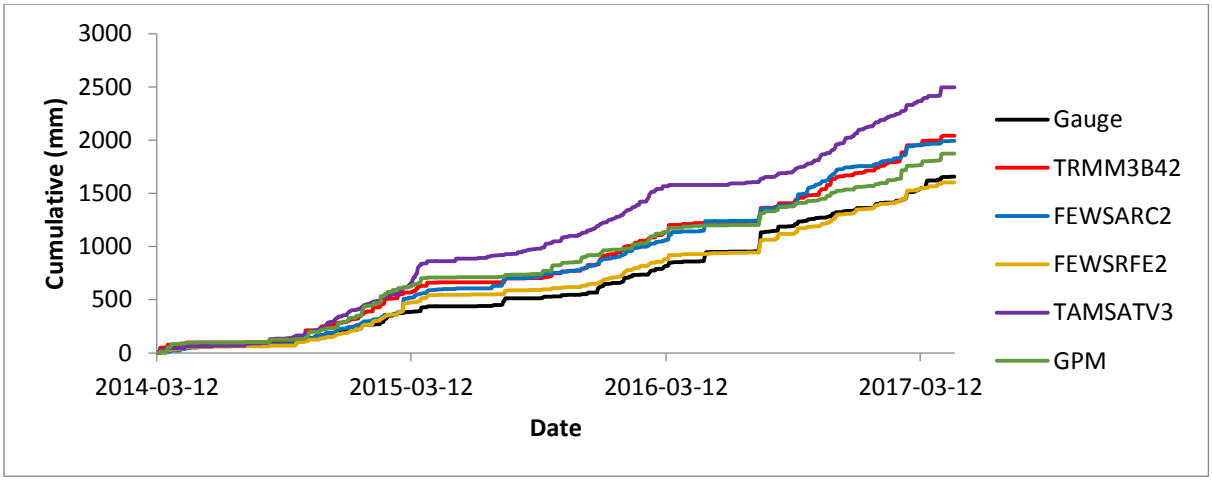

Figure 8.45 Accumulated rainfall at U2E010 during the GPM period of analysis.

Tables of statistics are presented below.

Table 8.9 Statistics produced at U2E010.

	Gauge	TRMM3B42	FEWSARC2	FEWSRFE2	TAMSATv3
Total (mm)	4610,40	5292,30	5263,90	4227,10	5676,10
Max (mm)	90,00	98,10	112,00	76,70	49,00
Mean (mm)	1,72	1,98	1,97	1,58	2,12
BIAS		1,15	1,14	0,92	1,23
MAE (mm)		0,25	0,24	0,14	0,40
RMSE (mm)		7,13	4,63	5,06	6,92
RVE (%)		14,79	14,17	-8,31	23,12
RSQ		0,22	0,37	0,41	0,07
0 mm					
POD		0,52	0,73	0,67	0,52
FAR		0,43	0,53	0,52	0,60
CSI		0,37	0,40	0,39	0,29
5 mm					
POD		1,00	1,00	0,99	0,99
FAR		0,03	0,04	0,02	0,02
CSI		0,97	0,96	0,97	0,97

Table 8.10 Statistics produced at U2E010 during the GPM period of analysis.

	Gauge	TRMM3B42	FEWSARC2	FEWSRFE2	TAMSATv3	GPM
Total (mm)	1657,20	2040,20	1994,70	1603,20	2496,10	1874,60
Max (mm)	90,00	65,80	112,00	70,80	46,30	77,10
Mean (mm)	1,45	1,78	1,74	1,40	2,18	1,64
BIAS		1,23	1,20	0,97	1,51	1,13
MAE (mm)		0,33	0,29	0,05	0,73	0,19
RMSE (mm)		6,11	1,86	4,45	6,25	5,72
RVE (%)		23,11	20,37	-3,26	50,62	13,12
RSQ		0,24	0,31	0,39	0,08	0,29
0 mm						
POD		0,46	0,70	0,61	0,52	0,55
FAR		0,44	0,55	0,54	0,63	0,54
CSI		0,34	0,38	0,36	0,27	0,34
5 mm						
POD		1,00	1,00	1,00	0,98	1,00
FAR		0,00	0,07	0,00	0,02	0,02
CSI		1,00	0,93	1,00	0,96	0,98

- V2E002 (Rietvlei at Craigie Burn dam)

The time series of the products are presented below.

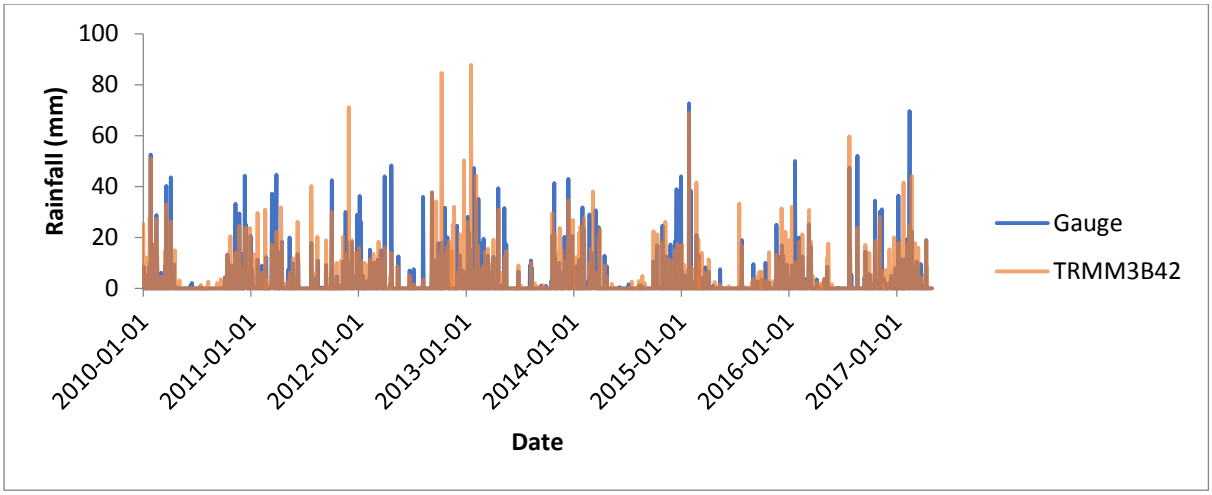

Figure 8.46 Time series of TRMM 3B42 against V2E002 measurements.

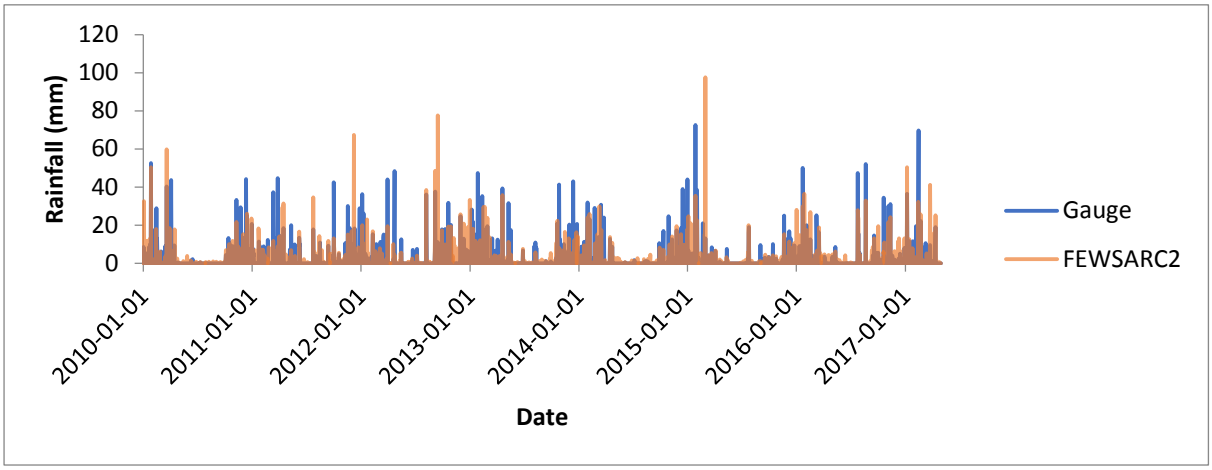

Figure 8.47 Time series of FEWS ARC2 against V2E002 measurements.

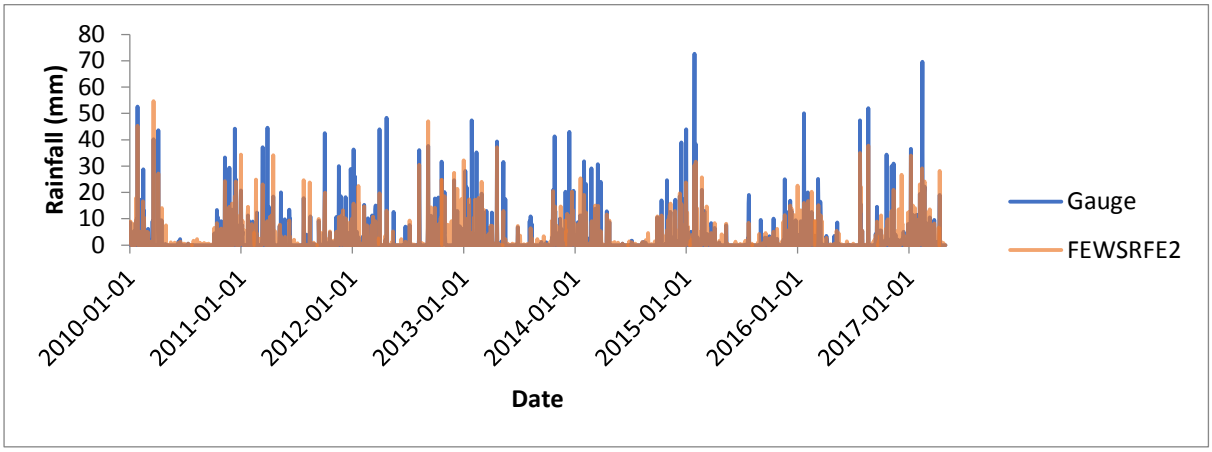

Figure 8.48 Time series of FEWS RFE2 against V2E002 measurements.

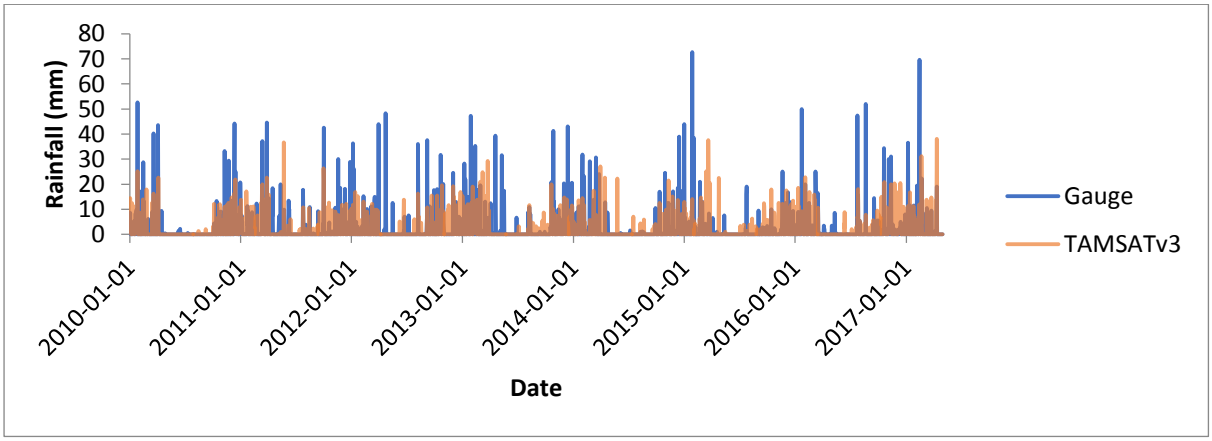

Figure 8.49 Time series of TAMSAT-3 against V2E002 measurements.

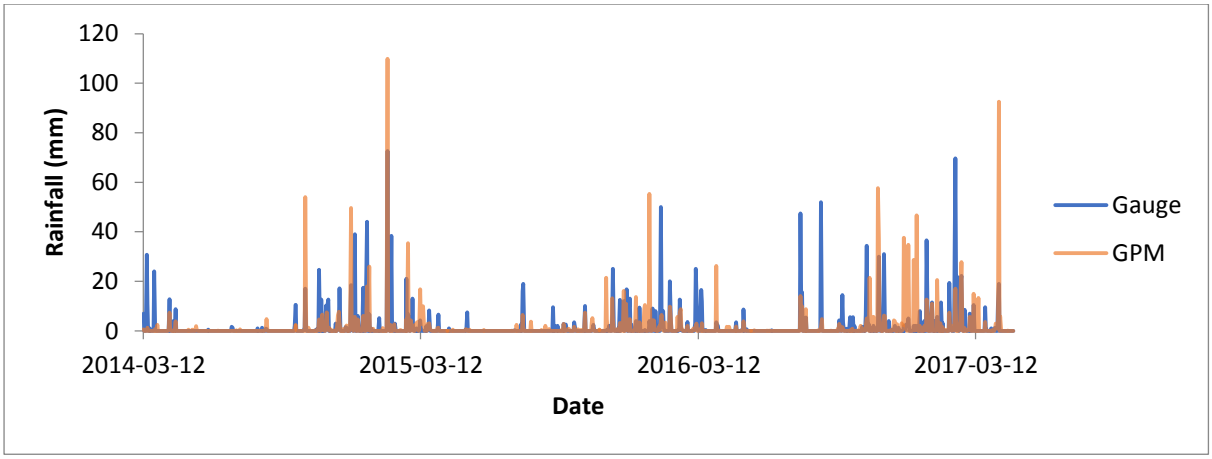

Figure 8.50 Time series of GPM against V2E002 measurements.

Average monthly rainfall totals are presented below.

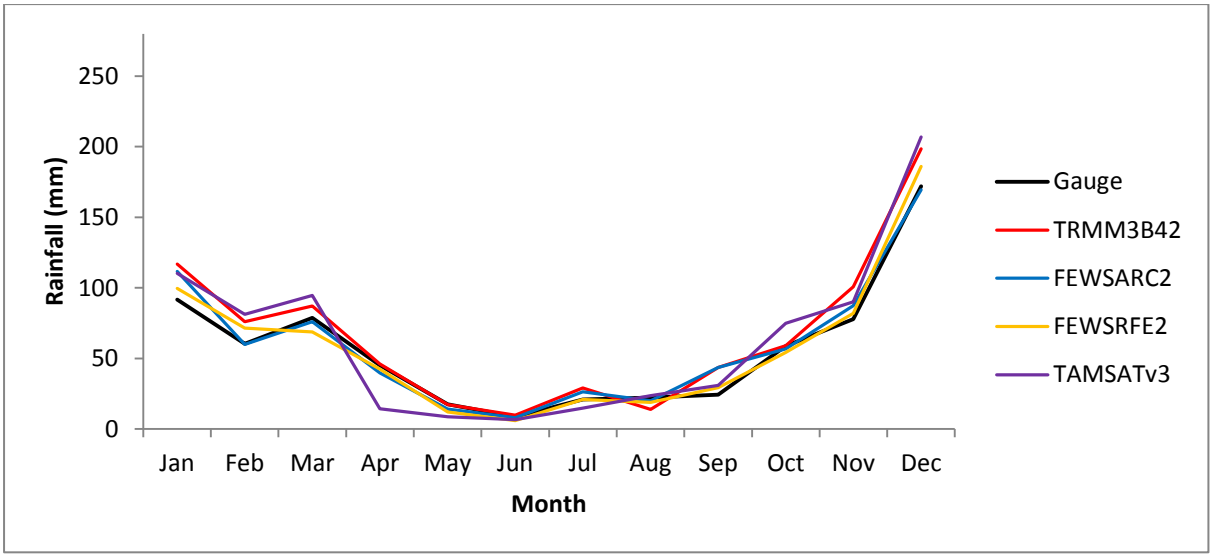

Figure 8.51 Average monthly rainfall totals at V2E002.

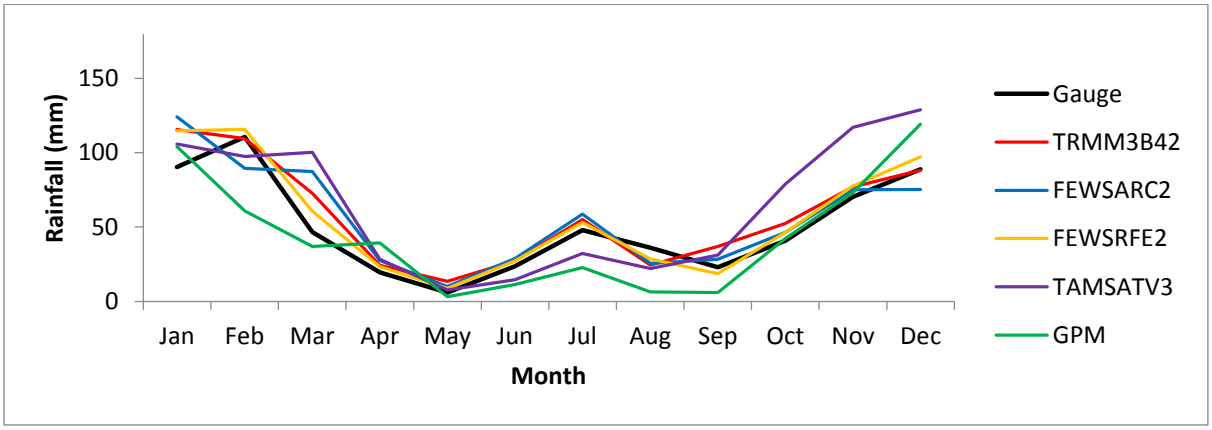

Figure 8.52 Average monthly rainfall totals at V2E002 during the GPM period of analysis.

Accumulated rainfall is presented below.

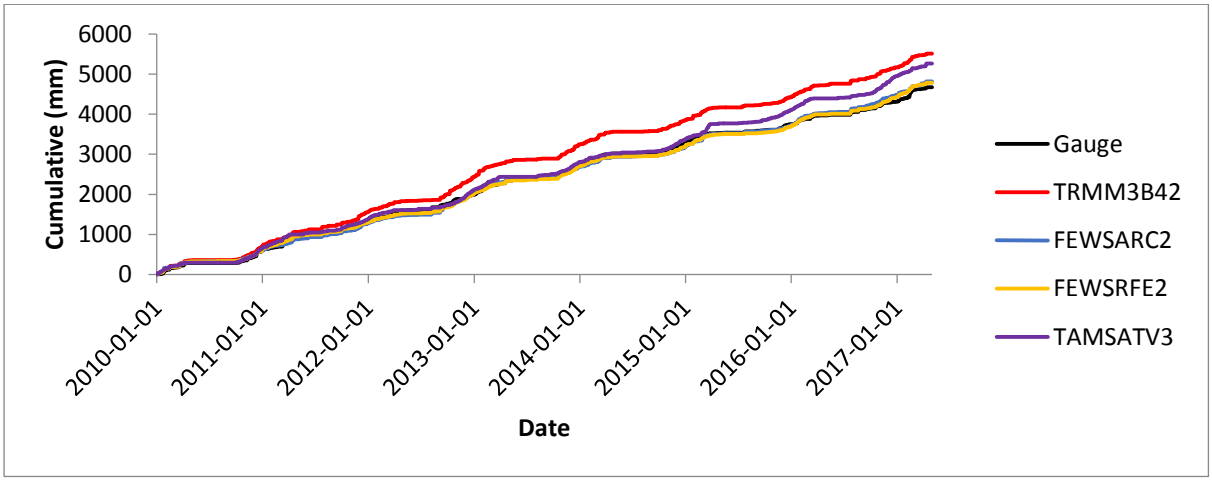

Figure 8.53 Accumulated rainfall at V2E002.

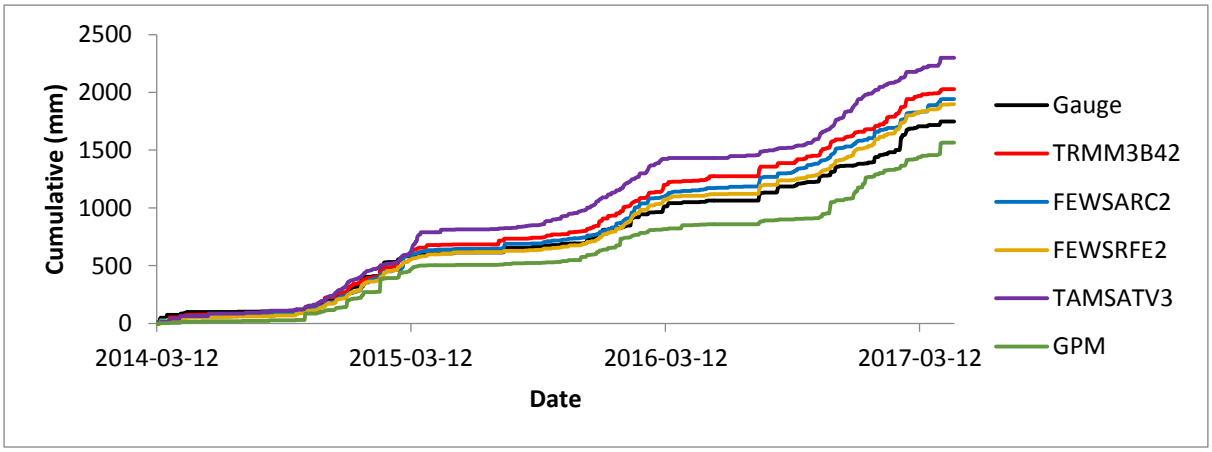

Figure 8.54 Accumulated rainfall at V2E002 during the GPM period of analysis.

Tables of statistics are presented below.

Table 8.11 Statistics produced at V2E002.

	Gauge	TRMM3B42	FEWSARC2	FEWSRFE2	TAMSATv3
Total (mm)	4667,80	5511,90	4816,40	4786,30	5259,40
Max (mm)	72,60	87,80	97,50	54,60	38,10
Mean (mm)	1,74	2,06	1,80	1,79	1,96
BIAS		1,18	1,03	1,03	1,13
MAE (mm)		0,32	0,06	0,04	0,22
RMSE (mm)		5,83	4,57	4,32	5,83
RVE (%)		18,08	3,18	2,54	12,67
RSQ		0,30	0,32	0,48	0,16
0 mm					
POD		0,73	0,73	0,87	0,65
FAR		0,36	0,52	0,49	0,51
CSI		0,51	0,41	0,47	0,38
5 mm					
POD		1	0,99	0,98	0,99
FAR		0	0,02	0,01	0,01
CSI		1	0,96	0,97	0,97

Table 8.12 Statistics produced at V2E002 during the GPM period of analysis.

	Gauge	TRMM3B42	FEWSARC2	FEWSRFE2	TAMSATv3	GPM
Total (mm)	1748,70	2027,70	1941,90	1896,30	2299,10	1565,70
Max (mm)	72,60	68,90	97,50	37,70	38,10	109,90
Mean (mm)	1,53	1,77	1,69	1,65	2,01	1,37
BIAS		1,16	1,11	1,08	1,31	0,90
MAE (mm)		0,24	0,17	0,13	0,48	0,16
RMSE (mm)		5,22	2,59	4,09	6,04	6,43
RVE (%)		15,95	11,05	8,44	31,47	-10,46
RSQ		0,35	0,37	0,53	0,13	0,22
0 mm						
POD		0,71	0,75	0,88	0,64	0,74
FAR		0,38	0,54	0,52	0,57	0,47
CSI		0,49	0,40	0,45	0,35	0,44
5 mm						
POD		1,00	0,96	0,98	0,96	0,97
FAR		0,00	0,04	0,02	0,04	0,06
CSI		1,00	0,93	0,97	0,93	0,92

- 0268883 6 (Mooi River SAWS)

The time series of the products are presented below.

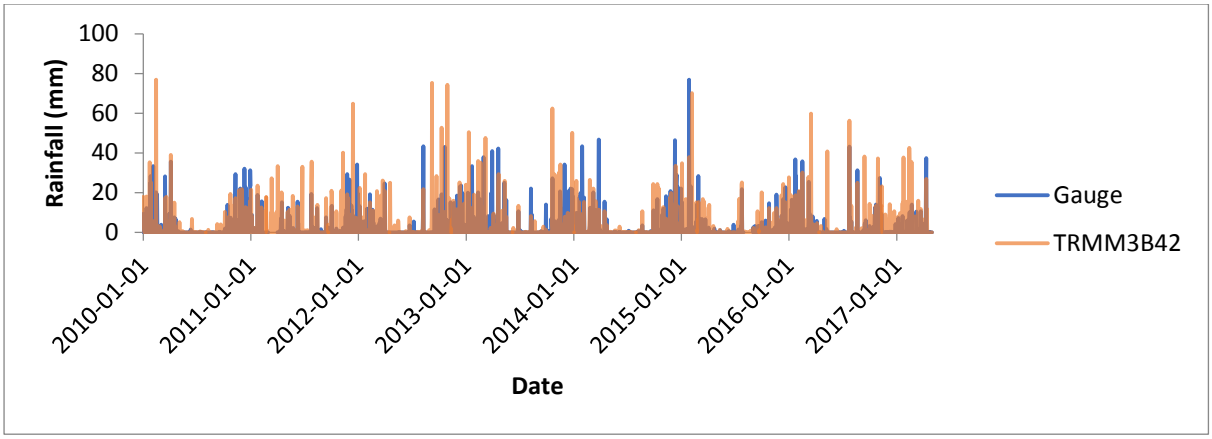

Figure 8.55 Time series of TRMM 3B42 against 0268883 6 measurements.

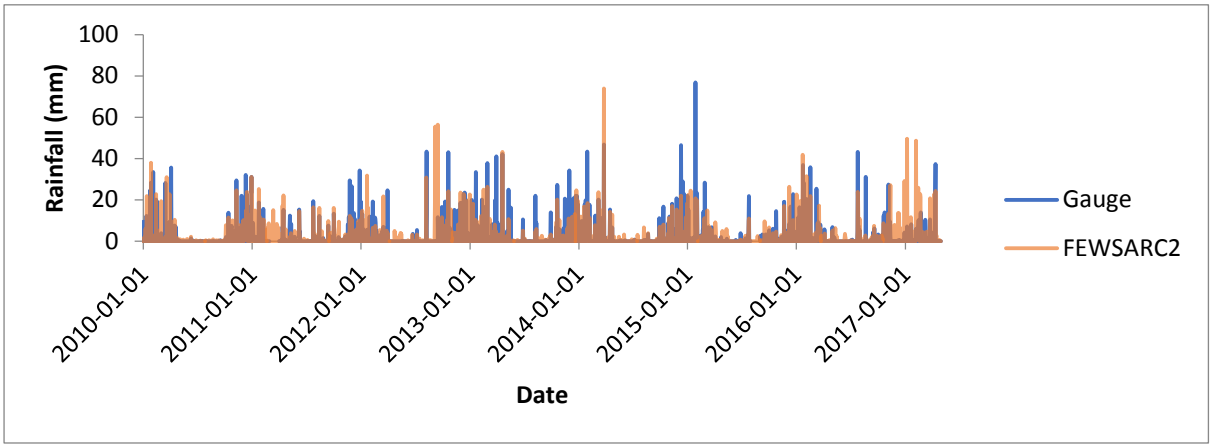

Figure 8.56 Time series of FEWS ARC2 against 0268883 6 measurements.

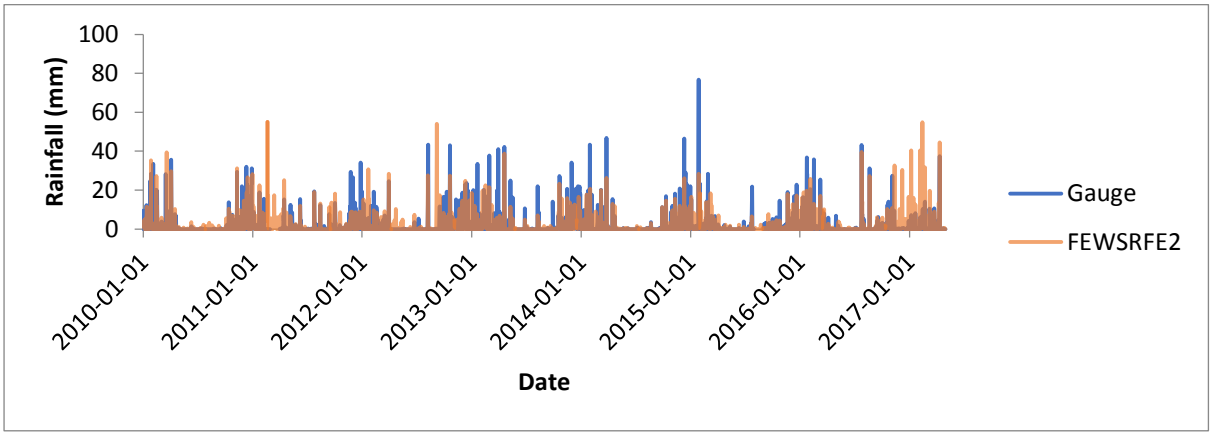

Figure 8.57 Time series of FEWS RFE2 against 0268883 6 measurements.

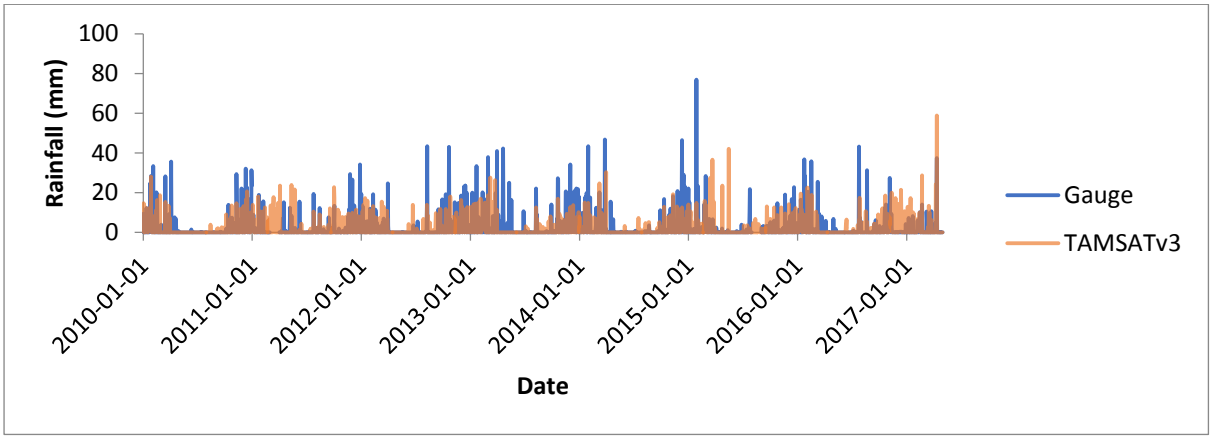

Figure 8.58 Time series of TAMSAT-3 against 0268883 6 measurements.

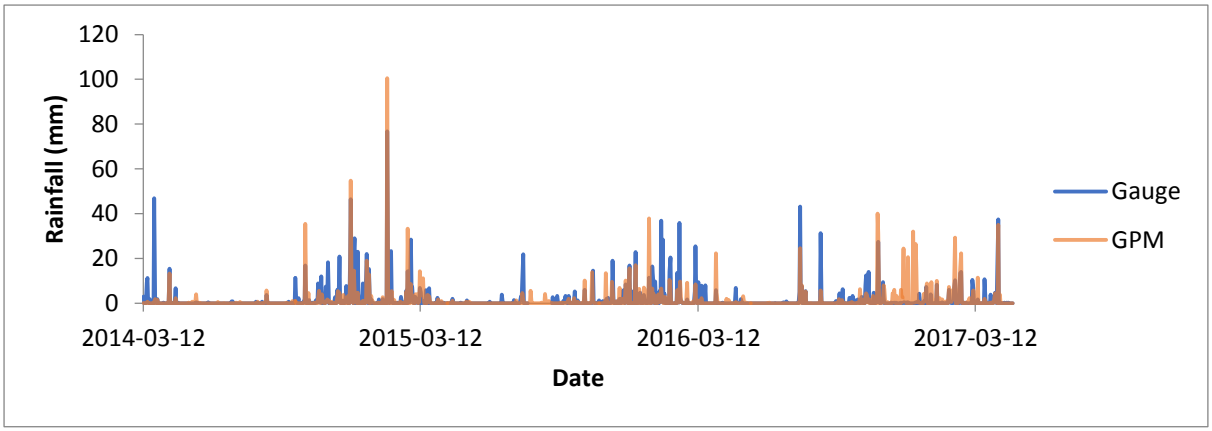

Figure 8.59 Time series of GPM against 0268883 6 measurements.

Average monthly totals are presented below.

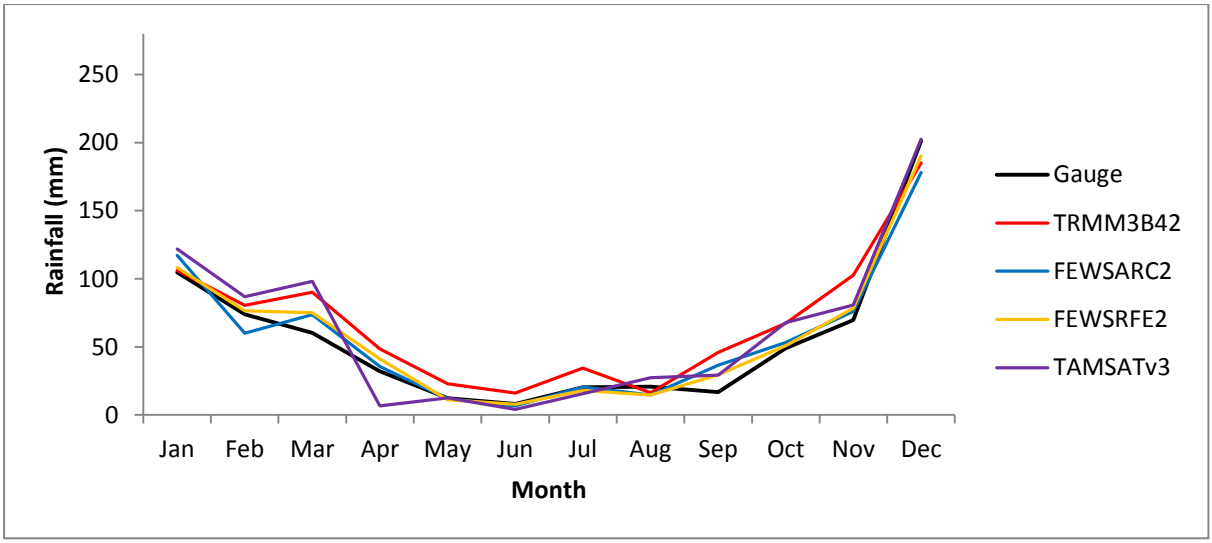

Figure 8.60 Average monthly rainfall totals at 0268883 6.

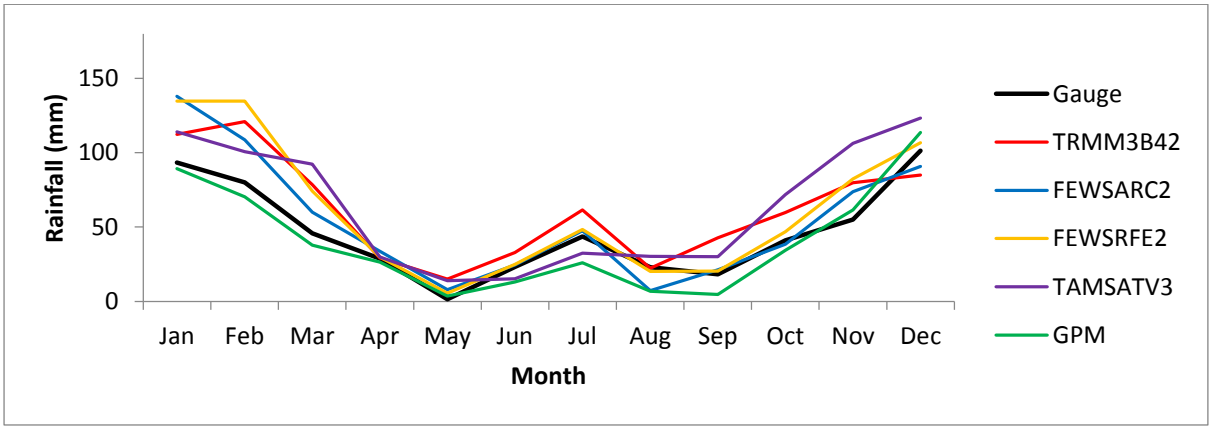

Figure 8.61 Average monthly rainfall totals at 0268883 6 during the GPM period of analysis.

Accumulated rainfall is presented below.

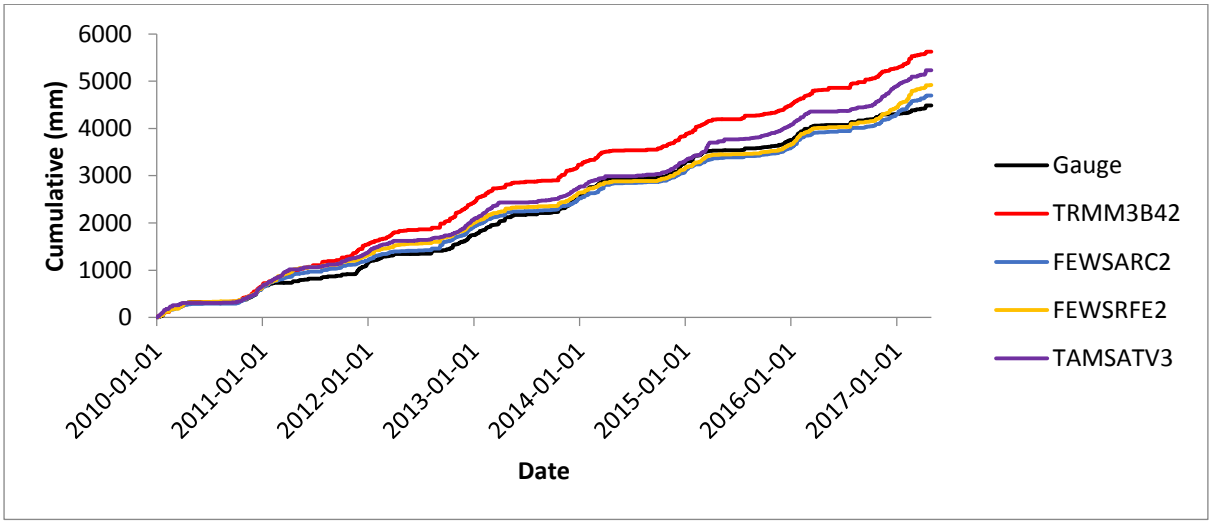

Figure 8.62 Accumulated rainfall at 0268883 6.

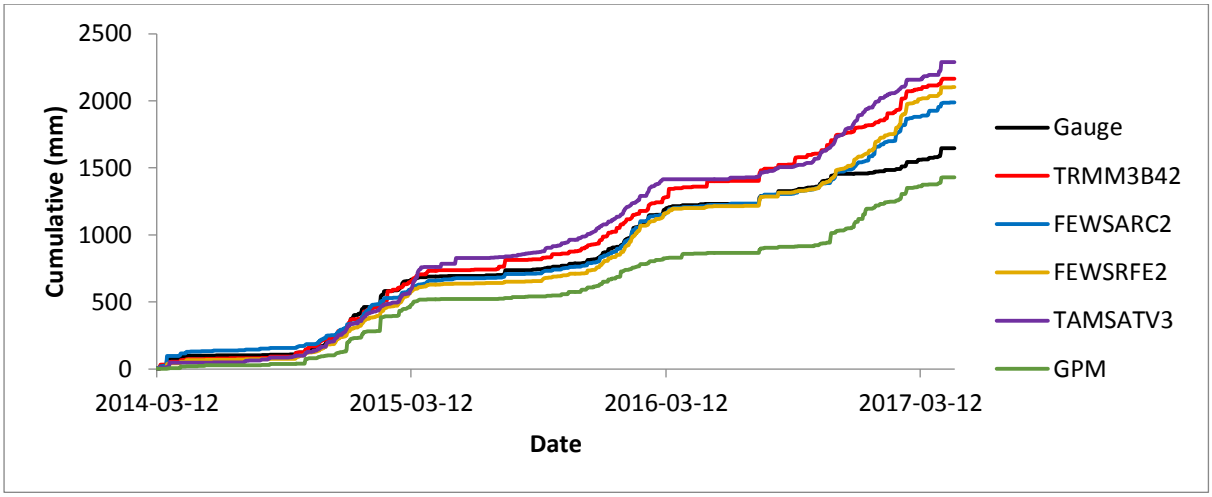

Figure 8.63 Accumulated rainfall at 0268883 6 during the GPM period of analysis.

Tables of statistics are presented below.

Table 8.13 Statistics produced at 0268883 6.

	Gauge	TRMM3B42	FEWSARC2	FEWSRFE2	TAMSATv3
Total (mm)	4488,60	5621,20	4696,20	4916,60	5231,10
Max (mm)	76,80	76,90	73,90	55,10	58,80
Mean (mm)	1,72	2,10	1,75	1,84	1,95
BIAS		1,25	1,05	1,10	1,17
MAE (mm)		0,42	0,08	0,16	0,28
RMSE (mm)		6,57	4,37	4,72	5,46
RVE (%)		25,23	4,63	9,54	16,54
RSQ		0,18	0,26	0,33	0,14
0 mm					
POD		0,58	0,65	0,77	0,57
FAR		0,34	0,41	0,39	0,44
CSI		0,44	0,45	0,51	0,39
5 mm					
POD		1,00	1,00	0,98	0,99
FAR		0,01	0,01	0,01	0,02
CSI		0,99	0,99	0,97	0,97

Table 8.14 Statistics produced at 0268883 6 during the GPM period of analysis.

	Gauge	TRMM3B42	FEWSARC2	FEWSRFE2	TAMSATv3	GPM
Total (mm)	1646,80	2164,90	1987,00	2101,80	2289,80	1429,50
Max (mm)	76,80	70,10	73,90	54,90	58,80	100,50
Mean (mm)	1,48	1,89	1,73	1,83	2,00	1,25
BIAS		1,31	1,21	1,28	1,39	0,87
MAE (mm)		0,45	0,30	0,40	0,56	0,19
RMSE (mm)		5,91	2,77	4,35	5,51	4,30
RVE (%)		31,46	20,66	27,63	39,05	-13,20
RSQ		0,22	0,30	0,40	0,14	0,43
0 mm						
POD		0,57	0,66	0,78	0,59	0,67
FAR		0,31	0,44	0,42	0,46	0,36
CSI		0,45	0,44	0,50	0,39	0,49
5 mm						
POD		1,00	1,00	1,00	0,98	1,00
FAR		0,00	0,00	0,00	0,00	0,00
CSI		1,00	1,00	1,00	0,98	1,00

- 0239698 5 (Pietermaritzburg SAWS)

The time series of the products are presented below.

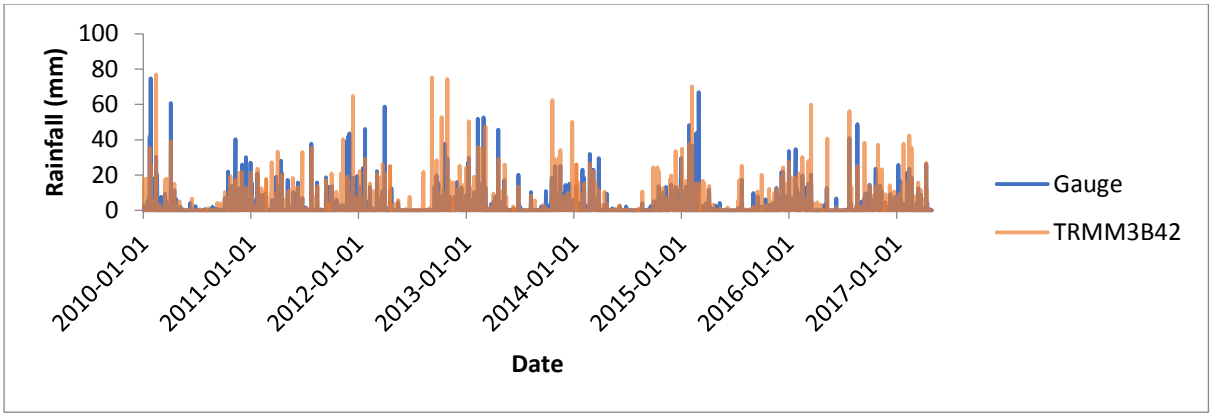

Figure 8.64 Time series of TRMM 3B42 against 0239698 5 measurements.

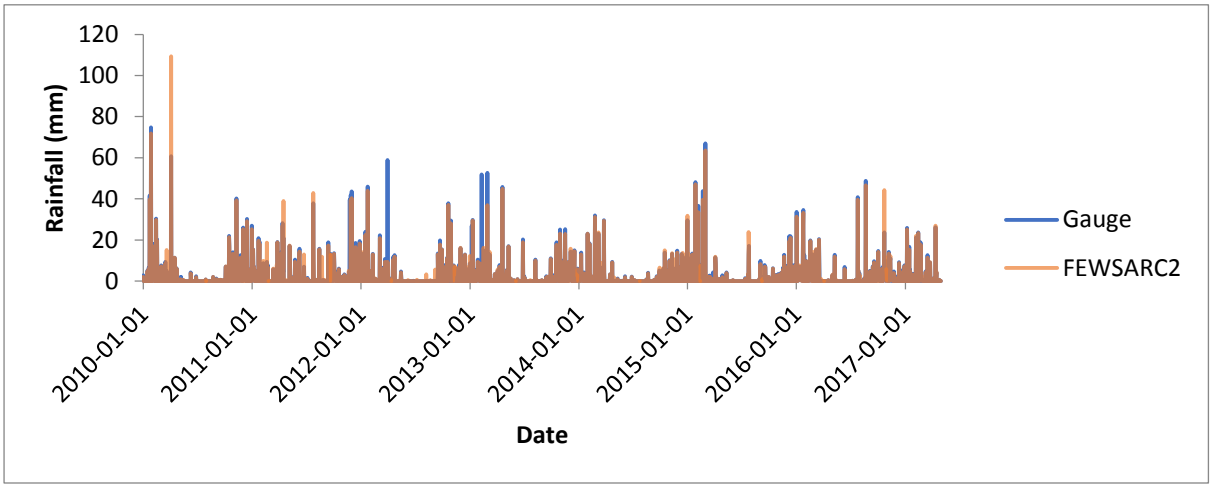

Figure 8.65 Time series of FEWS ARC 2 against 0239698 5 measurements.

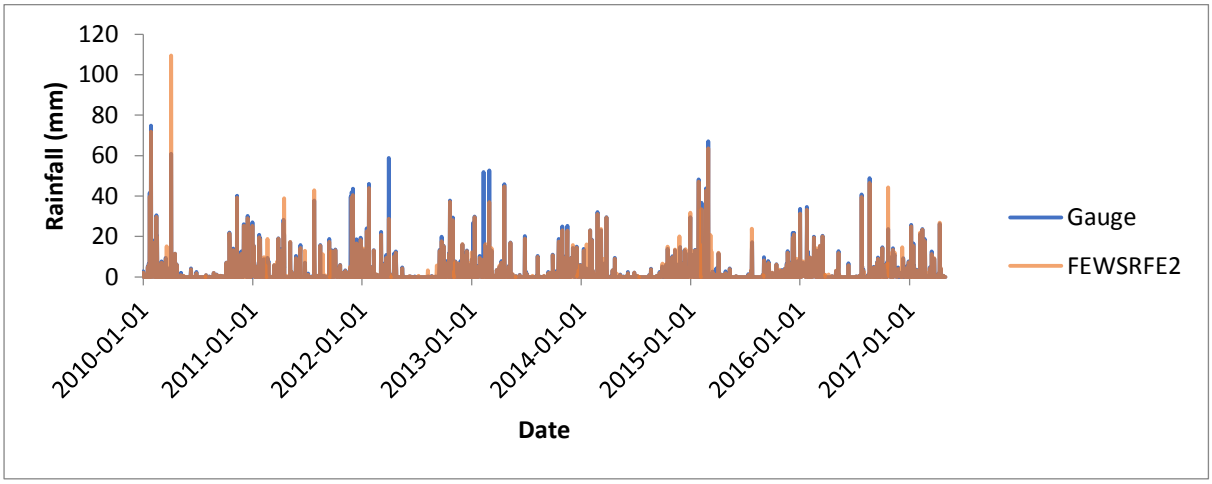

Figure 8.66 Time series of FEWS RFE2 against 0239698 5 measurements.

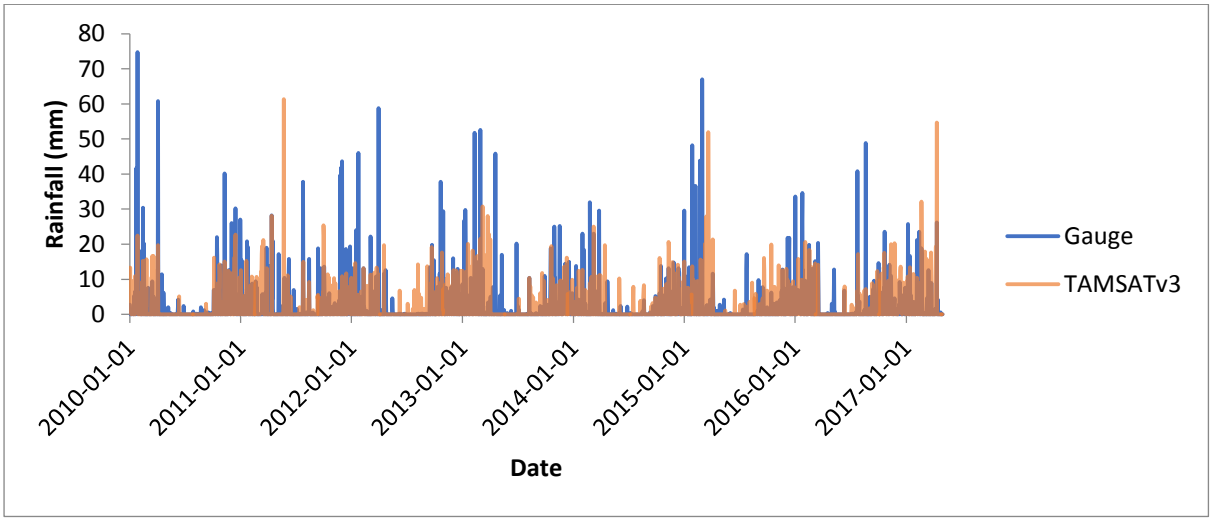

Figure 8.67 Time series of TAMSAT-3 against 0239698 5 measurements.

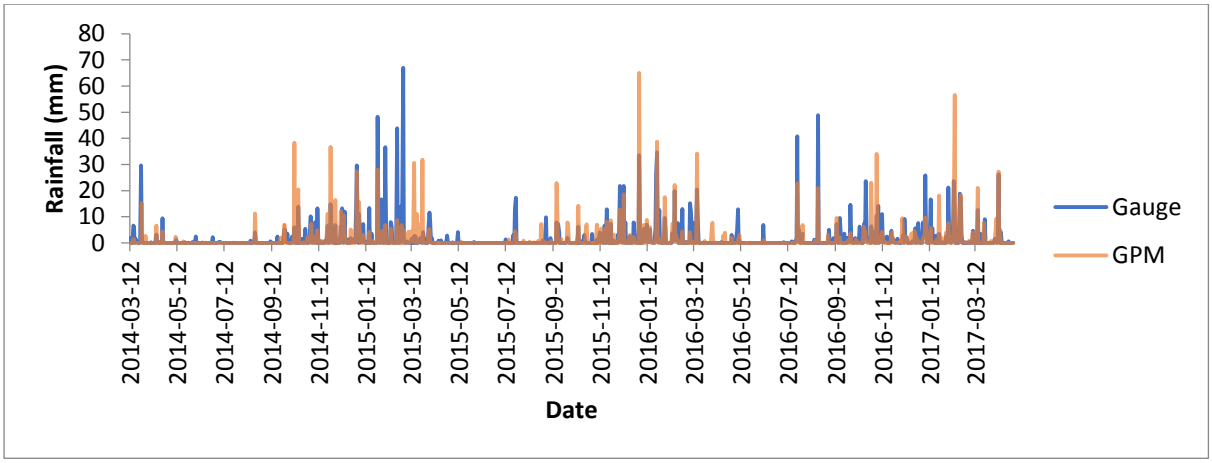

Figure 8.68 Time series of GPM against 0239698 5 measurements.

Average monthly rainfall totals are presented below.

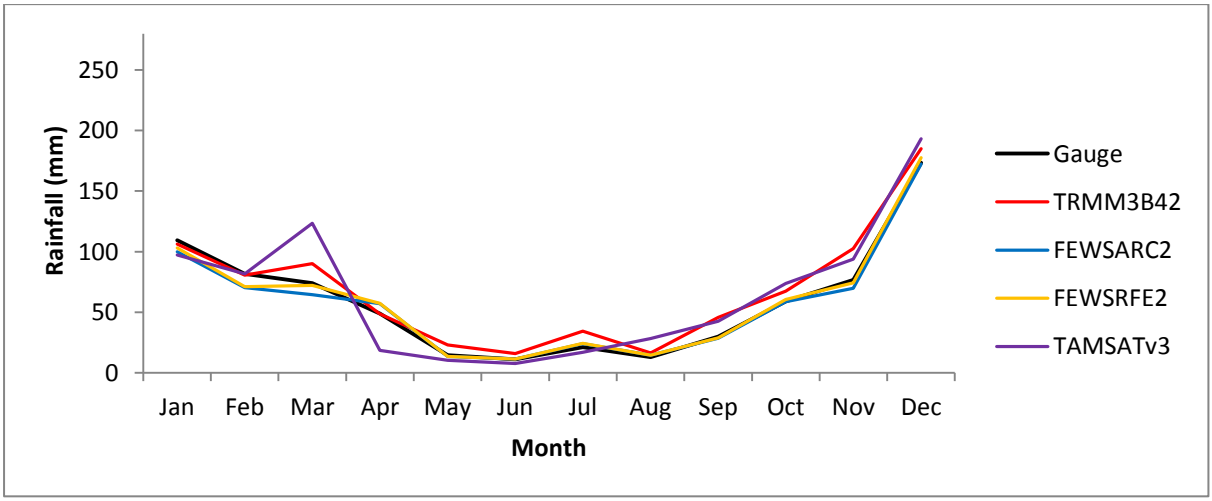

Figure 8.69 Average monthly rainfall totals at 0239698 5.

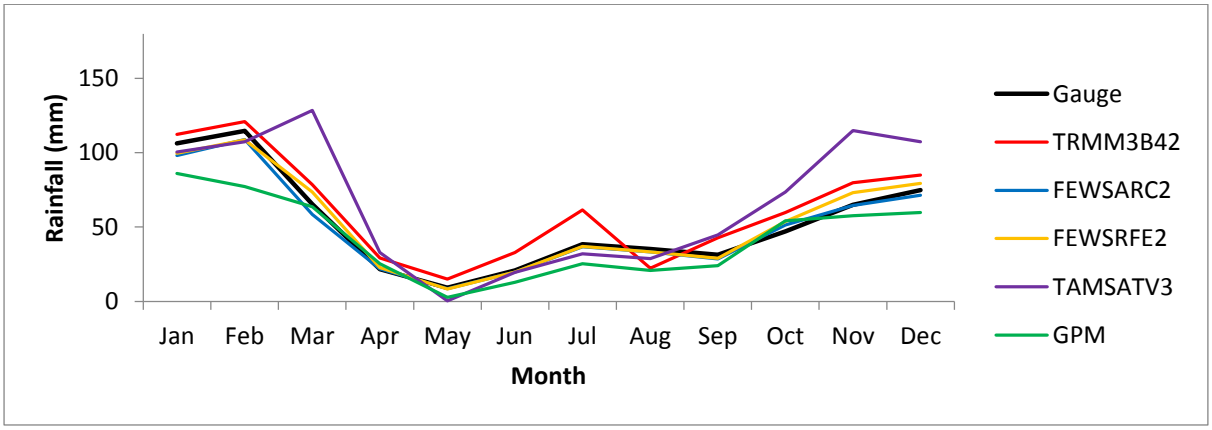

Figure 8.70 Average monthly rainfall totals at 0239698 5 during the GPM period of analysis.

Accumulated rainfall is presented below.

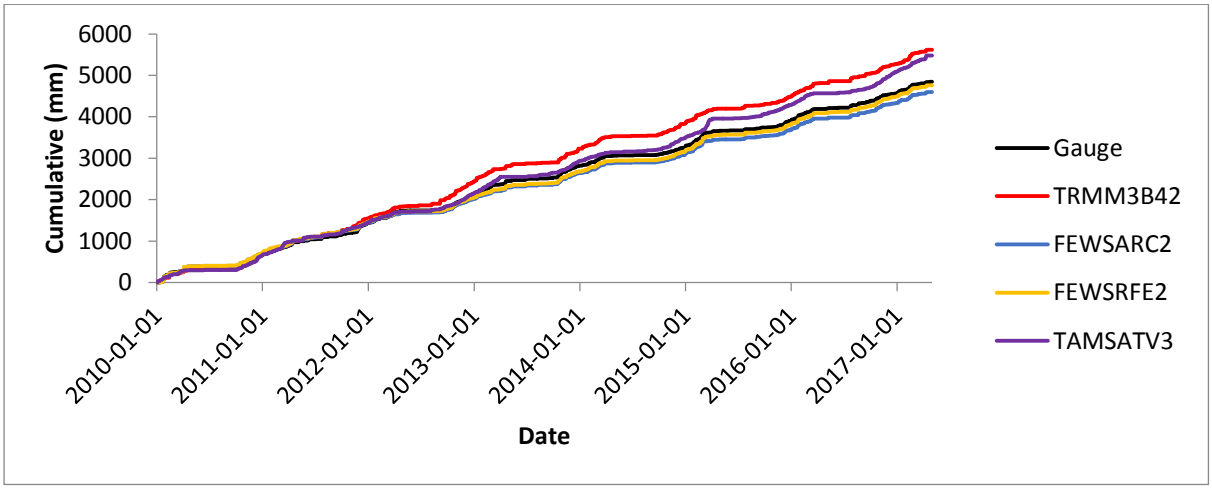

Figure 8.71 Accumulated rainfall at 0239698 5.

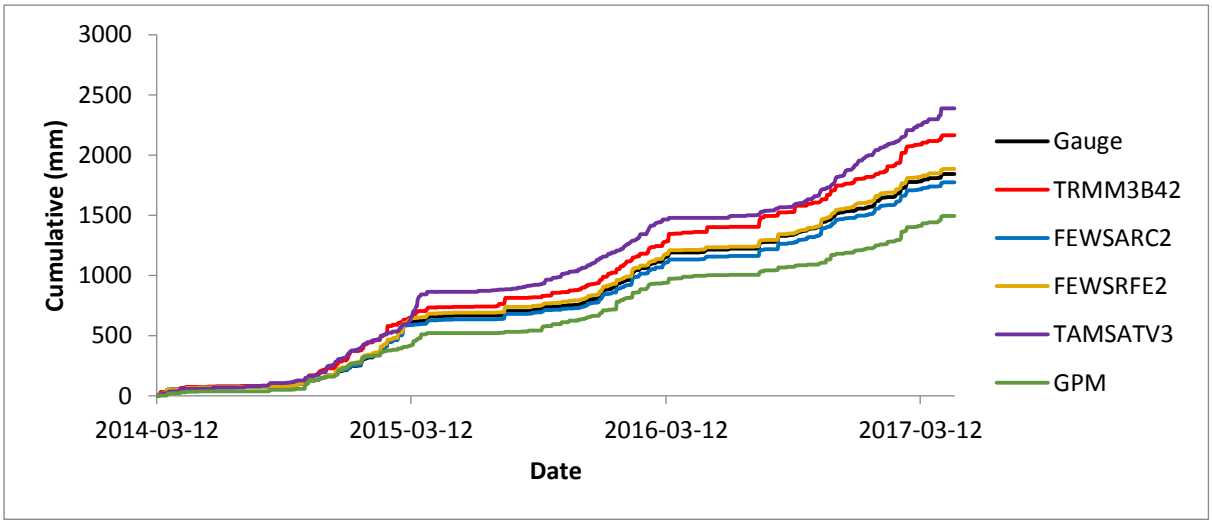

Figure 8.72 Accumulated rainfall at 0239698 5 during the GPM period of analysis.

Table 8.15 Statistics produced at 0239698 5.

	Gauge	TRMM3B42	FEWSARC2	FEWSRFE2	TAMSATv3
Total (mm)	4842,00	5621,20	4596,40	4761,30	5477,30
Max (mm)	74,80	76,90	109,40	109,40	61,30
Mean (mm)	1,81	2,10	1,72	1,78	2,05
BIAS		1,16	0,95	0,98	1,13
MAE (mm)		0,29	0,09	0,03	0,24
RMSE (mm)		5,92	2,04	2,14	5,93
RVE (%)		16,09	-5,07	-1,67	13,12
RSQ		0,31	0,86	0,87	0,12
0 mm					
POD		0,54	0,90	0,90	0,55
FAR		0,31	0,07	0,09	0,39
CSI		0,43	0,84	0,83	0,41
5 mm					
POD		1,00	0,98	0,98	0,99
FAR		0,02	0,01	0,01	0,02
CSI		0,98	0,96	0,96	0,97

Table 8.16 Statistics produced at 0239698 5 during the GPM period of analysis.

	Gauge	TRMM3B42	FEWSARC2	FEWSRFE2	TAMSATv3	GPM
Max (mm)	67,00	70,10	63,50	63,50	54,70	65,00
Mean (mm)	1,61	1,89	1,55	1,64	2,08	1,30
BIAS		1,18	0,96	1,02	1,30	0,81
MAE (mm)		0,28	0,06	0,04	0,48	0,31
RMSE (mm)		4,86	0,30	1,45	5,49	4,64
RVE (%)		17,50	-3,71	2,32	29,56	-18,98
RSQ		0,42	0,96	0,92	0,15	0,33
Total (mm)	1842,40	2164,90	1774,00	1885,10	2387,00	1492,80
0 mm						
POD		0,49	0,89	0,91	0,58	0,55
FAR		0,29	0,08	0,11	0,39	0,32
CSI		0,41	0,83	0,82	0,42	0,44
5 mm						
POD		1,00	0,98	0,98	0,97	1,00
FAR		0,00	0,01	0,01	0,00	0,00
CSI		1,00	0,97	0,97	0,97	1,00

8.2.2 Winter rainfall region

- 0022729 X (Worcester)

The time series of the products are presented below.

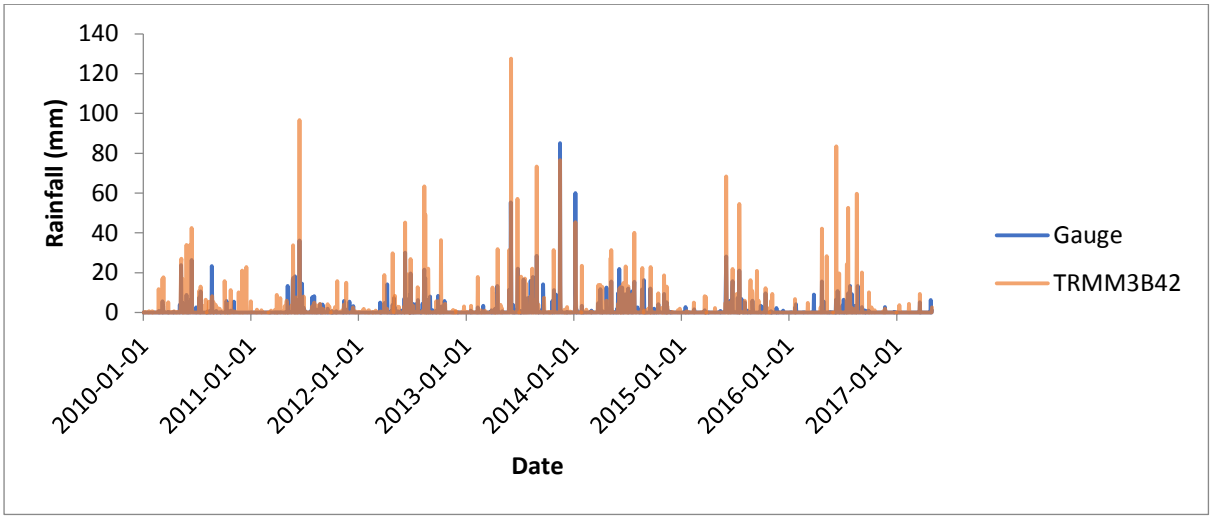

Figure 8.73 Time series of TRMM 3B42 against 0022729 X measurements.

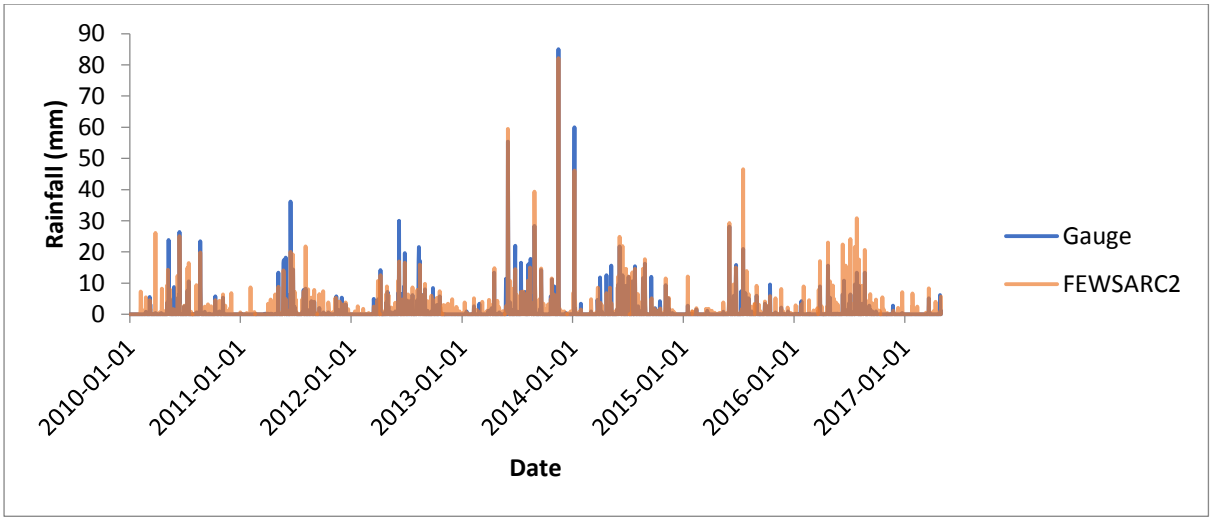

Figure 8.74 Time series of FEWS ARC2 against 0022729 X measurements.

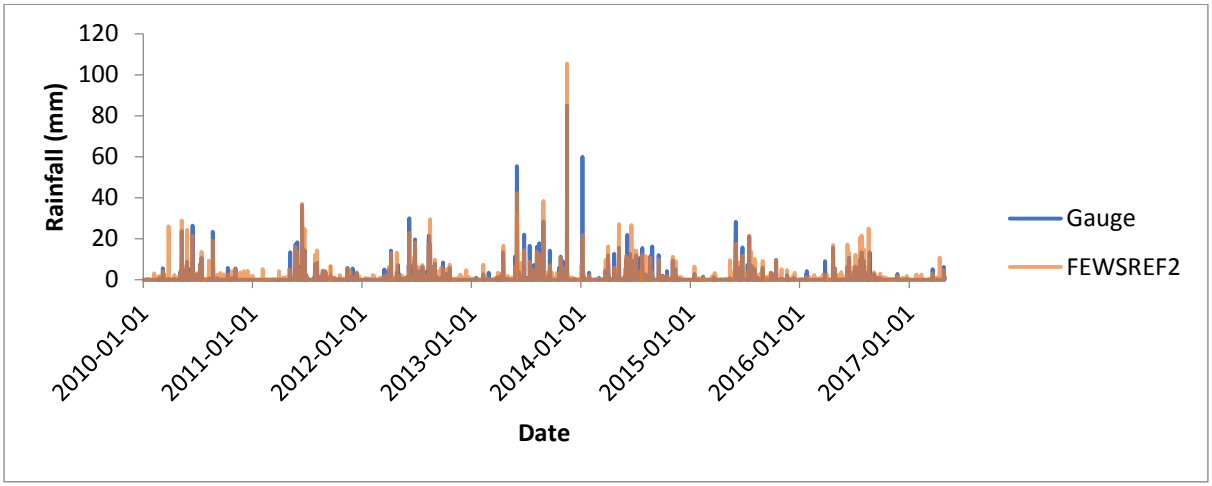

Figure 8.75 Time series of FEWS RFE2 against 0022729 X measurements.

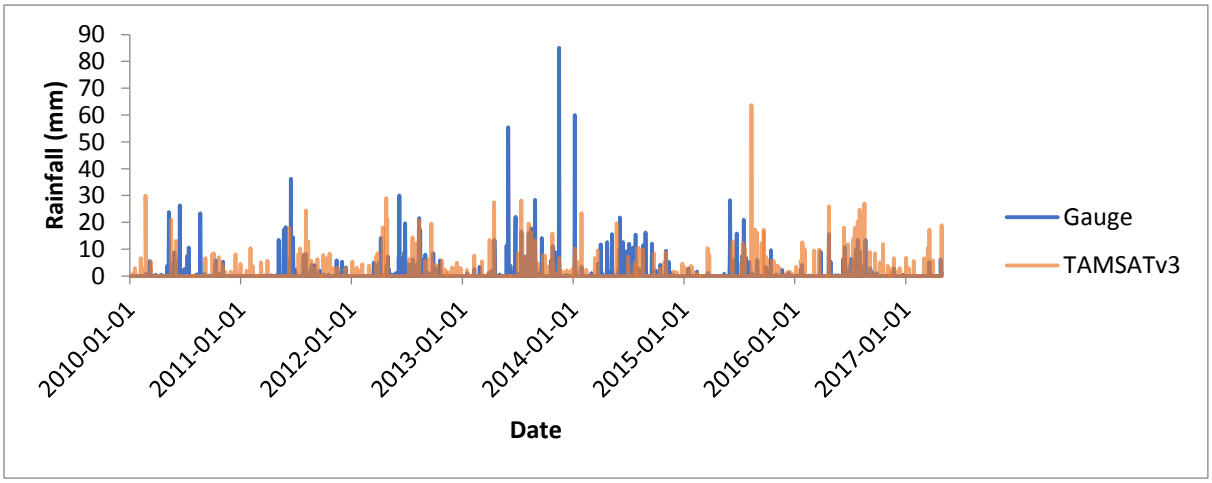

Figure 8.76 Time series of TAMSAT-3 against 0022729 X measurements.

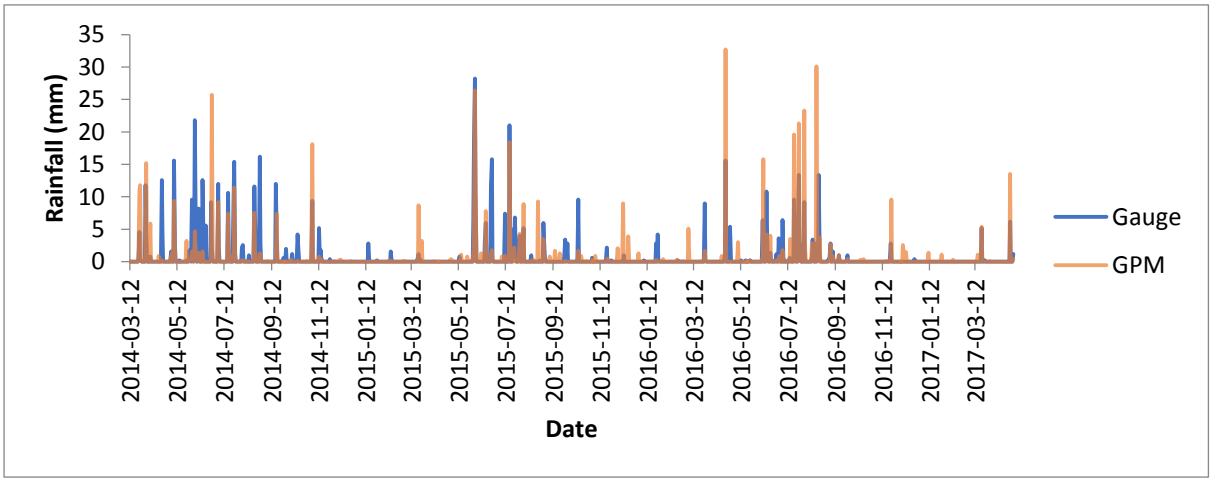

Figure 8.77 Time series of GPM against 0022729 X measurements.

Average monthly totals are presented below.

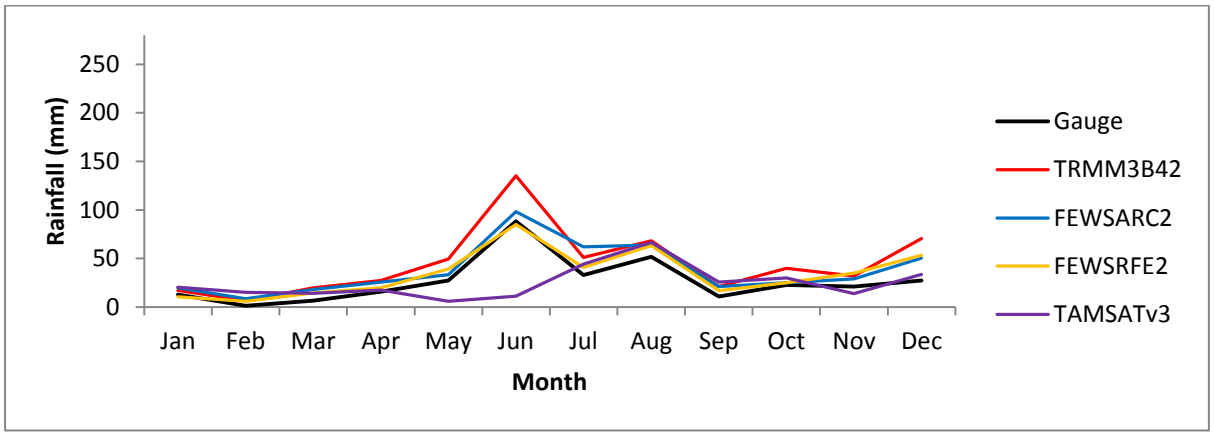

Figure 8.78 Average monthly rainfall totals at 0022729 X.

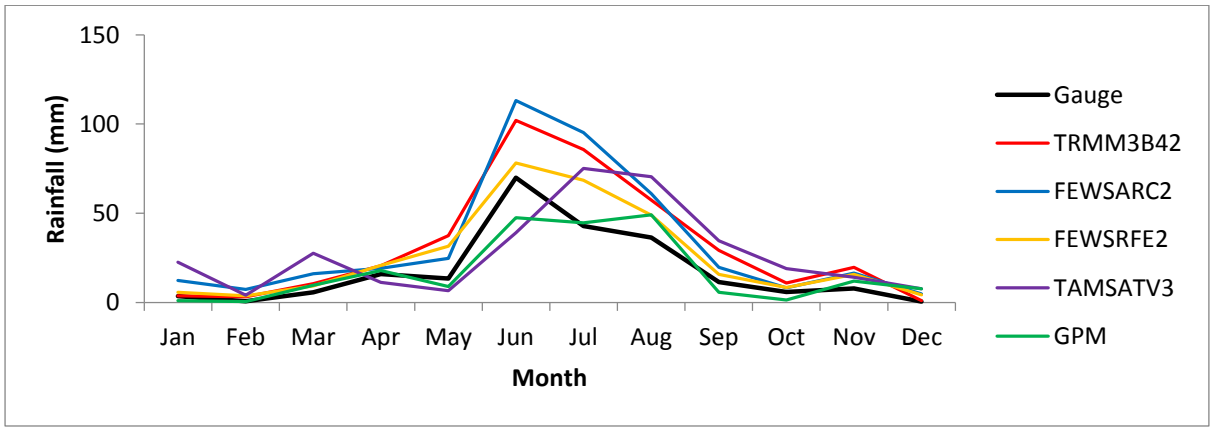

Figure 8.79 Average monthly rainfall totals at 0022729 X during the GPM period of analysis.

Accumulated rainfall is presented below.

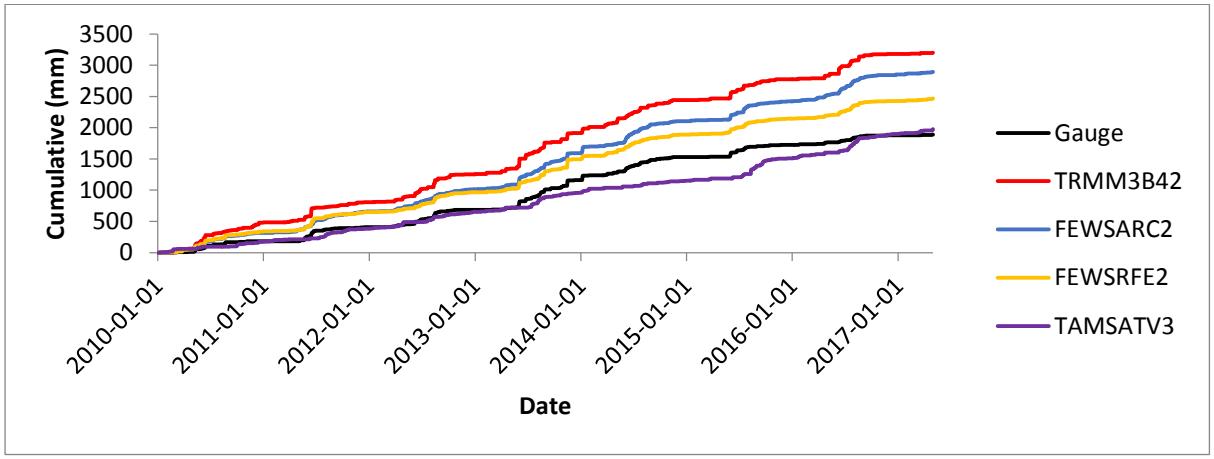

Figure 8.80 Accumulated rainfall at 0022729 X.

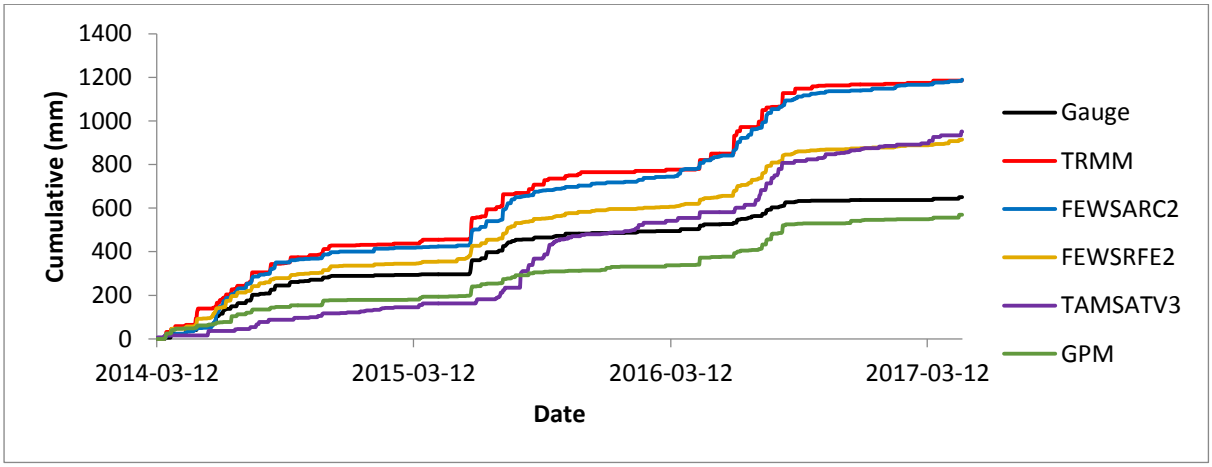

Figure 8.81 Accumulated rainfall at 0022729 X during the GPM period of analysis.

Tables of statistics are presented below.

Table 8.17 Statistics produced at 0022729 X.

	Gauge	**TRMM3B42**	**FEWSARC2**	**FEWSRFE2**	**TAMSATv3**
Total (mm)	1889,40	3198,30	2892,00	2465,00	1974,80
Max (mm)	85,00	127,50	82,10	105,40	63,70
Mean (mm)	0,71	1,19	1,08	0,92	0,74
BIAS		1,69	1,53	1,30	1,05
MAE (mm)		0,49	0,37	0,22	0,03
RMSE (mm)		4,98	1,82	2,17	4,34
RVE (%)		69,28	53,06	30,46	4,52
RSQ		0,39	0,70	0,69	0,02
0 mm					
POD		0,46	0,88	0,88	0,18
FAR		0,54	0,48	0,50	0,79
CSI		0,30	0,48	0,47	0,11
5 mm					
POD		0,97	0,99	1,00	1,00
FAR		0,05	0,03	0,02	0,05
CSI		0,93	0,96	0,98	0,95

Table 8.18 Statistics produced at 0022729 X during the GPM period of analysis.

	Gauge	TRMM3B42	FEWSARC2	FEWSRFE2	TAMSATv3	GPM
Total (mm)	650,80	1186,70	1189,40	914,00	952,00	569,90
Max (mm)	28,20	83,50	46,50	27,20	63,70	32,70
Mean (mm)	0,57	1,04	1,04	0,80	0,83	0,50
BIAS		1,82	1,83	1,40	1,46	0,88
MAE (mm)		0,47	0,47	0,23	0,26	0,07
RMSE (mm)		4,69	1,08	1,92	3,99	2,31
RVE (%)		82,34	82,76	40,44	46,28	-12,43
RSQ		0,30	0,68	0,54	0,01	0,32
0 mm						
POD		0,36	0,85	0,89	0,17	0,64
FAR		0,46	0,49	0,48	0,80	0,48
CSI		0,28	0,47	0,48	0,10	0,40
5 mm						
POD		0,97	1,00	1,00	1,00	1,00
FAR		0,03	0,05	0,00	0,00	0,00
CSI		0,93	0,95	1,00	1,00	1,00

- H1E007 (Doorn @ Kwaggaskloof Dam)

Time series of the products are presented below.

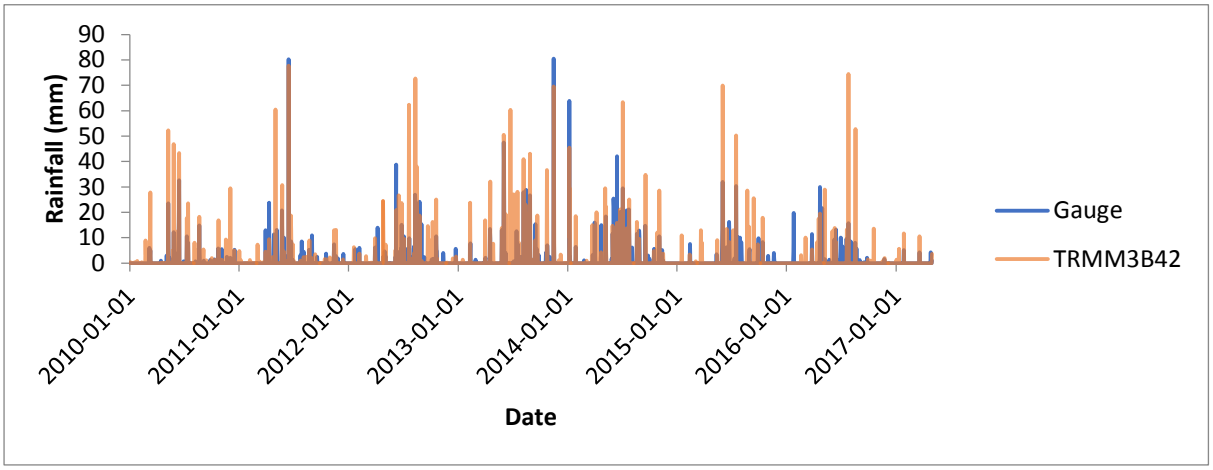

Figure 8.82 Time series of TRMM 3B42 against H1E007 measurements.

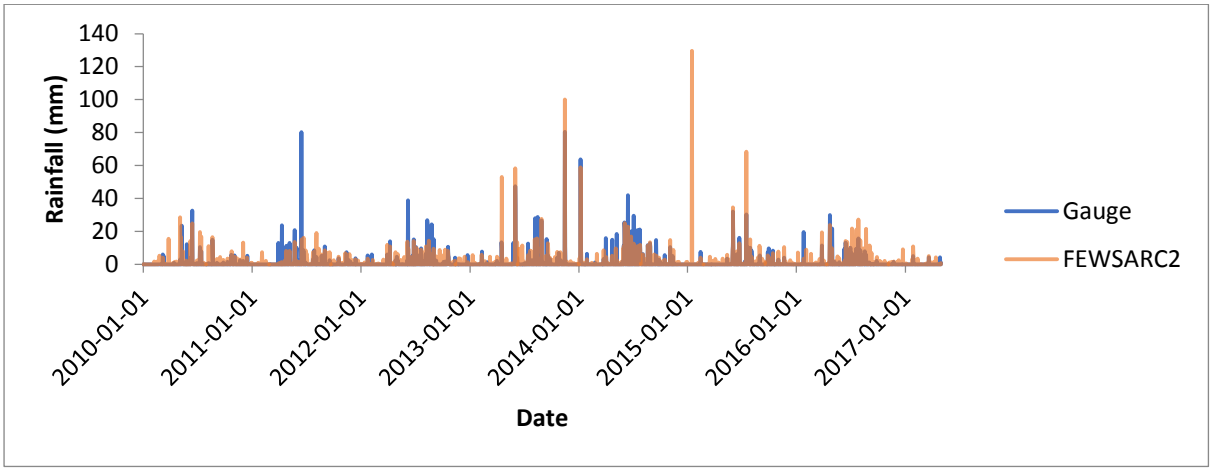

Figure 8.83 Time series of FEWS ARC2 against H1E007 measurements.

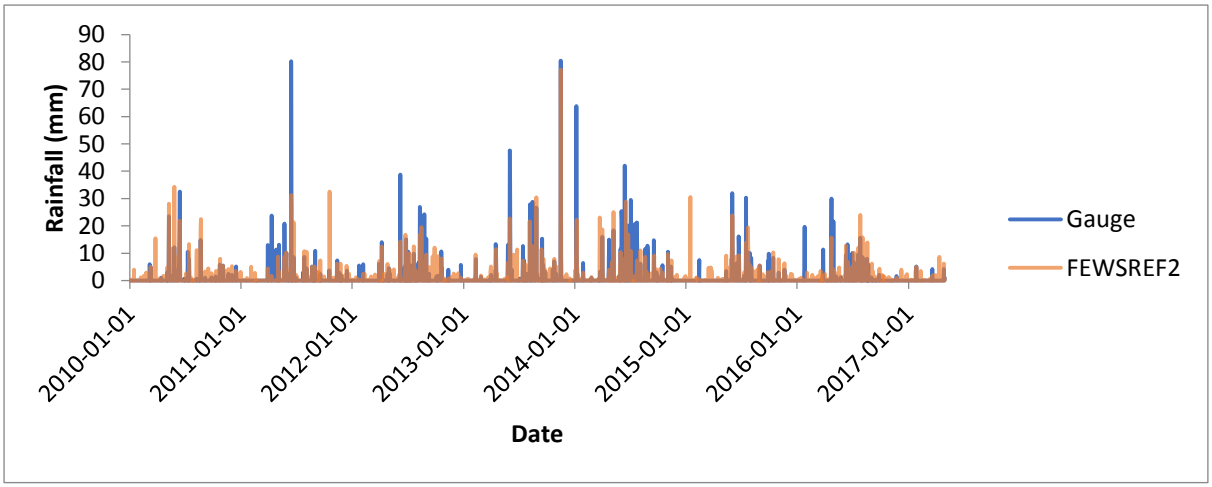

Figure 8.84 Time series of FEWS RFE2 against H1E007 measurements.

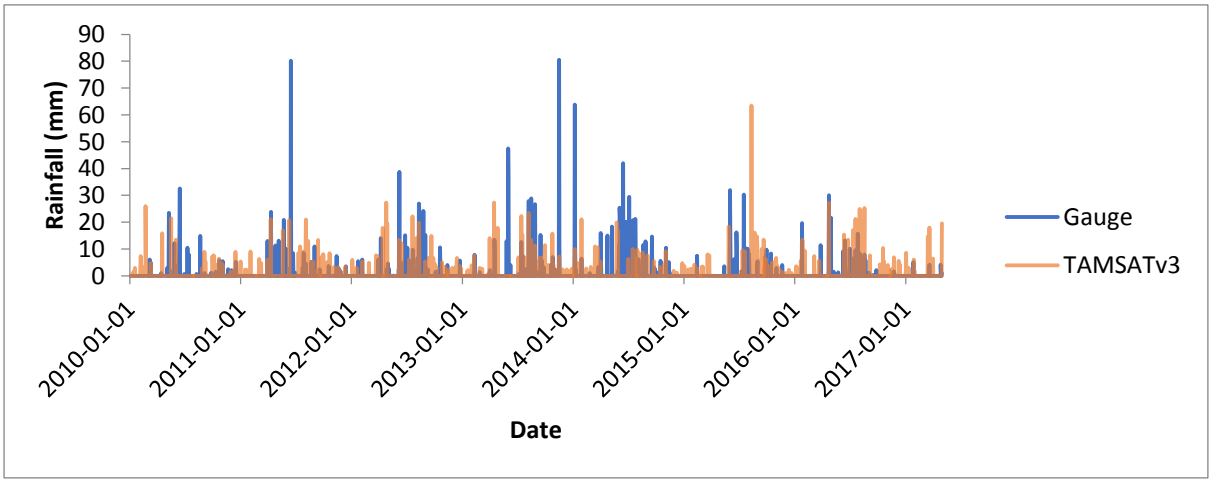

Figure 8.85 Time series of TAMSAT-3 against H1E007 measurements.

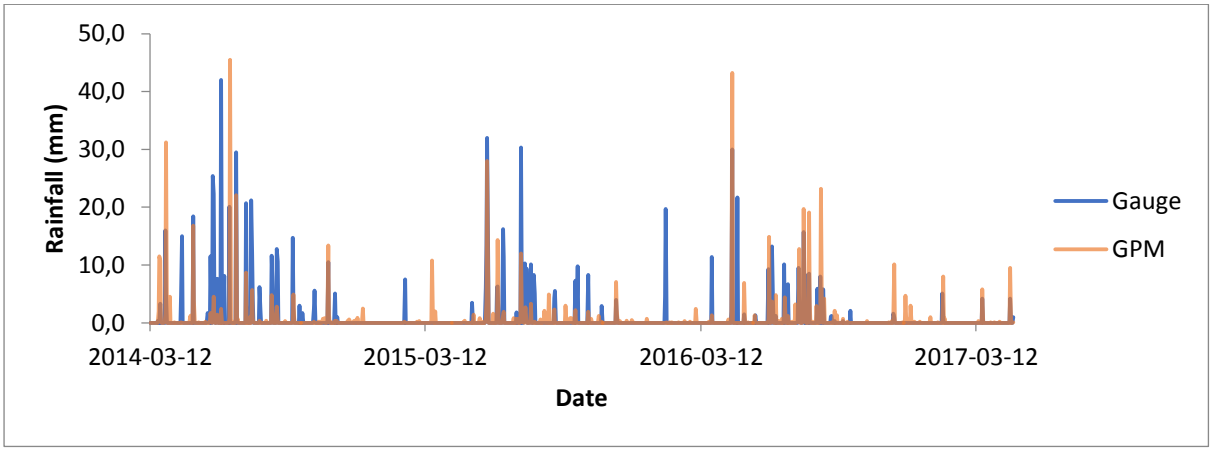

Figure 8.86 Time series of GPM against H1E007 measurements.

Average monthly rainfall totals are presented below.

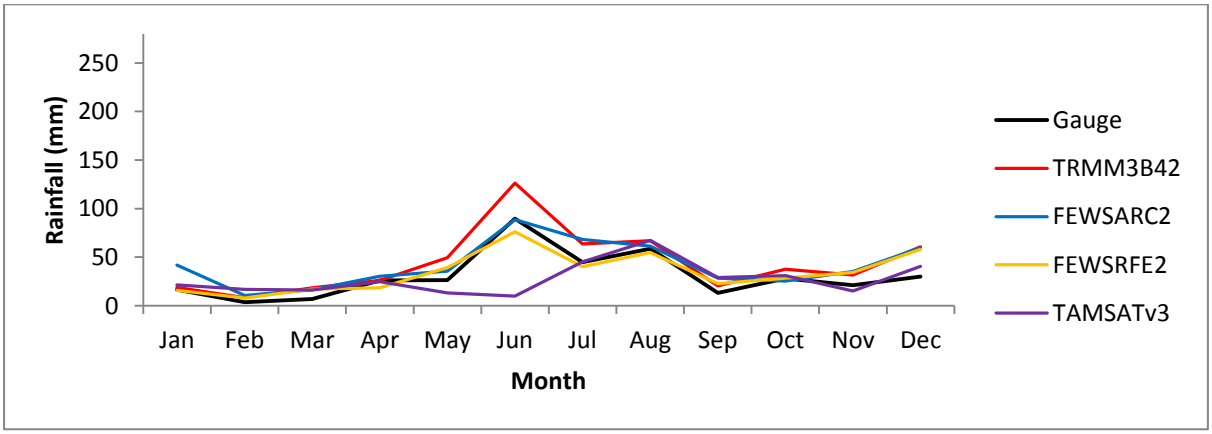

Figure 8.87 Average monthly rainfall totals at H1E007.

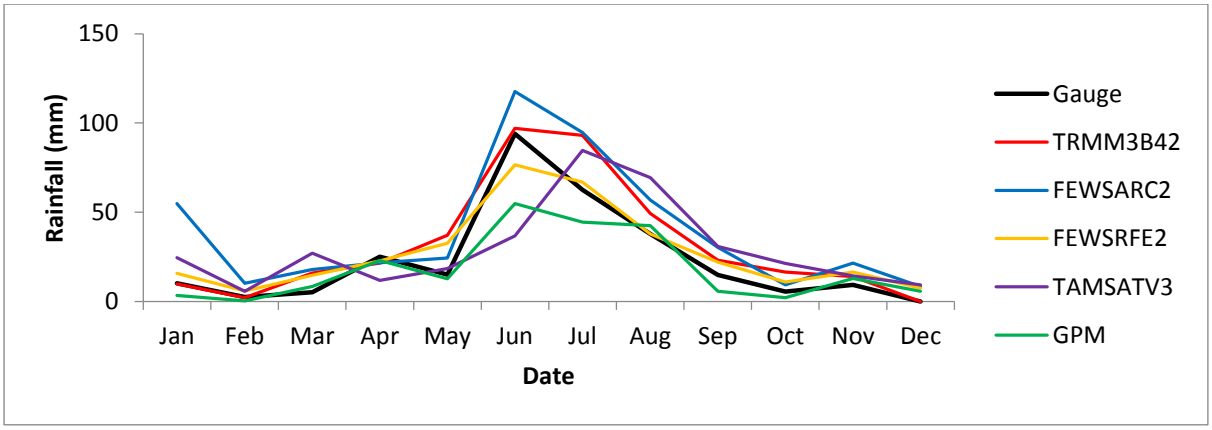

Figure 8.88 Average monthly rainfall totals at H1E007 during the GPM period of analysis.

Accumulated rainfall is presented below.

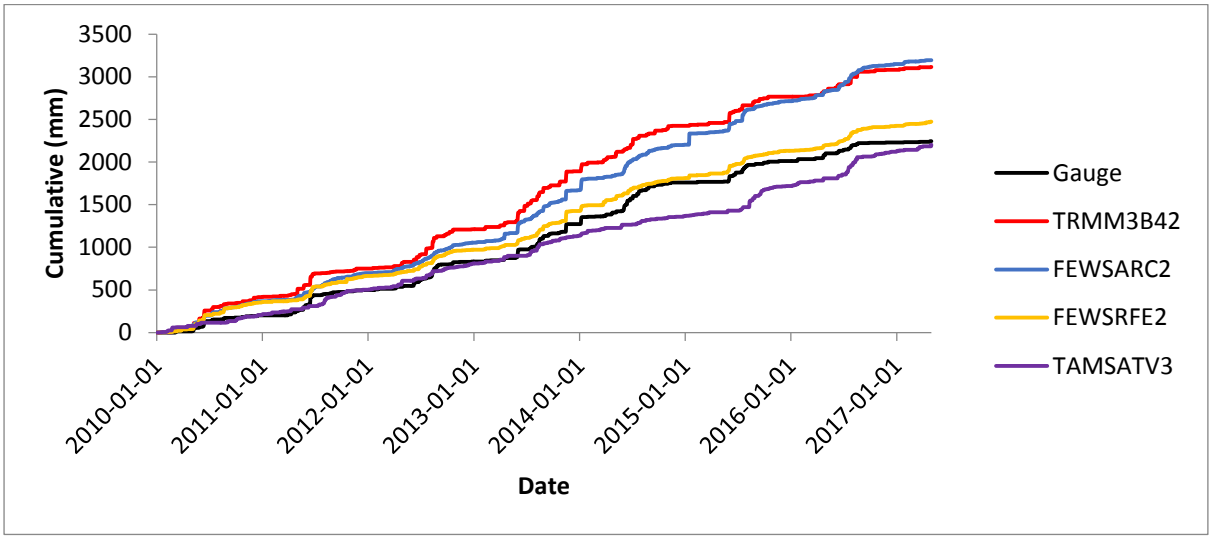

Figure 8.89 Accumulated rainfall at H1E007 during the GPM period of analysis.

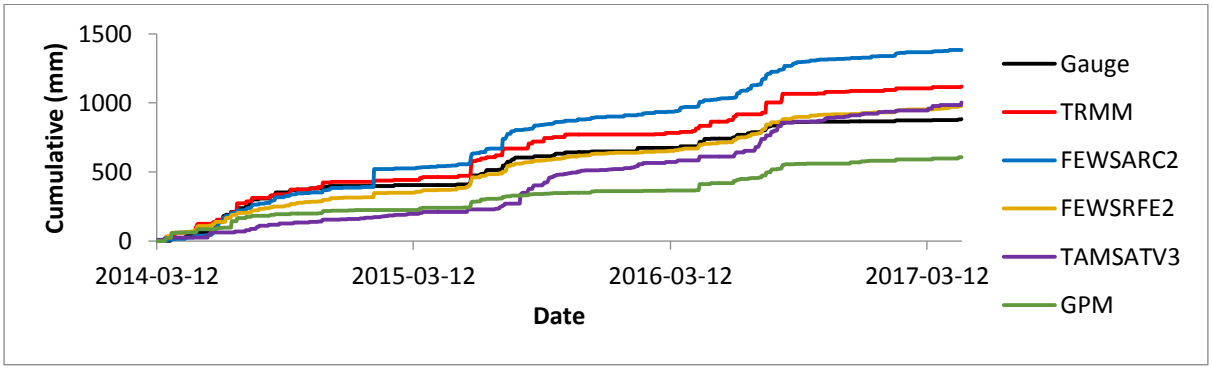

Figure 8.90 Accumulated rainfall at H1E007 during the GPM period of analysis.

Tables of statistics are presented below.

Table 8.19 Statistics produced at H1E007 during the GPM period of analysis.

	Gauge	TRMM3B42	FEWSARC2	FEWSRFE2	TAMSATv3
Total (mm)	2243,40	3113,70	3195,72	2472,00	2203,00
Max (mm)	80,50	77,70	129,65	77,20	63,40
Mean (mm)	0,84	1,16	1,19	0,92	0,82
BIAS		1,39	1,42	1,10	0,98
MAE (mm)		0,33	0,36	0,09	0,02
RMSE (mm)		4,67	4,01	3,21	4,91
RVE (%)		38,79	42,45	10,19	-1,80
RSQ		0,42	0,34	0,44	0,02
0 mm					
POD		0,47	0,84	0,72	0,21
FAR		0,51	0,67	0,68	0,83
CSI		0,31	0,31	0,28	0,10
5 mm					
POD		1,00	1,00	0,99	0,96
FAR		0,01	0,00	0,01	0,00
CSI		0,99	1,00	0,97	0,96

Table 8.20 Statistics produced at H1E007 during the GPM period of analysis.

	Gauge	TRMM3B42	FEWSARC2	FEWSRFE2	TAMSATv3	GPM
Total (mm)	882,70	1118,60	1384,02	978,50	1004,20	607,10
Max (mm)	42,00	74,50	129,65	30,60	63,40	45,50
Mean (mm)	0,77	0,98	1,21	0,85	0,88	0,53
BIAS		1,27	1,57	1,11	1,14	0,69
MAE (mm)		0,21	0,44	0,08	0,11	0,24
RMSE (mm)		4,56	4.83	3,06	4,62	3,32
RVE (%)		26,72	56,79	10,85	13,76	-31,22
RSQ		0,29	0,27	0,29	0,01	0,21
0 mm						
POD		0,39	0,87	0,73	0,19	0,78
FAR		0,49	0,69	0,72	0,87	0,61
CSI		0,28	0,30	0,25	0,08	0,35
5 mm						
POD		1,00	1,00	0,97	1,00	1,00
FAR		0,00	0,00	0,03	0,00	0,08
CSI		1,00	1,00	0,94	1,00	0,92

- H9E002 (Krantzkloof at Korinte-Vet Dam)

Time series of the products against gauge measurements are presented below.

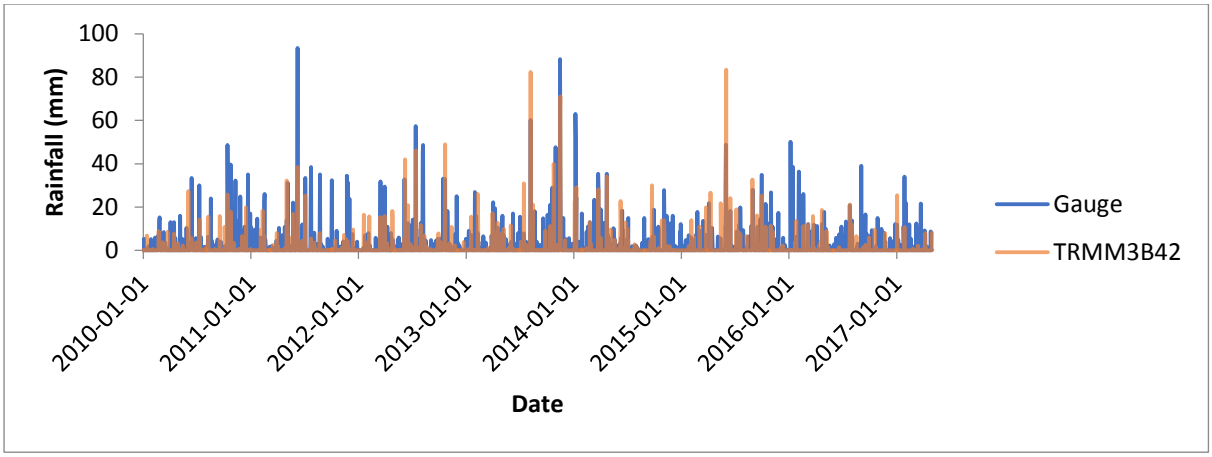

Figure 8.91 Time series of TRMM 3B42 against H9E002 measurements.

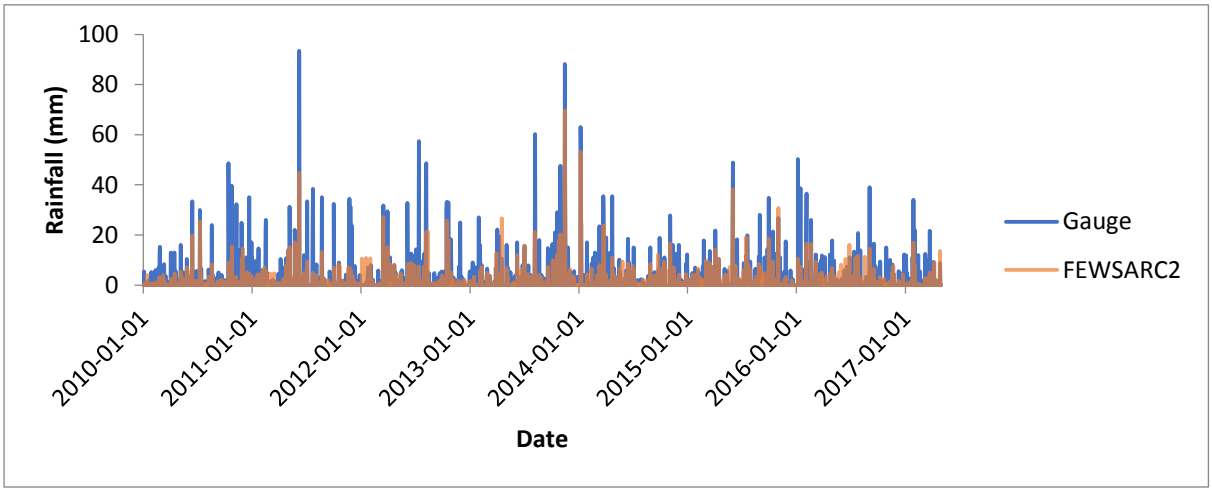

Figure 8.92 Time series of FEWS ARC2 against H9E002 measurements.

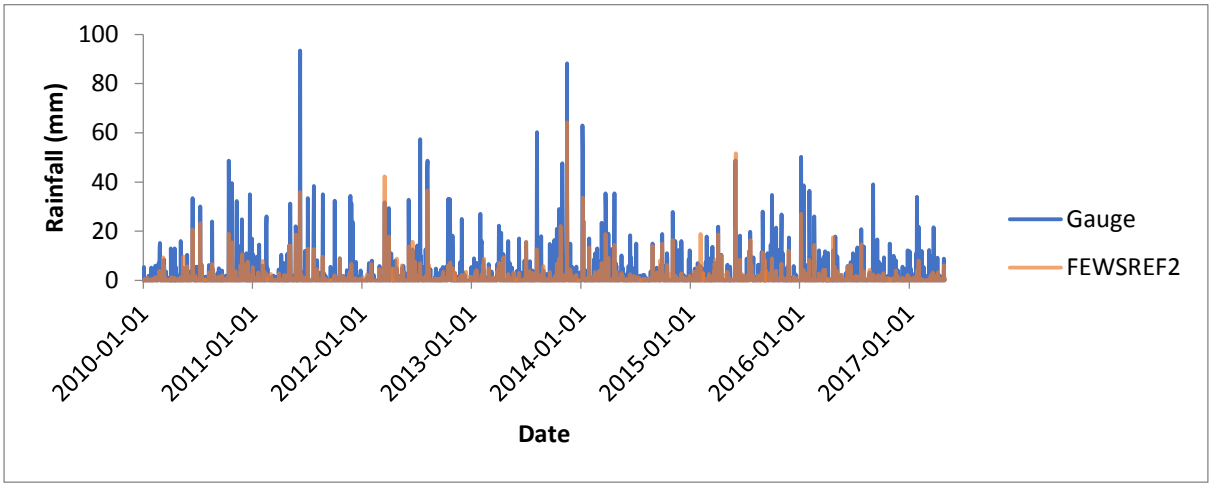

Figure 8.93 Time series of FEWS RFE2 against H9E002 measurements.

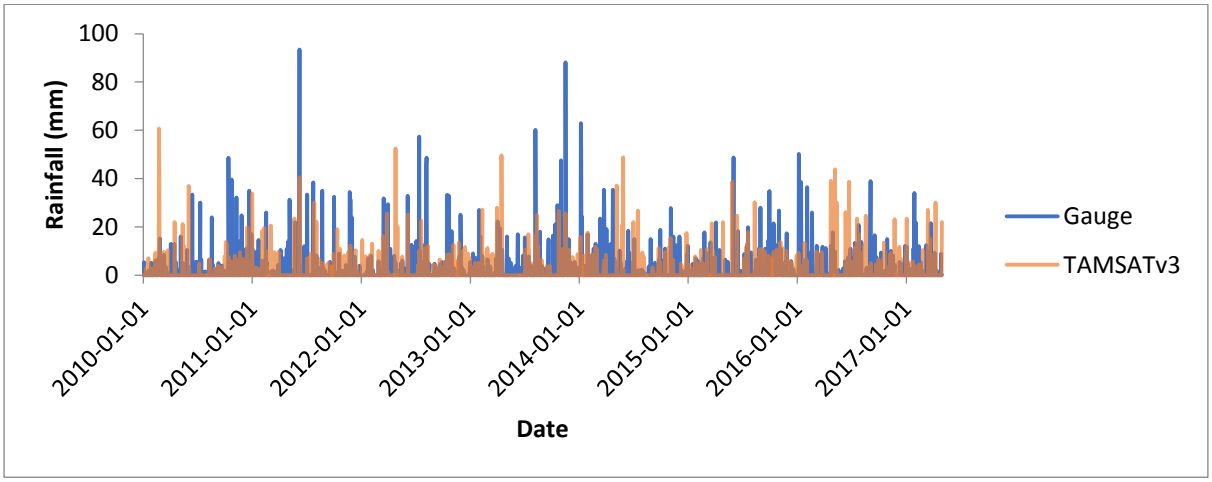

Figure 8.94 Time series of TAMSAT-3 against H9E002 measurements.

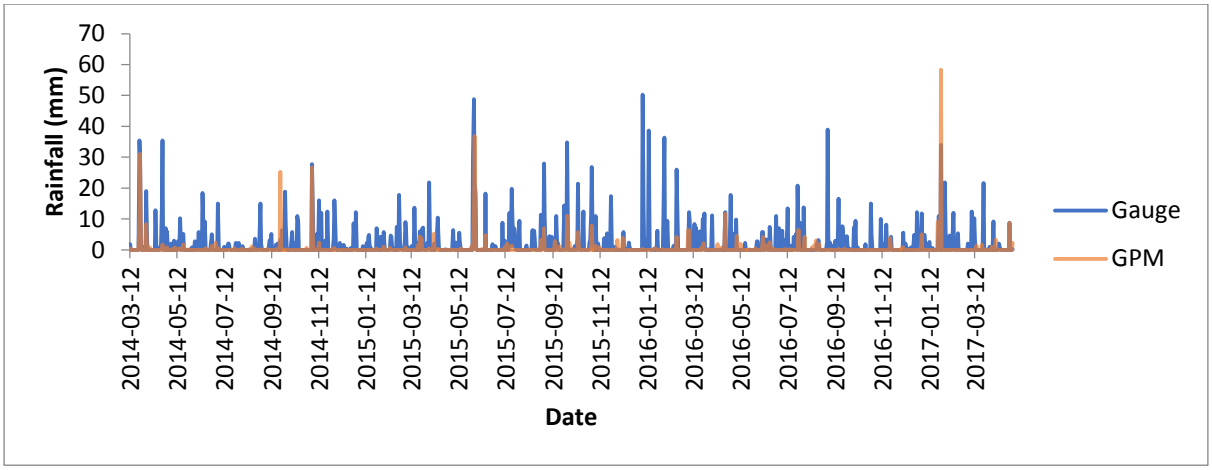

Figure 8.95 Time series of GPM against H9E002 measurements.

Average monthly rainfall totals are presented below.

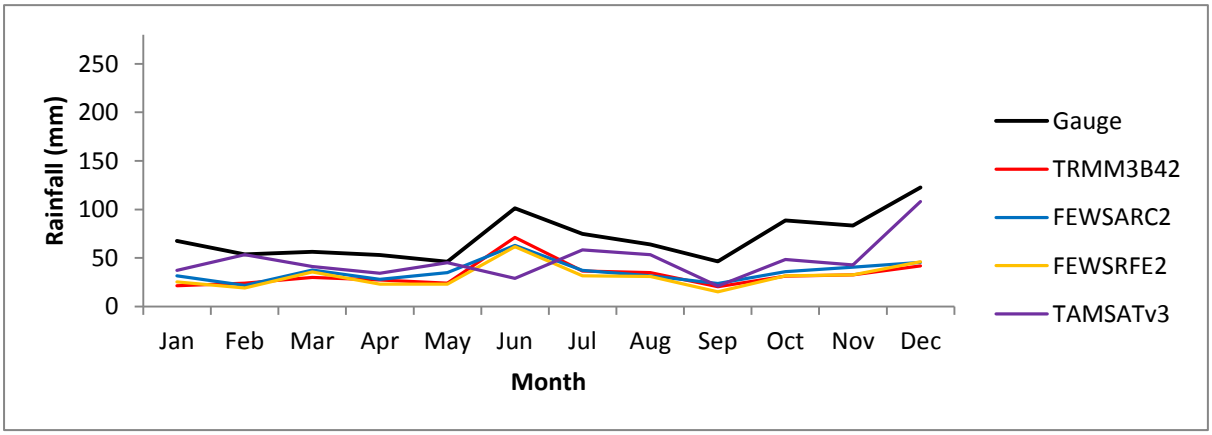

Figure 8.96 Average monthly rainfall totals at H9E002.

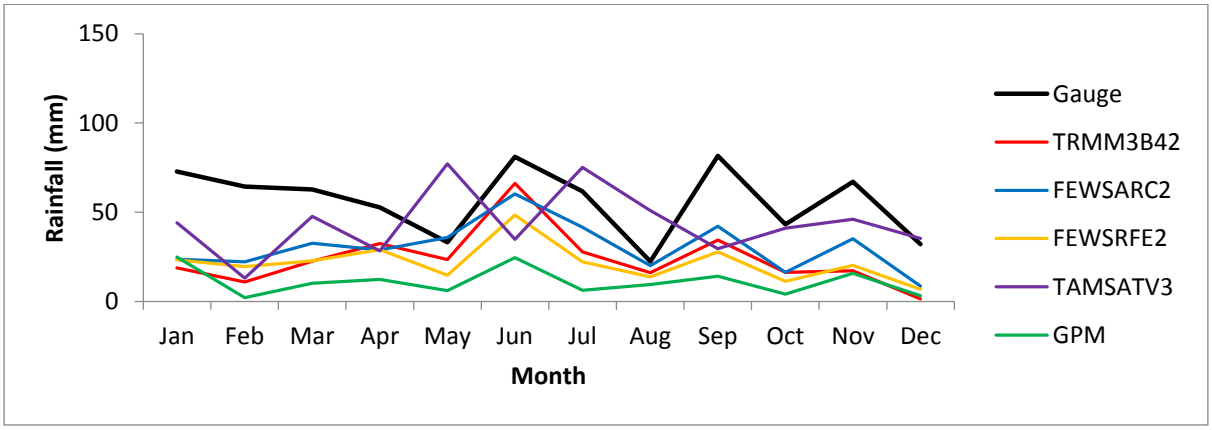

Figure 8.97 Average monthly rainfall totals at H9E002 during the GPM period of analysis.

Accumulated rainfall of all products are presented below against accumulated gauge rainfall.

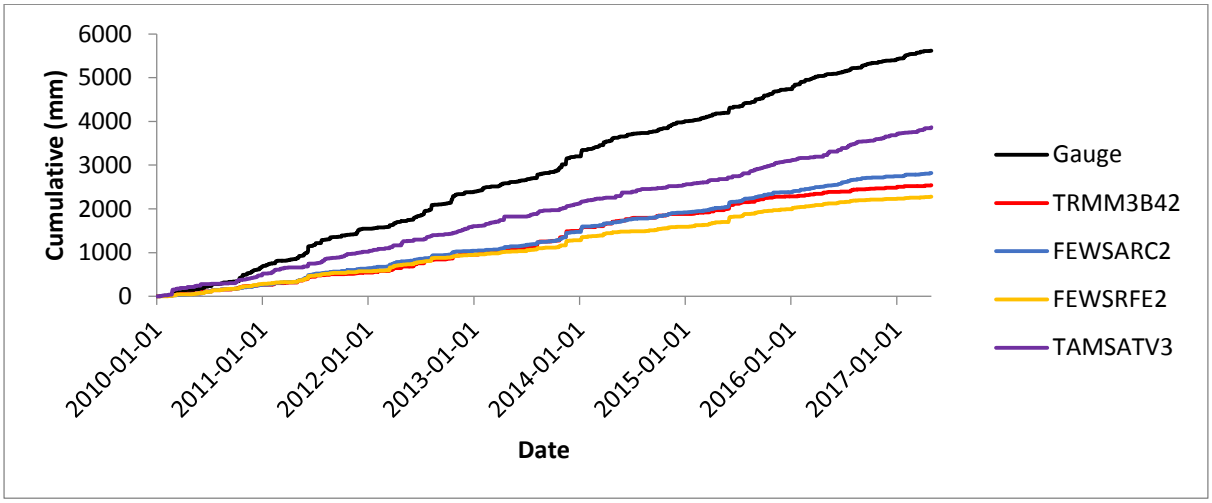

Figure 8.98 Accumulated rainfall at H9E002.

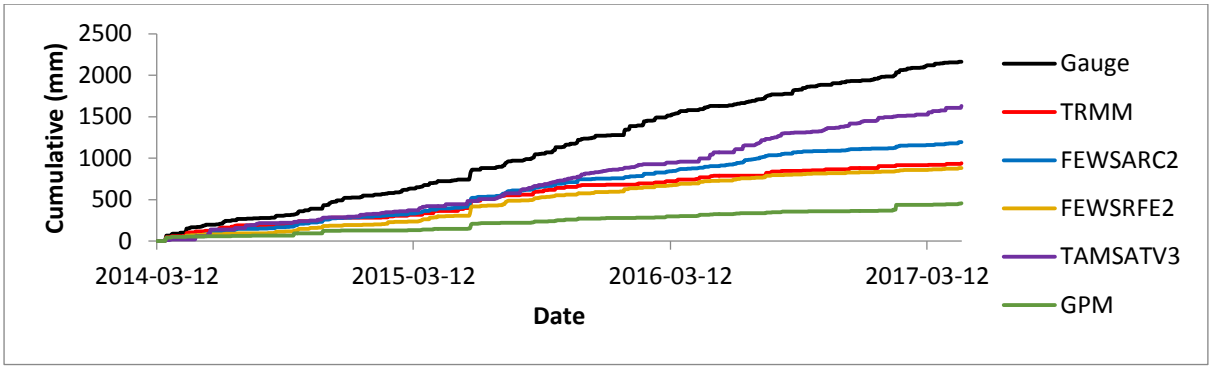

Figure 8.99 Accumulated rainfall at H9E002 during the GPM period of analysis.

Table 8.21 Statistics produced at H9E002.

	Gauge	TRMM3B42	FEWSARC2	FEWSRFE2	TAMSATv3
Total (mm)	5618,30	2541,10	2820,28	2276,50	3863,90
Max (mm)	93,40	83,40	69,73	64,30	60,70
Mean (mm)	2,10	0,95	1,05	0,85	1,44
BIAS		0,45	0,50	0,41	0,69
MAE (mm)		1,15	1,05	1,25	0,66
RMSE (mm)		6,16	4,11	4,82	7,51
RVE (%)		-54,77	-49,80	-59,48	-31,23
RSQ		0,20	0,54	0,52	0,02
0 mm					
POD		0,31	0,70	0,67	0,22
FAR		0,33	0,21	0,25	0,61
CSI		0,27	0,59	0,54	0,16
5 mm					
POD		0,97	1,00	0,99	0,98
FAR		0,03	0,01	0,01	0,00
CSI		0,95	0,99	0,98	0,98

Table 8.22 Statistics produced at H9E002 during the GPM period of analysis.

	Gauge	TRMM3B42	FEWSARC2	FEWSRFE2	TAMSATv3	GPM
Total (mm)	2163,60	939,00	1192,57	881,80	1628,60	455,40
Max (mm)	50,20	83,40	38,08	51,60	48,80	58,30
Mean (mm)	1,89	0,82	1,04	0,77	1,42	0,40
BIAS		0,43	0,55	0,41	0,75	0,21
MAE (mm)		1,07	0,85	1,12	0,47	1,49
RMSE (mm)		5,57	1,87	4,05	6,96	4,96
RVE (%)		-56,60	-44,88	-59,24	-24,73	-78,95
RSQ		0,12	0,51	0,46	0,00	0,19
0 mm						
POD		0,20	0,71	0,68	0,18	0,26
FAR		0,36	0,20	0,24	0,66	0,47
CSI		0,18	0,60	0,56	0,14	0,21
5 mm						
POD		1,00	1,00	1,00	1,00	0,94
FAR		0,04	0,02	0,00	0,00	0,00
CSI		0,96	0,98	1,00	1,00	0,94

- H6E001 (Thee Waters Kloof at Theewaterskloof Dam)

Time series of the products against gauge measurements are presented below.

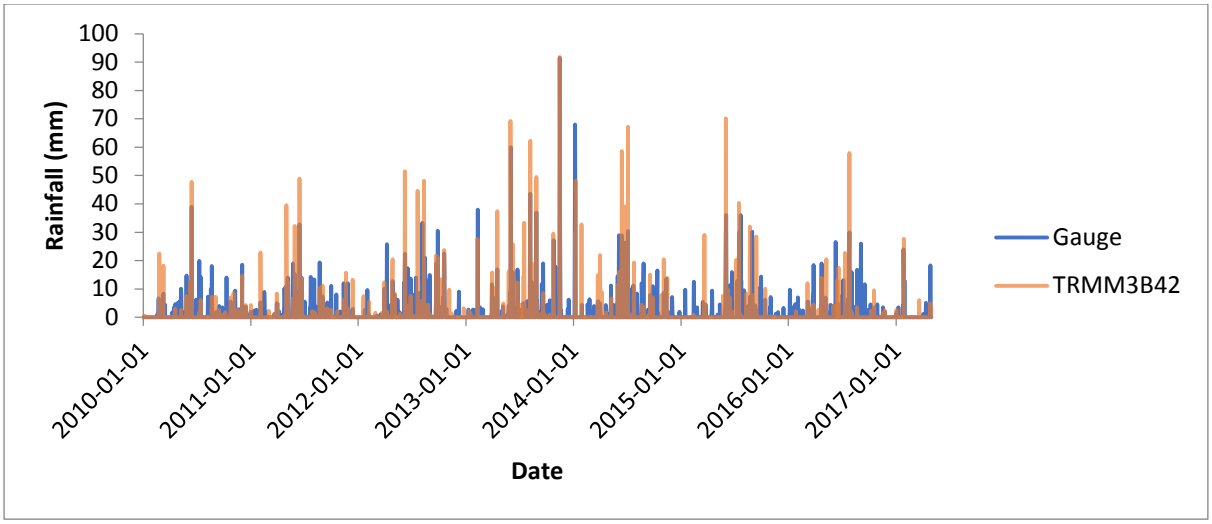

Figure 8.100 Time series of TRMM 3B42 against H6E001 measurements.

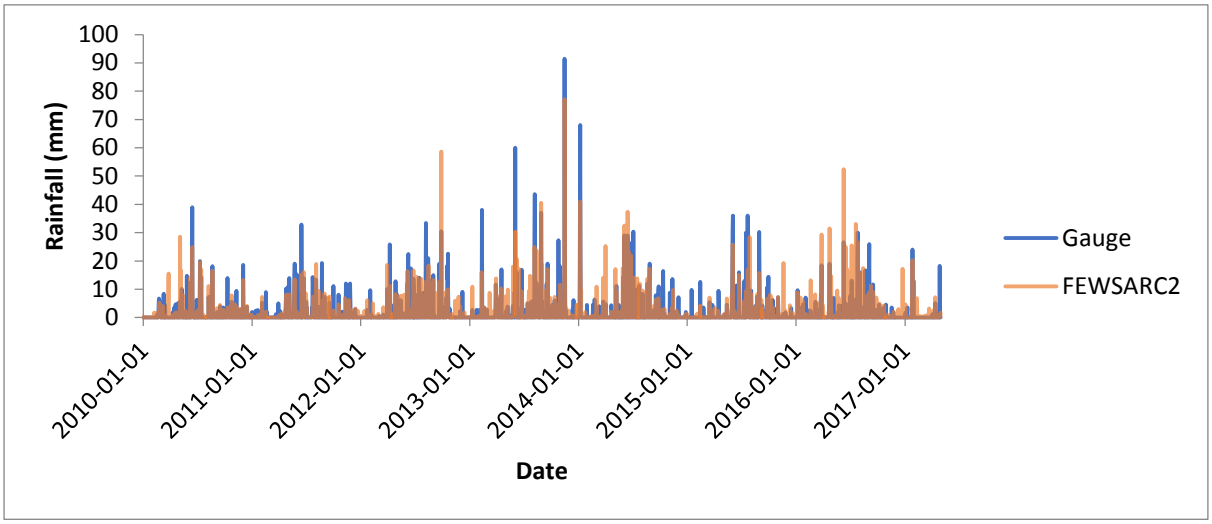

Figure 8.101 Time series of FEWS ARC2 against H6E001 measurements.

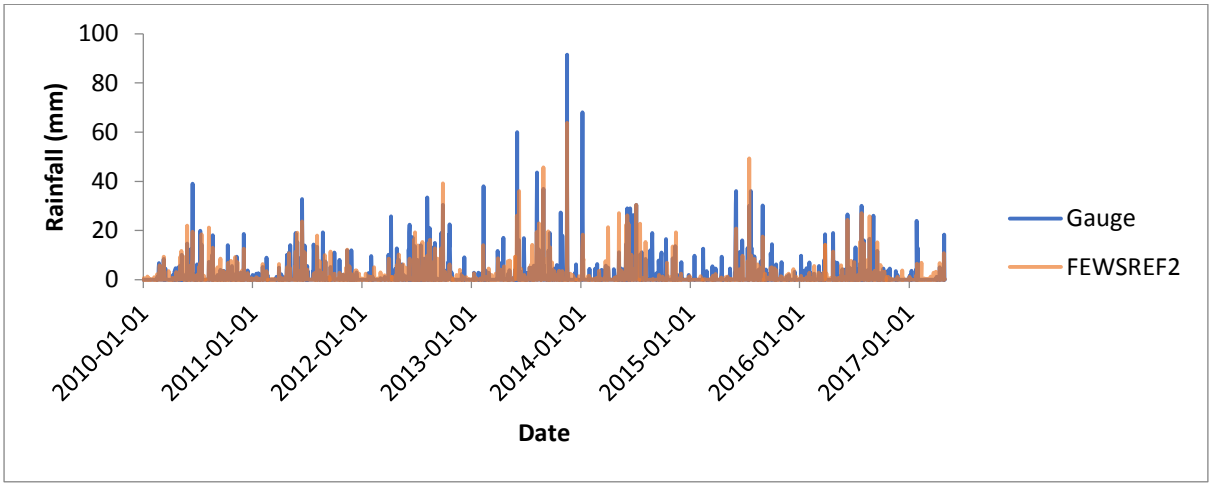

Figure 8.102 Time series of FEWS RFE2 against H6E001 measurements.

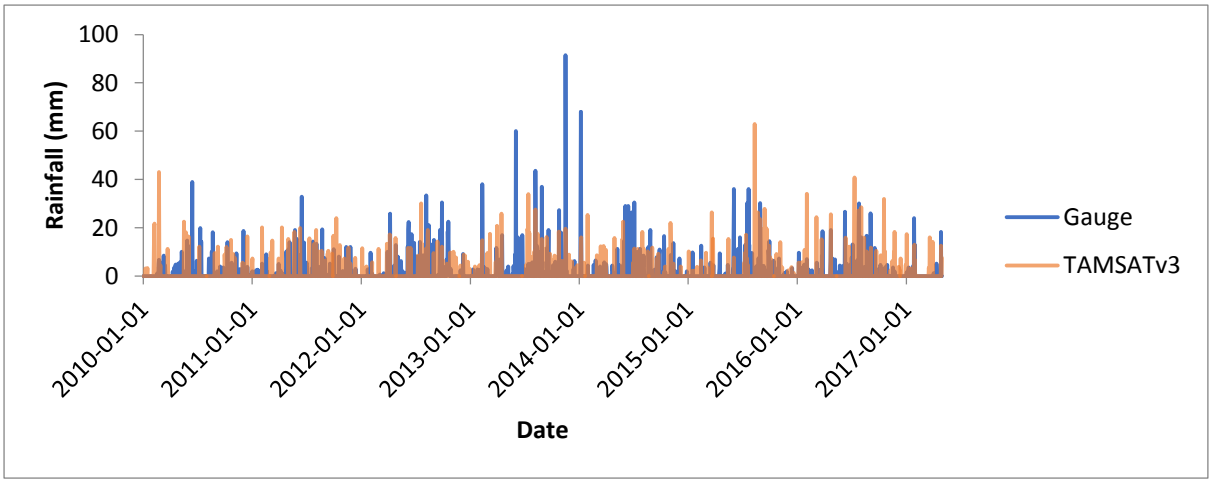

Figure 8.103 Time series of TAMSAT-3 against H6E001 measurements.

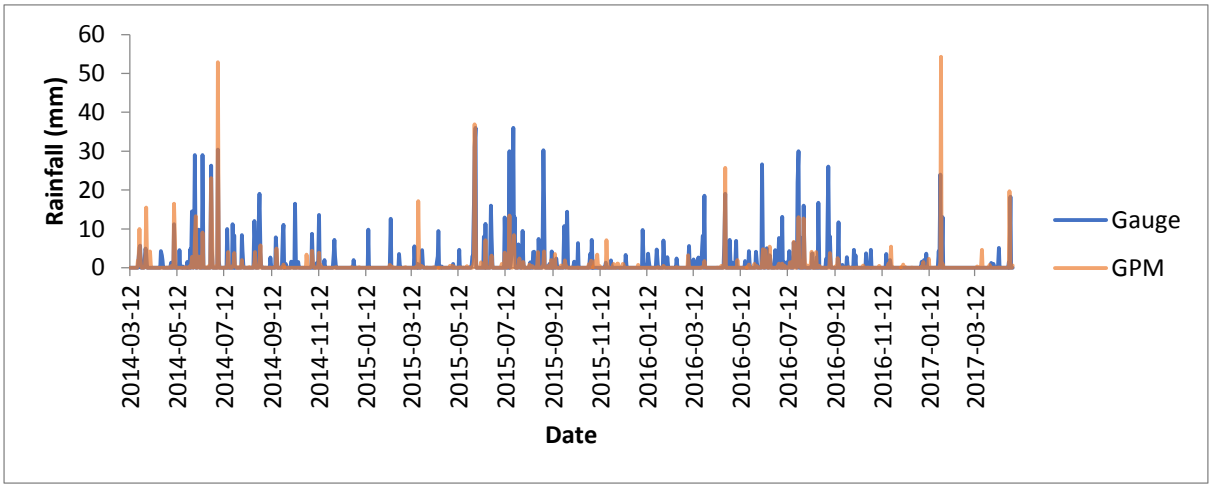

Figure 8.104 Time series of GPM against H6E001 measurements.

Average monthly rainfall totals are presented below.

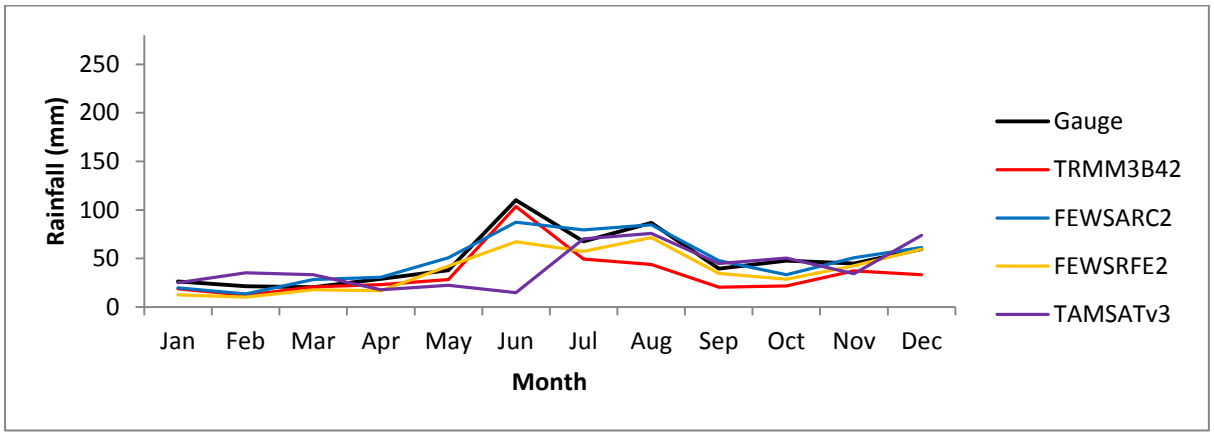

Figure 8.105 Average monthly rainfall totals at H6E001.

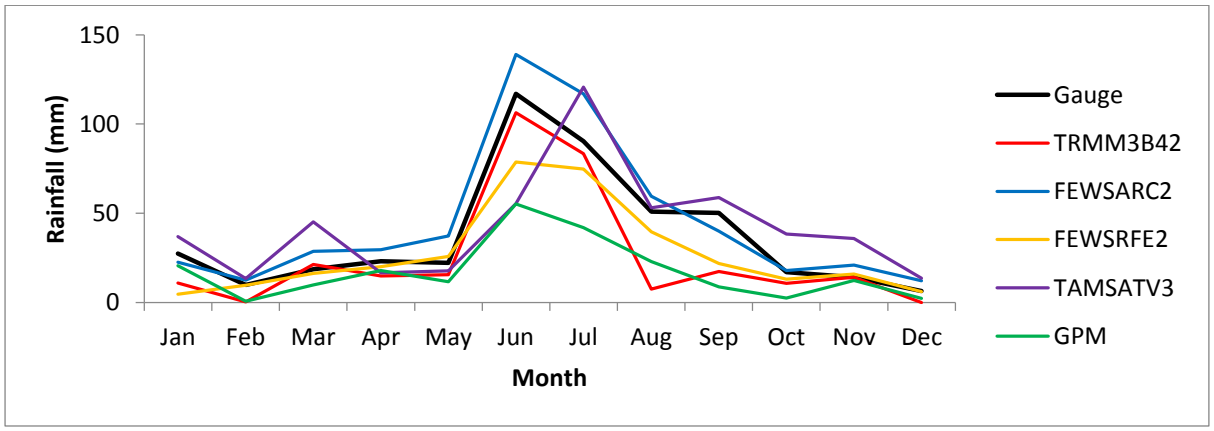

Figure 8.106 Average monthly rainfall totals at H6E001 during the GPM period of analysis.

Accumulated rainfall of all products are presented below against accumulated gauge rainfall.

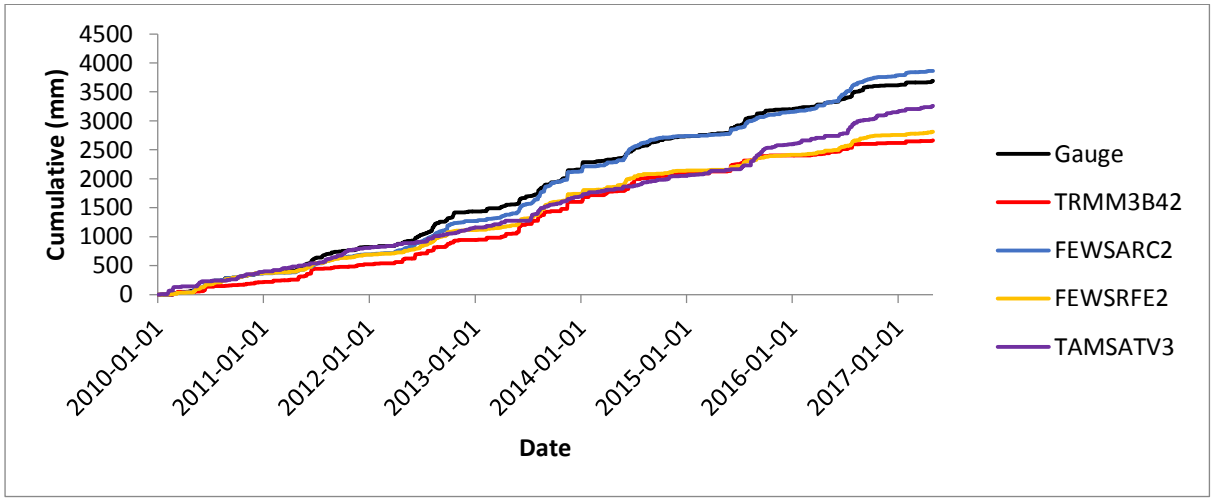

Figure 8.107 Accumulated rainfall at H6E001.

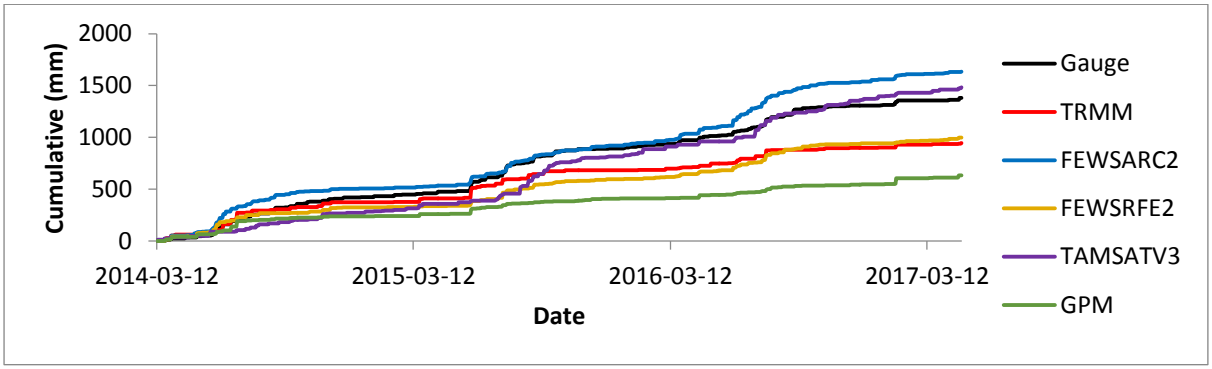

Figure 8.108 Accumulated rainfall at H6E001 during the GPM period of analysis.

Table 8.23 Statistics produced at H6E001.

	Gauge	TRMM3B42	FEWSARC2	FEWSRFE2	TAMSATv3
Total (mm)	3689,90	2661,80	3864,21	2812,50	3259,70
Max (mm)	91,50	91,80	77,15	63,70	63,00
Mean	1,38	0,99	1,44	1,05	1,22
BIAS		0,72	1,05	0,76	0,88
MAE (mm)		0,38	0,07	0,33	0,16
RMSE (mm)		4,81	2,99	3,67	5,87
RVE (%)		-27,86	4,72	-23,78	-11,66
RSQ		0,34	0,53	0,45	0,03
0 mm					
POD		0,35	0,81	0,76	0,19
FAR		0,39	0,47	0,50	0,74
CSI		0,29	0,47	0,43	0,12
5 mm					
POD		1,00	1,00	1,00	0,98
FAR		0,03	0,03	0,03	0,04
CSI		0,97	0,97	0,97	0,94

Table 8.24 Statistics produced at H6E001 during the GPM period of analysis.

	Gauge	TRMM3B42	FEWSARC2	FEWSRFE2	TAMSATv3	GPM
Total (mm)	1381,90	944,40	1634,36	998,80	1482,70	633,70
Max	36,00	70,10	52,45	49,30	63,00	54,30
Mean	1,21	0,82	1,43	0,87	1,29	0,55
BIAS		0,68	1,18	0,72	1,07	0,46
MAE (mm)		0,38	0,22	0,33	0,09	0,65
RMSE (mm)		4,63	1,86	3,30	5,68	3,97
RVE (%)		-31,66	18,27	-27,72	7,29	-54,14
RSQ		0,25	0,49	0,40	0,03	0,20
0 mm						
POD		0,22	0,83	0,68	0,23	0,49
FAR		0,48	0,50	0,53	0,71	0,61
CSI		0,18	0,45	0,38	0,15	0,28
5 mm						
POD		1,00	1,00	1,00	1,00	1,00
FAR		0,06	0,04	0,03	0,00	0,06
CSI		0,94	0,96	0,97	1,00	0,94

- H4E007 (Haweqwas Stateforest @ Stettynskloof Dam)

Time series of the products against gauge measurements are presented below.

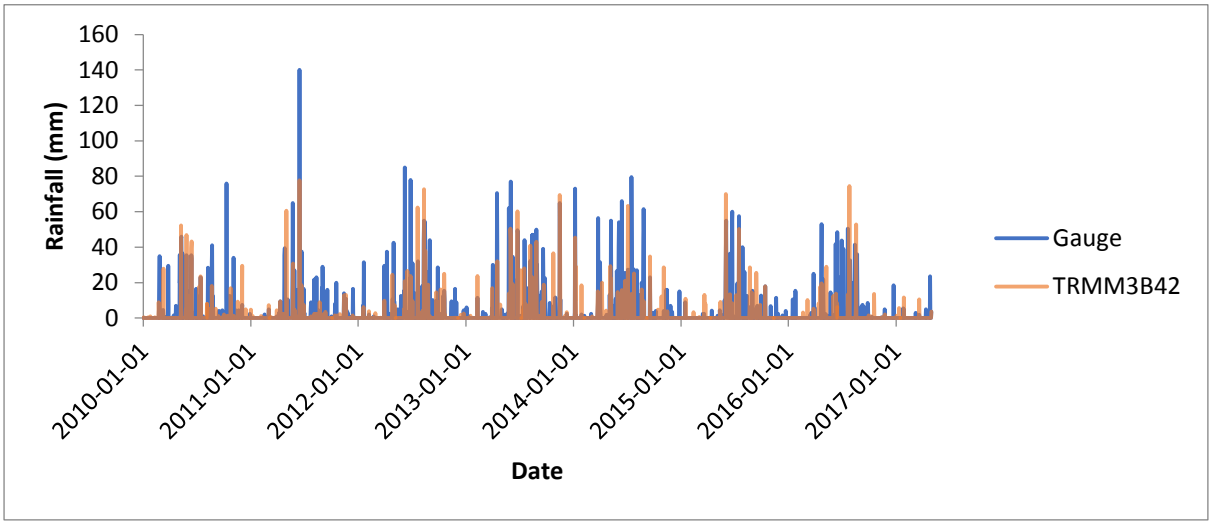

Figure 8.109 Time series of TRMM 3B42 against H4E007 measurements.

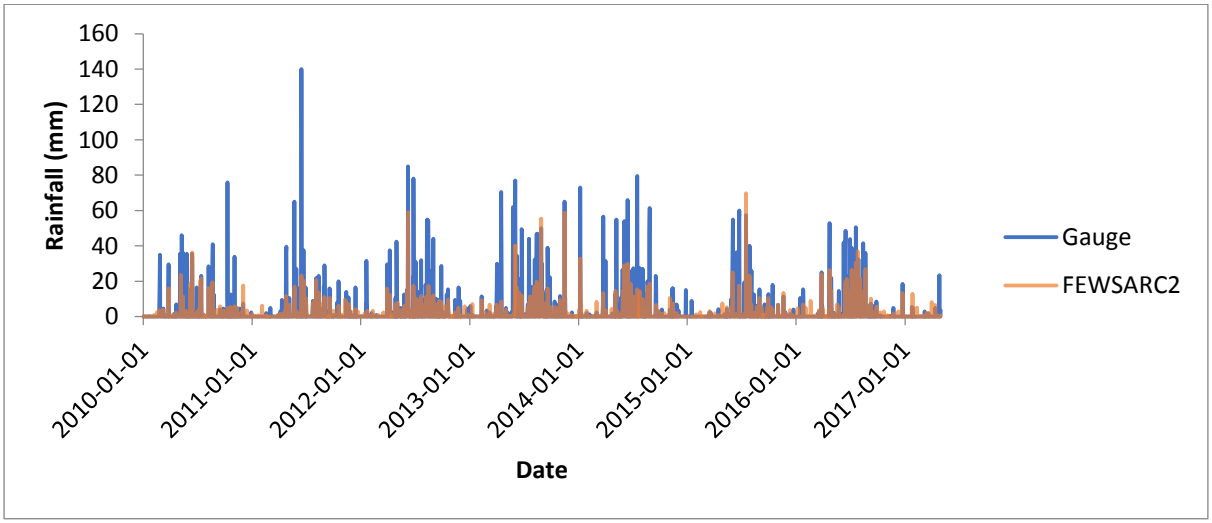

Figure 8.110 Time series of FEWS ARC2 against H4E007 measurements.

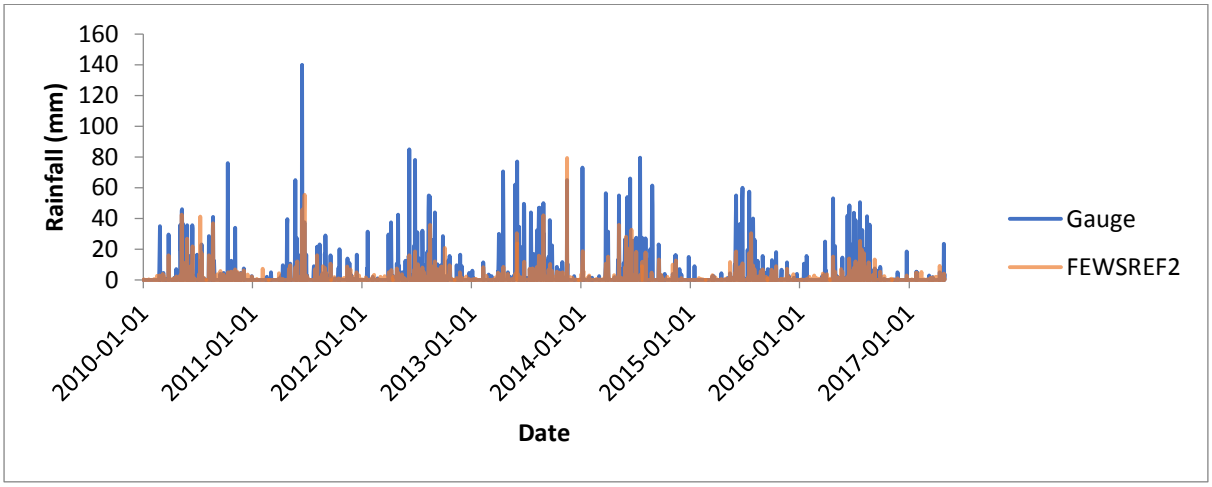

Figure 8.111 Time series of FEWS RFE2 against H4E007 measurements.

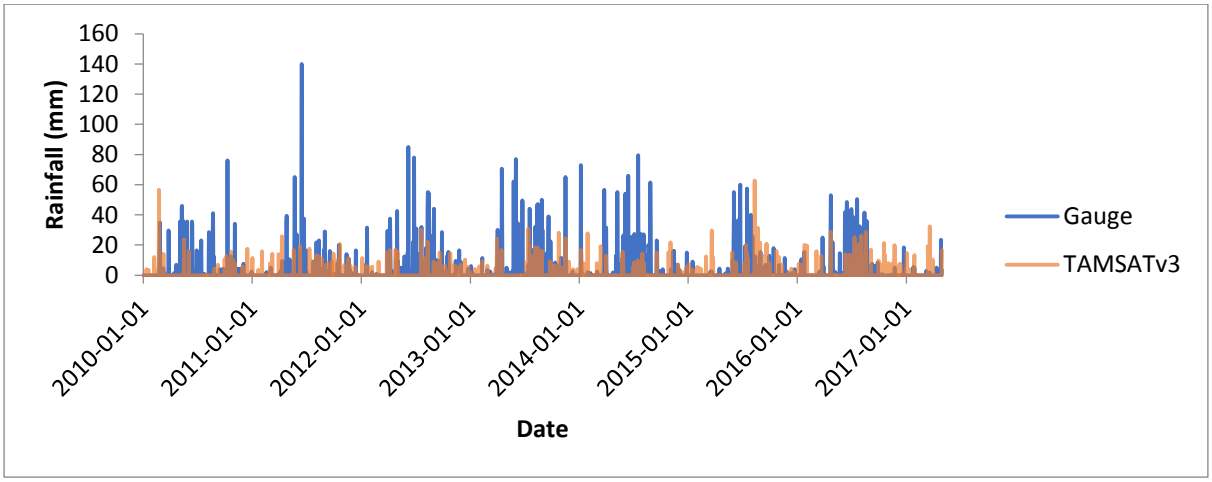

Figure 8.112 Time series of TAMSAT-3 against H4E007 measurements.

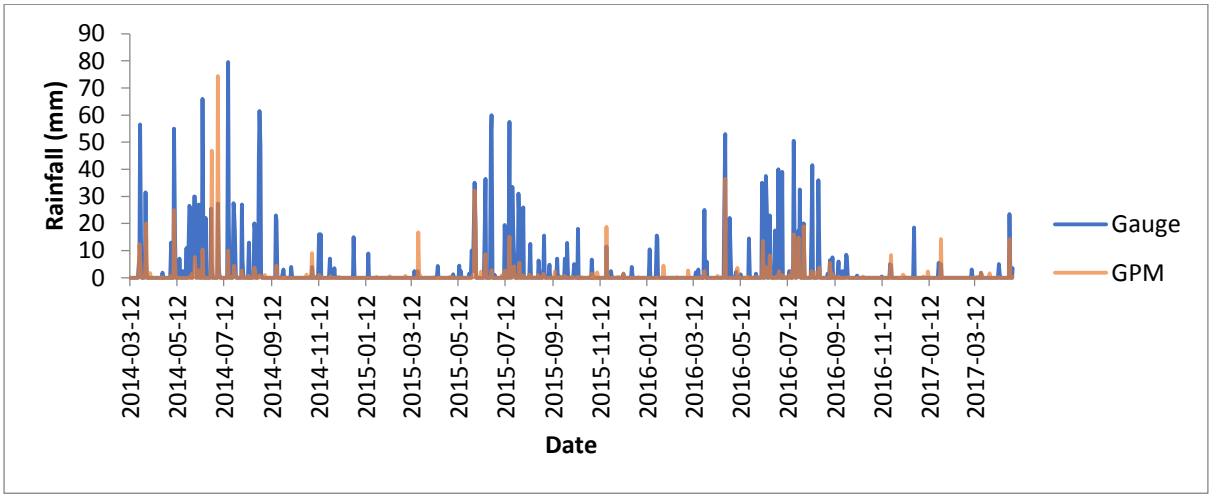

Figure 8.113 Time series of GPM against H4E007 measurements.

Average monthly rainfall totals are presented below.

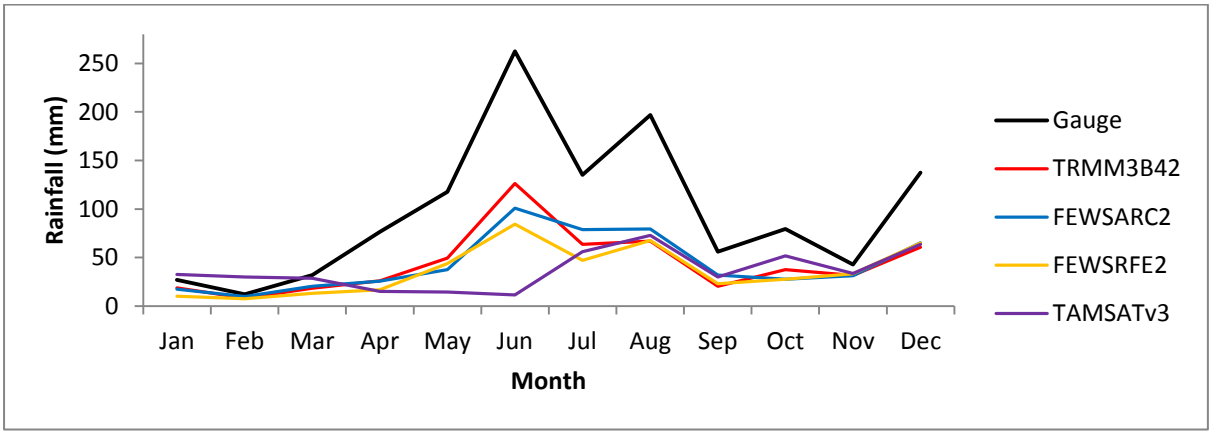

Figure 8.114 Average monthly rainfall totals at H4E007.

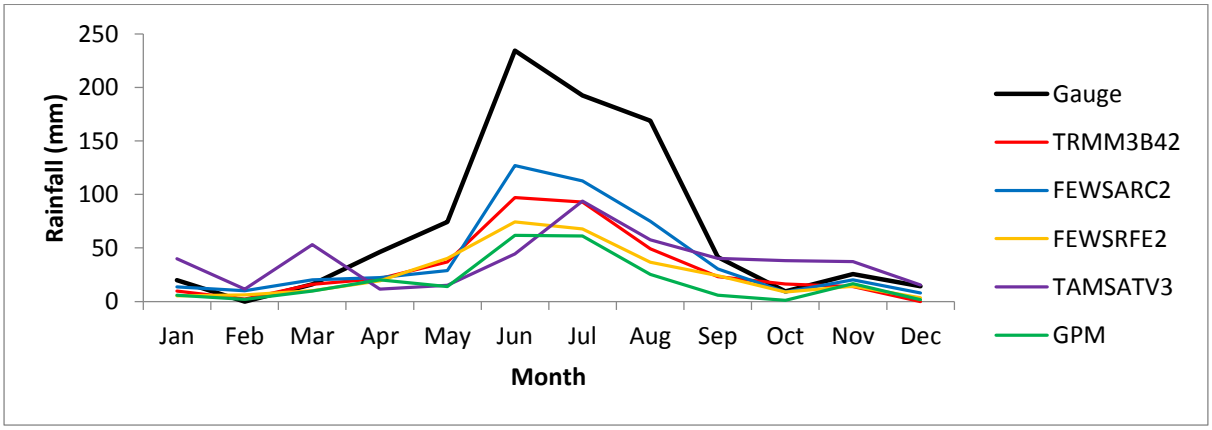

Figure 8.115 Average monthly rainfall totals at H4E007 during the GPM period of analysis.

Accumulated rainfall of all products are presented below against accumulated gauge rainfall.

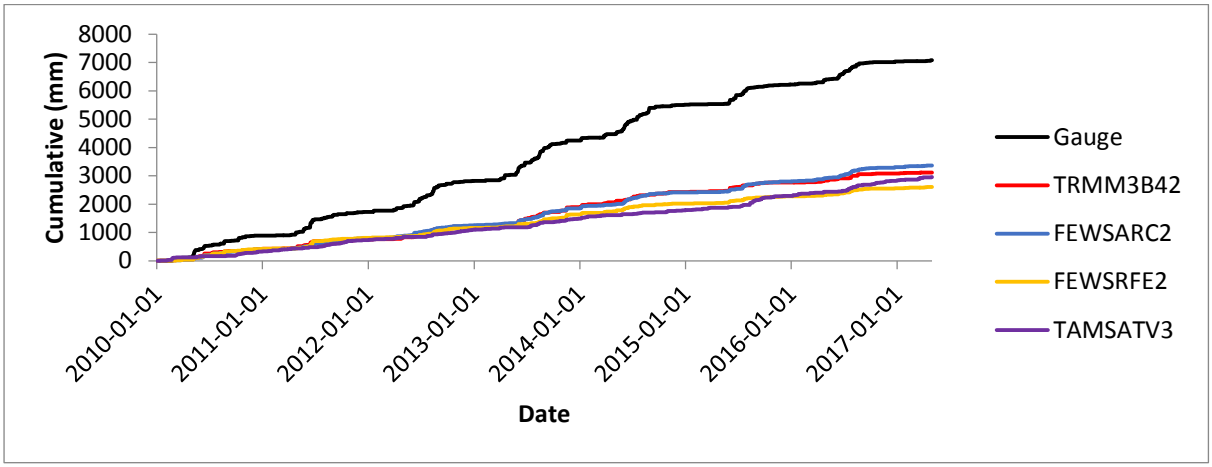

Figure 8.116 Accumulated rainfall at H4E007.

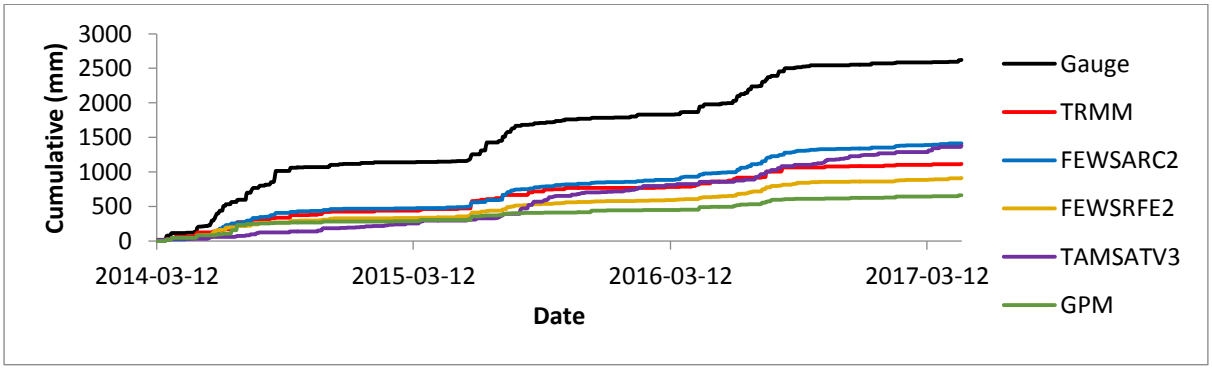

Figure 8.117 Accumulated rainfall at H4E007 during the GPM period of analysis.

Tables of statistics are presented below.

Table 8.25 Statistics produced at H4E007.

	Gauge	TRMM3B42	FEWSARC2	FEWSRFE2	TAMSATv3
Total (mm)	6984,20	3113,70	3362,76	2604,60	2957,20
Max (mm)	85,00	77,70	69,70	79,30	62,70
Mean (mm)	2,61	1,16	1,26	0,97	1,10
BIAS		0,45	0,48	0,37	0,42
MAE (mm)		1,45	1,35	1,64	1,50
RMSE (mm)		8,17	6,14	7,59	9,62
RVE (%)		-55,42	-51,85	-62,71	-57,66
RSQ		0,23	0,51	0,33	0,01
0 mm					
POD		0,33	0,77	0,60	0,16
FAR		0,39	0,45	0,48	0,74
CSI		0,27	0,47	0,39	0,11
5 mm					
POD		1,00	1,00	1,00	0,94
FAR		0,04	0,02	0,03	0,11
CSI		0,96	0,98	0,97	0,85

Table 8.26 Statistics produced at H4E007 during the GPM period of analysis.

	Gauge	TRMM3B42	FEWSARC2	FEWSRFE2	TAMSATv3	GPM
Total (mm)	2739,60	1118,60	1415,99	912,20	1381,30	665,60
Max (mm)	79,50	74,50	69,70	35,70	62,70	74,30
Mean (mm)	2,39	0,98	1,24	0,80	1,21	0,58
BIAS		0,41	0,52	0,33	0,50	0,24
MAE (mm)		1,41	1,15	1,59	1,19	1,81
RMSE (mm)		8,27	4,50	7,41	9,48	7,95
RVE (%)		-59,17	-48,31	-66,70	-49,58	-75,70
RSQ		0,15	0,54	0,32	0,00	0,18
0 mm						
POD		0,23	0,78	0,60	0,14	0,59
FAR		0,44	0,47	0,51	0,81	0,43
CSI		0,20	0,46	0,37	0,09	0,41
5 mm						
POD		1,00	1,00	1,00	1,00	1,00
FAR		0,03	0,04	0,06	0,15	0,08
CSI		0,97	0,96	0,94	0,85	0,92

- H3E002 (Montagu)

Time series of the products against gauge measurements are presented below.

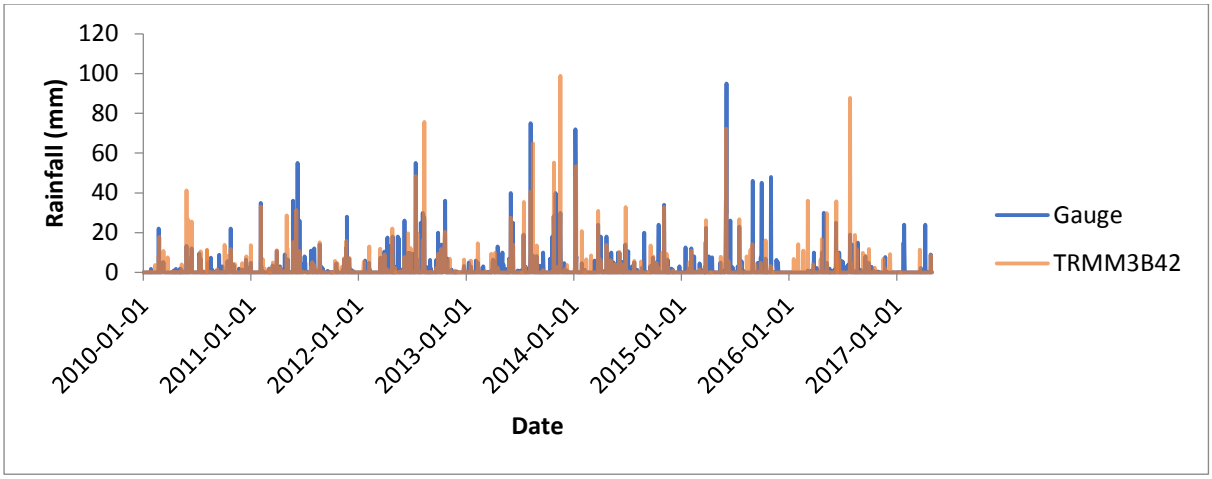

Figure 8.118 Time series of TRMM 3B42 against H3E002 measurements.

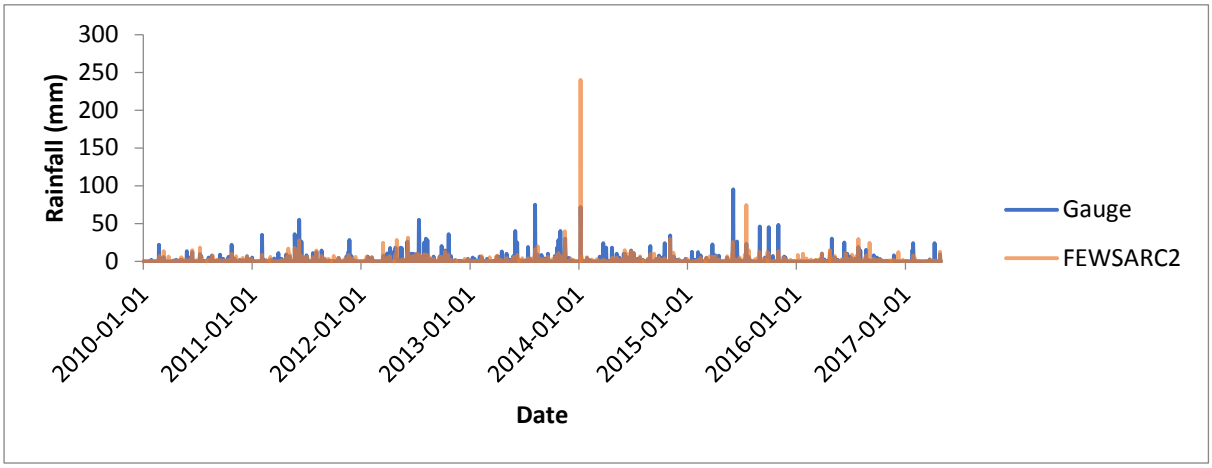

Figure 8.119 Time series of FEWS ARC2 against H3E002 measurements.

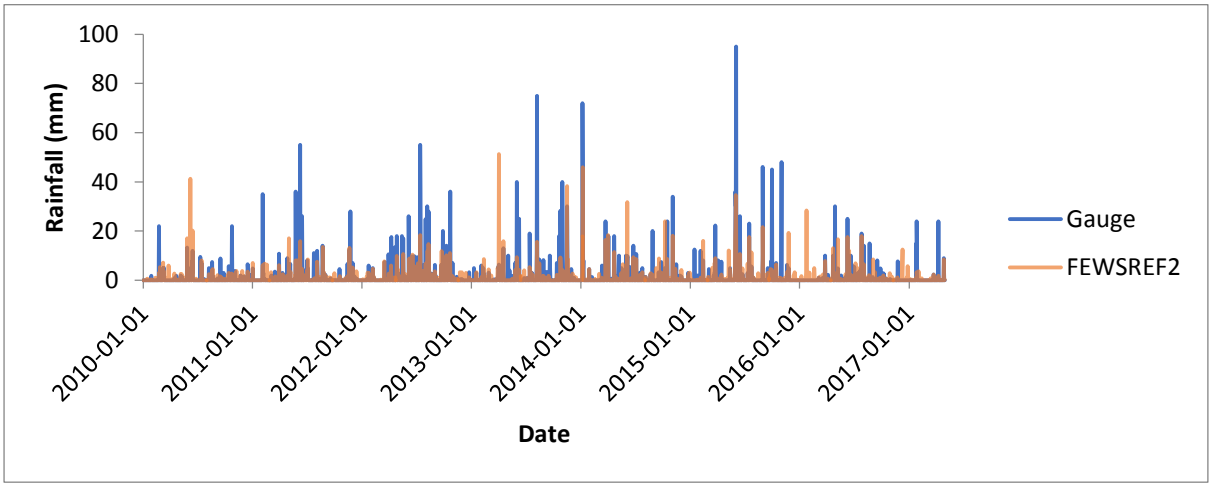

Figure 8.120 Time series of FEWS RFE2 against H3E002 measurements.

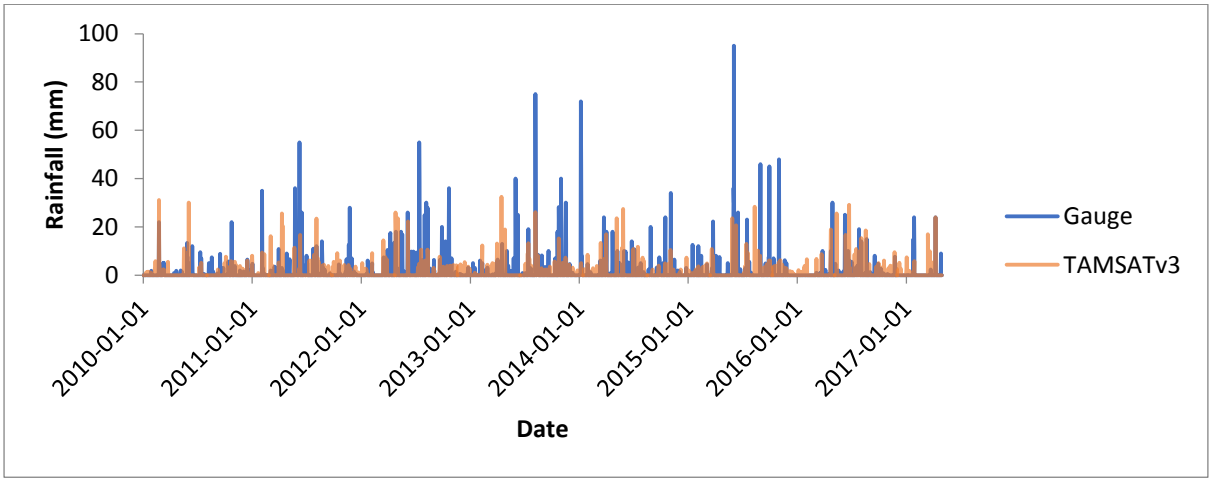

Figure 8.121 Time series of TAMSAT-3 against H3E002 measurements.

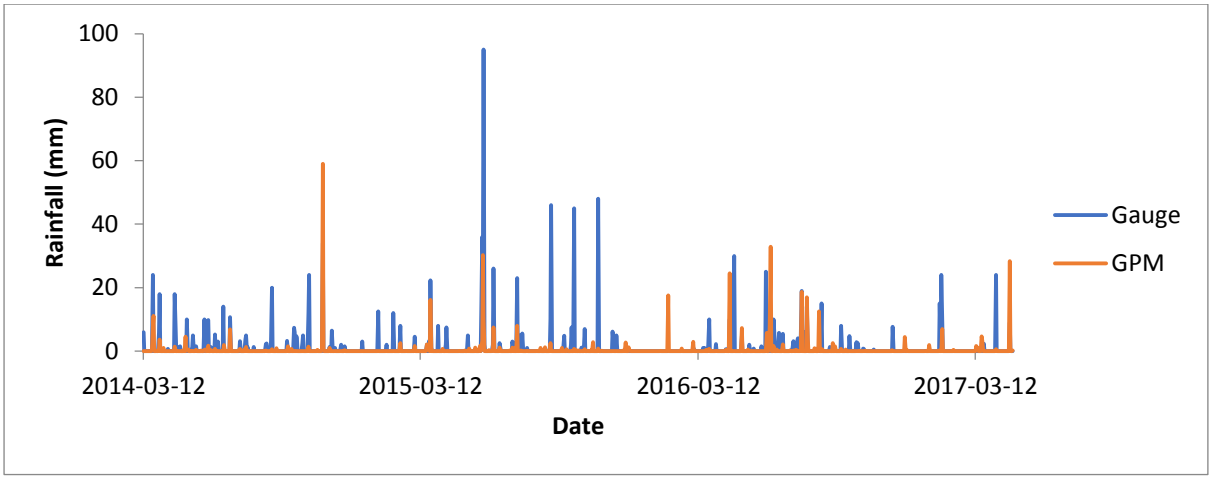

Figure 8.122 Time series of GPM against H3E002 measurements.

Average monthly rainfall totals are presented below.

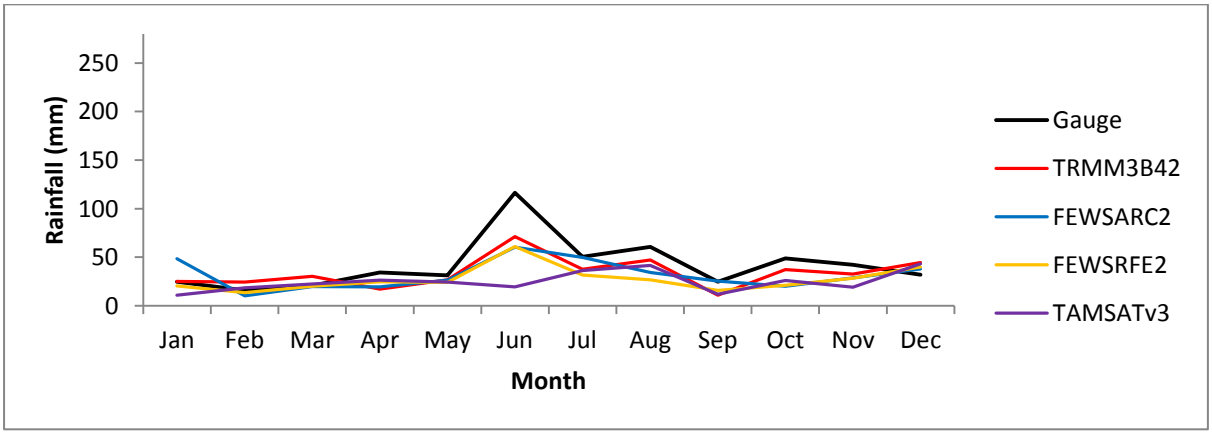

Figure 8.123 Average monthly rainfall totals at H3E002.

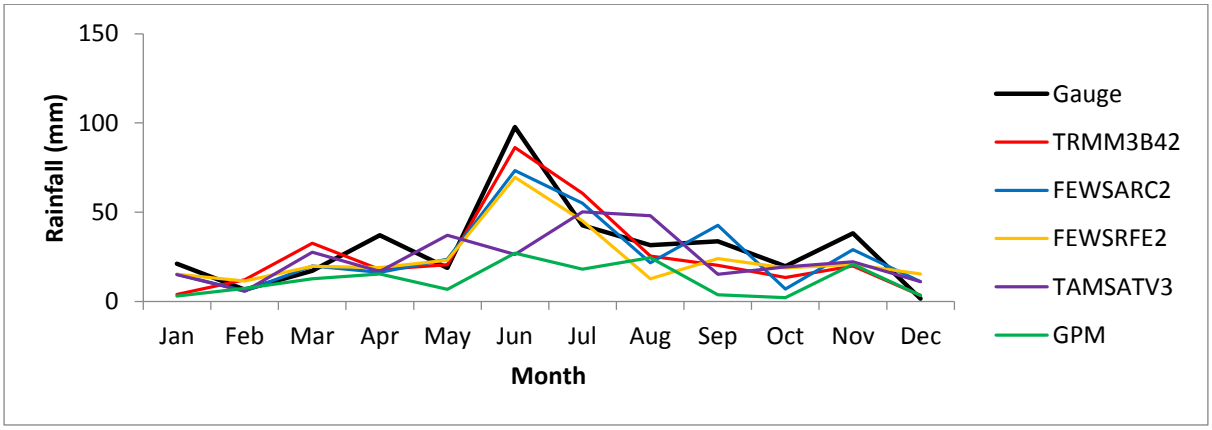

Figure 8.124 Average monthly rainfall totals at H3E002 during the GPM period of analysis.

Accumulated rainfall of all products are presented below against accumulated gauge rainfall.

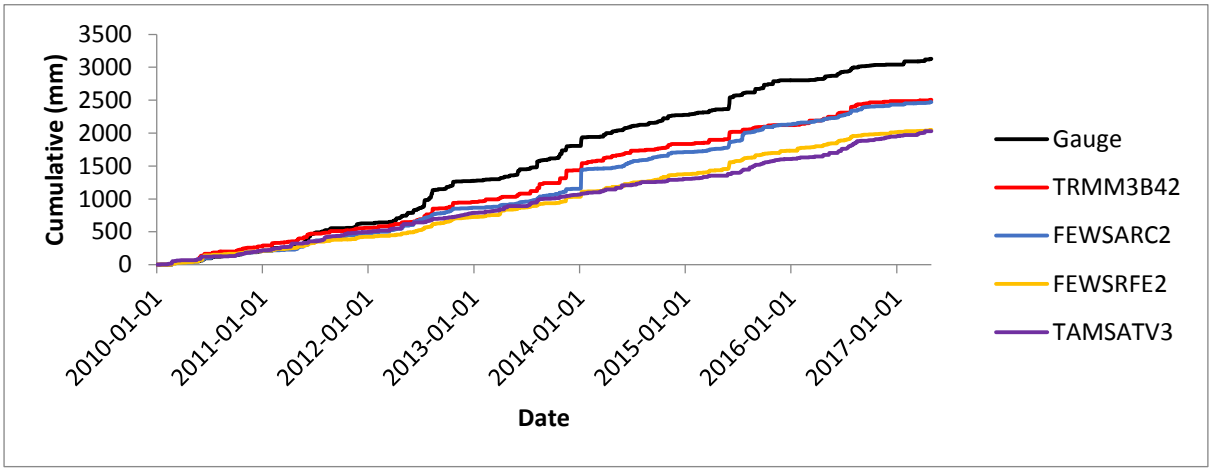

Figure 8.125 Accumulated rainfall at H3E002.

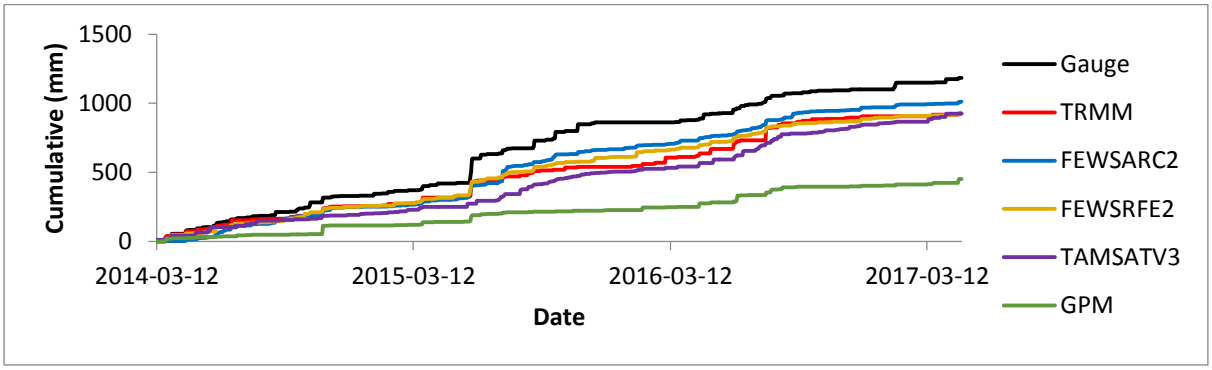

Figure 8.126 Accumulated rainfall at H3E002 during the GPM period of analysis.

Tables of statistics are presented below.

Table 8.27 Statistics produced at H3E002.

	Gauge	TRMM3B42	FEWSARC2	FEWSRFE2	TAMSATv3
Total (mm)	3126,70	2507,00	2472,90	2046,70	2026,80
Max (mm)	95,00	98,80	239,88	51,30	32,50
Mean (mm)	1,17	0,94	0,92	0,76	0,76
BIAS		0,80	0,79	0,65	0,65
MAE (mm)		0,23	0,24	0,40	0,41
RMSE (mm)		5,23	4,66	4,34	5,47
RVE (%)		-19,82	-20,91	-34,54	-35,18
RSQ		0,24	0,24	0,31	0,03
0 mm					
POD		0,39	0,68	0,66	0,25
FAR		0,36	0,49	0,51	0,71
CSI		0,32	0,41	0,39	0,16
5 mm					
POD		0,97	1,00	0,98	0,93
FAR		0,04	0,05	0,08	0,07
CSI		0,93	0,95	0,90	0,86

Table 8.28 Statistics produced at H3E002 during the GPM period of analysis.

	Gauge	TRMM3B42	FEWSARC2	FEWSRFE2	TAMSATv3	GPM
Total (mm)	1185,00	927,20	1011,59	926,10	924,40	453,20
Max (mm)	95,00	87,80	74,58	34,60	29,20	59,00
Mean (mm)	1,03	0,81	0,88	0,81	0,81	0,40
BIAS		0,78	0,85	0,78	0,78	0,38
MAE (mm)		0,22	0,15	0,23	0,23	0,64
RMSE (mm)		5,25	1,57	4,07	5,58	4,72
RVE (%)		-21,76	-14,63	-21,85	-21,99	-61,76
RSQ		0,18	0,23	0,34	0,01	0,15
0 mm						
POD		0,30	0,76	0,72	0,22	0,44
FAR		0,43	0,59	0,59	0,79	0,56
CSI		0,25	0,36	0,35	0,12	0,28
5 mm						
POD		0,96	1,00	1,00	0,92	1,00
FAR		0,04	0,07	0,10	0,08	0,00
CSI		0,92	0,93	0,90	0,85	1,00

- H2E003 (Lakenvlei at Lakenvallei Dam)

Time series of the products against gauge measurements are presented below.

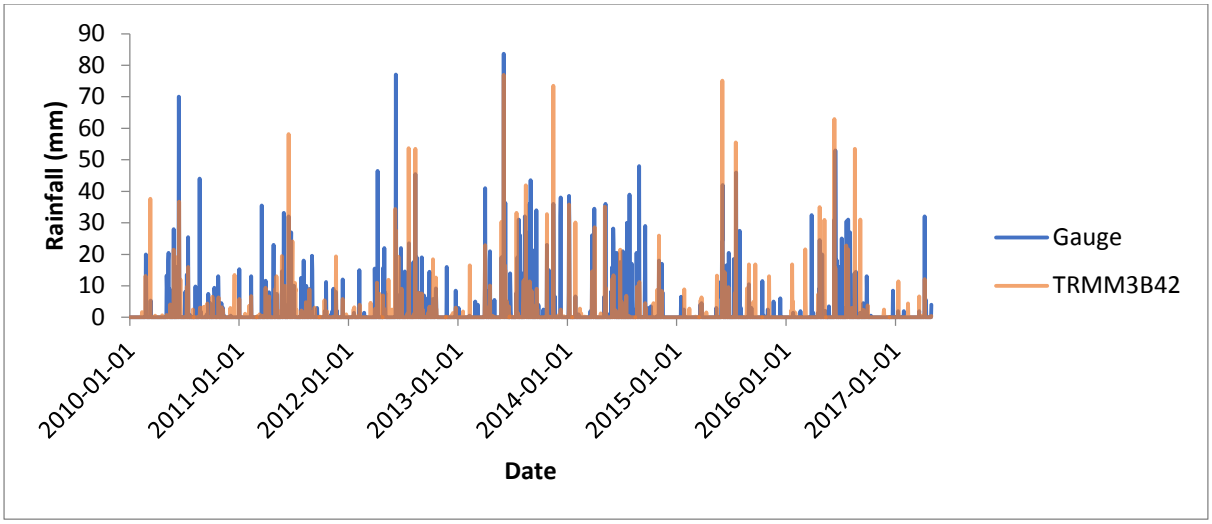

Figure 8.127 Time series of TRMM 3B42 against H2E003 measurements.

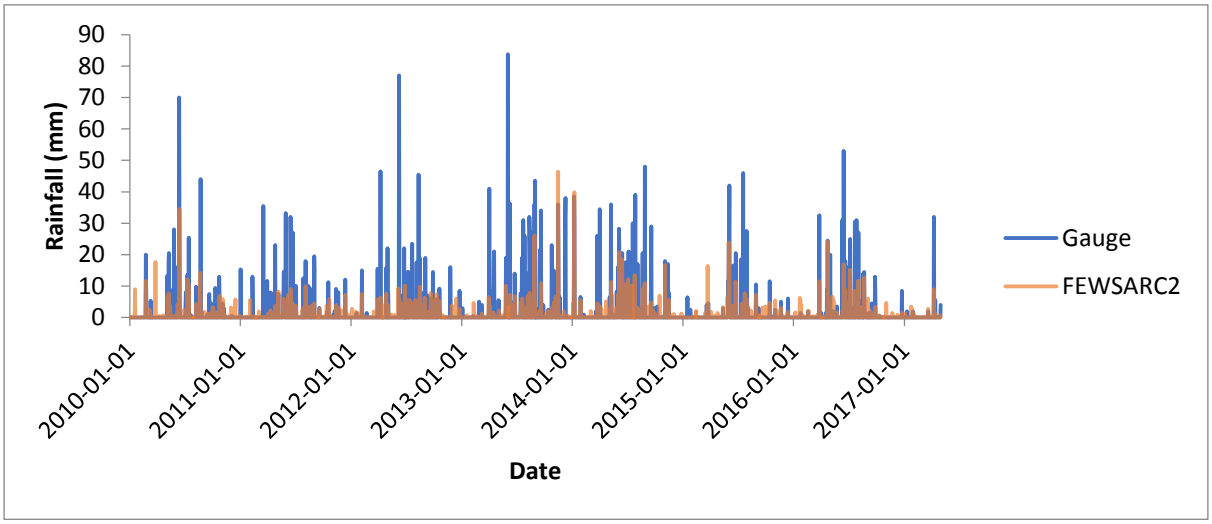

Figure 8.128 Time series of FEWS ARC2 against H2E003 measurements.

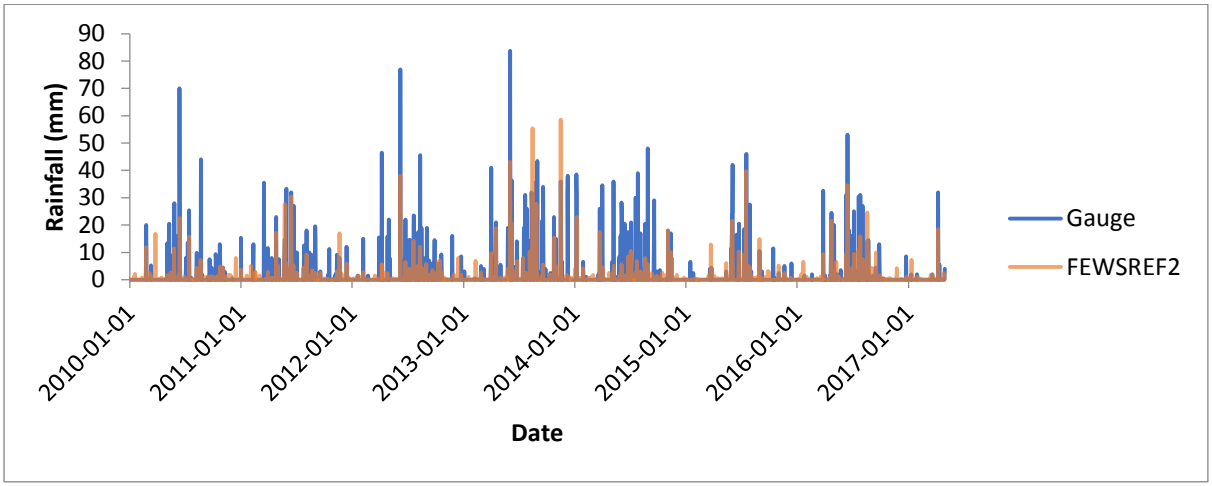

Figure 8.129 Time series of FEWS RFE2 against H2E003 measurements.

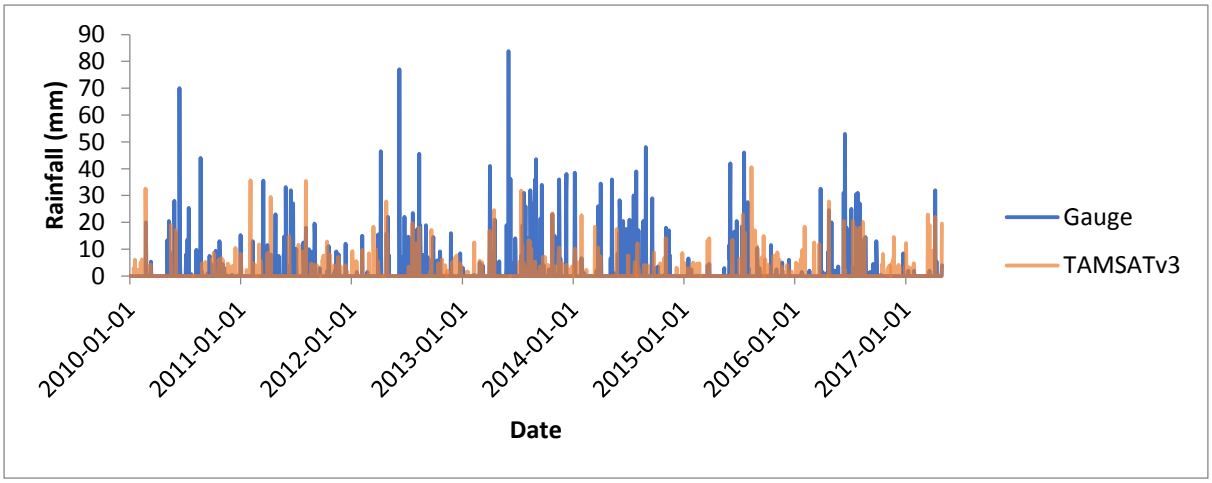

Figure 8.130 Time series of TAMSAT-3 against H2E003 measurements.

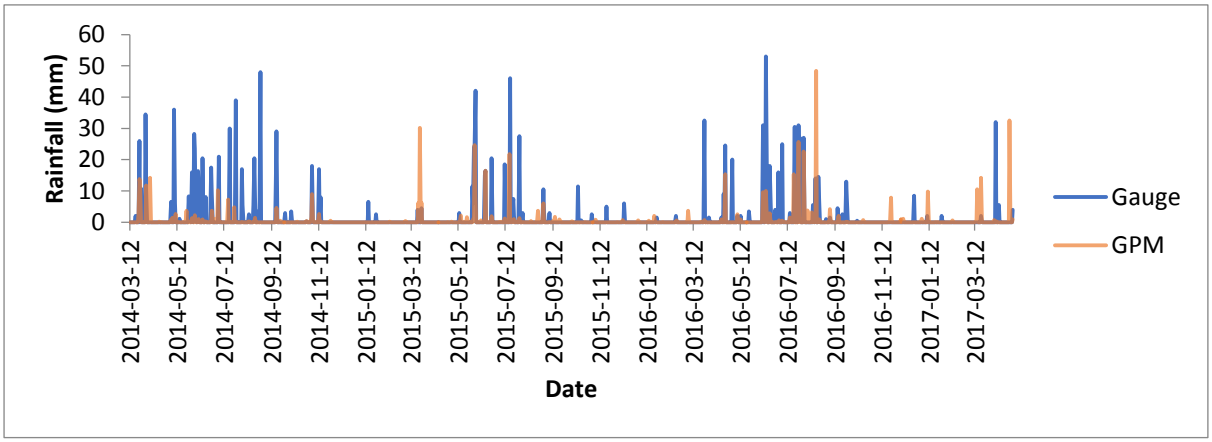

Figure 8.131 Time series of GPM against H2E003 measurements.

Average monthly rainfall totals are presented below.

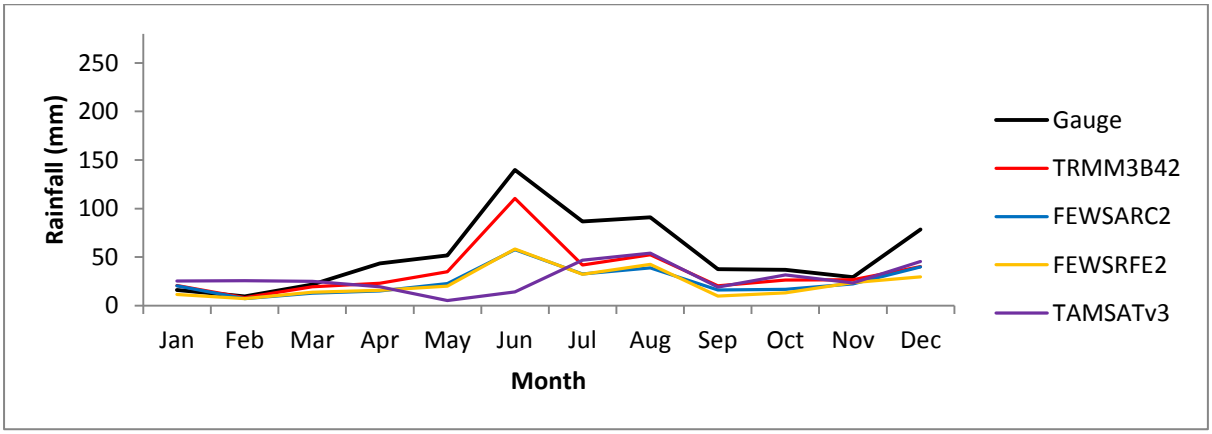

Figure 8.132 Average monthly rainfall totals at H2E003.

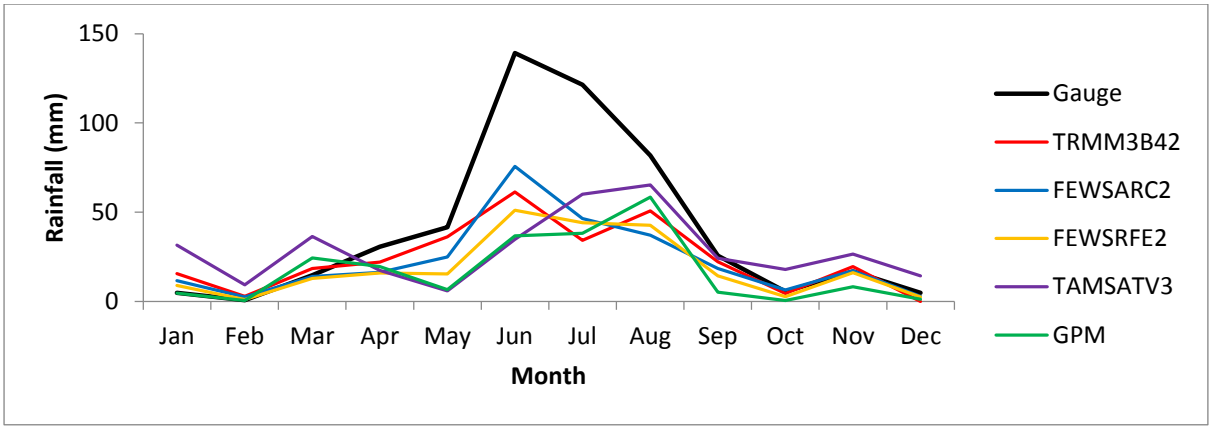

Figure 8.133 Average monthly rainfall totals at H2E003 during the GPM period of analysis.

Accumulated rainfall of all products are presented below against accumulated gauge rainfall.

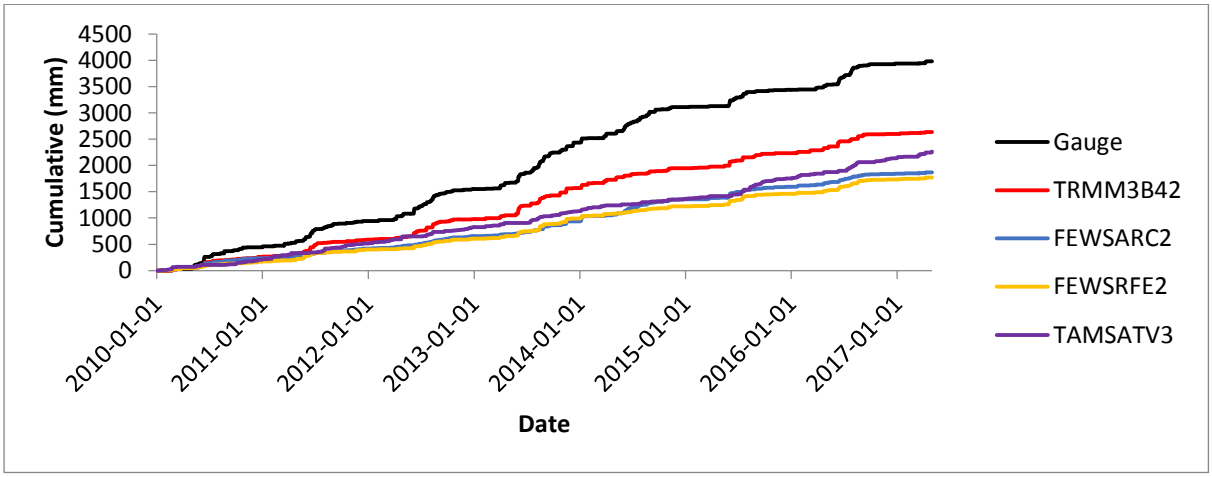

Figure 8.134 Accumulated rainfall at H2E003.

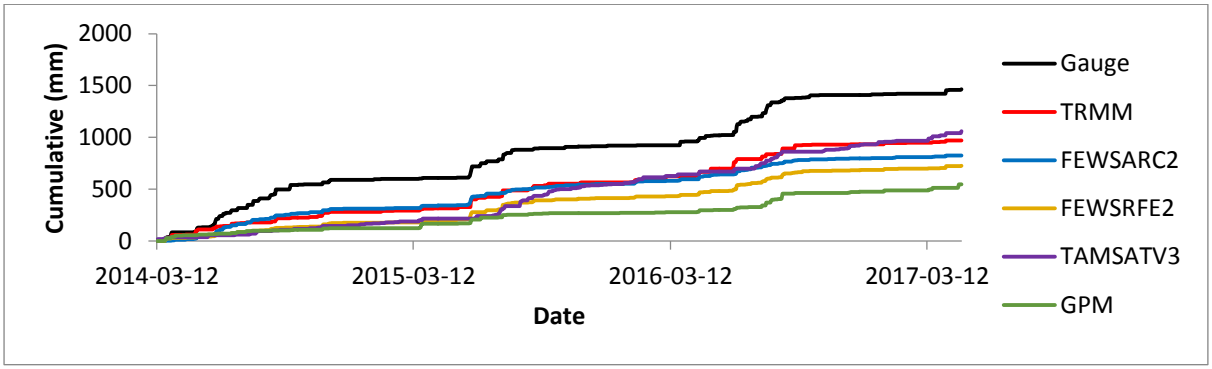

Figure 8.135 Accumulated rainfall at H2E003 during the GPM period of analysis.

Tables of statistics are presented below.

Table 8.29 Statistics produced at H2E003.

	Gauge	TRMM3B42	FEWSARC2	FEWSRFE2	TAMSATv3
Total (mm)	3981,80	2633,90	1866,54	1772,40	2262,60
Max (mm)	83,70	76,90	46,35	58,60	40,50
Mean (mm)	1,49	0,98	0,70	0,66	0,85
BIAS		0,66	0,47	0,45	0,57
MAE (mm)		0,50	0,79	0,83	0,64
RMSE (mm)		6,02	4,79	5,11	6,48
RVE (%)		-33,85	-53,12	-55,49	-43,18
RSQ		0,17	0,25	0,28	0,01
0 mm					
POD		0,36	0,67	0,63	0,22
FAR		0,61	0,59	0,61	0,78
CSI		0,23	0,34	0,32	0,13
5 mm					
POD		1,00	1,00	0,98	1,00
FAR		0,00	0,00	0,00	0,07
CSI		1,00	1,00	0,98	0,93

Table 8.30 Statistics produced at H2E003 during the GPM period of analysis.

	Gauge	TRMM3B42	FEWSARC2	FEWSRFE2	TAMSATv3	GPM
Total (mm)	1463,60	969,60	826,05	725,50	1061,50	548,00
Max (mm)	53,00	75,10	24,18	39,70	40,50	48,40
Mean (mm)	1,28	0,85	0,72	0,63	0,93	0,48
BIAS		0,66	0,56	0,50	0,73	0,37
MAE (mm)		0,43	0,56	0,64	0,35	0,80
RMSE (mm)		6,11	2,98	4,67	6,06	5,41
RVE (%)		-33,75	-43,56	-50,43	-27,47	-62,56
RSQ		0,09	0,34	0,26	0,01	0,07
0 mm						
POD		0,26	0,76	0,65	0,18	0,57
FAR		0,65	0,64	0,69	0,85	0,62
CSI		0,17	0,32	0,27	0,09	0,30
5 mm						
POD		1,00	1,00	0,96	1,00	1,00
FAR		0,00	0,00	0,00	0,00	0,00
CSI		1,00	1,00	0,96	1,00	1,00

8.3 Appendix C

The time series of the ACRU simulations of steamflow are presented in this section.

8.3.1 Upper uMngeni streamflow modelling

- U2H006 (Karkloof at Shafton)

The time series of the simulated streamflow against weir gauge streamflow are presented below.

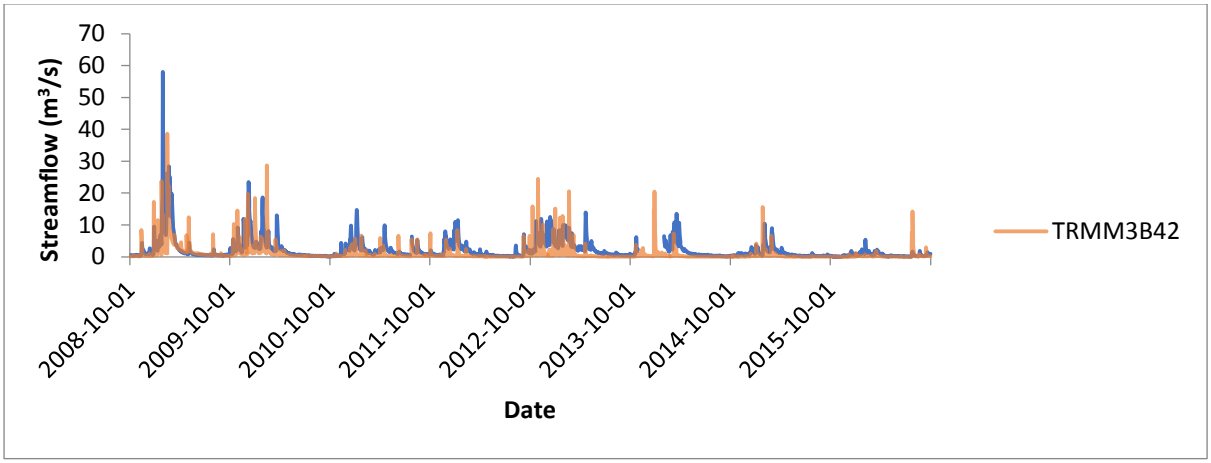

Figure 8.136 Time series of simulated streamflow driven with TRMM 3B42 against U2H006 streamflow.

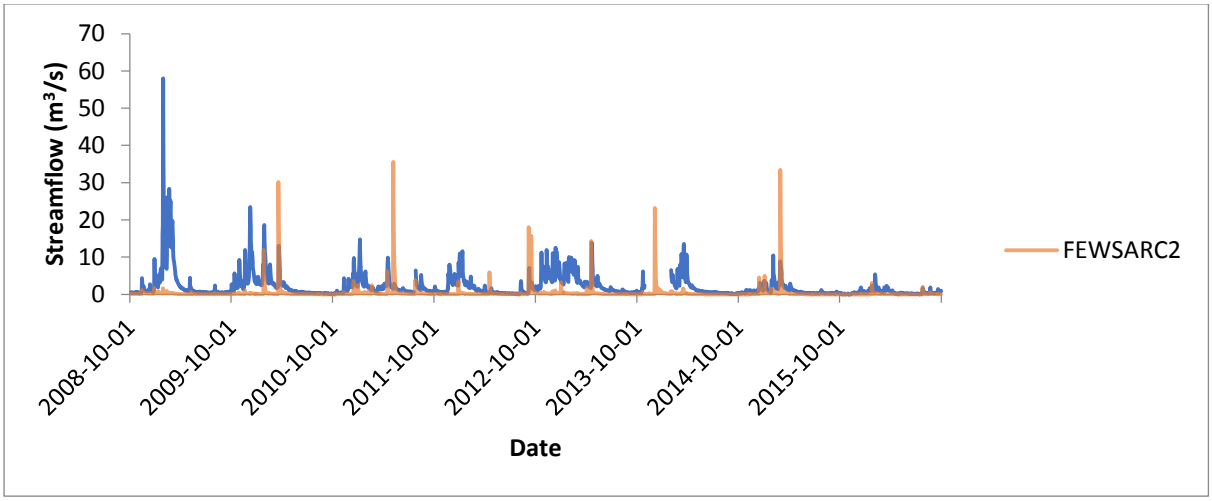

Figure 8.137 Time series of simulated streamflow driven with FEWS ARC2 against U2H006 streamflow.

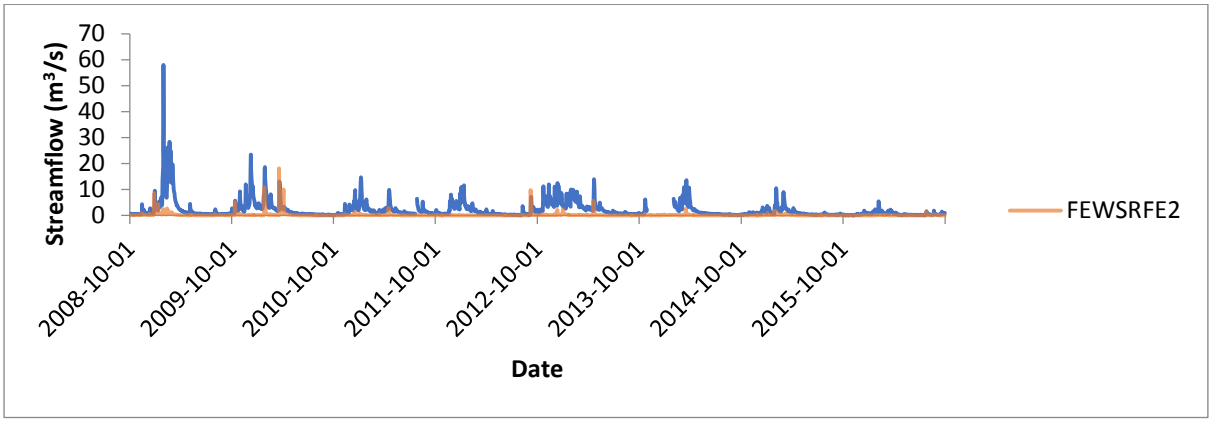

Figure 8.138 Time series of simulated streamflow driven with FEWS RFE2 against U2H006 streamflow.

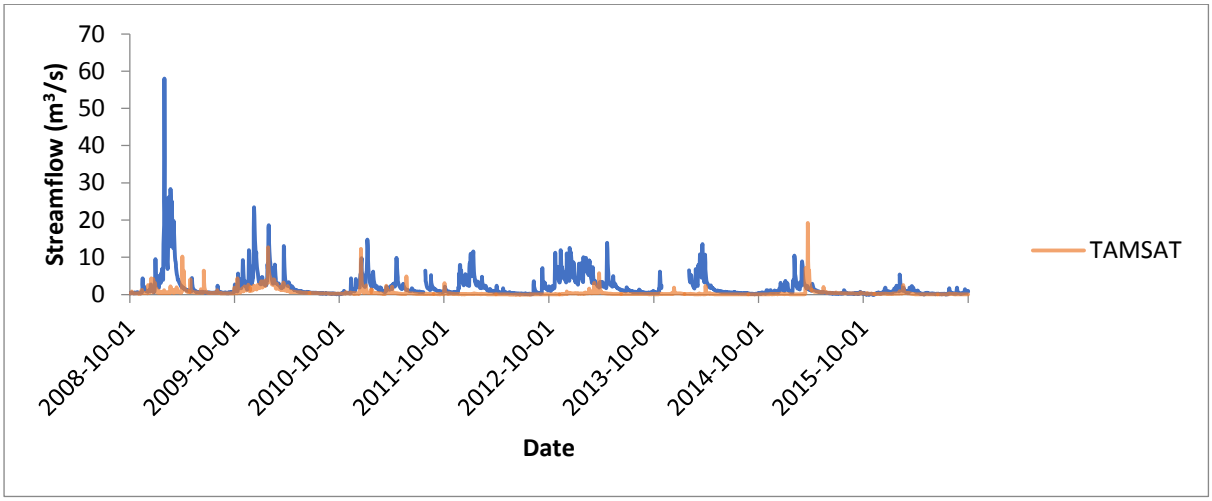

Figure 8.139 Time series of simulated streamflow driven with TAMSAT-3 against U2H006 streamflow.

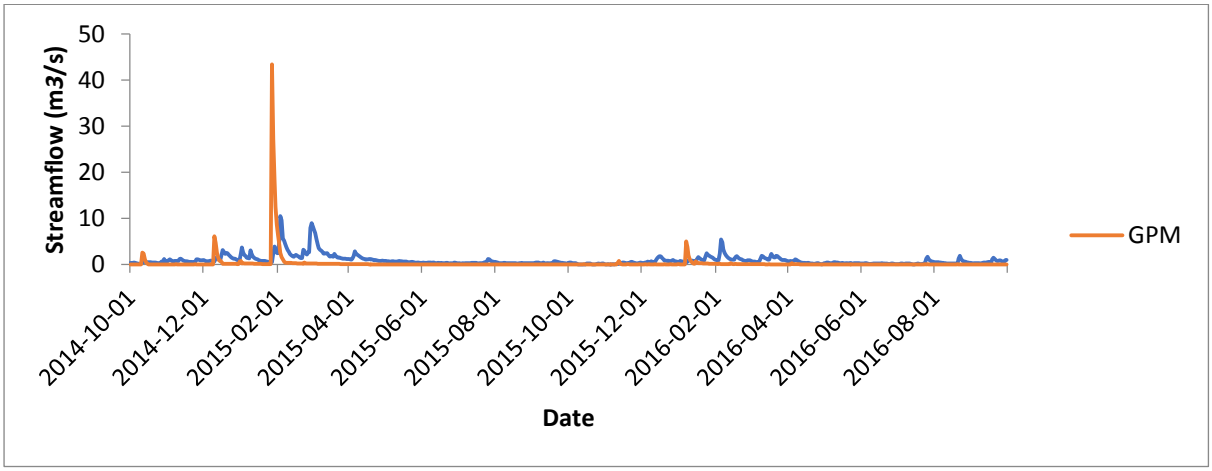

Figure 8.140 Time series of simulated streamflow driven with GPM against U2H006 streamflow.

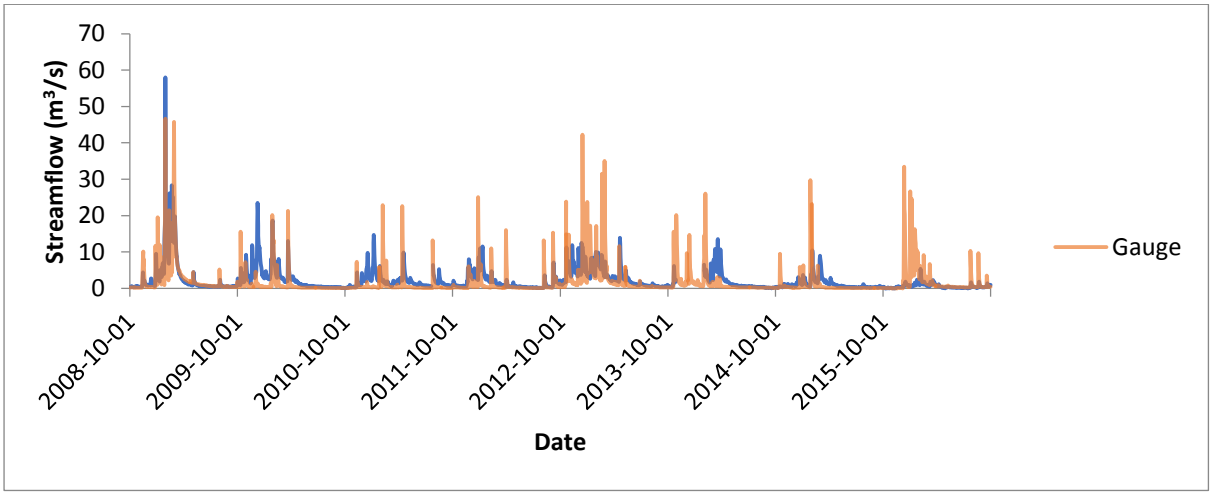

Figure 8.141 Time series of simulated streamflow driven with rain gauge measurements against U2H006 streamflow.

- U2H007 (Lions River- Mpofana River at Weltervreden)

The time series of the simulated streamflow against weir gauge streamflow are presented below.

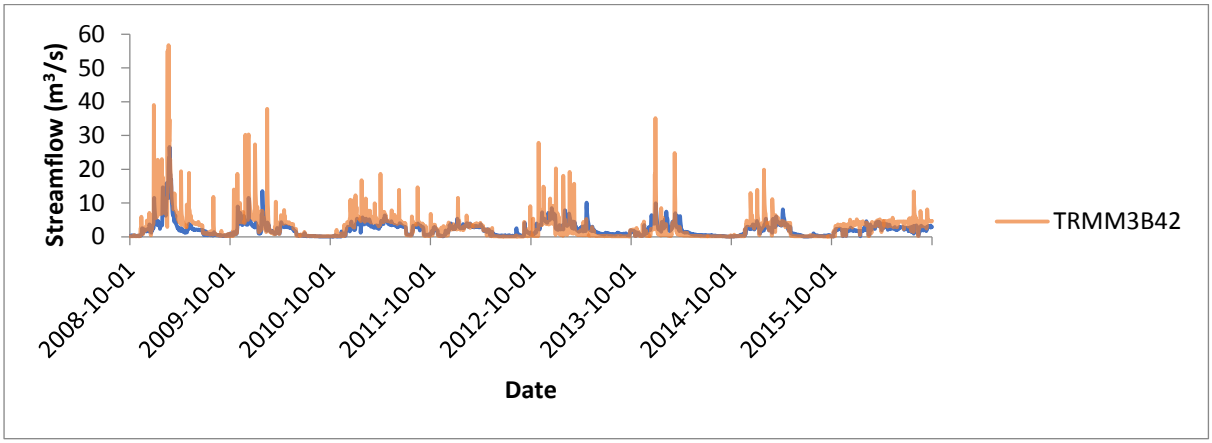

Figure 8.142 Time series of simulated streamflow driven with TRMM 3B42 against U2H007 streamflow.

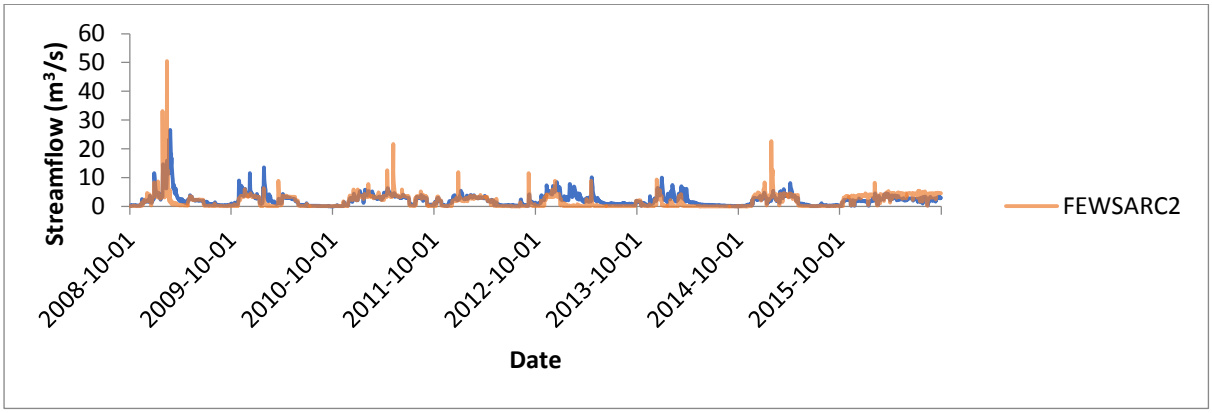

Figure 8.143 Time series of simulated streamflow driven with FEWS ARC2 against U2H007 streamflow.

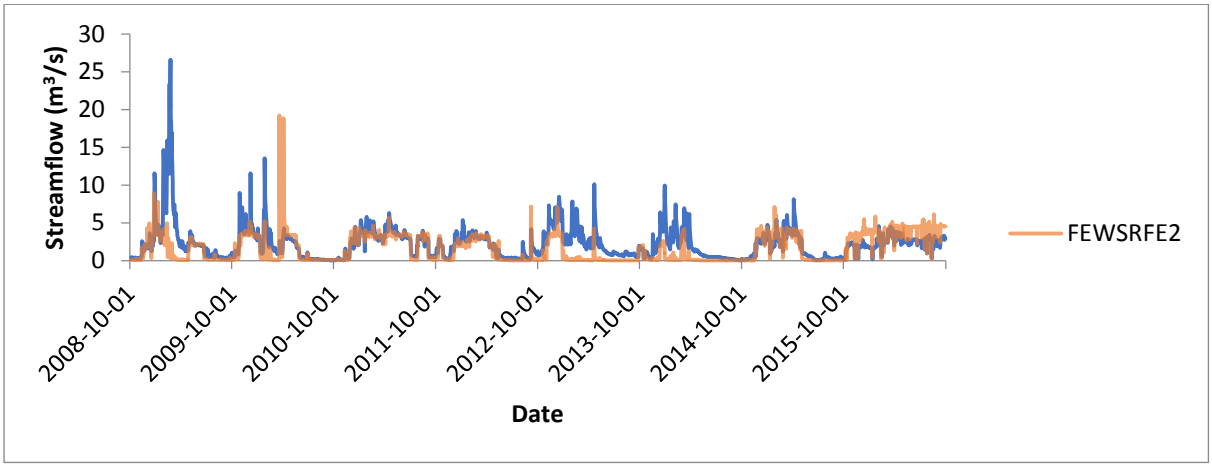

Figure 8.144 Time series of simulated streamflow driven with FEWS RFE2 against U2H007 streamflow.

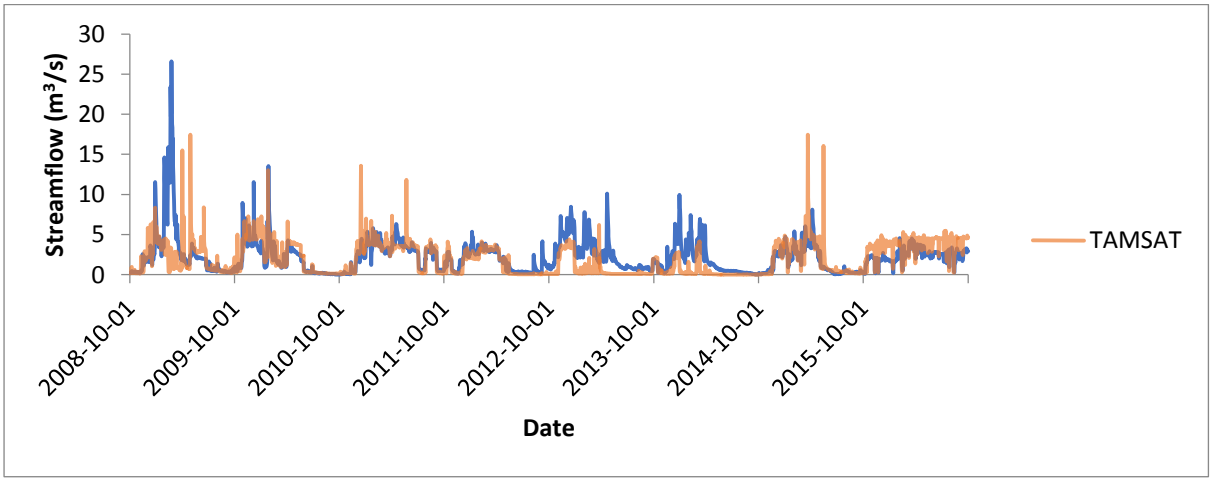

Figure 8.145 Time series of simulated streamflow driven with TAMSAT-3 against U2H007 streamflow.

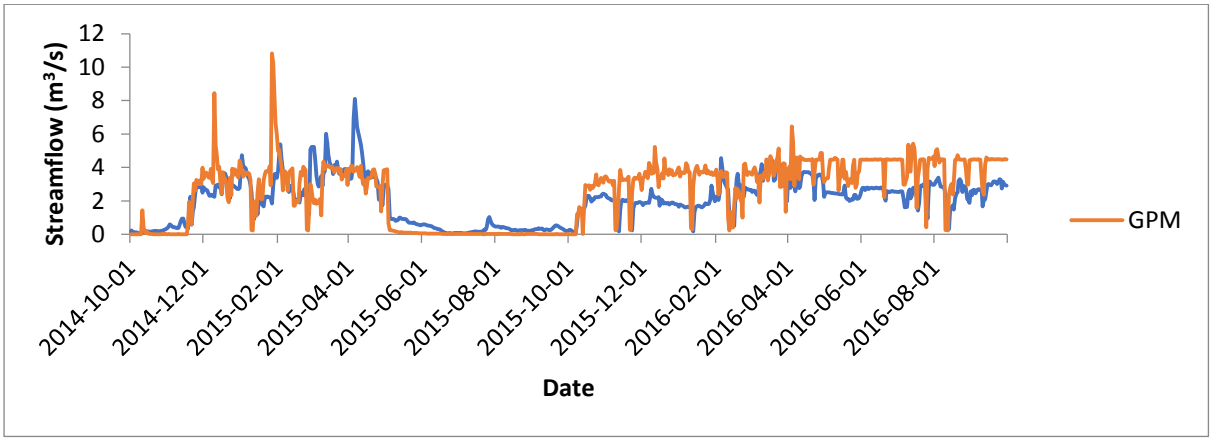

Figure 8.146 Time series of simulated streamflow driven with GPM against U2H007 streamflow.

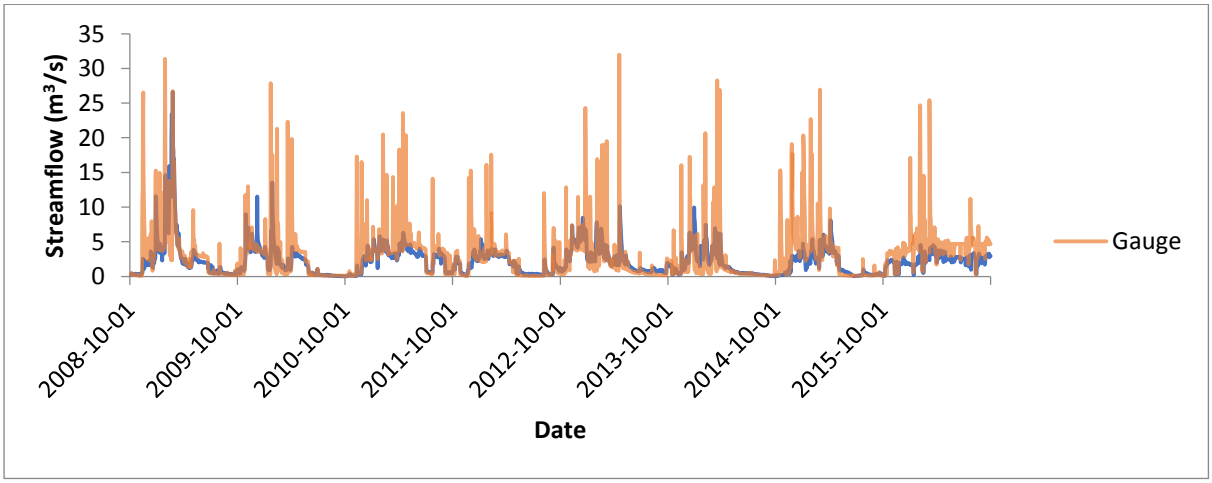

Figure 8.147 Time series of simulated streamflow driven with rain gauge measurements against U2H007 streamflow.

- U2H013 (Mgeni River at Petrus Stroom)

The time series of the simulated streamflow against weir gauge streamflow are presented below.

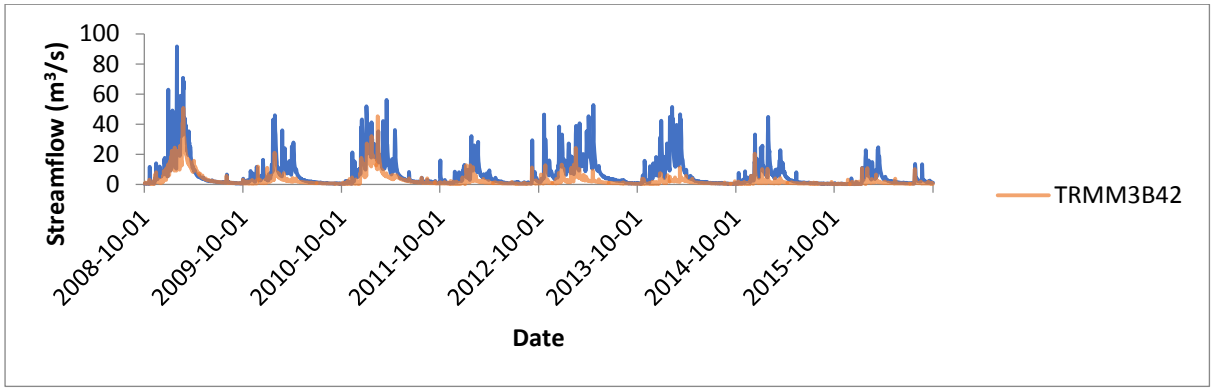

Figure 8.148 Time series of simulated streamflow driven with TRMM 3B42 against U2H013 streamflow.

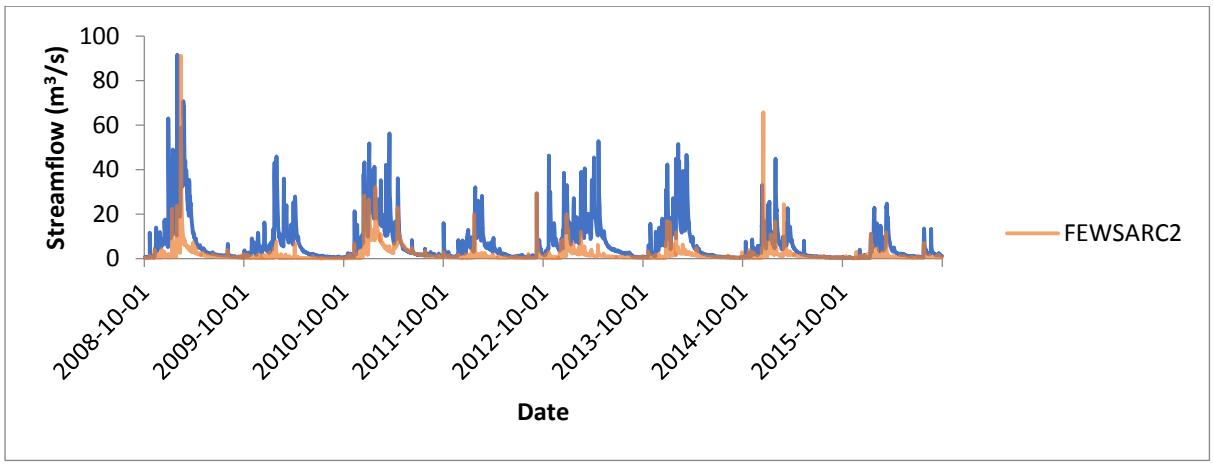

Figure 8.149 Time series of simulated streamflow driven with FEWS ARC2 against U2H013 streamflow.

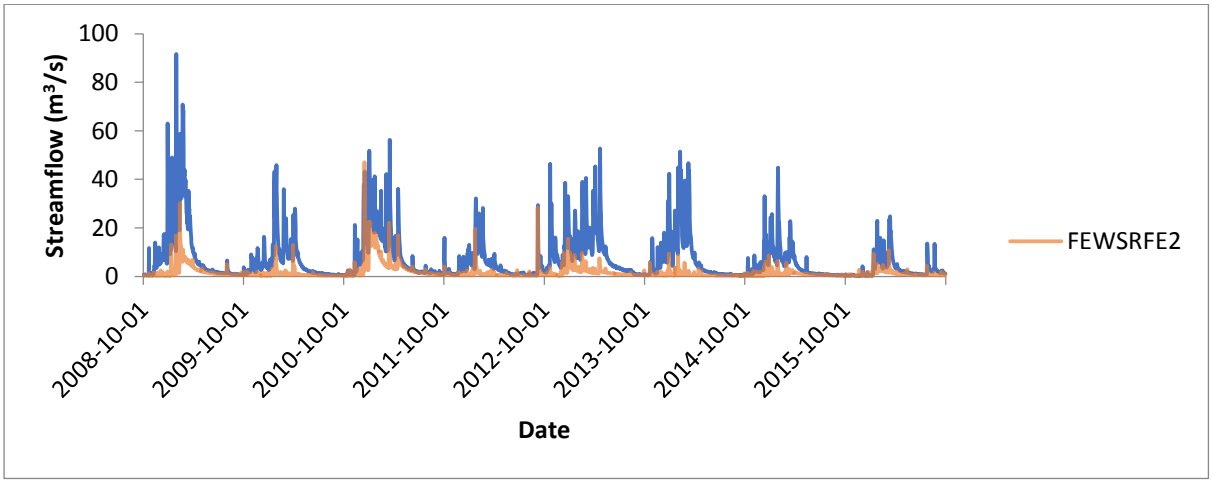

Figure 8.150 Time series of simulated streamflow driven with FEWS RFE2 against U2H013 streamflow.

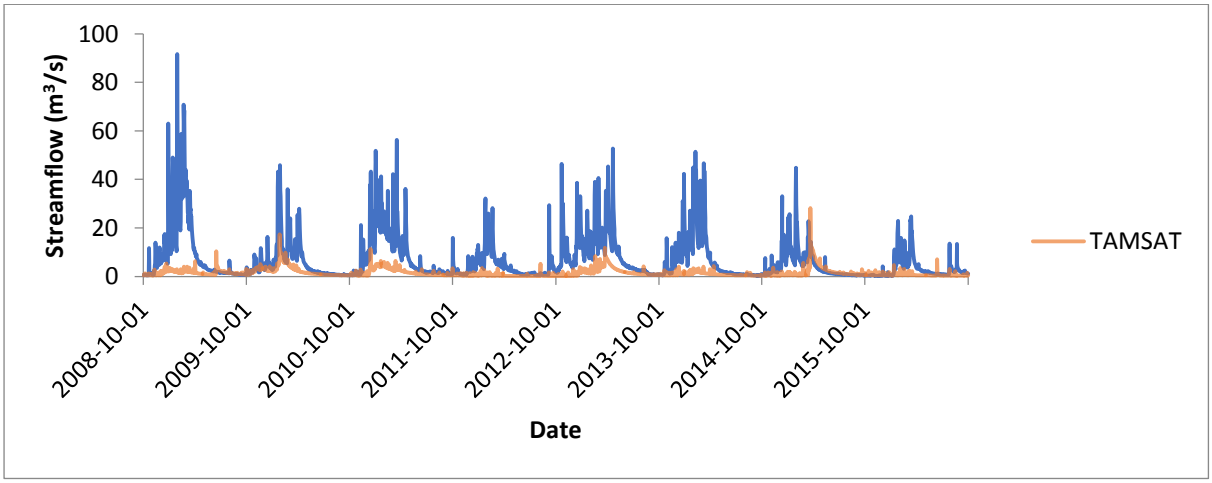

Figure 8.151 Time series of simulated streamflow driven with TAMSAT-3 against U2H013 streamflow.

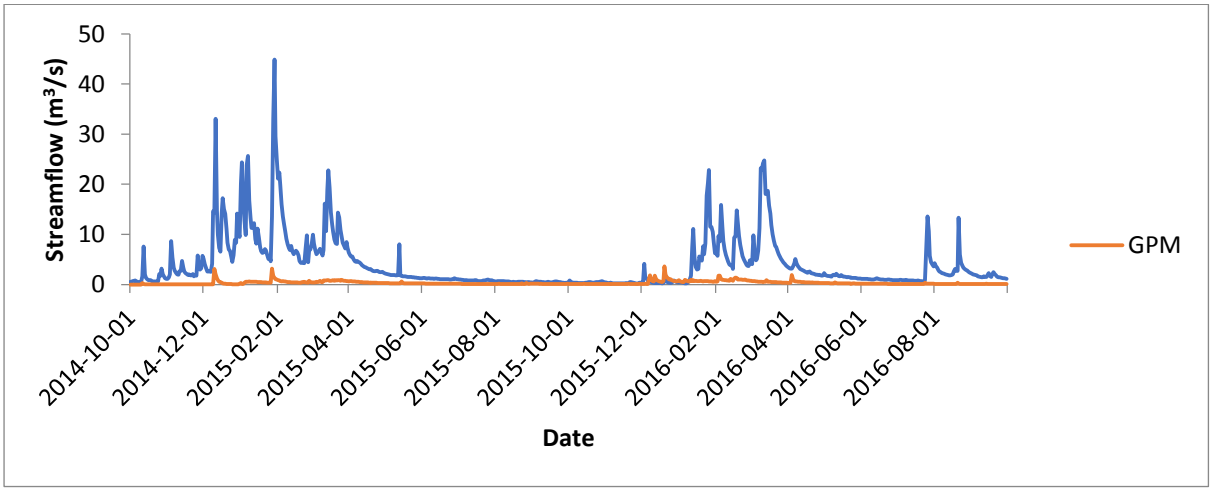

Figure 8.152 Time series of simulated streamflow driven with GPM against U2H013 streamflow.

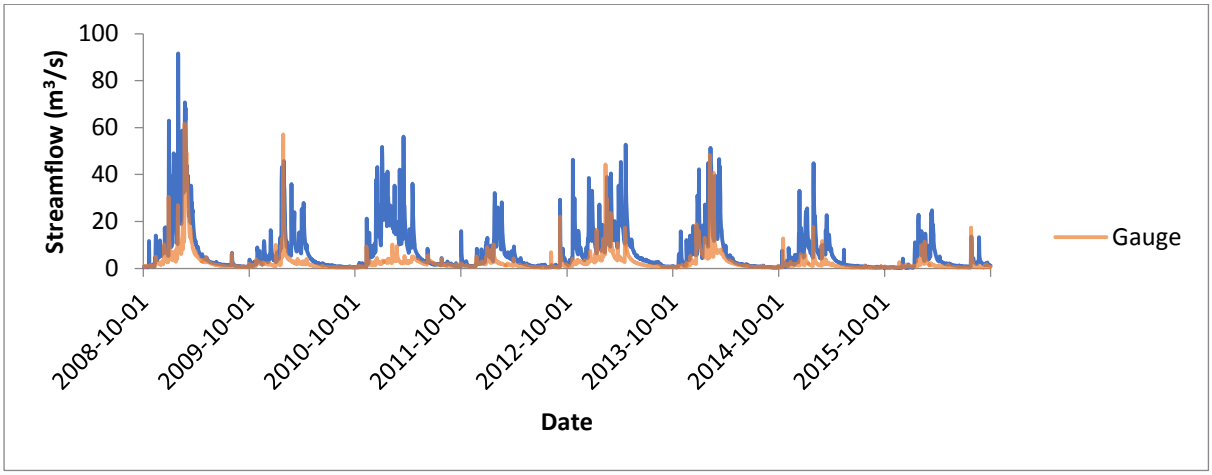

Figure 8.153 Time series of simulated streamflow driven with rain gauge measurements against U2H013 streamflow.

8.3.2 Upper uThukela streamflow modelling

The time series of streamflow the upper uThukela modelling are presented below.

- V6H004 (Sondags River at Kleinfontein)

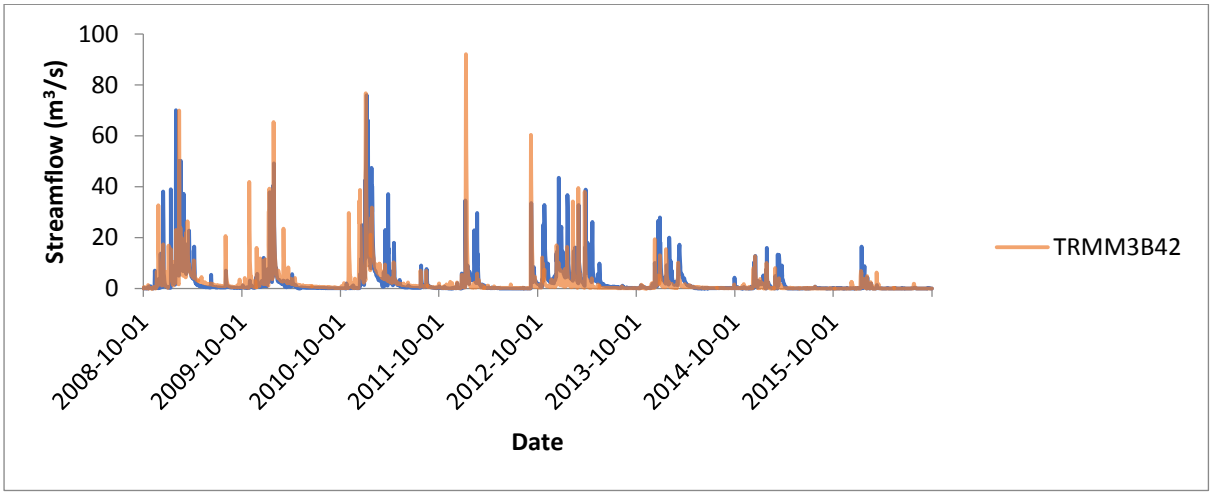

Figure 8.154 Time series of simulated streamflow driven with TRMM 3B42 against V6H004 streamflow.

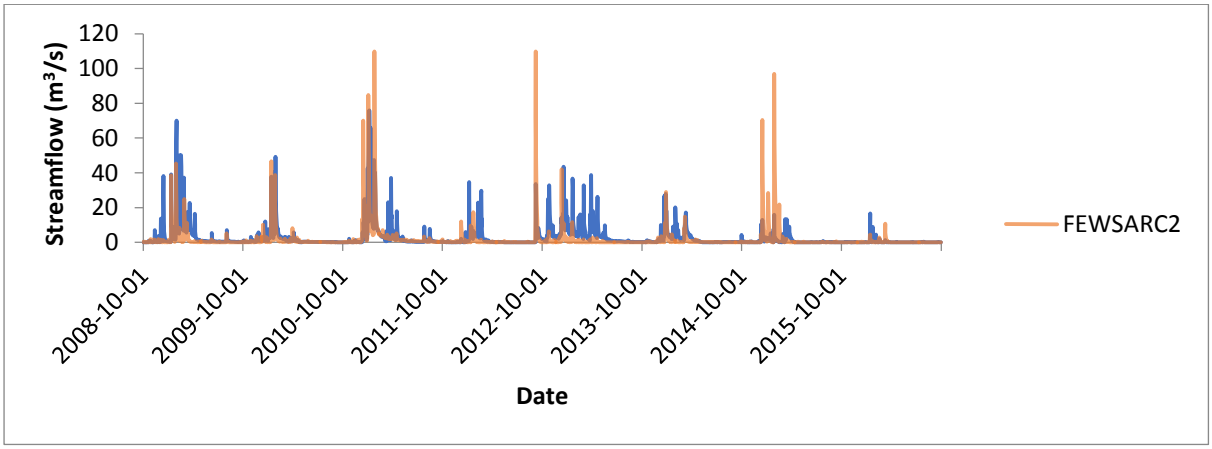

Figure 8.155 Time series of simulated streamflow driven with FEWS ARC2 against V6H004 streamflow.

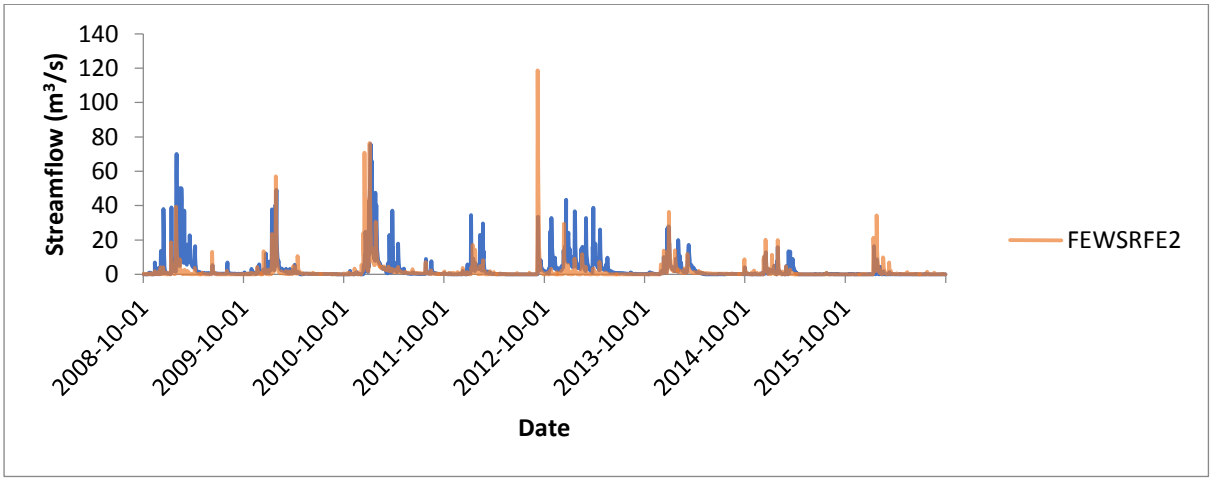

Figure 8.156 Time series of simulated streamflow driven with FEWS RFE2 against V6H004 streamflow.

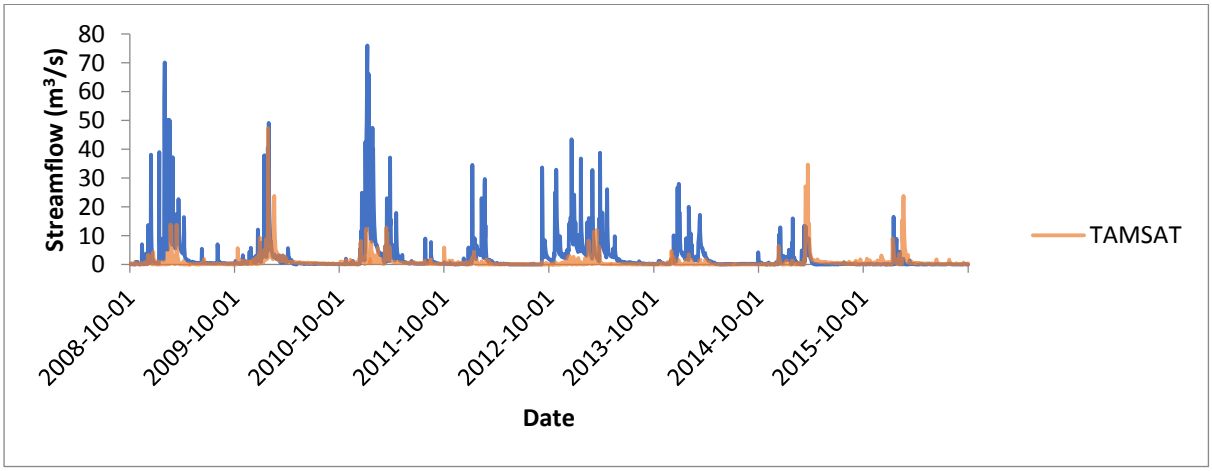

Figure 8.157 Time series of simulated streamflow driven with TAMSAT-3 against V6H004 streamflow.

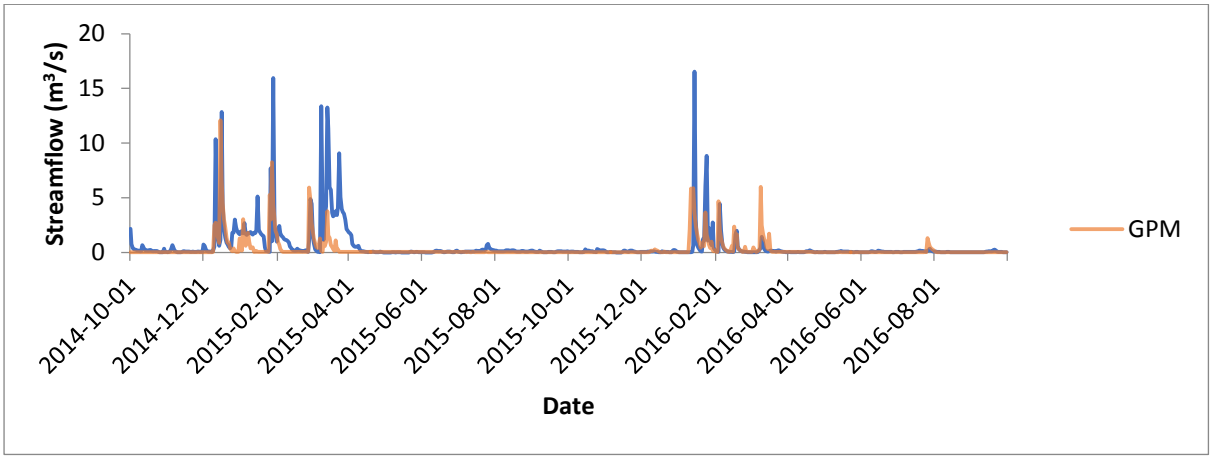

Figure 8.158 Time series of simulated streamflow driven with GPM against V6H004 streamflow.

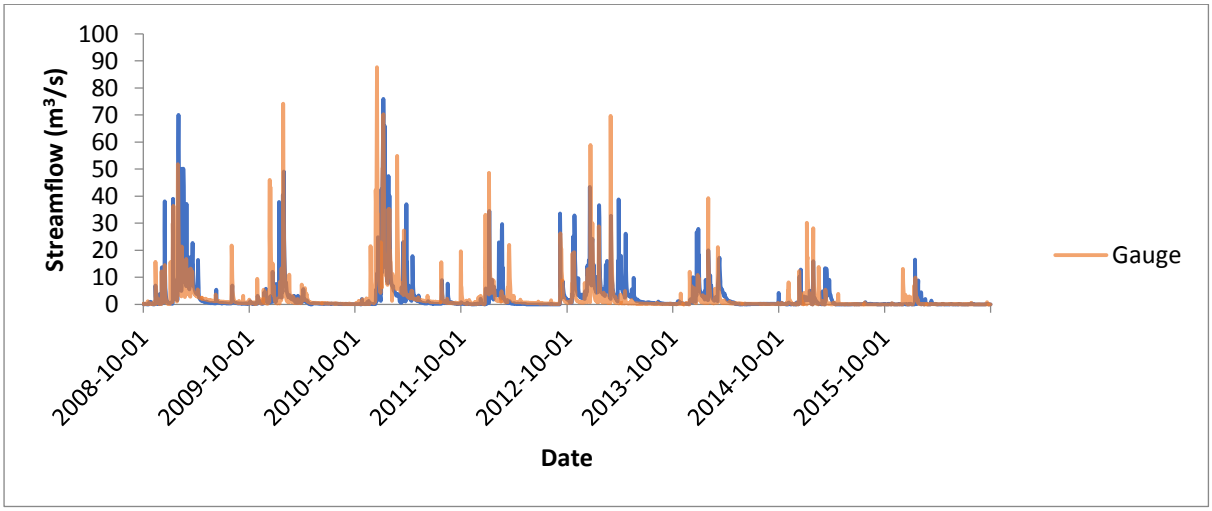

Figure 8.159 Time series of simulated streamflow driven with rain gauge measurements against V6H004 streamflow.

- V7H017 (Boesmans River at Drakensberg Loc1)

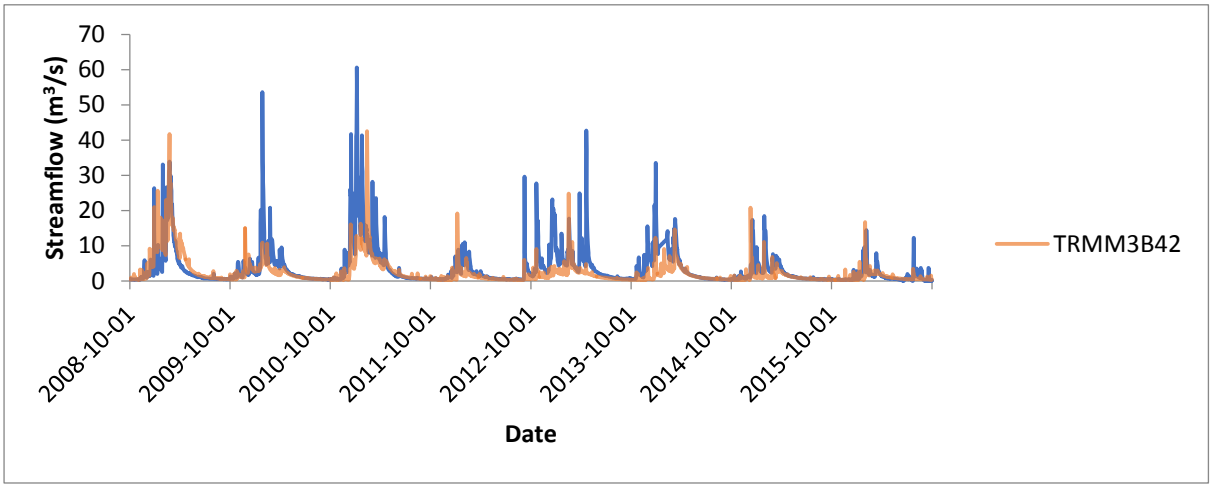

Figure 8.160 Time series of simulated streamflow driven with TRMM 3B42 against V7H017 streamflow.

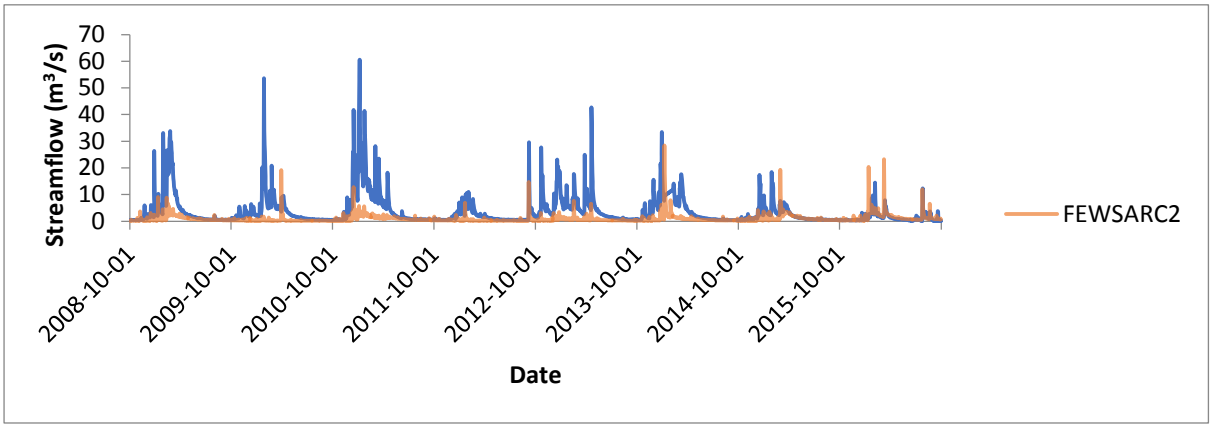

Figure 8.161 Time series of simulated streamflow driven with FEWS ARC2 against V7H017 streamflow.

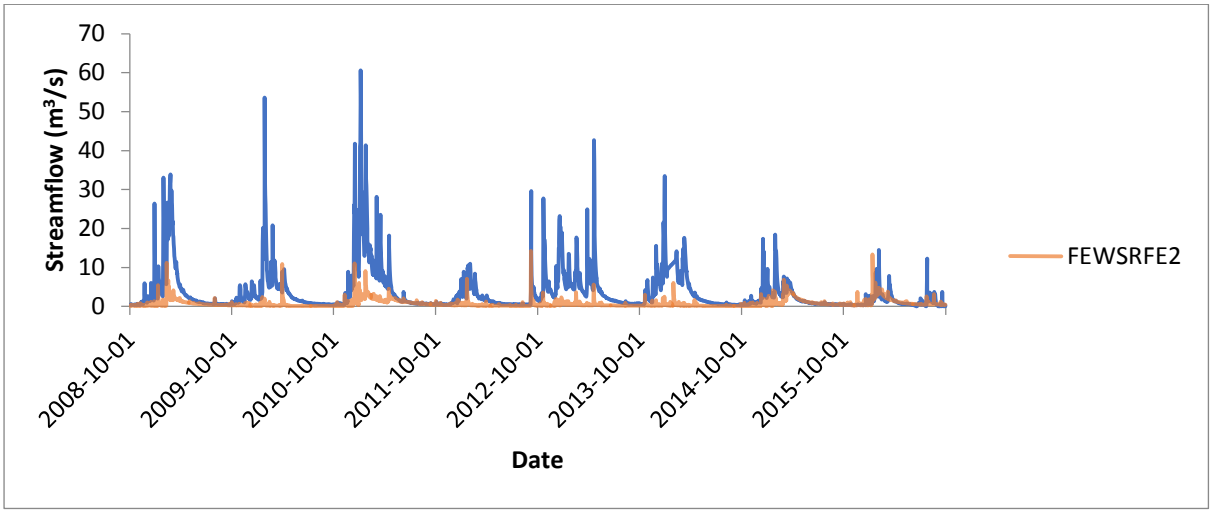

Figure 8.162 Time series of simulated streamflow driven with FEWS RFE2 against V7H017 streamflow.

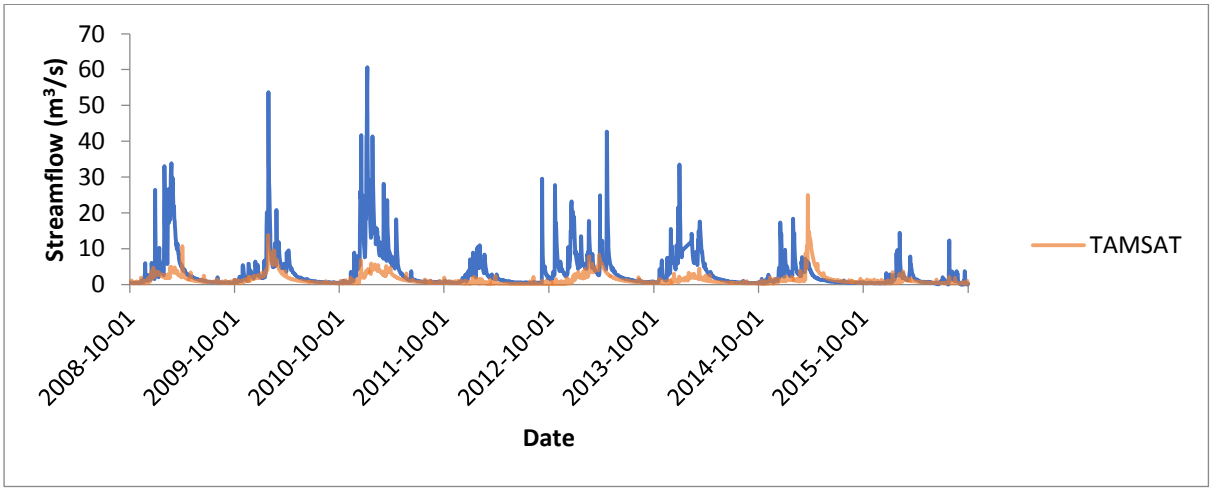

Figure 8.163 Time series of simulated streamflow driven with TAMSAT-3 against V7H017 streamflow.

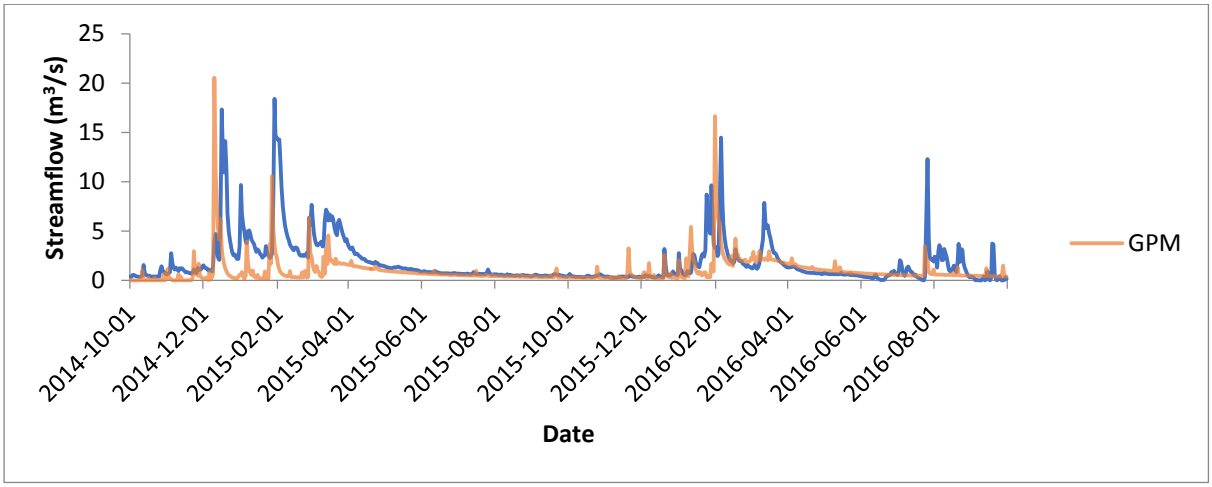

Figure 8.164 Time series of simulated streamflow driven with GPM against V7H017 streamflow.

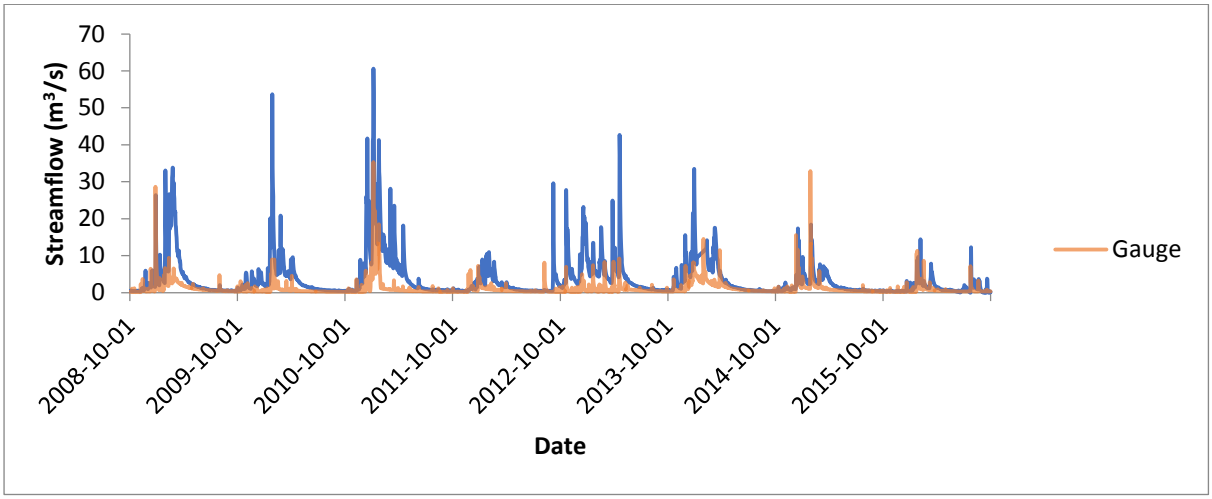

Figure 8.165 Time series of simulated streamflow driven with rain gauge measurements against V7H017 streamflow.

- V2H006 (Little Mooi River at Dartington)

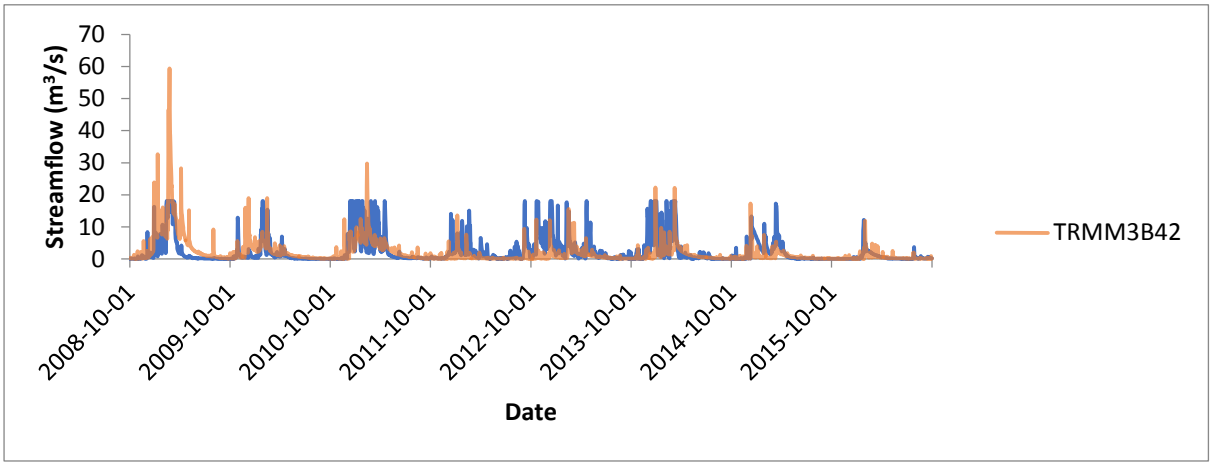

Figure 8.166 Time series of simulated streamflow driven with TRMM 3B42 against V2H006 streamflow.

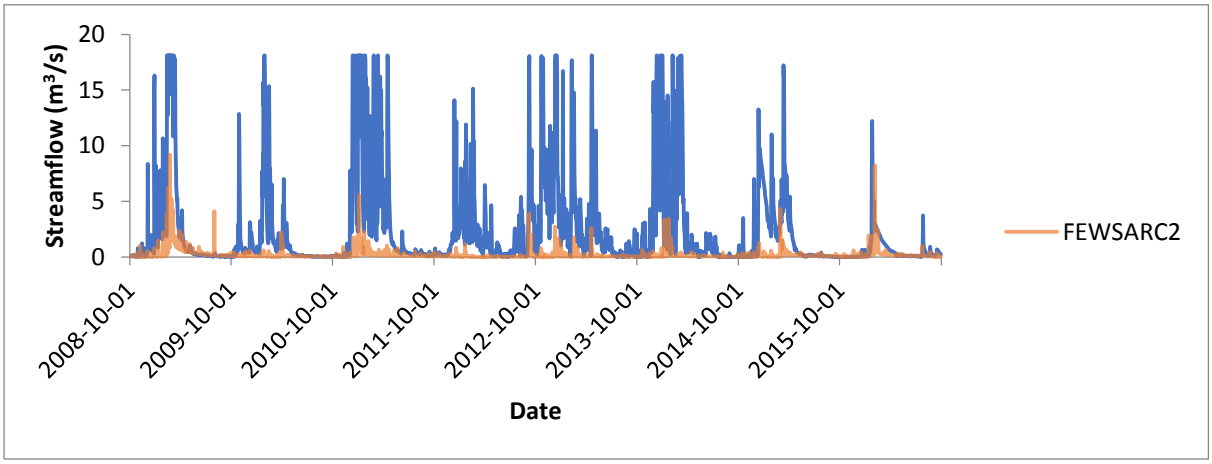

Figure 8.167 Time series of simulated streamflow driven with FEWS ARC2 against V2H006 streamflow.

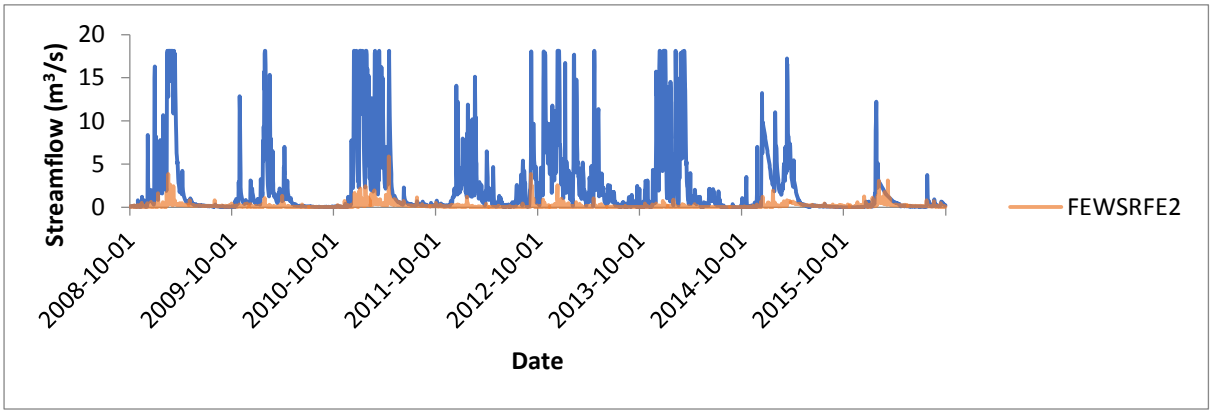

Figure 8.168 Time series of simulated streamflow driven with FEWS RFE2 against V2H006 streamflow.

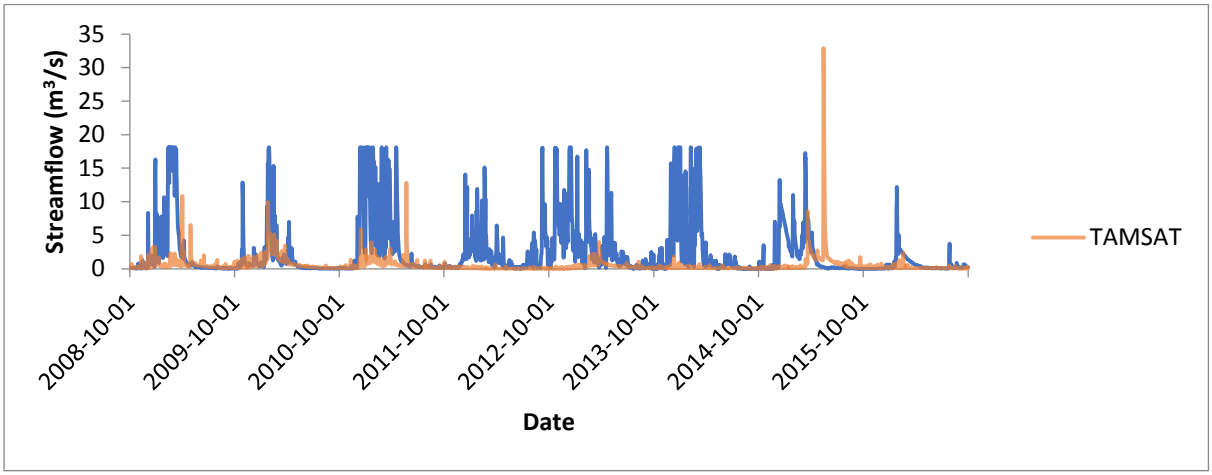

Figure 8.169 Time series of simulated streamflow driven with TAMSAT-3 against V2H006 streamflow.

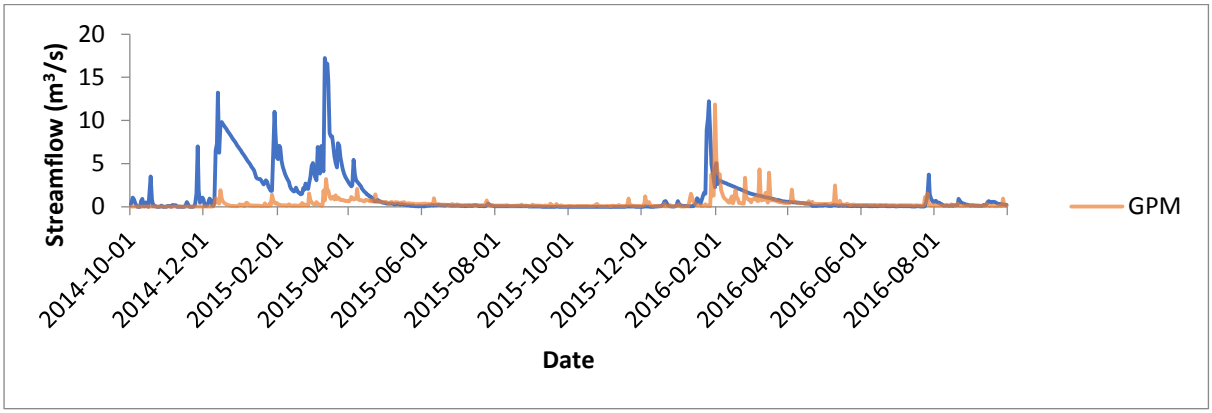

Figure 8.170 Time series of simulated streamflow driven with GPM against V2H006 streamflow.

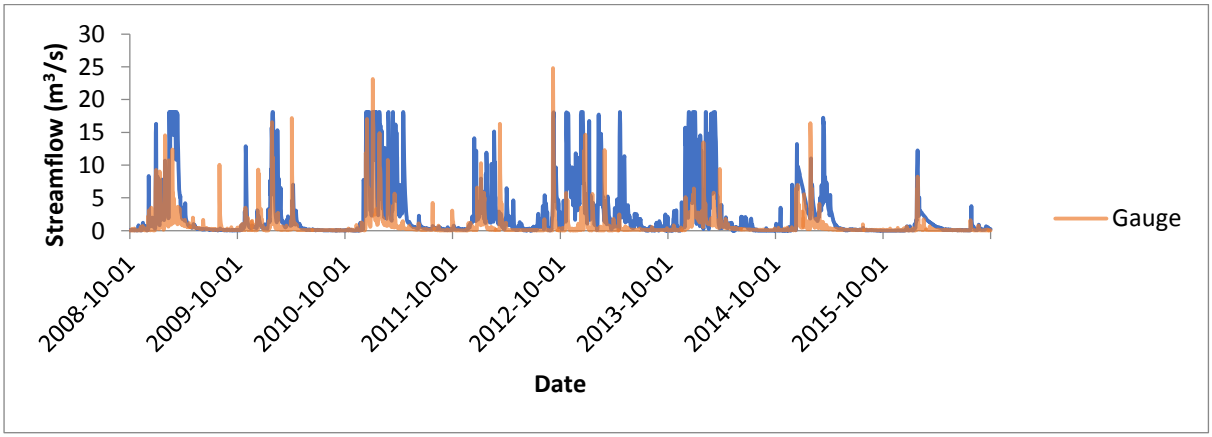

Figure 8.171 Time series of simulated streamflow driven with rain gauge measurements against V2H006 streamflow.

8.3.3 Upper and central Breede streamflow modelling

The time series of simulated streamflows of the upper and central Breede against weir data are presented below.

- H1H013 (Koekedou River at Ceres)

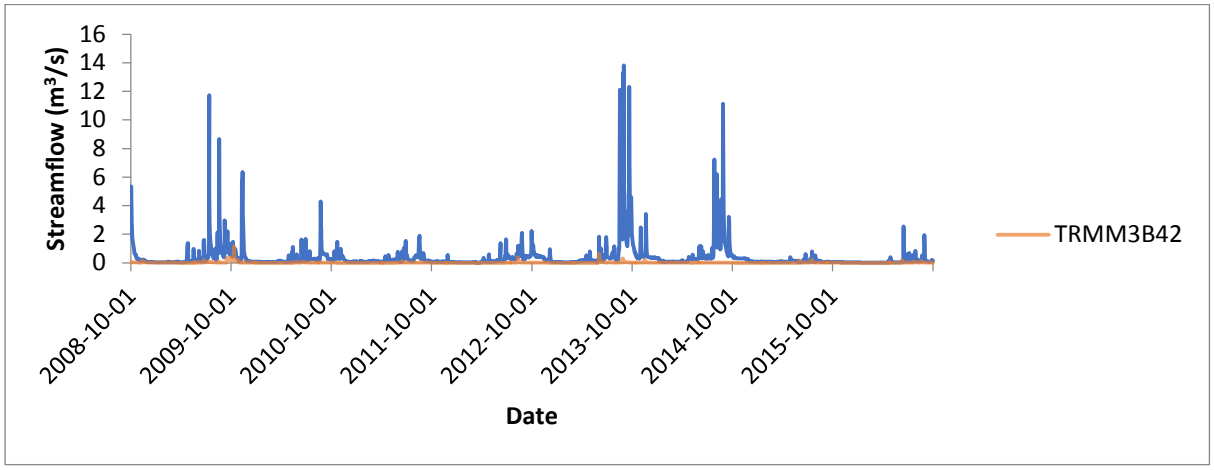

Figure 8.172 Time series of simulated streamflow driven with TRMM 3B42 against H1H013 streamflow.

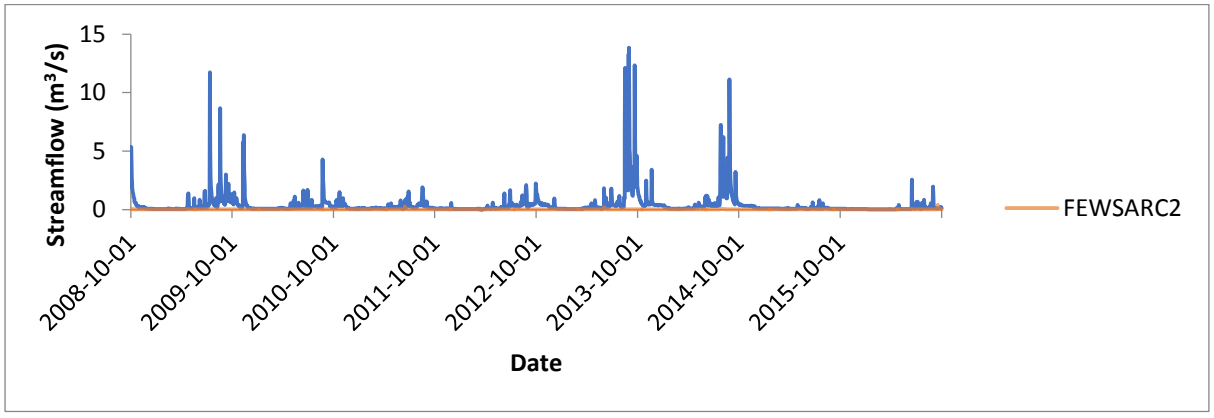

Figure 8.173 Time series of simulated streamflow driven with FEWS ARC2 against H1H013 streamflow.

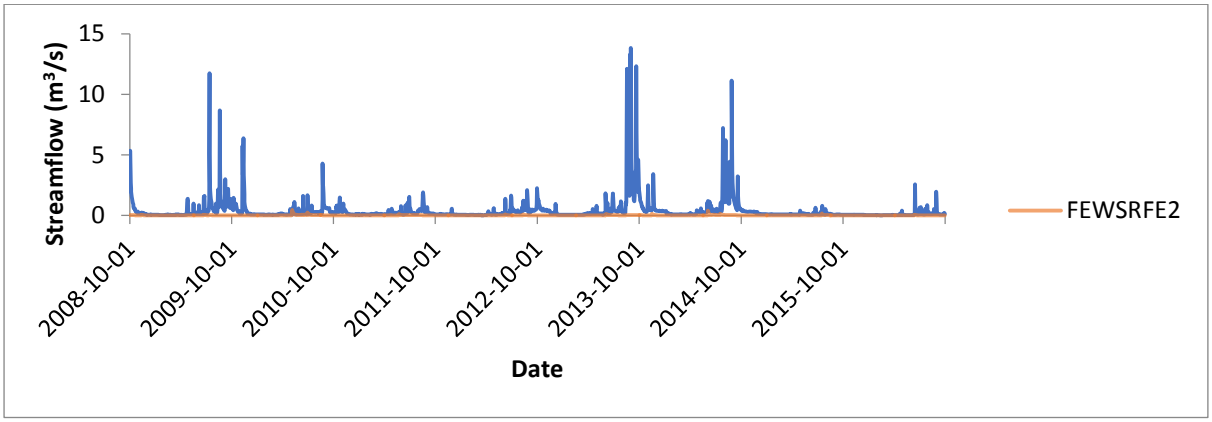

Figure 8.174 Time series of simulated streamflow driven with FEWS RFE2 against H1H013 streamflow.

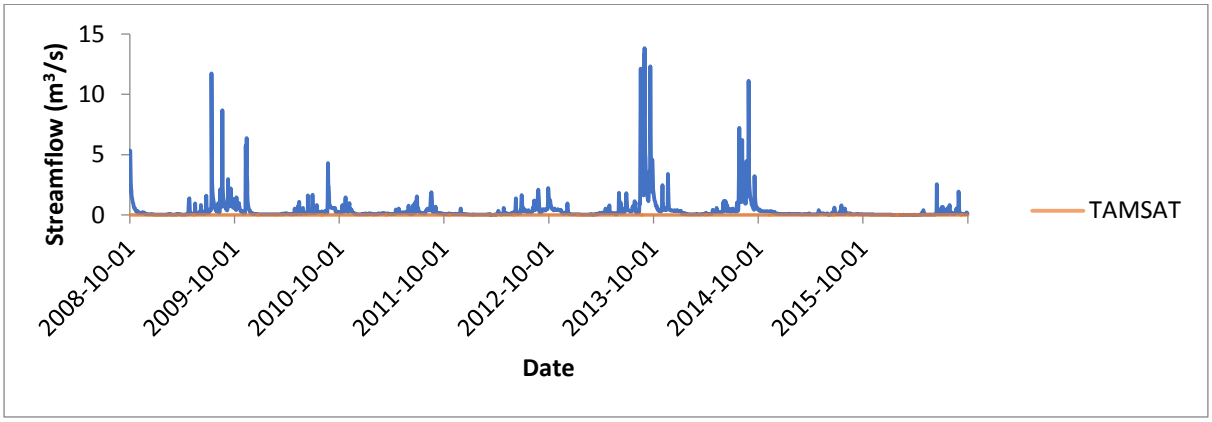

Figure 8.175 Time series of simulated streamflow driven with TAMSAT-3 against H1H013 streamflow.

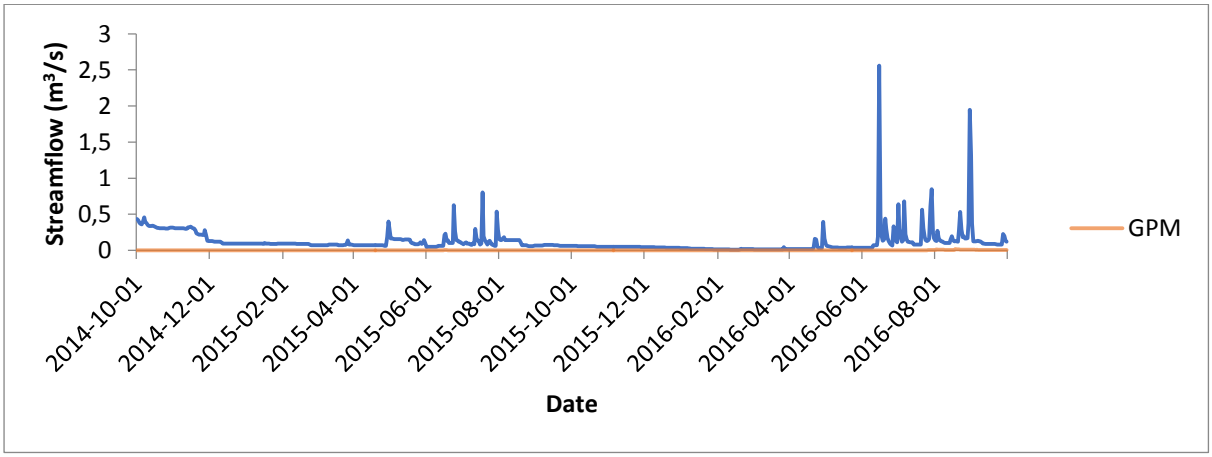

Figure 8.176 Time series of simulated streamflow driven with GPM against H1H013 streamflow.

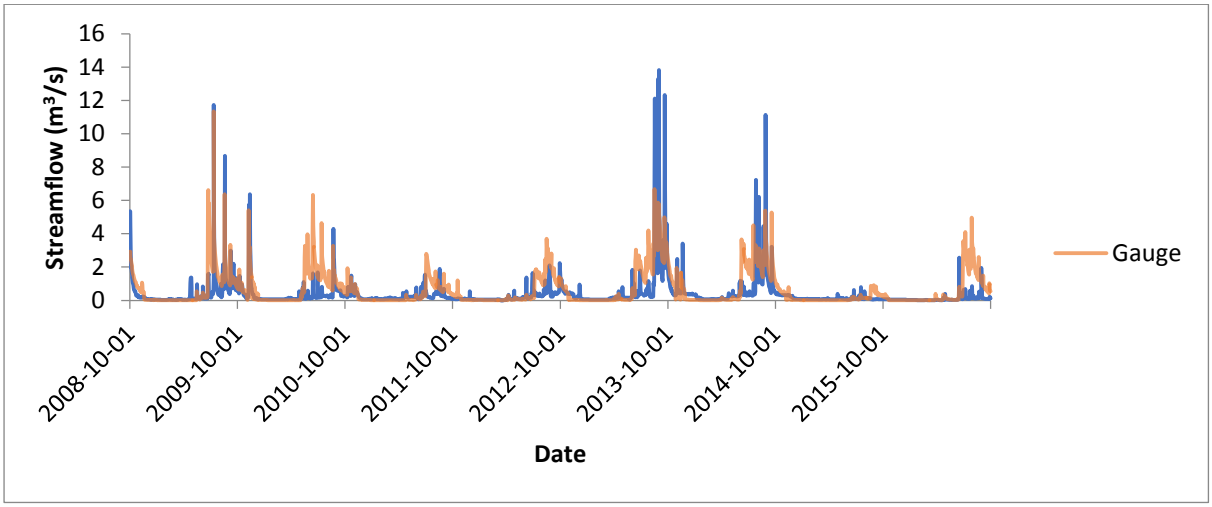

Figure 8.177 Time series of simulated streamflow driven with rain gauge measurements against H1H013 streamflow.

- H4H016 (Keisers at Mc Gregor Toeken Geb)

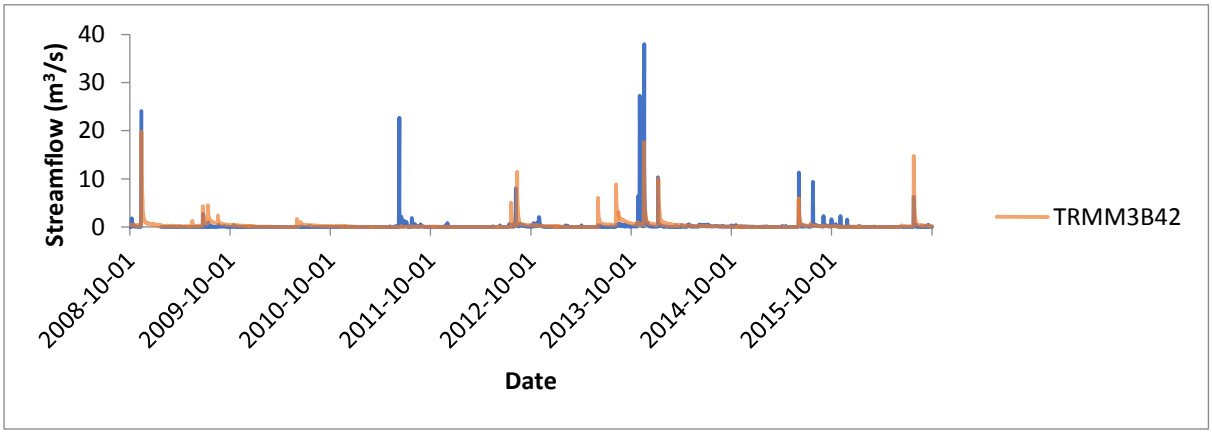

Figure 8.178 Time series of simulated streamflow driven with TRMM 3B42 against H4H016 streamflow.

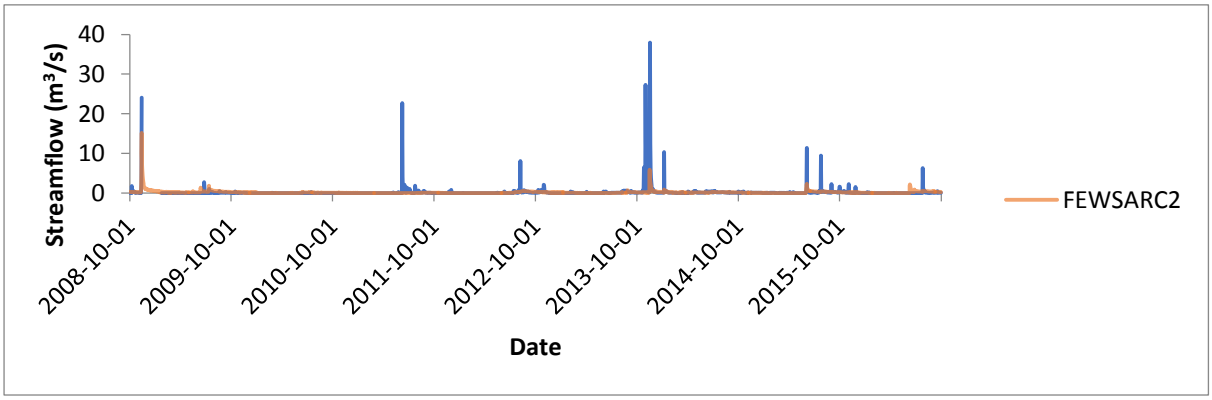

Figure 8.179 Time series of simulated streamflow driven with FEWS ARC2 against H4H016 streamflow.

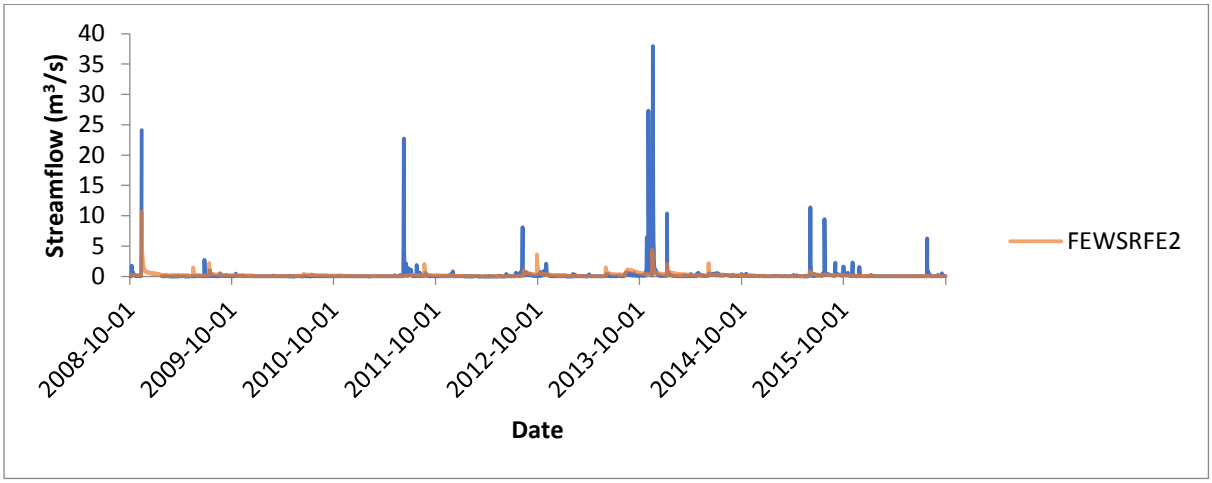

Figure 8.180 Time series of simulated streamflow driven with FEWS RFE2 against H4H016 streamflow.

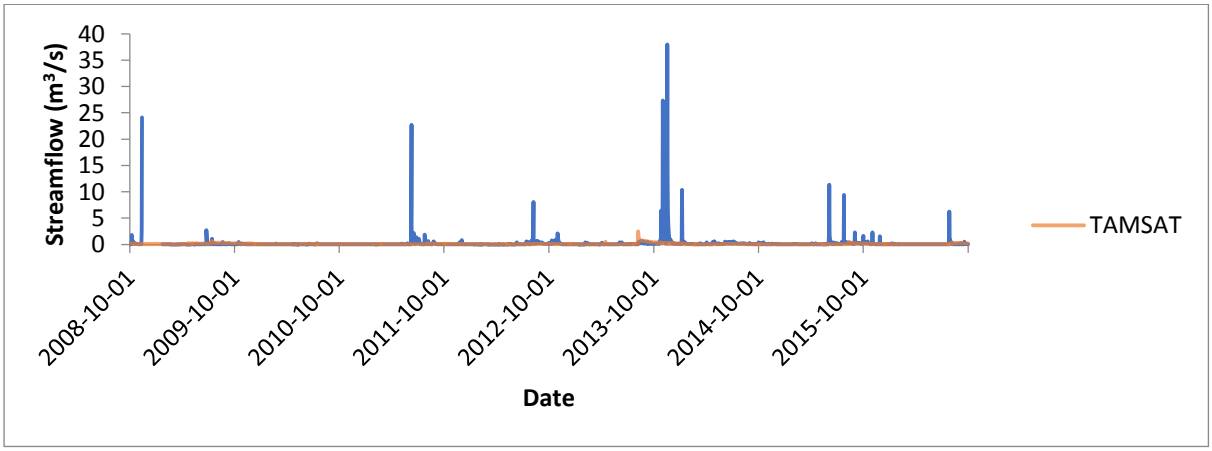

Figure 8.181 Time series of simulated streamflow driven with TAMSAT-3 against H4H016 streamflow.

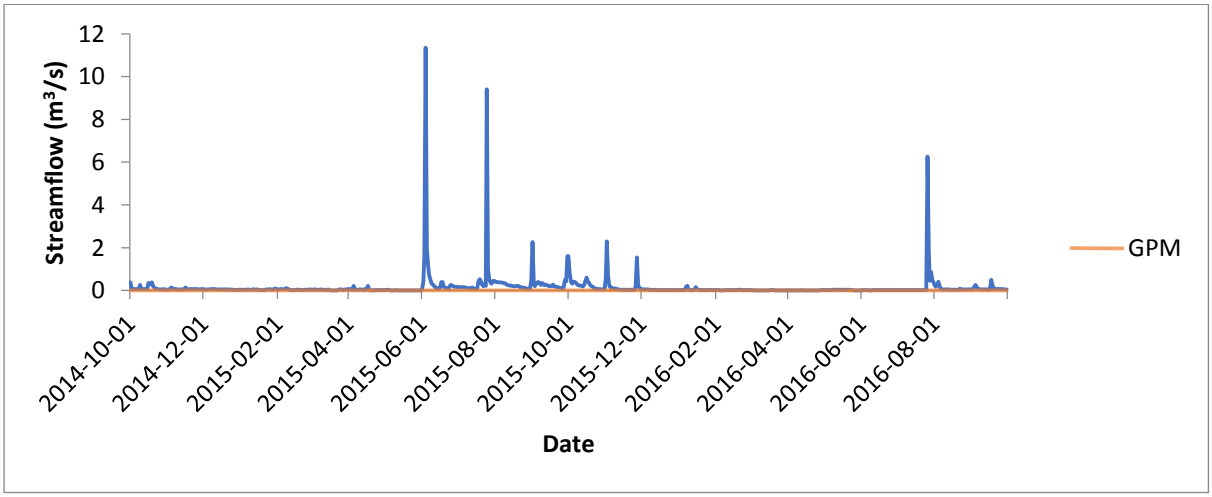

Figure 8.182 Time series of simulated streamflow driven with GPM against H4H016 streamflow.

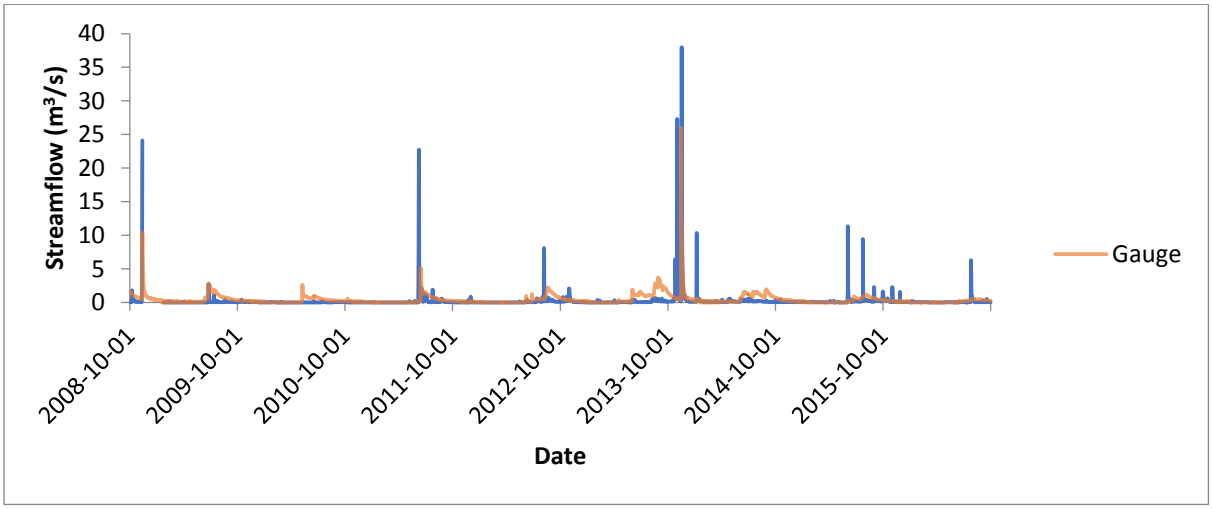

Figure 8.183 Time series of simulated streamflow driven with rain gauge measurements against H4H016 streamflow.

- H4H018 (Poesjenels at Le Chasseur)

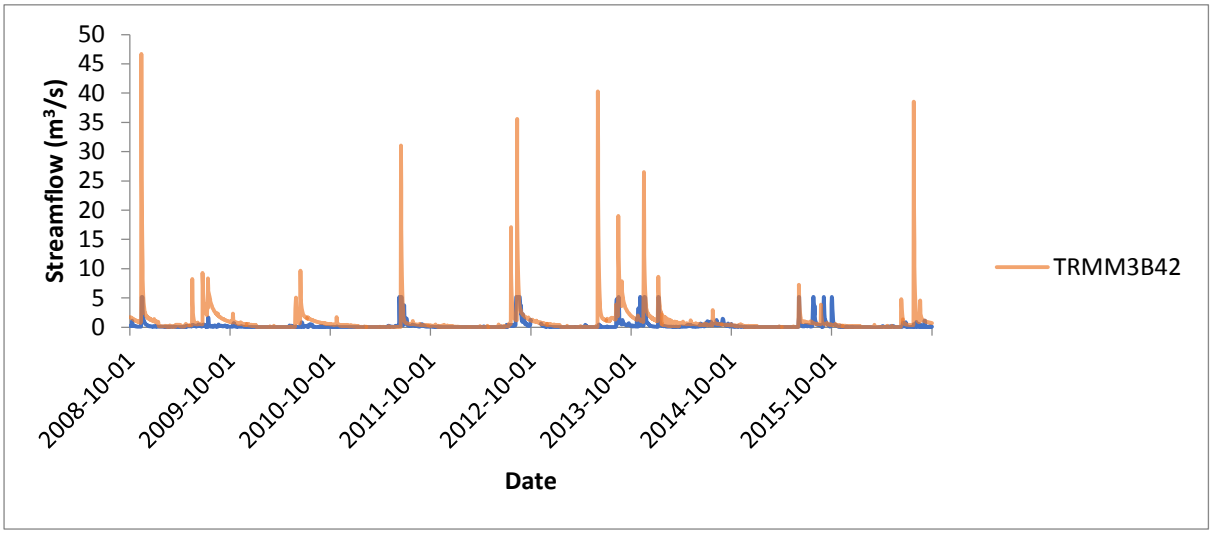

Figure 8.184 Time series of simulated streamflow driven with TRMM 3B42 against H4H018 streamflow.

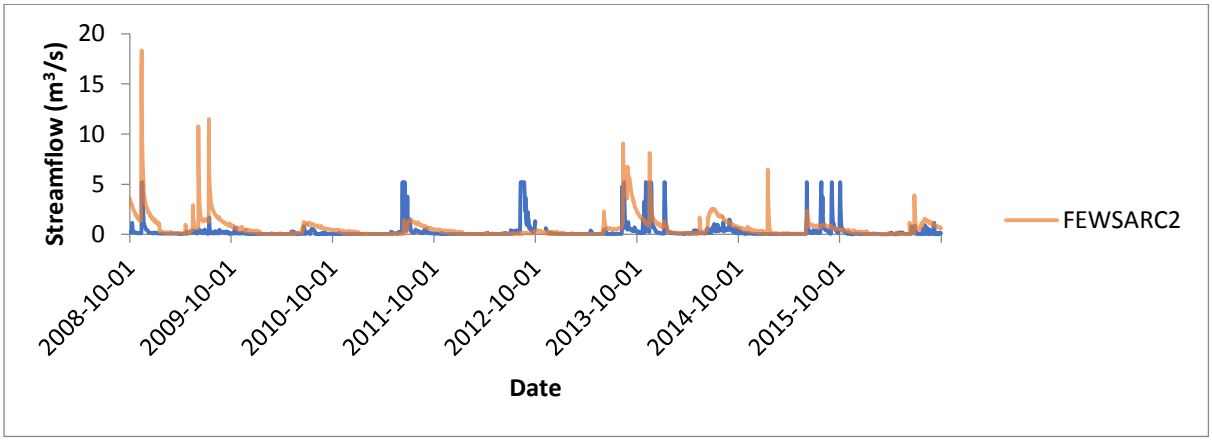

Figure 8.185 Time series of simulated streamflow driven with FEWS ARC2 against H4H018 streamflow.

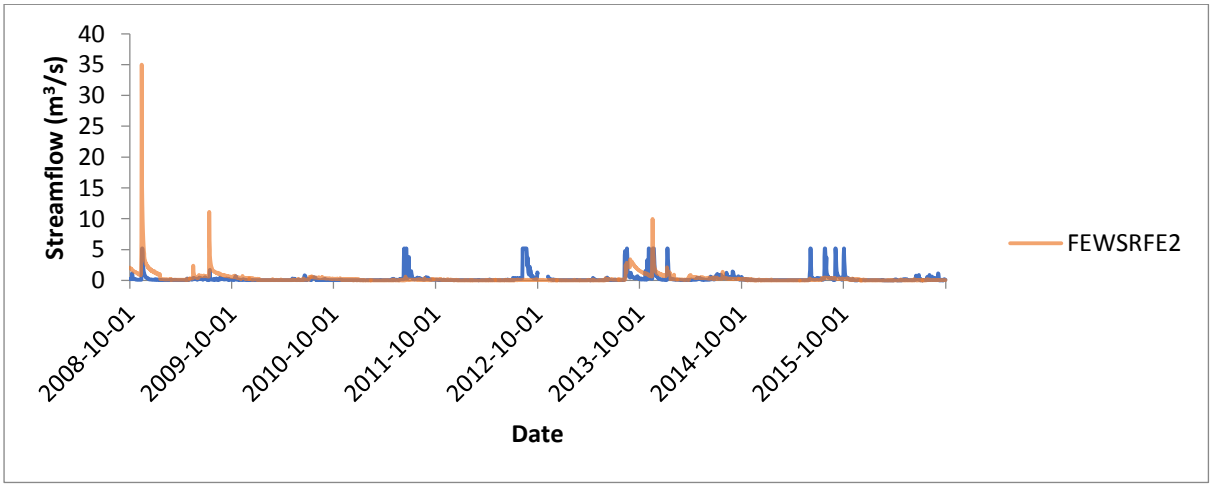

Figure 8.186 Time series of simulated streamflow driven with FEWS RFE2 against H4H018 streamflow.

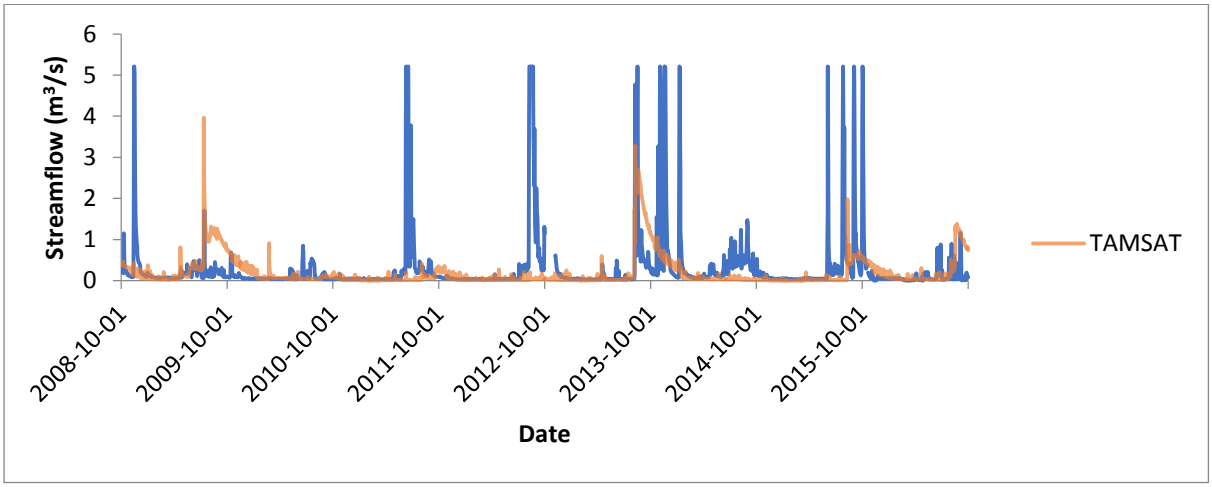

Figure 8.187 Time series of simulated streamflow driven with TAMSAT-3 against H4H018 streamflow.

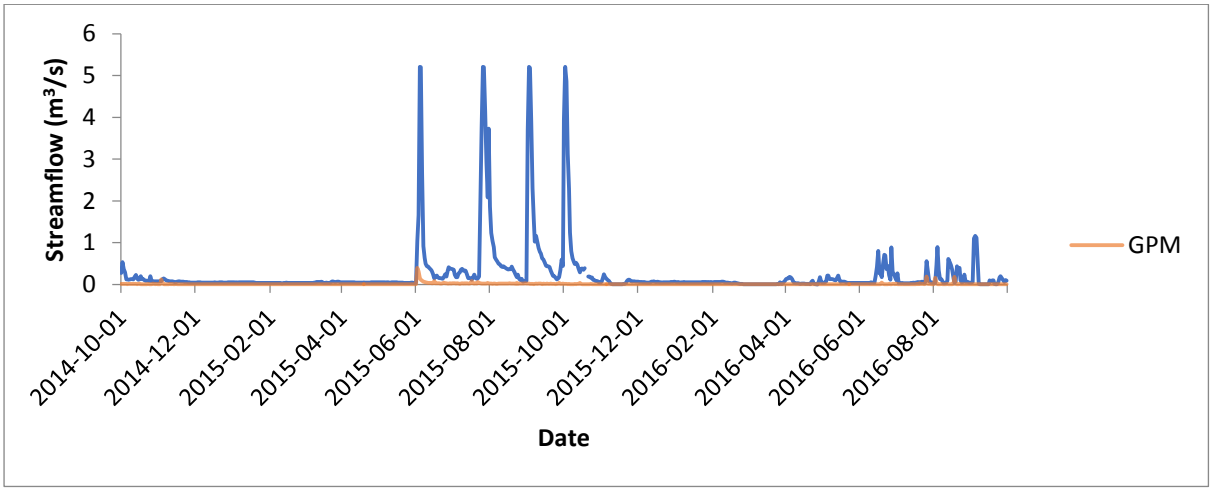

Figure 8.188 Time series of simulated streamflow driven with GPM against H4H018 streamflow.

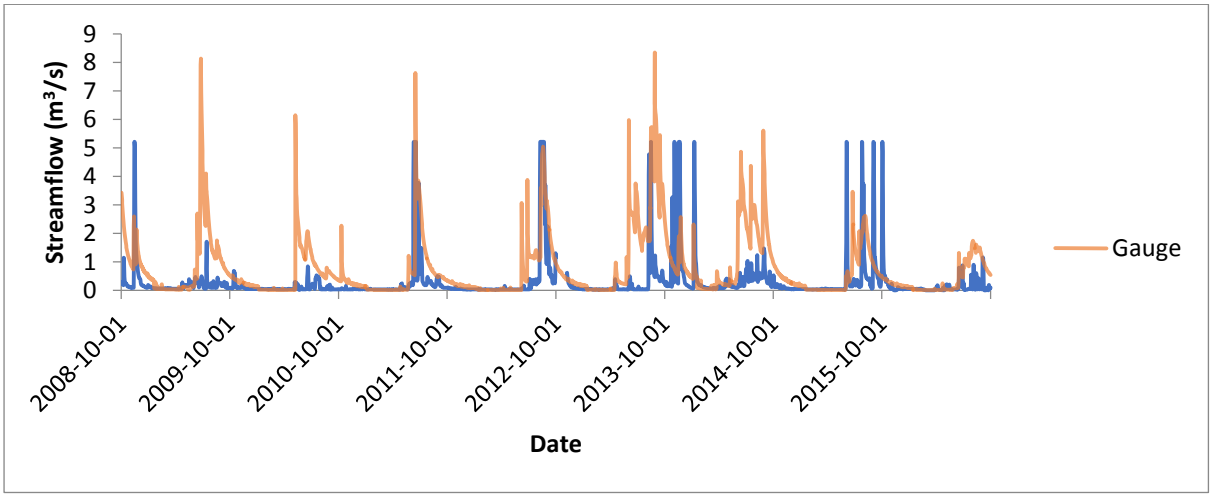

Figure 8.189 Time series of simulated streamflow driven with rain gauge measurements against H4H018 streamflow.